



UNIVERSIDAD MIGUEL HERNÁNDEZ

Programa de Doctorado en Biología Molecular y Celular

Instituto de Investigación, Desarrollo e Innovación
en Biotecnología Sanitaria de Elche (IDiBE)

DESCUBRIMIENTO Y CARACTERIZACIÓN DE LA ACTIVIDAD ANTIVIRAL INDUCIDA POR LAS MOLECULAS TIPO CRP DE PEZ CEBRA (*DANIO RERIO*)

TESIS DOCTORAL

Melissa Belló Pérez

DIRECTOR

Luis Pérez García-Estañ

CODIRECTOR

Alberto Falcó Graciá

2019

PREFACIO

La memoria correspondiente a la presente tesis doctoral se presenta **con un compendio de publicaciones**. A continuación se detallan las publicaciones científicas que constan en este documento:

Publicación 1. Bello-Perez M, Falco A, Medina R, Encinar JA, Novoa B, Perez L, et al. Structure and functionalities of the human c-reactive protein compared to the zebrafish multigene family of c-reactive-like proteins. *Dev Comp Immunol.* 2017;69:33-40. doi: 10.1016/j.dci.2016.12.001. PubMed PMID: 27965017.

Publicación 2. Bello-Perez M, Falco A, Medina-Gali R, Pereiro P, Encinar JA, Novoa B, et al. Neutralization of viral infectivity by zebrafish c-reactive protein isoforms. *Molecular immunology.* 2017;91:145-55.

Publicación 3. Bello-Perez M, Falco A, Novoa B, Perez L, Coll J. Hydroxycholesterol binds and enhances the anti-viral activities of zebrafish monomeric c-reactive protein isoforms. *PloS one.* 2019;14(1):e0201509.

***Publicación 4.** Bello-Perez M., Pereiro P, Coll J, Novoa B, Perez L, Falco A. Zebrafish C-reactive protein isoforms inhibit SVCV replication by blocking autophagy through the interaction with cell membrane cholesterol. Autophagy. *Enviado.

Publicación 5. Bello-Perez M, Falco A, Galiano V, Coll J, Perez L, Encinar JA. Discovery of nonnucleoside inhibitors of polymerase from infectious pancreatic necrosis virus (IPNV). *Drug Des Devel Ther.* 2018;12:2337-59. doi: 10.2147/DDDT.S171087. PubMed PMID: 30104863; PubMed Central PMCID: PMC6072831.

Publicación 6. Bello-Perez M, Medina-Gali R, Coll J, Perez L. Viral interference between infectious pancreatic necrosis virus and spring viremia of carp virus in zebrafish. *Aquaculture.* 2019;500:370-7.

La presente tesis doctoral se ha desarrollado en el Instituto de Investigación, Desarrollo e Innovación en Biotecnología Sanitaria de Elche (IDiBE) de la Universidad Miguel Hernández (UMH), bajo la dirección de los doctores Luis Pérez García-Estañ y Alberto Falcó Graciá, con el **apoyo de una beca para la contratación de personal investigador de carácter predoctoral de la Comunidad Valenciana (identificación ACIF/2016/207) y el Fondo Social Europeo (FSE) 2014-2020.**

Siguiendo la normativa interna de la UMH, la memoria consta de los siguientes apartados:

1. Resumen
2. Introducción general
3. Objetivos, antecedentes y sistema modelo
4. Resumen de los resultados obtenidos
5. Discusión global
6. Conclusiones
7. Bibliografía
8. Compendio de publicaciones
9. Anexo 1 (material no publicado presente en la tesis)
10. Anexo 2 (indicios de calidad extra)





D. Luis Pérez García-Estañ, Profesor Titular de la Universidad Miguel Hernández, y D. Juan Alberto Falcó Graciá, doctor en el Instituto de Investigación, Desarrollo e Innovación en Biotecnología Sanitaria de Elche de la Universidad Miguel Hernández,

CERTIFICAN:

Que el trabajo de investigación para optar al título de doctor, titulado: "Descubrimiento y caracterización de la actividad antiviral inducida por las moléculas tipo CRP de pez cebra (*Danio rerio*)", del que es autora Melissa Belló Pérez, ha sido realizado bajo su dirección en el Instituto de Investigación, Desarrollo e Innovación en Biotecnología Sanitaria de Elche de la Universidad Miguel Hernández.

Para que conste y surta los efectos oportunos, firman el presente certificado en Elche, a de de 2019.

Fdo: Dr. Luis Pérez García-Estañ
Director

Fdo: Dr. Juan Alberto Falcó Graciá
Codirector



Dr. Ricardo Mallavia, Catedrático del Departamento de Química Inorgánica de la Universidad Miguel Hernández y coordinador del Programa de Doctorado en Biología Molecular y Celular del Instituto de Investigación, Desarrollo e Innovación en Biotecnología Sanitaria de Elche, de la Universidad Miguel Hernández (UMH).

CERTIFICA que la doctoranda Melissa Belló Pérez, ha completado el Programa de formación Doctoral en Biología Molecular y Celular, alcanzado los objetivos establecidos en el mismo. Y que la tesis reúne los indicios de calidad exigidos para el campo de evaluación. La estudiante es la primera firmante de los siguientes artículos indexados en el *Journal of Citation Report*:

- Bello-Perez M, Falco A, Medina R, Encinar JA, Novoa B, Perez L, et al. Structure and functionalities of the human c-reactive protein compared to the zebrafish multigene family of c-reactive-like proteins. *Dev Comp Immunol*. 2017;69:33-40. doi: 10.1016/j.dci.2016.12.001. PubMed PMID: 27965017.

La revista pertenece al primer cuartil en las áreas *Fisheries* y *Zoology* y al tercer cuartil en el área de *Immunology* y posee un índice de impacto de 2,913.

- Bello-Perez M, Falco A, Medina-Gali R, Pereiro P, Encinar JA, Novoa B, et al. Neutralization of viral infectivity by zebrafish c-reactive protein isoforms. *Molecular immunology*. 2017;91:145-55.

La revista pertenece al segundo cuartil en las áreas *Immunology* y *Biochemistry & molecular biology* y posee un índice de impacto de 3,188.

- Bello-Perez M, Falco A, Novoa B, Perez L, Coll J. Hydroxycholesterol binds and enhances the anti-viral activities of zebrafish monomeric c-reactive protein isoforms. *PloS one*. 2019;14(1):e0201509.

La revista pertenece al primer cuartil en el área *Multidisciplinary Sciences* y posee un índice de impacto de 2,766.

- Bello-Perez M., Pereiro P, Coll J, Novoa B, Perez L, Falco A. Zebrafish C-reactive protein isoforms inhibit SVCV replication by blocking autophagy through the interaction with cell membrane cholesterol. Autophagy. **Enviado.*

La revista pertenece al primer cuartil en el área *Cell biology* y posee un índice de impacto de 11,1.

- Bello-Perez M, Falco A, Galiano V, Coll J, Perez L, Encinar JA. Discovery of nonnucleoside inhibitors of polymerase from infectious pancreatic necrosis virus (IPNV). *Drug Des Devel Ther*. 2018;12:2337-59. doi: 10.2147/DDDT.S171087. PubMed PMID: 30104863; PubMed Central PMCID: PMC6072831.

La revista pertenece al segundo cuartil en las áreas *Chemistry, medicinal y Pharmacology & pharmacy* y posee un índice de impacto de 2,935.

- Bello-Perez M, Medina-Gali R, Coll J, Perez L. Viral interference between infectious pancreatic necrosis virus and spring viremia of carp virus in zebrafish. Aquaculture. 2019;500:370-7.

La revista pertenece al primer cuartil en las áreas *Fisheries* y *Marine & Freshwater biology* y posee un índice de impacto de 2,710.

Por ello, DA SU CONFORMIDAD para la defensa por compendio de publicaciones de la Tesis doctoral “Descubrimiento y caracterización de la actividad antiviral inducida por las moléculas tipo CRP de pez cebra (*Danio rerio*)”.

Y para que así conste al efecto de certificar la presencia de indicios de calidad
firmo la presente.

Fdo.

En Elche, a de de 2019.

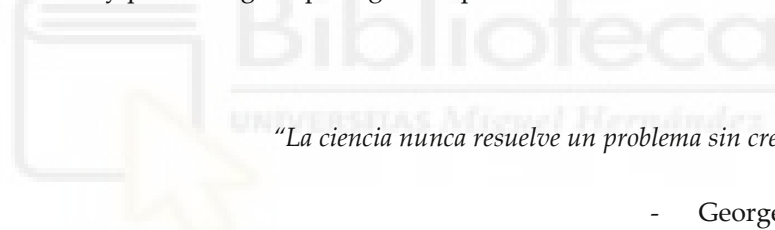
AGRADECIMIENTOS

Me gustaría agradecer al Dr. Alberto Falcó y al Dr. Luis Pérez el apoyo y guía que me han ofrecido a lo largo de esta etapa. Asimismo, esta tesis no hubiese sido posible sin la preocupación y la predisposición a ayudarme de los doctores Julio Coll y Beatriz Novoa y de todo su equipo, en especial el Dr. Antonio Figueras, la Dra. Patricia Pereiro y Paula Pérez.

Gracias al Dr. José Antonio Encinar por sus consejos y discusiones científicas, al Dr. José Manuel González Ros por ayudarme a agilizar todo este proceso, al Dr. José Luis Neira por amenizarme los fines de semana de trabajo y, por supuesto, a los doctores Ricardo Mallavia y Amparo Estepa por confiar en mí y convencerme de que esto merecería la pena.

Gracias a mis compañeros por hacerme más fuerte, a mis amigos y a mi familia porque de principio a fin he sentido que estabais orgullosos de que hiciese esto. Gracias a Diego Sanz, porque además me ha ayudado en el diseño de las ilustraciones.

Y como no, gracias a la ciencia, por enamorarme cada día un poco más, por los retos a los que me somete y por conseguir que algo me apasione tanto.



"La ciencia nunca resuelve un problema sin crear otros 10 más"

- George Bernard Shaw

ÍNDICE

ABREVIATURAS	1
RESUMEN	5
ABSTRACT	6
INTRODUCCIÓN	9
1. EL SISTEMA INMUNE: CONSIDERACIONES GENERALES	9
1.1. El sistema inmune	9
1.2. La inmunidad innata y adaptativa	9
2. NUEVOS CONCEPTOS DEL SISTEMA INMUNE	11
3. INTEGRACIÓN DE RESPUESTAS DEL SISTEMA INMUNE	13
3.1. Quimiotaxis	13
3.2. Autofagia	14
3.3. Las pentraxinas	16
4. EVOLUCIÓN DEL SISTEMA INMUNE	17
5. LAS PENTRAXINAS	20
5.1. Consideraciones generales	20
5.2. La proteína C-reactiva (CRP)	22
5.3. Actividad antimicrobiana de las CRPs	23
5.4. Evolución de las CRPs	24
5.5. Potencial actividad antiviral de las pentraxinas	27
OBJETIVOS, ANTECEDENTES Y SISTEMA MODELO	31
1. El pez cebra como sistema modelo para el estudio de las pentraxinas cortas	32
2. Los rabdovirus de peces: SVCV y VHSV	34
MATERIAL Y MÉTODOS	39
1. ANIMALES DE ESTUDIO	39
2. LÍNEAS CELULARES	39
3. VIRUS	40
4. CONSTRUCCIÓN DE PLÁSMIDOS QUE CODIFICAN <i>zfcrp1-7</i>	40

5. TRANSFECCIÓN DE CÉLULAS CON pMCV1.4-zfcrp1-7 Y PRODUCCIÓN DE SOBRENADANTES ENRIQUECIDOS.....	40
6. PRODUCCIÓN DE CRPs RECOMBINANTES.....	41
7. PRODUCCIÓN DE ANTICUERPOS EN CONEJO PARA RECONOCER LAS ISOFORMAS DE zfCRP1-7.....	42
8. CARACTERIZACIÓN DE LOS ssCRPs.....	42
8.1. <i>Western blot</i>	42
8.2. <i>Dot-blot</i>	43
9. INFECCIONES DE PECES CEBRA ADULTOS Y RECOLECCIÓN DE ÓRGANOS Y PLASMA SANGUÍNEO.....	43
9.1. Infecciones <i>in vivo</i>	43
9.2. Recolección de órganos de peces cebra adultos.....	43
9.3. Recolección de sangre de peces cebra adultos.....	44
10. EXTRACCIÓN DE ARN, RT y qPCR.....	44
11. MICROMATRICES.....	45
12. ANÁLISIS PROTEÓMICO DE LAS zfCRPs INDUCIDAS POR LA INFECCIÓN CON SVCV EN EL PLASMA DE PECES CEBRA.....	45
13. ESTUDIO DEL EFECTO DE LAS zfCRPs EN LA INFECCIÓN DE SVCV.....	46
13.1. Ensayos de neutralización <i>in vitro</i>	46
13.2. Ensayos de neutralización <i>in vivo</i>	46
13.3. Ensayos de neutralización con ssCRPs empobrecidos (deplet-ssCRPs).....	47
13.4. Ensayos de neutralización con LPS	47
14. ENSAYOS DE ACTIVIDAD ANTIVIRAL DE LAS zfCRPs.....	47
14.1. Ensayos para determinar la inhibición de la unión del virus a la célula.....	48
14.2. Ensayos de fusión mediada por la proteína G de SVCV.....	48
14.3. Actividad de los sobrenadantes condicionados por el tratamiento con ssCRPs	49
14.4. Determinación de los niveles de replicación de SVCV <i>in vitro</i> en etapas tempranas después de la adsorción.....	49
14.5. Análisis de la capacidad de los ssCRPs para inducir el sistema de interferón.....	49
15. EVALUACIÓN DEL PAPEL DE LA IL6 EN LA INDUCCIÓN DE <i>zfcrps</i>	49
16. PREDICCIONES <i>IN SILICO</i>	50

16.1. Estructuras tridimensionales de las zfCRPs.....	50
16.2. Energías libres de unión de las zfCRPs a lípidos de membrana.....	50
17. ESTUDIO DE LA UNIÓN DE zfCRPs A LÍPIDOS.....	50
17.1. Unión en fase sólida.....	50
17.2. Análisis de secuencias de péptidos superpuestas (Pepscan).....	51
18. EVALUACIÓN DEL EFECTO DE LA METIL- β -CICLODEXTRINA (M β CD) Y EL COLESTEROL (CH) SOBRE LA INFECCIÓN DE SVCV.....	51
19. ANÁLISIS DEL EFECTO DEL 25-HOC SOBRE LA ACTIVIDAD ANTIVIRAL DE LAS zfCRPs.....	52
20. ENSAYOS PARA LA DETERMINACIÓN DEL PAPEL DE LAS zfCRPs, 25-HOC, M β CD Y CH SOBRE LA AUTOFAGIA.....	52
20.1. Inmunofluorescencias.....	52
20.2. Determinación de autofagosomas intracelulares.....	53
20.3. Ensayos <i>in vivo</i>	53
20.4. Ensayos funcionales <i>in vitro</i>	54
21. ANÁLISIS ESTADÍSTICO.....	54
RESULTADOS.....	57
1. DESCRIPCIÓN DE LOS NIVELES DE EXPRESIÓN DE LAS <i>zfcrps</i> TRAS DIFERENTES ESTÍMULOS.....	57
2. EVALUACIÓN DE LA ACTIVIDAD ANTIVIRAL DE LAS zfCRPs.....	59
2.1. Caracterización de los sobrenadantes enriquecidos con zfCRPs (ssCRPs).....	59
2.2. Actividad antiviral de las zfCRPs.....	61
3. ANÁLISIS DE LA AFINIDAD DE LAS zfCRPs A LÍPIDOS.....	63
4. DETERMINACIÓN DEL MECANISMO ANTIVIRAL DE LAS zfCRPs.....	65
5. IMPLICACIÓN DEL COLESTEROL EN LA ACCIÓN ANTIVIRAL DE LAS zfCRPs.....	69
DISCUSIÓN.....	73
1. REGULACIÓN DE LA EXPRESIÓN GÉNICA DE LAS PENTRAXINAS CORTAS DE PEZES ANTE DIFERENTES ESTÍMULOS.....	73
2. ACTIVIDAD ANTIVIRAL DE LAS zfCRPs.....	76
3. RECONOCIMIENTO DE LIGANDOS POR LAS zfCRPs.....	78

4. EVALUACIÓN DE LA CAPACIDAD BLOQUEADORA DE LA ENTRADA DEL VIRUS.....	79
5. REGULACIÓN DE MECANISMOS CON ACCIÓN ANTIVIRAL.....	79
5.1. Sistema de interferón.....	79
5.2. La regulación de la autofagia como mecanismo de defensa antiviral.....	80
6. INFLUENCIA DE LOS LÍPIDOS EN LA ACTIVIDAD ANTIVIRAL DE LAS zfCRPs.....	82
CONCLUSIONES.....	87
BIBLIOGRAFÍA.....	89
COMPENDIO DE PUBLICACIONES.....	109
Publicación 1.....	111
Publicación 2.....	133
Publicación 3.....	171
Publicación 4 (enviada).....	197
ANEXO 1.....	243
ANEXO 2.....	247

ABREVIATURAS

En la siguiente lista, para cada sigla se proporciona el término del que procede en inglés y su correspondiente en castellano. En el caso de siglas comúnmente utilizadas en castellano como ADN y ARN, se obviará el término en inglés. Asimismo, sólo se incluye el término en inglés en aquellas siglas en las que el vocablo al que se hace referencia nunca se utiliza en castellano. Respecto a las abreviaturas de especies, se citan tanto su nombre científico como su nombre común en castellano.

Aa: aminoácido	CyHV-3: <i>Cyprinid herpesvirus 3</i> , herpesvirus de los ciprínidos 3.
ADN: ácido desoxirribonucleico	DAPI: 4,6-diamidino-2-fenilindol
ADNc: ADN complementario	DCs: <i>dendritic cells</i> , células dendríticas
Af: <i>Achatina fulica</i> , caracol gigante africano	DMSO: dimetilsulfóxido
AMPs: <i>antimicrobial peptides</i> , péptidos antimicrobianos	dpf: días post-fertilización
AP: <i>alternative pathway</i> , vía alternativa del sistema de complemento	EPC: células de <i>Epithelioma papulosum cyprini</i>
APC: <i>antigen presenting cell</i> , célula presentadora de antígenos	FBS: <i>fetal bovine serum</i> , suero fetal bovino
APP: <i>acute phase protein</i> , proteína de fase aguda	FcR: <i>Fc receptor</i> , receptor transmembrana de inmunoglobulinas
ARN: ácido ribonucleico	ffu: <i>foci forming units</i> , unidades formadoras de focos
ARNm: ARN mensajero	ΔG: energía libre de Gibbs/de unión
ATG16L1: <i>autophagy related 16 like 1 complex</i>	G: <i>glycoprotein</i> , glicoproteína de membrana de los rhabdovirus
BCA: <i>bicinchoninic acid assay</i> , ensayo de ácido bicinchonínico	GFP: <i>green fluorescence protein</i> , proteína verde fluorescente
Cc: <i>Cyprinus carpio</i> , carpa común	GlcNAc: <i>N-acetylglucosamine</i> , N-acetilglucosamina
Ch: colesterol	7β-HOC: 7β-hidroxcolesterol
CP: <i>classical pathway</i> , vía clásica del sistema de complemento	25-HOC: 25-hidroxcolesterol
CQ: cloroquina	27-HOC: 27-hidroxcolesterol
CRP: <i>C-reactive protein</i> , proteína C-reactiva	24S-HOC: 24S-hidroxcolesterol
Cs: <i>Cynoglossus semilaevis</i> , perteneciente al género lengua	hCRP: proteína C-reactiva humana
	HIV: <i>human immunodeficiency virus</i> , virus de la inmunodeficiencia humana

H3K4me3: trimetilación de la histona 3 en la lisina 4	MHC: <i>major histocompatibility complex</i> , complejo mayor de histocompatibilidad
IFN: interferón	MOI: <i>multiplicity of infection</i> , multiplicidad de infección
Igs: inmunoglobulinas	N: <i>nucleoprotein</i> , nucleocápsida de rabdovirus
IL1β: interleuquina 1 beta	NAC: N-acetilcisteína
IL4: interleuquina 4	NF-κB: <i>nuclear factor kappa-light-chain-enhancer of activated B cells</i> , factor nuclear potenciador de las cadenas ligeras kappa de las células B activadas
IL6: interleuquina 6	NK: <i>natural killer</i> , linfocito natural citolítico
IL13: interleuquina 13	NO: <i>nitric oxide</i> , óxido nítrico
IL18: interleuquina 18	NOS: <i>reactive nitrogen species</i> , especies reactivas de nitrógeno
IFN-γ: interferón gamma	Nv: <i>nonvirion protein</i>
ISG: <i>interferon-stimulated gene</i> , gen estimulado por interferón	OIE: Oficina Internacional de Epizooatis
i.p.: intraperitoneal	P: <i>phosphoprotein</i> , fosfoproteína de los rabdovirus
7KC: 7-ketcolesterol	PAMPs: <i>pathogen-associated molecular patterns</i> , patrones moleculares asociados a patógenos
L: <i>polymerase</i> , ARN polimerasa ARN dependiente de rabdovirus	PBMC: células mononucleares de sangre periférica
LB: Luria Bertani	PC: <i>phosphatidylcholine</i> , fosfatidilcolina
LC3: <i>microtubule-associated protein light chain 3</i>	PCR: <i>polymerase chain reaction</i> , reacción en cadena de la polimerasa
LD: <i>lipid droplets</i> , gotas de lípidos	pCRP: proteína C-reactiva pentamérica
LP: <i>lectin pathway</i> , vía de la lectina del sistema de complemento	PE: <i>phosphatidylethanolamine</i> , fosfatidiletanolamina
Lp: <i>Limulus polyphemus</i> , cangrejo herradura del Atlántico	Pfu: <i>plaque forming units</i> , unidades formadoras de placas
LPS: lipopolisacárido	PI: punto isoeléctrico
3-MA: 3-metiladenina	PI3KC3: <i>the class III phosphatidylinositol 3-kinase complex</i>
M: <i>matrix protein</i> , proteína de la matriz de los rabdovirus	
MAC: <i>membrane attack complex</i> , complejo de ataque de membrana	
MALT: <i>mucosa-associated lymphoid tissue</i> , tejido linfoide asociado a mucosas	
MβCD: metil-β-ciclodextrina	
mCRP: proteína C-reactiva monomérica	

PI3P: <i>phosphatidylinositol 3-phosphate</i> , fosfatidilinositol 3-fosfato	ssCRP: sobrenadante enriquecido con CRP
PRRs: <i>pattern recognition receptors</i> , receptores de reconocimiento de patrones	ssGFP: sobrenadante enriquecido con GFP
PTMs: modificaciones post-taduccionales	SVCV: <i>spring viremia of carp virus</i> , virus de la viremia primaveral de la carpa
PTX3: <i>pentraxin 3</i> , pentraxina 3	TCR: <i>t-cell receptor</i> , receptores de linfocitos T
Rb: <i>Oplegnathus fasciatus</i> , pez pico rayado	TLRs: <i>toll-like receptors</i> , receptores tipo toll
rCRP: proteína C-reactiva recombinante producida en insecto	TLR7: <i>toll-like receptor 7</i> , receptor tipo toll 7
Rf: <i>Sebastes schlegelii</i> , pez roca coreano	TNF-α: <i>tumor necrosis factor alpha</i> , factor de necrosis tumoral alfa
ROS: <i>reactive oxygen species</i> , especies reactivas de oxígeno	ULK1: <i>Unc-51 like autophagy activating kinase 1 complex</i>
RSIV: <i>red sea bream iridovirus</i> , iridovirus de la dorada japonesa.	VHSV: <i>viral hemorrhagic septicemia virus</i> , virus de la septicemia hemorrágica vírica
SAA: <i>serum amyloid A</i> , proteína de suero amiloide A	VLR: <i>variable lymphocyte receptor B</i>
SAP: <i>serum amyloid protein</i> , proteína amiloide del suero	VSV: <i>vesicular stomatitis virus</i> , virus de la estomatitis vesicular
s.d: <i>standard deviation</i> , desviación estándar	zfCRP: CRP de pez cebra
SDS-PAGE: electroforesis en gel de poliacrilamida con dodecilsulfato sódico	ZF4: <i>zebrafish embrionic fibroblast</i> , fibroblastos embrionicos de pez cebra
Ss: <i>Salmo salar</i> , salmón común	

RESUMEN

La proteína C-reactiva (CRP) es una pentraxina corta cuyos niveles séricos en mamíferos aumentan en presencia de estímulos desencadenantes de la respuesta de fase aguda y, por tanto, es ampliamente utilizada en clínica como biomarcador de inflamación. Clásicamente, la CRP ha sido descrita como una molécula de reconocimiento de patrones bacterianos y de células dañadas que actúa como primera línea de defensa del huésped. El presente trabajo aporta evidencias sobre una nueva función de esta molécula que se añade a su ya extensa lista de actividades descritas.

En esta tesis se ha demostrado, *in vitro* e *in vivo*, la actividad protectora de las CRPs de pez cebra (zfCRP1-7) frente al virus de la viremia primaveral de la carpa (SVCV). Asimismo, se ha descubierto que existe una alta afinidad de las zfCRPs por los colesteroles, mostrando una unión preferencial por el 25-hidroxicolesterol (25-HOC), un lípido cuya actividad anti-SVCV ha sido descrita previamente y que muestra efectos sumatorios con la protección ofrecida por las zfCRPs. La exploración de los posibles mecanismos responsables de la protección antiviral conferida por las zfCRPs descartó la interferencia de estas moléculas con el proceso de entrada (unión al receptor y fusión) del virus, sugiriendo la regulación de algún mecanismo antiviral en la célula. También se ha descartado que esta actividad antiviral sea mediada por el sistema de interferón, el cual incluso se reprime tras el tratamiento de las células con zfCRPs. De acuerdo con nuestros resultados, las zfCRPs bloquean la autofagia o la vía endocítica del virus, dos procesos que convergen en el ciclo de replicación de otros virus. Por tanto, en este estudio se propone que la inhibición de la infectividad de SVCV se produce como consecuencia del bloqueo de la fusión de los endosomas/autofagosomas que contienen SVCV con el lisosoma. Este bloqueo evita la acidificación requerida para la actividad fusogénica de la proteína G vírica y, por tanto, impide la liberación del virus al citoplasma y su replicación. Este efecto también se observó tras el tratamiento de las células con 25-HOC o metil- β -ciclodextrina (secuestrador de colesterol) previo a la infección con SVCV, sugiriendo la alteración de los niveles de colesterol celulares como causa de la actividad antiviral. La desregulación de estos niveles parece estimular la producción de especies reactivas de oxígeno, lo que llevaría a la inhibición de la fusión autofagosoma-lisosoma.

ABSTRACT

C-reactive protein (CRP) is a short pentraxin whose serum levels in mammals increase in the presence of stimuli that trigger the acute phase response and, therefore, it is widely used in clinic as an inflammation biomarker. CRP has been classically described as a molecule of recognition of bacterial patterns and damaged cells that acts as the first line of defence of the host. The present work provides evidence of a novel function of this molecule expanding its already wide range of biological activities.

Our work demonstrates *in vitro* and *in vivo* the protective activity of zebrafish's C-reactive proteins (zfCRPs) on the infection of the spring viremia of carp virus (SVCV). Likewise, a high affinity of zfCRPs for cholesterol was found, showing a preferential binding by 25-hydroxycholesterol (25-HOC), a lipid whose anti-SVCV activity has been previously described, showing additive antiviral effects over the protection conferred by the zfCRPs. The exploration of the possible mechanisms responsible for the zfCRPs antiviral activity ruled out the interference of these molecules with the process of viral entry (binding and fusion), suggesting the regulation of some antiviral mechanism in the cell. We could not find a relationship of the CRP antiviral activity with the stimulation of interferon system, which appears to be repressed after the treatment of the cells with zfCRPs. According to our results, zfCRPs block autophagy or the endocytic pathway of the virus, two processes that converge in the replication cycle of other viruses. Therefore, this study proposed that the inhibition of SVCV infectivity is consequence of blocking the fusion of the endosomes/autophagosomes containing SVCV with the lysosome. This blocking prevents the acidification required for the fusogenic activity of the viral G protein and, consequently prevents the release of the virus to the cytoplasm and its replication. This effect was also observed after treatment of the cells with 25-HOC or methyl- β -cyclodextrin (a cholesterol depleting agent) prior to infection with SVCV, suggesting the involvement of cellular cholesterol levels in antiviral activity. Deregulation of membrane cholesterol seems to stimulate the production of reactive oxygen species, which has an inhibitory effect of the autophagosome-lysosome fusion.

Introducción

Obj., ant., s. modelo Mat. y métodos Resultados Discusión Conclusiones Bibliografía Publicaciones Anexos

INTRODUCCIÓN

INTRODUCCIÓN

1. EL SISTEMA INMUNE: CONSIDERACIONES GENERALES

1.1. El sistema inmune

Los seres vivos están constantemente amenazados por un gran número de patógenos: virus, bacterias, hongos y parásitos. Sin embargo, en condiciones normales los individuos presentan un estado saludable. Esta capacidad de resistencia es conferida por el **sistema inmune**. Principalmente éste diferencia las células propias, o aquellas exógenas pero inocuas, de los organismos invasores. De esta manera, garantiza la integridad del cuerpo frente a los intrusos mediante una serie de órganos, células y moléculas solubles [1, 2]. No obstante, no siempre es así en individuos inmunocompetentes y el organismo no es capaz de eliminar el agente patógeno [3, 4].

Los avances en inmunología han permitido aumentar el conocimiento de algunas enfermedades y desarrollar/mejorar estrategias terapéuticas como las vacunas [5, 6], los adyuvantes [7, 8], los anticuerpos terapéuticos [9, 10] y los inmunomoduladores [11]. Se han creado vacunas exitosas contra numerosos microorganismos patógenos responsables de enfermedades como la viruela, la poliomelitis, la difteria y el tétanos. Sin embargo, la amenaza que representan las enfermedades infecciosas no ha desaparecido. Por ejemplo los virus de la inmunodeficiencia humana (HIV) [12], el dengue [13] y la malaria [14] causan miles de muertes anuales en la población humana.

Este panorama, al que se le suman las alergias, el cáncer, las enfermedades autoinmunes y los rechazos de trasplantes, convierte la búsqueda de nuevas estrategias para combatir situaciones patológicas en uno de los principales retos de la inmunología actual. Es por ello que una mayor comprensión del sistema inmune es incuestionablemente necesaria para abordar estos problemas.

1.2. La inmunidad innata y adaptativa

Clásicamente, el sistema inmune de los vertebrados se diferenciaba en dos ramas: el sistema inmune innato y el sistema inmune adaptativo. Sin embargo, es tal la integración de estos sistemas que actualmente esta clasificación se considera exclusivamente didáctica [15, 16].

INTRODUCCIÓN

El **sistema inmune innato** es la primera línea de defensa frente a la agresión de patógenos y está presente evolutivamente desde los organismos invertebrados [17]. Este sistema está activo desde el origen de cada individuo y no requiere un reconocimiento o exposición previo del/al patógeno, sino que responde “inespecíficamente” desde su entrada **a) mediante barreras naturales:** la piel, las mucosas y el tracto gastrointestinal [2, 18] y **b)** a través de la inflamación [19, 20].

Cuando un patógeno invade a otro organismo, se inicia rápidamente una respuesta inflamatoria que incluye elementos celulares y humorales. Esta respuesta empieza tras el reconocimiento de estructuras moleculares, denominadas patrones moleculares asociados a patógenos (PAMPs), que son identificados por receptores de reconocimiento de patrones (PRRs) [21] presentes en la mayoría de células [22]. La identificación de los PAMPs estimula la expresión y liberación de citoquinas, aminas biogénicas y prostaglandinas que inducen un estado de “alerta” en las células del individuo [19, 23]. Las quimioquinas y algunas moléculas del sistema de complemento producidas en respuesta al patógeno, junto con cambios vasculares [24], contribuyen a la atracción de leucocitos circulantes hacia los tejidos dañados [19]. Para eliminar los patógenos y las células dañadas/infectadas, las citoquinas también pueden inducir las proteínas de fase aguda (lectinas, pentraxinas, moléculas del sistema de complemento, etc.) y, los leucocitos, moléculas efectoras como especies reactivas de oxígeno y nitrógeno, ROS y NOS y péptidos antimicrobianos [25].

Si bien generalmente el sistema inmune innato es capaz de neutralizar las amenazas, en otras no consigue dar una solución definitiva. Aun así su función es esencial ya que ralentiza la infección y contribuye a la activación del **sistema inmune adaptativo**. En el sistema inmune adaptativo de mamíferos, las células dendríticas o los macrófagos capturan al patógeno transformándose en células presentadoras de antígenos (APC) que, posteriormente, migrarán hasta los nódulos linfáticos profesionales. Allí presentarán, a través de las moléculas del complejo mayor de histocompatibilidad (MHC), antígenos derivados del procesamiento de los patógenos fagocitados a las células T *naïve*, que se activarán y diferenciarán en células efectoras [26, 27].

La especificidad de la respuesta inmune adaptativa y su capacidad de establecer una memoria específica y de larga duración de cada encuentro con un patógeno ha clasificado, tradicionalmente, las respuestas inmunes en innatas o adaptativas [16, 28]. No obstante, la inmunidad adaptativa aparece en la evolución por primera vez en los peces, en la divergencia entre los ciclostomos (peces sin mandíbula) y los peces cartilaginosos (ya con mandíbula) hace aproximadamente 450 millones de años [29]. Por lo tanto, es difícil concebir

que la memoria inmunológica sea exclusiva de tan sólo un 1% del total de los seres vivos, los vertebrados [30], o que el sistema inmune innato no posea algún tipo de mecanismo que le confiera “memoria” en cierto grado.

2. NUEVOS CONCEPTOS DEL SISTEMA INMUNE

El dogma de la inmunología contemporánea afirma que sólo los vertebrados poseen memoria inmunológica, la cual se caracteriza por ser específica y estar vinculada al sistema inmune adaptativo. Sin embargo, esta afirmación es incapaz de explicar resultados que demuestran una defensa mejorada en huéspedes carentes de sistema inmune adaptativo cuando se producen re-infecciones con el mismo patógeno u otro diferente [30-32]. Esta respuesta inmune innata mejorada recibe el nombre de **inmunidad entrenada** (*trained immunity*, en inglés) y su aparición ha revolucionado el campo de la inmunología, ya que extiende el concepto de memoria inmunológica en tres aspectos: taxonómico, celular y temporal [33]. Así, actualmente la memoria inmunológica abarca fenómenos: a) con duraciones muy diversas (desde pocos días en invertebrados hasta toda la vida en el caso de mamíferos), b) que se dan incluso en invertebrados, plantas, bacterias y arqueas y c) que no se limita a los linfocitos, sino que también se producen en otras células como los linfocitos citolíticos naturales (NK), los macrófagos y los monocitos [15, 30-38].

El entrenamiento de las células de la inmunidad innata para que adquieran memoria inmunológica parece ser consecuencia de la adquisición de marcas epigenéticas en el ADN y en las histonas que modulan la activación de la transcripción de genes del sistema inmune [39, 40]. Una de las modificaciones de histonas más extendidas es la trimetilación de la histona 3 en la lisina 4 (H3K4me3), que está asociada con una configuración abierta de la cromatina y, por tanto, con un estado transcripcional activo [41-43]. Esto explicaría una mejora de la defensa innata (en términos de rapidez y magnitud) como consecuencia de una mejor accesibilidad de los factores de transcripción a los promotores de genes implicados en la respuesta inmune [30].

Estos descubrimientos sugieren la posibilidad de nuevas estrategias de vacunación mediante la potenciación de la inmunidad entrenada que permitiría desarrollar vacunas que: a) funcionasen en organismos invertebrados y plantas, b) fueran eficaces en pacientes inmunodeprimidos [31] y, c) sobre todo, que modulasen la resistencia general del huésped. Además, estas nuevas vacunas, al ser efectivas contra un amplio espectro de patógenos al

INTRODUCCIÓN

mismo tiempo [44], reducirían los gastos asociados a investigación, desarrollo, producción e implementación que supone la generación de vacunas específicas.

No obstante, el campo de investigación sobre la inmunidad entrenada acaba de nacer y, por tanto, ciertas cuestiones todavía no tienen respuesta. En este sentido, un claro ejemplo es el desconocimiento sobre la duración de la protección ofrecida por la inmunidad entrenada [45].

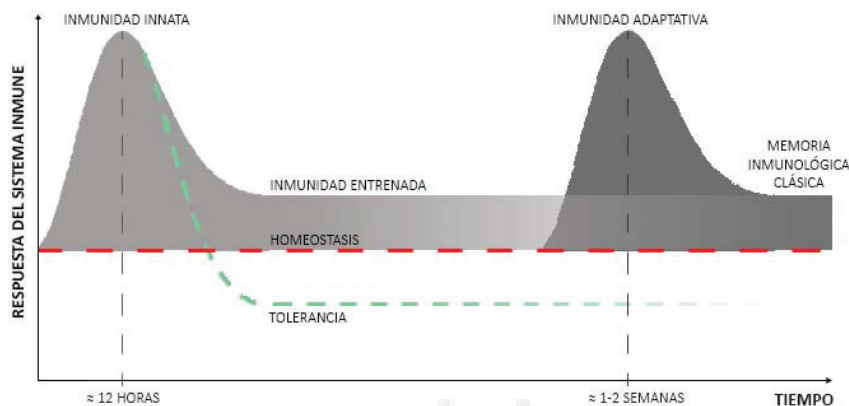


Figura 1. Representación gráfica de las respuestas coordinadas que ofrece el sistema inmune para proteger al organismo frente a un encuentro con un patógeno. Las zonas sombreadas en gris representan la zona de protección. Esta figura ha sido diseñada a partir de [46].

Que el sistema inmune innato carece de memoria no es el único concepto en inmunología que ha quedado obsoleto. La separación clásica entre respuesta inmune innata y adaptativa es otro. Actualmente sabemos que esta separación es artificial, pues en realidad la protección que ofrece el sistema inmune está formada por diferentes respuestas coordinadas temporalmente según las necesidades del huésped para enfrentarse al patógeno. Tras el encuentro con un patógeno, se desencadena una respuesta inmune innata que regresa a sus niveles basales una vez neutralizada la infección. Sin embargo, esto no es siempre así, pudiendo suceder dos fenómenos opuestos: que la respuesta quede inhibida (tolerancia) o, por el contrario, aumentada, de manera que frente a un segundo encuentro con un patógeno se produjese más rápido de lo normal (inmunidad entrenada) [46]. Esta primera reacción del sistema inmune, que aparece durante las primeras 12 horas, también alerta a otras células más especializadas sobre la invasión, lo que permite el reclutamiento y activación de los linfocitos. Esta última respuesta no decae totalmente con el tiempo debido a la formación de poblaciones linfocitarias de memoria que, en un futuro, mediarán una

respuesta específica más rápida si el organismo es invadido por el mismo patógeno [47] (**Figura 1**).

3. INTEGRACIÓN DE RESPUESTAS DEL SISTEMA INMUNE

Como se ha descrito previamente, establecer una línea que separe la respuesta inmune innata de la adaptativa es difícil ya que, por ejemplo existen células, moléculas y procesos que conectan y/o participan en ambos sistemas. Por tanto, el sistema inmune consiste en realidad en una sucesión temporal y coordinada de respuestas relacionadas íntimamente.

3.1. Quimiotaxis

Para que la comunicación entre elementos del sistema inmune tenga lugar, es esencial la migración de las APCs a los órganos linfoides secundarios, donde se realiza la presentación de antígenos a los linfocitos T [48]. Esta migración ocurre porque los receptores presentes en las membranas de las APCs reconocen quimioquinas que transmiten un mensaje de desplazamiento [49, 50]. Este mensaje permite que las APCs se acoplen al endotelio de los vasos sanguíneos donde sufren un cambio morfológico que les permite cruzarlo [51].

Los quimioatractantes no están únicamente involucrados en la migración de las APCs, sino que también regulan el tráfico de células del sistema inmune innato como los granulocitos (neutrófilos, eosinófilos y basófilos), los macrófagos y los mastocitos [52]. En esta línea, algunos componentes del sistema de complemento, como veremos a continuación, también funcionan como quimioatractantes, contribuyendo a la rápida movilización de leucocitos al sitio de lesión [53].

El sistema de complemento de los vertebrados está formado por aproximadamente 35 proteínas que se encuentran en el plasma sanguíneo [54]. Cuando se produce una infección, los factores del complemento se dirigen hacia los tejidos diana donde pueden realizar tres funciones: **a)** quimiotaxis de leucocitos al sitio de infección, **b)** opsonización del patógeno favoreciendo así la fagocitosis o **c)** formación de poros en las membranas de las bacterias [55]. Asimismo, la activación del sistema de complemento puede llevarse a cabo a través de tres vías: la clásica (CP), la alternativa (AP) y la de lectina (LP). No obstante, en la mayoría de los casos, todas ellas comparten un objetivo final común: la formación del

INTRODUCCIÓN

complejo de ataque de membrana, el cual forma poros en las bicapas de fosfolípidos de las células diana [56].

Pese a que cada vía de activación del sistema de complemento se inicia de una manera distinta e implica moléculas diferentes, en todas ellas intervienen dos moléculas llamadas convertasa de C3 y convertasa de C5 encargadas de escindir las moléculas C3 y C5, respectivamente en C3a y C3b, y C5a y C5b. Cada una de estas moléculas resultantes tiene una función diferente entre las que destacamos C3a y C5a que funcionan como quimiotrayentes de leucocitos al tejido diana [55, 56].

3.2. Autofagia

Otra prueba de la gran integración de las respuestas del sistema inmune es que existen procesos tales como la autofagia, que participan tanto en las respuestas innatas como en las adaptativas. El término autofagia hace referencia a un mecanismo evolutivamente conservado en eucariotas en el que los componentes citoplasmáticos innecesarios (como orgánulos dañados o proteínas desnaturalizadas) son engullidos por una vesícula de doble membrana: autofagosoma. Posteriormente, el autofagosoma se fusiona con un lisosoma para formar el autolisosoma cuyo contenido se degrada y se recicla [57-60]. Este proceso, en el que se diferencian básicamente dos etapas, **a)** la inducción del autofagosoma y **b)** la fusión del autofagosoma con el lisosoma, implica una multitud de moléculas que forman tres complejos principales: ULK1, PI3KC3 y ATG16L1 [60, 61] (**Tabla 1**).

Tabla 1. Complejos de moléculas implicados en la formación del autofagosoma

Complejos	Moléculas integrantes del complejo
ULK1	ULK1/2, FIP200, ATG13 y ATG101
PI3KC3	BECLIN-1, VPS24, VPS15 y ATG14L
ATG16L1	ATG16L1, ATG5 y ATG12

Para mantener la homeostasis celular se requieren unos niveles basales de autofagia. No obstante, frente a una diversa variedad de situaciones de estrés, entre ellas las infecciones, las células incrementan la actividad de este proceso. La autofagia se inicia porque el complejo ULK1 activa el complejo PI3KC3 que crea subdominios ricos en PI3P en regiones de dobles membranas, llamadas fagoforos, que proceden del retículo endoplasmático y de las mitocondrias asociadas a las membranas del retículo. A

continuación, el complejo ATG16L1 es reclutado por las proteínas de unión a PI3P al fagoforo, donde anclará la molécula LC3 mediante su conjugación con fosfatidiletanolamina (PE). La unión LC3-PE media en la extensión del fagoforo a través del reclutamiento de membranas de múltiples fuentes. La autofusión de estas membranas crea una estructura cerrada de doble membrana: el autofagosoma, que envuelve el material que será degradado gracias a la fusión del mismo con el lisosoma [60-62] (**Figura 2**).

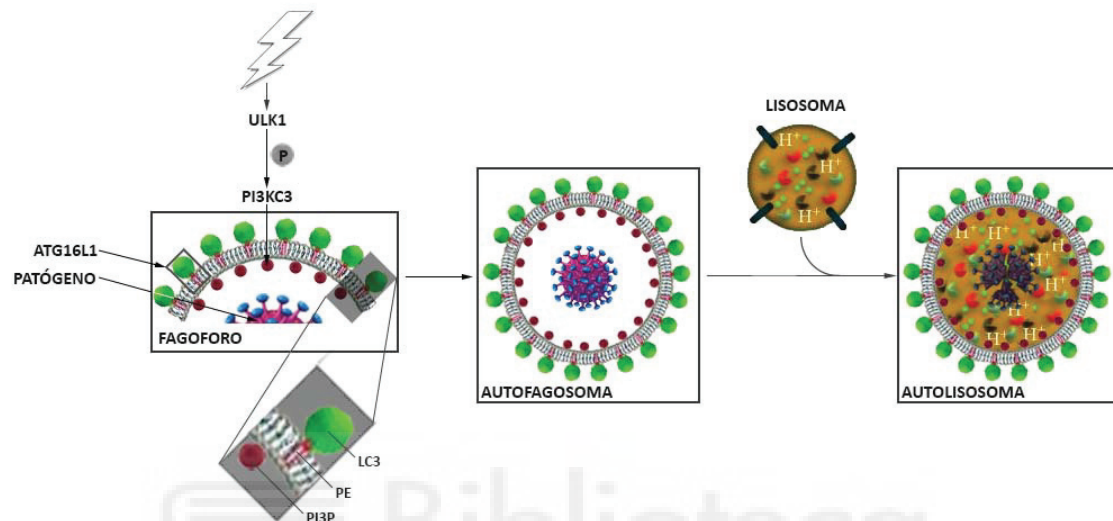


Figura 2. Representación gráfica de la activación de la autofagia con el fin de eliminar un patógeno.

Pese a que la autofagia fue inicialmente descrita como un proceso metabólico [63], recientemente se ha demostrado que no sólo proporciona una homeostasis celular básica, sino que también está involucrada en la inmunidad ya que: **a)** elimina directamente los patógenos [62, 64, 65], **b)** regula la producción de citoquinas y el proceso de inflamación [66], **c)** activa la señalización mediada por PRRs [59, 67] y **d)** participa en la presentación de antígenos [57-59].

Las investigaciones en el campo de la autofagia han revelado que las células utilizan una forma especializada de este proceso, conocida como xenofagia, para degradar patógenos intracelulares [65]. En este proceso cobra un papel importante la ubiquitinación, es decir, la marca que será reconocida por los adaptadores de autofagia que reclutan LC3 para introducir los patógenos en el autofagosoma [64].

Asimismo, se ha identificado una asociación entre la autofagia y la inflamación consistente en un circuito de retroalimentación negativa [68]. Esta regulación, en la que la secreción de ciertas citoquinas que estimulan la autofagia se ve inhibida por la misma, se interpreta como una estrategia para evitar respuestas exacerbadas, tales como las observadas en enfermedades como fibrosis quística, enfermedad pulmonar obstructiva crónica y

INTRODUCCIÓN

enfermedad de Crohn [57]. Las citoquinas proinflamatorias, como el factor de necrosis tumoral (TNF), la interleuquina 1 beta (IL1 β) y los interferones de tipo I y II, la inducen mejorando en algunos casos el control de la infección. A su vez, las anti-inflamatorias, como la interleuquina 4 (IL4) y la interleuquina 13 (IL13), la inhiben a través de la activación de mTOR (responsable de la inhibición del complejo ULK) [69]. Por otro lado, y relacionado con este aspecto, la autofagia también regula la activación del inflamasoma y viceversa. La existencia de esta regulación es lógica, pues una de las funciones del inflamasoma es promover la maduración de las citoquinas proinflamatorias IL1 β e IL18 que, como ya se ha comentado anteriormente, son reguladas negativamente por la autofagia [66].

Otro proceso relevante para la inmunidad que se encuentra regulado por la autofagia es el suministro de PAMPs citosólicos a los PRRs localizados en las membranas de los endosomas [70]. Por ejemplo, la autofagia trasloca los intermediarios de replicación del virus de la estomatitis vesicular (VSV) al TLR7 en células dendríticas (DCs), un PRR encargado del reconocimiento de ssARN. Sin embargo, la relación entre la autofagia y la señalización de PRR es más amplia que el suministro de PAMPs a PRRs endosómicos. Recientemente se ha demostrado que la estimulación de varios TLRs por sus ligandos activa la autofagia como un mecanismo de defensa capaz de eliminar los patógenos intracelulares de una manera directa [59, 67]. No obstante, como se comentará en la discusión de esta tesis, la autofagia no siempre funciona como un mecanismo de defensa frente a las infecciones, ya que, en ocasiones, la replicación de los virus es favorecida por la activación de este mecanismo [71].

Por otra parte, existen evidencias de que la autofagia participa en la presentación de antígenos. Los autofagosomas, que expresan MHC-II, son capaces de presentar antígenos a los linfocitos T CD4 $^{+}$ [57]. Esta presentación, que conlleva un retraso de la fusión del autofagosoma con el lisosoma, permite el montaje de una respuesta inmune adaptativa contra el antígeno secuestrado [58].

3.3. Las pentraxinas

Aunque el papel inmunológico de las pentraxinas será descrito ampliamente más adelante, cabe comentar en este apartado que las pentraxinas, caracterizadas como componentes humorales del sistema inmune innato, tienen características muy similares a los anticuerpos, hasta el punto de que han sido consideradas por algunos autores como anticuerpos ancestrales [72, 73]. Entre sus semejanzas con los anticuerpos naturales o pre-existentes, éstas: **a)** reconocen y opsonizan patógenos, **b)** activan el sistema de complemento

a través de la vía clásica [74, 75], **c)** aumentan sus niveles en sangre rápidamente en la respuesta de fase aguda, **d)** tienen afinidad por fosfolípidos como la fosfatidilcolina (PC) y la fosfaetanolamina (PE) y **e)** reconocen múltiples sitios de unión para aumentar las posibilidades de actividad frente a patógenos [20, 76].

No obstante, las pentraxinas y los anticuerpos no son moléculas redundantes: **a)** los anticuerpos reconocen a los patógenos específicamente a diferencia de las pentraxinas que lo hacen a través de PAPMs [77] y **b)** las pentraxinas se liberan generalmente más rápido y en mayor cantidad al torrente sanguíneo en respuesta a una infección [20], de ahí que algunas de ellas sean importantes proteínas de fase aguda (APPs) [76]. La importancia de las pentraxinas en nuestra especie se reafirma por el hecho de que no se conocen individuos deficientes en proteína C-reactiva (CRP) [78].

4. EVOLUCIÓN DEL SISTEMA INMUNE

La separación didáctica que se ha realizado entre sistema inmune innato y adaptativo se debe a que si bien todas las formas de vida poseen sistema inmune innato, el adaptativo aparece evolutivamente más tarde, como consecuencia de las innovaciones moleculares asociadas a los vertebrados. Así, con el origen de los peces aparecieron nuevos tipos celulares y tejidos inexistentes en los organismos invertebrados que fueron clasificados como parte del sistema inmune adaptativo [79, 80].

Ya los primeros gnatóstomos (vertebrados con mandíbula) presentan linfocitos y células dendríticas además de los llamados tejidos linfoideos, como por ejemplo el timo y el bazo [79]. En estos nuevos tipos celulares está activada la maquinaria necesaria para desencadenar la denominada respuesta del sistema inmune adaptativo. Entre los principales grupos moleculares involucrados en esta respuesta destacan: MHC, receptores de linfocitos T (TCR) e inmunoglobulinas (Igs) [80].

Existen dos tipos de MHC: MHC-I y MHC-II. Estas moléculas están implicadas en el reconocimiento y la presentación de antígenos. Cuando MHC-I interacciona con un antígeno, éste es procesado por las células que expresan MHC-I en su membrana (todas las células nucleadas) para su posterior presentación a los linfocitos T CD8⁺. Esta presentación, consecuencia de la interacción del complejo MHC-péptido con el receptor TCR presente en los linfocitos, será la responsable de la activación de éstos, encargados de destruir las células infectadas. Por el contrario, la presencia de MHC-II se encuentra restringida a las superficies

INTRODUCCIÓN

de las APCs, que tras el reconocimiento de un antígeno interaccionan con los receptores TCR de los linfocitos T CD4⁺. Esta interacción concluye con la activación y diferenciación de los linfocitos B, que producirán anticuerpos específicos frente al antígeno presentado, así como células B de memoria [81-84].

Las IgGs han supuesto una gran ventaja evolutiva en los cordados, pues presentan una enorme especificidad de reconocimiento de antígenos. Estas proteínas variables se expresan en las membranas de los linfocitos B a modo de receptores y son capaces de interaccionar con antígenos. La unión antígeno-Ig permite la conversión de los linfocitos B en células plasmáticas capaces de secretar IgGs solubles circulantes (anticuerpos). Los anticuerpos se diseminan por todo el organismo para reconocer epítopos específicos de patógenos y marcarlos para su posterior destrucción mediada por los fagocitos y el sistema de complemento [85-89].

Los primeros indicios de inmunidad adaptativa aparecen en las lampreas (vertebrados agnatos, sin mandíbula), que poseen homólogos a IgGs, denominados receptores VLR (*variable lymphocyte receptor B*, en inglés), capaces de reconocer antígenos y secretarse al medio ante una estimulación. Actualmente se conocen tres isoformas de VLR: VLRA, VLRB y VLRC. Remarcablemente, las células que expresan en su membrana la primera y la tercera isoforma también expresan genes específicos de linfocitos T, mientras que aquellas que expresan la segunda, inducen genes específicos de linfocitos B. Asimismo, en este organismo también están presentes los genes que codifican MHC-I y MHCII. Es decir, existe un sistema inmune adaptativo, aunque muy primitivo, anterior al presente en los vertebrados con mandíbula. Este sistema, sin embargo, no depende de la recombinación V(D)J a partir de la cual se generan los anticuerpos y los TCR [79, 90-92].

A pesar de la aparición del sistema inmune adaptativo en vertebrados, el innato no ha desaparecido y ambos conviven en estos organismos. De hecho, muchos elementos del sistema innato parecen ser críticos en la defensa frente a infecciones, ya que se han mantenido a lo largo de la evolución. Por ello, incluso en los invertebrados más primitivos encontramos ortólogos de **moléculas de reconocimiento de patógenos, moléculas efectoras** y **moléculas de señalización** presentes también en humanos. Aun así, en vertebrados se ha reducido la presión selectiva sobre estos elementos y, con ello, la abundancia de isoformas. Asimismo, otros de estos elementos han adaptado sus funciones para coordinar su actividad con la respuesta inmune adaptativa.

Muchos invertebrados poseen células con apariencia y función similar a la de macrófagos que, dependiendo de la especie, reciben un nombre diferente (amebocitos, hemocitos o coelomocitos) [25]. Estas células expresan PRRs, que son sistemas de reconocimiento muy sencillos que tienen como diana motivos conservados en diferentes grupos de patógenos. Aunque existen muchas familias de PRR, la más ampliamente estudiada es la formada por los receptores tipo toll (TLRs) [93]. Los TLRs son proteínas transmembrana cuyo dominio extracelular reconoce componentes específicos de hongos, virus, bacterias y protistas [93, 94]. Se conservan desde los invertebrados (esponjas, cnidarios, oligoquetos, moluscos, crustáceos e insectos) [25] y parecen tener especial trascendencia en los invertebrados marinos, ya que, mientras los gnatóstomos poseen alrededor de 10 TLRs, el repertorio en éstos se incrementa enormemente, habiéndose descrito hasta 253 TLRs distintos en el caso del erizo de mar púrpura (*Strongylocentrotus purpuratus*) [23].

La interacción PRR-PAMP inicia una cascada de señalización para activar la respuesta inmune del huésped. Esta cascada culmina con la activación del factor nuclear de transcripción kappaB (NF- κ B) que controla la expresión, entre otras, de moléculas solubles mensajeras que activan las respuestas inmunitarias locales y sistémicas [94]. Estas moléculas mensajeras son las citoquinas, que no sólo se encuentran en los vertebrados sino también en muchos invertebrados [95]. De hecho, el factor de necrosis tumoral alfa (TNF- α), el interferón gamma (IFN- γ) y la interleuquina 8 (IL8) están presentes en gusanos, moluscos e insectos [25].

A parte de moléculas de reconocimiento y moléculas de señalización, también hay moléculas efectoras comunes en vertebrados e invertebrados. Un claro ejemplo de ello son los péptidos antimicrobianos (AMPs), componentes humorales de la inmunidad innata que se encuentran presentes desde los procariotas hasta los organismos más desarrollados.

Otro caso de familia de moléculas efectoras conservadas evolutivamente son las pentraxinas, que fueron inicialmente descritas como parte del sistema inmune innato de invertebrados y vertebrados, no obstante, estudios recientes también muestran su intervención en el sistema inmune adaptativo [96, 97].

5. LAS PENTRAXINAS

5.1. Consideraciones generales

Uno de los principales componentes de la respuesta humoral del sistema inmune son las pentraxinas, una superfamilia de PRRs filogenéticamente muy conservada que se secretan al medio donde reconocen PAMPs (membranas celulares dañadas, componentes nucleares y antígenos microbianos) y reclutan otros elementos de defensa del huésped. Según la estructura primaria de sus subunidades, se dividen en pentraxinas largas y cortas (~50 y 25 kDa, respectivamente). Ambos grupos presentan un dominio homólogo en el extremo C-terminal de ≈ 200 aa, en el que se diferencia “la firma de las pentraxinas” (His-x-Cys-x-Ser/Thr-Trp-x-Ser, donde x puede ser cualquier aa), pero sólo las pentraxinas largas presentan un dominio N-terminal adicional [75, 98, 99]. Actualmente, se conocen diversas pentraxinas largas; no obstante la más estudiada es la pentraxina 3 (PTX3). En cuanto a las pentraxinas cortas, existen dos: la CRP, que es la molécula prototípica dentro de este grupo, y la proteína amiloide sérica (SAP) [72, 76, 99-102].

Las pentraxinas recibieron su nombre al descubrir que la CRP humana (hCRP) presentaba una estructura simétrica de cinco protómeros idénticos, cada uno de ellos formados por un sándwich β con dos láminas β antiparalelas [103]. Sin embargo, esta estructura pentamérica no se conserva en todas las especies. Por ejemplo, se ha descrito como dímero en la rana (*Xenopus*) y en el carpín dorado (*Carassius auratus*) [104], como trímero en el pez cebra (*Danio rerio*) [105] y como hexámero en el cangrejo de herradura chino (*Tachypleus tridentatus*) [106]. Asimismo, la SAP del cangrejo de herradura del Atlántico (*Limulus polyphemus*) se organiza en heptámeros y octámeros [107].

La capacidad funcional de las pentraxinas está polarizada estructuralmente y se distribuye entre los dos planos que forma el anillo oligomérico. Así, mientras una de las caras del anillo (cara de reconocimiento) actúa ligando PAMPs (**Tabla 2**), la otra (cara efectora) puede interactuar con el factor C1q del sistema de complemento o con FcRs (receptores presentes en la superficie de los linfocitos para el reconocimiento de anticuerpos unidos a patógenos) [20, 108]. La principal característica de la cara de reconocimiento es la presencia de un bolsillo hidrofóbico, que en el caso de la hCRP presenta dos sitios de unión a Ca^{2+} . Dado que las características hidrofóbicas de este bolsillo son diferentes para cada pentraxina, cada una de éstas muestra mayor afinidad por un ligando distinto [101]. Por ejemplo, en el caso de la hCRP este bolsillo une preferentemente, y dependientemente de Ca^{2+} , residuos de PC presentes en bacterias y en membranas de células dañadas [109]. Esta

unión se produce gracias a dos tipos de interacciones: la de los grupos metilo hidrofóbicos de la cola de PC con Phe⁶⁶ y la de los nitrógenos cargados positivamente de la cabeza de colina, con el Glu⁸¹ [110]. Por otra parte, en el caso de la cara efectora de la hCRP, los aa que parecen interaccionar con C1q son Asp¹¹² y Tyr¹⁷⁵ [74, 111].

Tabla 2. Ligandos microbianos de las pentraxinas humanas prototipo

Tipo de pentraxina	Ligandos		Referencia
	Motivos de membrana	Microorganismos	
CRP	Fosfatidilcolina (PC)	<i>Streptococcus pneumoniae</i> (+) <i>Aspergillus fumigatus</i> <i>Saccharomyces cerevisiae</i> <i>Leishmania donovani</i>	[101, 112]
SAP	Fosfatidiletanolamina (PE) Lipopolisacáridos (LPS)	<i>Salmonella typhimurium</i> (-) <i>Saccharomyces cerevisiae</i> <i>Influenza virus</i>	[77, 101]
PTX3	Proteína transmembrana KpOmpA de <i>Klebsiella pneumoniae</i>	<i>Pseudomonas aeruginosa</i> (-) <i>Klebsiella pneumoniae</i> (-) <i>Salmonella typhimurium</i> (-) <i>Aspergillus fumigatus</i> <i>Paracoccidioides brasiliensis</i> <i>Saccharomyces cerevisiae</i> <i>Influenza virus</i> <i>Citomegalovirus</i>	[77]

(+), bacterias grampositivas; (-), bacterias gramnegativas

Frente a una infección aguda ocurre una respuesta rápida y sistémica, caracterizada por el aumento de determinadas proteínas en suero, con un papel clave en el desencadenamiento de la reacción inflamatoria. Entre estas proteínas, llamadas proteínas de fase aguda (APP), está conservada evolutivamente la presencia mayoritaria de las pentraxinas cortas.

5.2. La proteína C-reactiva (CRP)

La APP más relevante en mamíferos, la CRP, se identificó en 1930 en los pacientes infectados por *Streptococcus pneumoniae* como consecuencia de su interacción con los residuos de fosfocolina (PC) del polisacárido C de la pared celular del pneumococo, razón por la cual se le asignó dicho nombre [99, 101, 113, 114]. Esta proteína, que comparte un 51% de identidad con la SAP en humanos, fue ampliamente estudiada, ya que, al formar parte de la reacción de fase aguda, aumentaba en sangre durante la inflamación y las infecciones bacterianas. Por tanto, la detección de sus niveles funciona como un biomarcador muy útil en clínica. Además, actualmente también se utiliza para predecir riesgo cardiovascular, ya que existe una estrecha relación entre el aumento de los niveles de CRP en sangre y el riesgo de padecer enfermedad coronaria, isquemia o muerte súbita [115-117]. De hecho, los humanos sanos tienen niveles bajos de CRP en sangre (0-5 mg/L) [118] que pueden aumentar hasta 1000 veces en 24 h debido a la síntesis *de novo*, mayoritariamente desde el hígado, estimulada por las interleuquinas 6 (IL6) y 1 β y su posterior secreción al torrente sanguíneo [78, 108, 113, 119, 120].

Como se ha expuesto anteriormente, la hCRP tiene una estructura pentamérica formada por la interacción no covalente de 5 monómeros de 206 aa cada uno, que se disponen en dos láminas β antiparalelas y una hélice α [74, 110]. Existen ciertas condiciones bajo las cuales la CRP pentamérica (pCRP) se puede disociar en monómeros (mCRP) de manera irreversible: pH ácido, altas concentraciones de urea, temperaturas elevadas, ausencia de calcio, detergentes y monocapas/bicapas lipídicas [114]. Estas dos conformaciones tienen funciones biológicas diferentes [121, 122]: **a)** la mCRP induce respuestas proinflamatorias en los neutrófilos y las células endoteliales, en contraste con las funciones antiinflamatorias del pCRP [123-125]; **b)** aunque ambas conformaciones pueden unirse a C1q y activar la vía clásica del sistema de complemento, sólo la mCRP recluta inhibidores del complemento como el factor H y C4b, que reducen la inflamación previniendo la actividad proinflamatoria excesiva de la mCRP [126, 127]; **c)** la pCRP genera superóxido por estallido respiratorio y, por tanto, apoptosis, mientras que la mCRP puede retrasar este proceso desencadenando la supervivencia celular en neutrófilos; **d)** mCRP, pero no pCRP, induce la generación de ROS mediadas por la unión a balsas lipídicas [128]; y **e)** la pCRP inhibe la producción del óxido nítrico (NO) mientras que la mCRP estimula la expresión de este mensajero celular [129].

5.3. Actividad antimicrobiana de las CRPs

Dado que la hCRP tiene afinidad por ligandos bacterianos y sus niveles en sangre se elevan enormemente tras las infecciones bacterianas [130, 131], ésta ha sido tradicionalmente considerada como una proteína antibacteriana. Hoy sabemos que esta actividad en humanos no se debe a una acción directa de la CRP sobre las bacterias sino a una activación del sistema de complemento [76, 101, 132-134] y a una mejora de la presentación de antígenos y de las respuestas citotóxicas [96, 135].

La hCRP es capaz de activar la vía clásica del sistema de complemento a través de su unión, dependiente de Ca^{2+} , al C1q de una manera más rápida y efectiva que los anticuerpos [76]. Como se ha comentado en el apartado 3, el sistema de complemento puede eliminar las bacterias a través de dos mecanismos: opsonización o lisis de membrana [134]. Sin embargo, cuando la activación de este sistema se debe a la CRP, como se favorece la unión al factor H, se fomenta la opsonización respecto a la lisis celular al impedir el ensamblaje del complejo de ataque de la membrana (MAC: C5b-C9) [101, 132, 133]. Esta opsonización mejora el reconocimiento de las bacterias por los receptores del complemento presentes en fagocitos profesionales, promoviendo su endocitosis [134]. La opsono-fagocitosis dependiente de complemento es crítica para la eliminación de algunas bacterias que expresan PC en la superficie, por ejemplo, *Streptococcus pneumoniae*, *Haemophilus influenzae*, *Pseudomonas aeruginosa*, *Neisseria meningitidis*, *Salmonella enterica* y *Morganella morganii* [134].

Algunos estudios han propuesto que la CRP no actúa sola, sino que colabora con otros PRRs del plasma para formar complejos estables de reconocimiento de PAMPs que permiten la activación de más de una vía del sistema de complemento [136]. Por ejemplo, la interacción entre la hCRP y las ficolinas permite que la CRP reconozca y estabilice su anclaje con ciertas bacterias que no son reconocidas de forma independiente. Esta colaboración no sólo aumenta el reconocimiento de *S. enterica*, sino que también activa el complemento por la vía de las lectinas en la superficie del patógeno [76].

Aparte de activar la respuesta inmune humoral vía sistema de complemento, la hCRP también puede activar la respuesta celular del sistema inmune [98, 137]. Una vez la hCRP opsoniza una bacteria, interacciona con FcRs presentes en la mayoría de las células hematopoyéticas humanas [138, 139]. Esta unión mejora **a)** la fagocitosis de bacterias [140], **b)** la presentación de antígenos por células dendríticas [135], **c)** la citotoxicidad mediada por linfocitos y células NK [96] y **d)** la reducción de la respuesta autoinmune como consecuencia de una mejor fagocitosis de células apoptóticas [141].

INTRODUCCIÓN

Por otra parte, existen estudios que sugieren que la hCRP se une a otros receptores, aún desconocidos, aparte de los FcRs. En este sentido se ha observado que la hCRP promueve la diferenciación de linfocitos T *naïve* a linfocitos T CD4⁺, una diferenciación que, pese a ser independientemente de FcR y de Ca²⁺, requiere un receptor, pues se insensibiliza con el uso de proteasas [97].

5.4. Evolución de las CRPs

Como se ha comentado en el apartado 4, la CRP está muy conservada filogenéticamente (desde moluscos y artrópodos hasta mamíferos); no obstante, aunque en mamíferos existe una clara diferenciación entre CRP y SAP, la diferenciación de estas proteínas en organismos ancestrales no está tan clara. Tradicionalmente esta diferenciación se ha realizado por la afinidad a los ligandos (la CRP se une preferentemente a PC y la SAP a PE). Sin embargo, en muchos peces la identidad de estas moléculas se ha basado en la homología de secuencia con ortólogos de otras especies y, por tanto, pueden haberse clasificado como CRP o SAP erróneamente [100]. Por ello, hay que tener en cuenta que cuando se habla de CRP o SAP en organismos no mamíferos en muchas ocasiones no se sabe con seguridad a qué tipo de pentraxina corta se hace referencia.

Pese a la notable conservación de algunas características de las CRPs desde invertebrados hasta mamíferos, existen diferencias a lo largo de la evolución en cuanto a la distribución de su expresión (**Tabla 3**), número de isoformas, estructura molecular, ligandos y funciones que, muy probablemente, tienen un significado biológico (**Tabla 4**). Por ejemplo, la CRP, que es la principal APP en humanos [78, 113], no se comporta así o no es la principal en todos los organismos: en ratones es la SAP la pentraxina que funciona como APP [142, 143] y en salmón, la SAA (proteína de suero amiloide A) [144]. Asimismo, como se había comentado anteriormente, la estructura oligomérica que le da nombre a la familia tampoco se mantiene en todas las especies [104-107]. Tampoco los monómeros tienen el mismo tamaño en cada especie dado que experimentan distintos cambios post-traduccionales [145]. Incluso en algunos casos como en el caracol *Achatina fulica*, los monómeros que forman el oligómero no son idénticos, sino que cada uno tiene un peso molecular diferente [146]. Los cambios estructurales a nivel molecular suelen estar asociados a cambios funcionales, de ahí que CRPs de diferentes organismos presenten afinidades desiguales y requisitos diferentes para interaccionar con los mismos ligandos. Por ejemplo, la necesidad de Ca²⁺ reportada en las pentraxinas cortas humanas para unirse a sus ligandos no se observa en la CRP del

cangrejo *Limulus polyphemus*, [147] y la SAP de trucha arcoíris (*Oncorhynchus mykiss*) no sólo requiere Ca^{2+} , sino también N-Acetilglucosamina (GlcNAc) para unirse a LPS [148].

Tabla 3. Distribución por tejidos de las isoformas de CRP/SAP en los diferentes organismos adultos.

Isoforma	Tejidos									
	Sangre/H	Piel	Bazo	Branquias	Cerebro	Corazón	Hígado	Intestino	Músculo	Riñón
<i>Af-CRP</i>										
<i>Lp-CRP</i>										
<i>Lp-SAP</i>										
<i>SsCRP1a</i>	X	X			X	X		X		
<i>SsCRP1b</i>	X	X			X	X		X		
<i>SsCRP1c</i>	X	X			X	X		X		
<i>SsCRP2</i>	X	X			X	X		X		
<i>SsCRP3</i>	X	X			X	X		X		
<i>RfCRP</i>					X					
<i>CcCRP1</i>						X				
<i>CcCRP2</i>					X	X				
<i>RbSAP1</i>	X									
<i>CsCRP</i>		X								

Los niveles de expresión de CRP se representan de acuerdo a una escala de grises en la que la expresión mínima aparece en blanco y la máxima, en negro. "X" indica que no se ha determinado la expresión en ese tejido. H: hemolinfa; Af: *Achatina fulica*; Lp: *Limulus polyphemus*; Ss: *Salmo salar*; Rf: *Sebastes schlegelii*; Cc: *Cyprinus carpio*; Rb: *Oplegnathus fasciatus*; Cs: *Cynoglossus semilaevis*.

Por otra parte, la expresión basal de las isoformas de CRP en diferentes tejidos de los organismos estudiados sigue una distribución heterogénea. Por ejemplo, mientras la CRP del pez roca coreano (*Sebastes schlegelii*) se expresa mayoritariamente en bazo [149], los mayores niveles de CRP en la carpa común (*Cyprinus carpio*) se encuentran en sangre e intestino (**Tabla 3**). Sin embargo, cada una de las isoformas de CRP de este último organismo sigue un patrón de expresión específico. Ejemplo de ello es que en su riñón anterior existen niveles de expresión bajos de ccCRP1 pero altos de ccCRP2 [100] (**Tabla 3**). Esta expresión diferencial de CRPs entre tejidos y organismos sugiere: **a)** que la CRP no tenga las mismas funciones en todos los organismos y **b)** que las diversas isoformas de CRP de cada organismo no realicen funciones redundantes. Estos resultados, junto con el hecho de que algunos peces tengan numerosas isoformas de CRP/SAP [100] mientras que, por ejemplo, los humanos sólo dos, sugieren que las funciones de las CRPs y/o su relevancia ha cambiado a lo largo de la evolución.

INTRODUCCIÓN

Tabla 4. Características generales de las CRP/SAPs de invertebrados y vertebrados inferiores.

Especie	Isoformas	Estructura	Monómero (kDa)	Ligandos	APP	Actividad	Ref
Moluscos							
<i>Achatina fulica</i> (caracol gigante africano)	CRP	Pentámero	110, 90, 62 y 60	PC (Ca^{2+}), poly-L-arginina	nd	Bacteriostática sobre Gram-	[146, 150]
Artrópodos							
<i>Limulus polyphemus</i> (cangrejo herradura)	L-CRP L-SAP	L-CRP: Hexámero, L-SAP: Heptámero Octómero	≈24	L-CRP: LPS L-SAP: PE (Ca^{2+})	CRP: (+)	Aglutinación, citolisis de bacterias	[107, 147, 151, 152]
Peces							
<i>Salmo salar</i> (salmón del Atlántico)	CRP-1a CRP-1b CRP-1c CRP-2 CRP-3	Pentámero	≈37	nd	No	nd	[144, 153, 154]
<i>Oncorhynchus mykiss</i> (trucha arcoíris)	CRP SAP1, SAP2, SAP3	CRP: monómero SAP: SAP: pentámero	CRP ≈24 SAP ≈34,5	CRP: PC (Ca^{2+}) SAP: LPS (Ca^{2+} y GlcNAc)	CRP: (+) SAP: (-)	CRP: Opsoniza <i>Vibrio anguillarum</i>	[148, 155]
<i>Ictalurus punctatus</i> (pez gato)	CRP	Pentámero	nd	Polisacárido C de <i>Pneumococo</i> (Ca^{2+})	(+)	nd	[156]
<i>Sebastes schlegelii</i> (pez roca coreano)	RfCRP	nd	≈25	LPS	(+)	Antibacteriana frente <i>Escherichia coli</i> y <i>S. iniae</i> . Aglutina <i>E. Coli</i>	[149]
<i>Cyprinus carpio</i> (carpa común)	CcCRP1 CcCRP2	nd	≈25	nd	(+)	CyHV-3 aumenta sus niveles en sangre	[100, 157, 158]
<i>Gadus morhua</i> (bacalao común)	CRP-I CRP-II	Pentámero	≈30	PC	No	nd	[159-161]
Anfibios							
<i>Xenopus laevis</i> (rana africana)	CRP	Dímero	≈24	nd	No	nd	[104]

nd, no determinado; (+), APP positiva; (-), APP negativa; CyHV-3, herpesvirus de los ciprínidos tipo 3

5.5. Potencial actividad antiviral de las pentraxinas

En mamíferos, aunque las APPs se desencadenan tanto tras una infección bacteriana como tras una infección vírica [162], los cambios en los niveles séricos tras esta última son mucho menores (1 logaritmo frente a 3) [162-164]. Por el contrario, en el caso de los peces, los pocos estudios existentes indican que los niveles séricos de las CRPs aumentan de manera moderada en respuesta a infecciones tanto bacterianas como víricas. Es decir, que las CRPs son igualmente reactivas a cualquiera de estos dos estímulos en peces [157, 158, 165]. Dado que este aumento es significativo y se observa muy rápidamente, cuando todavía el daño tisular debido a la infección no es aparente, dicha estimulación frente a virus sugiere que esta respuesta podría ser consecuencia de una actividad directa o indirecta frente al virus. Por ejemplo, en la carpa se ha descrito aumentos séricos de hasta 2, 6 y 10 veces en respuesta a las infecciones por *Aeromonas salmonicida* [166], *Aeromonas hydrophila* [167] y el herpesvirus de los ciprínidos tipo 3 (CyHV-3) [168], respectivamente.

Asimismo, análisis transcripcionales revelan aumentos significativos de la expresión de *crps* en tejidos de diversas especies de peces en respuesta a la infección con CyHV-3 [158], el iridovirus de la dorada japonesa (RSIV) [169, 170], el virus de la septicemia hemorrágica viral (VHSV) [171, 172] y el virus de la viremia primaveral de la carpa (SVCV) [171, 173]. De manera similar, se ha observado una mayor expresión transcripcional de dichos genes en carpa común tratada con ácido poliinosínico-policitidílico (poly I:C, compuesto que imita el ARN vírico)[165] y en trucha arcoíris tratada oralmente con vacunas de ADN [174].

Pese a la existencia de multitud de estudios sobre pentraxinas cortas, fundamentalmente por su relevancia como biomarcador en humanos, la mayoría son en mamíferos. Existen, por tanto, importantes lagunas en el conocimiento de las funciones y la significancia biológica de estas proteínas en organismos ancestrales. Por esto, y dados los resultados previos que sugieren, aunque no ha sido descrita, una función asociada a contrarrestar infecciones víricas, estas proteínas son el objeto de estudio de esta tesis doctoral.



OBJETIVOS, ANTECEDENTES Y SISTEMA MODELO

OBJETIVOS

El **objetivo general** de este trabajo es determinar y caracterizar el papel antiviral de las moléculas tipo CRP en organismos ancestrales, concretamente en peces. Con este fin, se seleccionó el sistema modelo de pez cebra y SVCV. Para alcanzar el objetivo general se establecieron los siguientes objetivos específicos:

1. Describir los niveles de expresión de las proteínas C-reactivas de pez cebra (*zfcrps*) tras una infección de origen vírico.
2. Evaluar la actividad antiviral de las zfCRPs *in vitro* e *in vivo*.
3. Analizar la afinidad de las zfCRPs a diferentes lípidos de membrana.
4. Determinar el/los mecanismos responsables de la actividad antiviral de las zfCRPs.

Los estudios realizados para lograr cada objetivo específico se encuentran descritos en capítulos independientes, que se corresponden con las cuatro publicaciones enumeradas en el PREFACIO. Los resultados de cada publicación serán referenciados utilizando el número de publicación y el número de figura de cada artículo. Por ejemplo, la referencia de la figura 1 de la publicación 1 sería: (Fig.1, P1).

ANTECEDENTES

Además de las evidencias ya descritas en el apartado de introducción, existen **antecedentes** recientes sobre las zfCRPs que son muy relevantes para abordar los objetivos planteados:

- a) El pez cebra tiene siete isoformas de CRP [100], por lo que cada una de ellas podría tener diferentes afinidades por ligandos y, por tanto, diferentes funciones. Asimismo, en este estudio se sugiere que las múltiples posibilidades de combinación entre los monómeros de las diferentes isoformas podrían ampliar el espectro de reconocimiento de PAMPs [100].
- b) La expresión transcripcional de *crp* en los órganos internos de peces cebra supervivientes a la infección por VHSV y de peces supervivientes re-infectados sigue el mismo patrón de expresión que los genes del sistema de interferón. Dado que el sistema de interferón está implicado en la respuesta antiviral de los peces, se propone que las zfCRPs podrían ser también antivirales [172].

OBJETIVOS, ANTECEDENTES Y SISTEMA MODELO

- c) Los niveles de tránscritos de *crps* en aletas de peces cebra mutantes carentes de sistema inmune adaptativo (*rag1-/-*) aumentan tras la infección con SVCV, lo que sugiere una actividad antiviral de estas proteínas [175].
- d) Las histonas asociadas a las regiones promotoras de las zfCRPs están metiladas a 2 y 5 días post-infección con SVCV. Esta activación transcripcional de los genes *zfcrp* no sólo sugiere una función antiviral de las zfCRPs, también un papel de estas proteínas en la inmunidad entrenada [173].

SISTEMA MODELO

1. El pez cebra como sistema modelo para el estudio de las pentraxinas cortas.

Como los peces son los primeros organismos en los que se desarrolla el sistema inmune adaptativo, éste se considera "poco" evolucionado (no tiene recombinación de IgGs, maduración de IgMs, IgT e IgZ, ni linfocitos B fagocíticos) [172]. Aún así, los peces generalmente son capaces de hacer frente a los numerosos patógenos a los que se ven expuestos continuamente [176, 177]. Esta supervivencia sugiere que su sistema inmune innato apoya en gran medida al sistema inmune adaptativo y que incluso es capaz de suplir posibles carencias.

Para comprobar la existencia de una actividad antiviral de moléculas presentes en el sistema inmune innato de peces, como las CRPs, se ha elegido el pez cebra como modelo experimental. Éste destaca como sistema modelo para estudios en vertebrados, en general, por su pequeño tamaño, la obtención de un gran número de embriones por apareamiento, su rápido desarrollo hasta la edad adulta, los bajos costes de mantenimiento y manejo, la posible manipulación genética, disponibilidad de mutantes, etc [178]. Además, el pez cebra es un buen modelo para el estudio de la respuesta antiviral en peces, ya que es susceptible a la infección experimental de una variedad de familias víricas que afectan a peces de gran importancia comercial: *Birnaviridae*, *Rhabdoviridae* e *Iridoviridae* [179].

Otra ventaja de este sistema animal es que ofrece la posibilidad de estudiar la respuesta del huésped frente a patógenos en fase de embrión y larva. Los embriones de los peces se desarrollan externamente y, por tanto, están expuestos muy tempranamente a un gran número de patógenos. Por este motivo, desarrollan rápidamente su sistema inmune [180] y, como consecuencia, a uno y dos días post-fertilización (dpf) ya poseen macrófagos y neutrófilos funcionales, respectivamente. Esto permite que las infecciones en el laboratorio

OBJETIVOS, ANTECEDENTES Y SISTEMA MODELO

puedan desarrollarse en estado larvario (ya a 1-2 días dpf) con la posibilidad de bioimagen en tiempo real para el seguimiento de cualquier proteína de interés, ya que los embriones permanecen transparentes hasta que la larva tiene varios días [181].

Asimismo, pese a que el pez cebra adulto tiene sistema inmune adaptativo, las funciones del sistema inmune innato pueden ser estudiadas sin interferencia del adaptativo en las larvas. Esto es posible porque la respuesta adaptativa funcional en las larvas de esta especie no aparece hasta la 4^a-5^a semana post-fertilización (**Figura 3**) [180, 181].

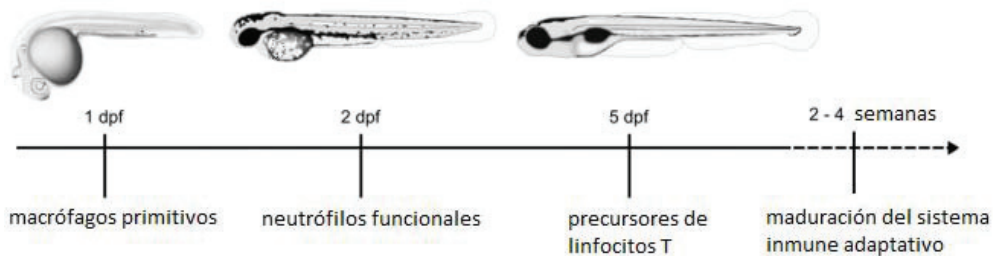


Figura 3. Esquema del desarrollo del sistema inmune del pez cebra. Tomada de [181].

A parte de las ventajas comentadas anteriormente, el pez cebra ofrece múltiples estrategias para estudiar funciones de genes, pues su manipulación génica está muy optimizada [182]. Por una parte, se puede anular transitoriamente la función de ciertos genes inyectando oligonucleótidos antisentido en embriones de una sola célula para bloquear la traducción del ARNm [183]. Por otra parte, se puede aumentar la expresión de un gen por inyección de ARNm, ADNc o de plásmidos en embriones (en estado de una sola célula) [182]. En muchas ocasiones la transgénesis puede conducirse junto con proteínas reporteras, como la proteína verde fluorescente (GFP), ligada a los genes o a los promotores de genes de interés, lo que permite visualizar procesos de interés a tiempo real mediante microscopía de fluorescencia [184].

Cabe también destacar que el genoma completo del pez cebra está secuenciado y estudios comparativos han desvelado que al menos el 70% del genoma codificante humano, incluyendo genes asociados con enfermedades, tiene ortólogos en pez cebra [185]. Adicionalmente, las células del sistema inmune innato de mamíferos también se encuentran conservadas en este organismo, que presenta macrófagos y neutrófilos muy similares (en términos de morfología y funcionalidad) a los de los mamíferos y un tipo de células consideradas como precursores de las NK [186]. Todas estas características, junto con la conservación de ciertas moléculas del sistema inmune innato (TLRs, AMPs, CRPs, sistema de complemento...) [187, 188], convierten al pez cebra en un buen sistema modelo para el

OBJETIVOS, ANTECEDENTES Y SISTEMA MODELO

estudio de numerosas afecciones. Los descubrimientos derivados de estos estudios podrían ser extrapolables a otros vertebrados superiores, incluidos los humanos [189].

2. Los rabdovirus de peces: SVCV y VHSV

Los rabdovirus se caracterizan por ser envueltos, tener morfología de bala y poseer un genoma de ARN monocatenario de cadena negativa (grupo V de la clasificación de Baltimore) que codifica cinco proteínas estructurales: la nucleocápsida (N), la fosfoproteína (P), la proteína de la matriz (M), una glicoproteína de membrana (G) y una ARN polimerasa ARN dependiente (L) [190]. En el caso de los rabdovirus pertenecientes al género *Novirhabdovirus*, están especializados en infectar organismos acuáticos y se caracterizan por tener un sexto gen, ubicado entre los genes G y L (**Figura 4**), que codifica una proteína no estructural denominada Nv (del inglés, *nonvirion protein*) [191], que parece participar en la patogénesis causada por los virus [192].

Genoma SVCV



Genoma VHSV



Figura 4. Organización del genoma y predicción de sus pesos moleculares en kDa del virus prototipo del género *Sprivivirus*, SVCV y del género *Novirhabdovirus*, VHSV. Modificada de [192].

De estas proteínas, las más utilizadas para detectar la presencia de los rabdovirus son: la glicoproteína G, porque se encuentra en la superficie externa del virus y la N, por ser la más abundante. La glicoproteína G es la encargada de mediar el proceso de entrada del virus al inducir la endocitosis (mediada por receptor) y la fusión de la membrana vírica con la celular del huésped. La proteína N, asociada con el ARN viral, da simetría helicoidal a la nucleocápside [193].

Pese a que muchos virus envueltos pueden penetrar en el citoplasma directamente mediante la fusión con la membrana plasmática, los rabdovirus utilizan la endocitosis de la

OBJETIVOS, ANTECEDENTES Y SISTEMA MODELO

célula huésped para su internalización [194]. El ciclo de replicación se inicia por la unión de la proteína G del virus a un receptor de la superficie celular que, en el caso de los rabdovirus de peces, se desconoce, aunque parece estar implicada la fibronectina [195]. Una vez adherido el virus a la célula, éste ingresa a través de la vía endocítica donde se transporta desde los endosomas tempranos hasta los tardíos. Los endosomas tardíos se fusionan con los lisosomas, produciendo una disminución de pH. Esta bajada de pH produce un cambio conformacional en la proteína G que permite la fusión de la envoltura vírica y la membrana endosomal. A partir de entonces se libera el genoma vírico al citoplasma [196].

El SVCV y el VHSV son dos rabdovirus que causan enfermedades hemorrágicas graves en los ciprínidos [190] y los salmoninos [197], respectivamente. A pesar de la cantidad de investigaciones realizadas, ambas enfermedades de obligada notificación por la Oficina Internacional de Epizootias (OIE) [198] causan anualmente pérdidas económicas masivas en la industria de la acuicultura a nivel mundial [199]. Por esta razón, la comprensión de la respuesta inmune de los peces frente a estos virus es fundamental para desarrollar medidas de control preventivas y profilácticas. En este sentido, sabemos que el primer sistema de defensa que utilizan los peces para protegerse frente a las infecciones virales, incluidas las de los rabdovirus, es el sistema del interferón tipo I. Este sistema está formado por un grupo de citoquinas cuya inducción provoca la transcripción de los genes estimulados por el interferón (ISG), que codifican proteínas efectoras para la defensa del huésped como por ejemplo las Mx, que controlan la replicación viral restringiendo la propagación del virus a las células vecinas [200].

En este trabajo, para demostrar que las zfCRPs conservan funciones ancestrales inexistentes o no descritas en mamíferos, se ha utilizado principalmente el SVCV. La elección de este virus se debe esencialmente a que el pez cebra es susceptible a su infección tanto en etapa adulta [201] como en fase de larva [175] a temperaturas cercanas a las óptimas para el desarrollo del pez. Asimismo, en este pez, los síntomas que cursan con la infección de SVCV son similares a los que se observan en otras especies, entre los que cabe destacar las hemorragias y la exoftalmia [202].

MATERIAL Y MÉTODOS

MATERIAL Y MÉTODOS

1. ANIMALES DE ESTUDIO

En la presente tesis se utilizaron peces cebra (*Danio rerio*) adultos XL (700–900 mg y 3–4 cm) obtenidos de un proveedor local (Fauna Flor, Elche, España). También se utilizaron peces cebra mutantes (*rag1*^{-/-}) con el gen activador de recombinación truncado, y sus correspondientes homólogos *wild type* (*rag1*^{+/+}), de ~6 meses y 0,5-1 g, los cuales se reprodujeron y caracterizaron en las instalaciones del Dr. Victoriano Mulero en la Universidad de Murcia. Todos los peces fueron mantenidos a 24–28 °C en tanques de 30 L equipados con un sistema de recirculación de agua declorada y alimentados diariamente con alimento comercial (Vipan BioVip, Alemania). Antes de los experimentos, los peces se aclimataron durante dos semanas a las condiciones del laboratorio.

Además de peces adultos, se utilizaron embriones de peces cebra *wild type* y transgénicos GFP-Lc3. Los embriones se obtuvieron mediante el desove natural de los apareamientos de adultos en las instalaciones de la Dra. Beatriz Novoa en el Instituto de Investigaciones Marinas-CSIC (Vigo, España).

Todos los procedimientos experimentales con pez cebra se realizaron de acuerdo con la Ley Española de Experimentación Animal (Real Decreto 53/2013) y la Directiva 2010/63/UE del Parlamento Europeo y del Consejo. Asimismo, todos los protocolos fueron aprobados por el comité de ética del gobierno regional sobre la experimentación con animales (Dirección General de Agricultura, Ganadería y Pesca, Generalitat Valenciana) y la Oficina Evaluadora de Proyectos de la Universidad Miguel Hernández y sus homólogos en las instituciones colaboradoras.

2. LÍNEAS CELULARES

En el presente estudio se utilizó la línea celular *Epithelioma papulosum cyprini* (EPC, ATCC #CRL-2872) procedente de *Pimephales promelas* y fibroblastos embrionarios de pez cebra (ZF4, ATCC #CRL-2050). Las células EPC se cultivaron en medio RPMI-1640 Dutch (Gibco, Invitrogen Corporation, Reino Unido) suplementado con un 10% de suero fetal bovino (FBS) (Sigma, St. Louis, EE.UU.), 1 mM de piruvato sódico, 2 mM de glutamina, 50 µg/mL de gentamicina y 2 µg/mL fungizona (Gibco BRL-Invitrogen, Carlsbad, CA, EE.UU.). Las células ZF4 se cultivaron con medio DMEM/F12 (Dulbecco's modified Eagle's, Gibco)

MATERIAL Y MÉTODOS

suplementado con 10 % FBS y 100 µg/mL de primocina (InvivoGen, San Diego, CA, EE.UU.). Ambos tipos celulares se mantuvieron a 28 °C con un 5 % de atmósfera de CO₂.

3. VIRUS

Las infecciones experimentales en este trabajo se realizaron con la cepa 07.71 de VHSV aislada de la trucha arcoíris y el aislado de carpita 56/70 de SVCV. Los aislados de VHSV y SVCV se propagaron en monocapas de EPC a 14 °C y de ZF4 a 22 °C, respectivamente, en los medios de cultivo celular descritos anteriormente, con la excepción del uso de un 2 % de FBS en lugar de un 10 %, y en ausencia de suplemento de CO₂. Los sobrenadantes de las monocapas infectadas se clarificaron por centrifugación a 4000 g y 4 °C durante 30 min y se mantuvieron a -80 °C hasta su uso.

4. CONSTRUCCIÓN DE PLÁSMIDOS QUE CODIFICAN *zfcrp1-7*

Cada uno de los genes *zfcrp1-7* y *gfp* sintetizados químicamente se subclonaron en el plásmido pMCV1.4 como se describe en la P2. Los plásmidos pMCV1.4-*zfcrp1-7* y pMCV1.4-*gfp* resultantes se utilizaron para transformar *E. coli* DH5- α mediante electroporación. Posteriormente, las bacterias transformadas se cultivaron en placas de agar Luria Bertani (LB) con kanamicina (50 µg/mL) durante 24 h a 37 °C y se seleccionó una colonia aislada de cada transformación. Esta colonia se cultivó en medio LB-kanamicina (50 µg/mL) a 37 °C en agitación. Las construcciones de plásmidos se aislaron con el kit de purificación Endofree Plasmid Midi (Qiagen, Alemania) de acuerdo con las instrucciones del fabricante.

5. TRANSFECCIÓN DE CÉLULAS CON pMCV1.4-*zfcrp1-7* Y PRODUCCIÓN DE SOBRENADANTES ENRIQUECIDOS

Para los experimentos en células transfectadas, las células EPC se transfecaron en placas de 96 pocillos con 100 ng de pMCV1.4-*zfcrp1-7* utilizando como agente transfectante FuGENE HD (Promega, WI, EE.UU.) durante 24 horas a 22 °C en un volumen total de 100 µL. Tras la transfección, se retiró el medio de cultivo y se añadió medio fresco durante 48 h. Todas las transfecciones realizadas durante esta tesis se realizaron mediante este procedimiento salvo las destinadas a la producción de sobrenadantes enriquecidos con zfCRPs (ssCRPs) o los sobrenadantes control (ssGFP). La eficiencia de transfección se determinó por el porcentaje de células fluorescentes después de la transfección con pMCV1.4-*gfp*.

Para la producción de ssCRP1-7 se transfecaron células EPC en botes de 25 cm² con pMCV1.4-zfcrp1-7. Tres días después de la transfección, el medio de las células fue retirado y se añadió medio RPMI 2 %. Dos días después, los sobrenadantes recogidos fueron procesados y almacenados en alícuotas a -80 °C hasta su uso.

6. PRODUCCIÓN DE CRPs RECOMBINANTES

Para la obtención de las proteínas recombinantes CRP2, CRP5 y CRP7, se ha utilizado el sistema Bac-to-Bac. Esta técnica se basa en la transposición de un casete de expresión desde un plásmido donador a un bácmido que se propaga en *E. coli*. La producción de estas proteínas fue realizada por GenScript (Piscataway, NJ, EE.UU.). Para más detalle, consultar la P3.

Brevemente, se sintetizó una construcción de ~ 3 Kpb, formada por el péptido señal gp67 + CRP1-7 + secuencia (DYKDDDK) + 6 x His, que se insertó en el plásmido donador pFastBac1 (Invitrogen). Los pFastBac1 recombinantes se transfecaron en células de *E. coli* DH10Bac (Invitrogen) que presentan, además de un bácmido con un segmento de ADN que codifica para el péptido LacZ, un plásmido auxiliar que codifica una transposasa que permite la transposición del gen de interés (contenido en el vector pFastBac1) al genoma del baculovirus. La transposición del gen de interés al bácmido interrumpe el marco de lectura del péptido LacZ permitiendo identificar las bacterias recombinantes por el desarrollo de colonias blancas. Posteriormente, los bácmidos recombinantes aislados se transfecaron en células de insecto *Spodoptera frugiperda* (Sf9) utilizando Cellfectin II (ThermoFisher, Massachusetts, EE.UU.) como se describe detalladamente en la P3. A 72 h post-transfección se obtuvieron sobrenadantes que contenían ~ 10⁷ pfu (unidades formadoras de placas)/mL de baculovirus recombinantes. Posteriormente, estos sobrenadantes se centrifugaron y dializaron frente a 50 mM Tris y 500 mM NaCl. Aprovechando las colas de His, las proteínas recombinantes se purificaron mediante cromatografía de afinidad de metales inmovilizados utilizando columnas de Ni²⁺. La identificación de las proteínas CRP se realizó mediante electroforesis en gel de poliacrilamida (SDS-PAGE) seguida de western blot. Sus concentraciones se determinaron utilizando el ensayo de ácido bicinconílico (BCA).

MATERIAL Y MÉTODOS

7. PRODUCCIÓN DE ANTICUERPOS EN CONEJO PARA RECONOCER LAS ISOFORMAS DE zfCRP1-7

Se generaron anticuerpos (GenScript) frente a los tres péptidos (p1, p2 y p3) más conservados en las zfCRPs: p1 (¹⁸SYVKLSPEKPLSLSAFTLC), p2 (¹⁸⁹DWDTIEYDVTGN) y p3 (¹²⁹RPGGTVLLGQDPDSYVGGPDC). Los tres anticuerpos fueron purificados mediante cromatografía de afinidad contra los péptidos sintéticos correspondientes acoplados a sefarosa activada con CNBr. Solamente el anticuerpo anti-p3 reconoció por *western blot* tanto las CRPs de los sobrenadantes enriquecidos como las rCRPs producidas en insecto. No obstante, el anticuerpo anti-p2 identificó CRPs en los ssCRPs por *dot-blot*.

8. CARACTERIZACIÓN DE LOS ssCRPs

La caracterización de los sobrenadantes incluyó la determinación de los niveles de tránscritos de *zfcrp1-7* por RT-qPCR (sección 10) y el reconocimiento por *western blot* y *dot-blot* de cada una de las isoformas de zfCRP utilizando los anticuerpos específicos citados en la sección 7.

8.1. Western blot

Se llevó a cabo una electroforesis en gel de poliacrilamida al 15 % durante 90 min a 100 V y bajo condiciones reductoras. Tras esta electroforesis, las proteínas fueron transferidas a membranas de nitrocelulosa (BioRad, 162-0115) a 4 °C y 15 V durante toda la noche en un tampón de transferencia (2,5 mM Tris, 9 mM glicina, 20 % metanol). Esta membrana fue bloqueada durante 2 h con una disolución de PBS con 8 % de leche en polvo y 0,05 % de Tween-20 (Sigma) y, posteriormente, incubada durante toda la noche a 4 °C con el anticuerpo anti-p3 diluido 1:500 en PBS con un 5 % de BSA (Sigma) y 0,05 % de Tween-20 (tampón blot). Tras estas incubaciones, las membranas fueron lavadas tres veces con una disolución de PBS con 0,05 % de Tween-20 e incubadas durante 1 h a temperatura ambiente con el anticuerpo secundario Alexa Fluor® 546 goat anti-rabbit IgG (ThermoFisher) diluido 1:200 en tampón blot. La actividad peroxidasa fue detectada por ECL Select™ Western Blotting Detection Reagent (Sigma) en un sistema de imágenes LIAS ChemLite 200F/400F (Avegene).

8.2. Dot-blot

En este ensayo las zfCRPs no fueron ni separadas por cromatografía ni electro-transferidas a la membrana. Se aplicaron 500 µl de ssCRPs directamente sobre la membrana de nitrocelulosa donde se fijaron por vacío. A partir de aquí, la detección de las zfCRPs se realizó del mismo modo que en los ensayos de *western blot* con la única diferencia de que el anticuerpo utilizado fue el anti-p2 en lugar del anti-p3.

9. INFECCIONES DE PECES CEBRA ADULTOS Y RECOLECCIÓN DE ÓRGANOS Y PLASMA SANGUÍNEO

9.1. Infecciones *in vivo*

Los peces cebra se aclimataron durante 2 semanas a 14 °C para la infección con VHSV o a 22 °C para la infección con SVCV. Tras este periodo de aclimatación, los peces fueron infectados durante 2 h por baño-inmersión con 10^7 pfu/mL de VHSV o 10^4 pfu/mL de SVCV. El grupo de peces control fue tratado con una cantidad correspondiente de medio celular fresco.

9.2. Recolección de órganos de peces cebra adultos

El tiempo post-infección al que se realiza el sacrificio de los peces mediante una sobredosis de anestesia (mesilato de tricaina, MS-222, Sigma) para recoger tejidos y/o sangre depende del experimento. A lo largo de esta tesis se han realizado ensayos con tejidos de animales sacrificados a diferentes días post-inefcción (**Tabla 5**).

Tabla 5. Tiempo post-infección de recogida de tejidos y/o sangre

Tipo de infección	Tiempo post-infección
SVCV	2 días
	5 días
	30 días
VHSV	2 días
	60 días
VHSV+VHSV	2 días en supervivientes de 60 días
<i>A. hydrophila</i> y <i>Vibrio fluvialis</i>	5 meses

MATERIAL Y MÉTODOS

En función del ensayo, los tejidos recogidos se utilizaron y procesaron de manera diferente. En los estudios de *microarray*, para la obtención de cada réplica biológica se recolectaron muestras conjuntas de órganos linfoideos (riñón anterior y bazo) o de aletas de tres peces. Sin embargo, para los estudios por RT-qPCR se utilizaron los tejidos aislados de cada pez. Estos tejidos se mantuvieron en RNAlater (Qiagen, Venlo, Países Bajos) a -70 °C hasta su uso.

9.3. Recolección de sangre de peces cebra adultos

Para los estudios proteómicos, la sangre de peces cebra adultos anestesiados se obtuvo cortando el extremo final de sus colas a 0, 24, 48 y 120 h post-infección de SVCV. Para obtener el plasma, la sangre se procesó como se describe en el apartado 2.5 de la P2. El plasma se mantuvo congelado a -70 °C hasta su uso.

10. EXTRACCIÓN DE ARN, RT y qPCR

Para evaluar la expresión de tránscritos de *crp1-7* en órganos de pez cebra mediante RT-qPCR, el ARN de cada uno de los tejidos se extrajo utilizando el kit E.Z.N.A HP Tissue RNA (Omega Bio-tek, GA, EE.UU.) y, posteriormente, se trató con DNAsa Turbo™ (Ambion, Thermo Fischer Scientific Inc.) para eliminar el ADN genómico residual. Sin embargo, para evaluar los niveles de tránscritos en EPC o ZF4, el ARN se extrajo utilizando el kit HP Total RNA (Omega Bio-tek) de acuerdo con las instrucciones del fabricante. Las concentraciones de ARN fueron estimadas mediante el espectrofotómetro NanoDrop® Spectrophotometer (Thermo-fisher Scientific, MA, EE.UU.) y la síntesis de ADNc se llevó a cabo utilizando la transcriptasa inversa M-MLV (Moloney murine leukemia virus, Invitrogen).

Finalmente, las PCR cuantitativas se realizaron usando el sistema ABI PRISM 7300 (Applied Biosystems, NJ, EE.UU). Las reacciones se llevaron a cabo en un volumen final de 20 µL que contenía 2 µL of ADNc, 900 nM de cada cebador (listados en cada publicación) y 10 µL de la master mix SYBR Green (Life Technologies, Reino Unido). Se incluyeron controles sin ADNc para cada análisis genético y todas las reacciones se realizaron utilizando duplicados técnicos. Las condiciones de reacción incluyeron: una desnaturalización inicial (95 °C durante 10 min), 40 ciclos de desnaturalización (95 °C durante 15 s) y una etapa de hibridación-elongación (65 °C durante 1 min). Además, en cada reacción se analizaron las curvas de disociación.

La expresión relativa de cada gen se determinó mediante el método $2^{-\Delta\Delta Ct}$ [203]. El valor de expresión de cada gen fue normalizado respecto a un gen endógeno de referencia (*ef1α* o *18S*, en función de la línea celular u organismo).

11. MICROMATRICES

Para la realización de la micromatriz se utilizó ARN extraído de los órganos linfoides (riñón anterior y bazo) de peces cebra adultos no infectados, infectados y supervivientes a la infección con VHSV o SVCV. Asimismo, se utilizaron peces cebra mutantes *rag1*^{-/-} y sus respectivos *wild types*. Las sondas específicas para cada *zfcrp1-7* se diseñaron mediante el programa Array Designer 4.3 (Premier Biosoft, Palo Alto CA, EE.UU.), la hibridación fue llevada a cabo por NIMGENETICS (Madrid, España) como fue descrito anteriormente en otros trabajos [172, 204], y la fluorescencia se detectó mediante el escáner Agilent (G2565B, AgilentTechnologies) usando el software Agilent Feature Extraction (v9.5). Los resultados de expresión génica se representaron con respecto a los grupos control utilizando las siguientes fórmulas: fluorescencia de cada gen en peces infectados / fluorescencia de cada gen en peces sin infectar; fluorescencia de cada gen en mutantes *rag 1*^{-/-} / fluorescencia de cada gen en peces *wild type*; fluorescencia de cada gen en los mutantes *rag 1*^{-/-} infectados / fluorescencia de cada gen en los mutantes *rag 1*^{-/-} sin infectar.

12. ANÁLISIS PROTEÓMICO DE LAS zfCRPs INDUCIDAS POR LA INFECCIÓN CON SVCV EN EL PLASMA DE PECES CEBRA

Las proteínas plasmáticas fueron precipitadas mediante un procedimiento con metanol/cloroformo. Posteriormente fueron cuantificadas por el ensayo BCA y digeridas con tripsina. Tras un proceso de purificación, 1 µg de cada muestra fue analizado mediante cromatografía líquida y espectrofotometría de masas en un aparato Sciex Triple-TOF 6600 (LC/LC-MS/MS) de las Instalaciones Proteómicas del Centro Nacional de Biotecnología (CNB, España). Las señales correspondientes a los péptidos obtenidos tras la digestión zfCRP1-7 fueron identificadas. Sólo las zfCRPs para las que se identificaron dos o más péptidos diferentes fueron consideradas para los análisis posteriores. Para más detalles de este procedimiento, consultar la sección 2.10 de la P2.

MATERIAL Y MÉTODOS

13. ESTUDIO DEL EFECTO DE LAS zfCRPs EN LA INFECCIÓN DE SVCV

13.1. Ensayos de neutralización *in vitro*

Para determinar si las zfCRPs interfieren en la replicación del SVCV se utilizaron diferentes estrategias. En primer lugar se estimó el efecto de las zfCRPs sobre la infección *in vitro*. Para ello, monocapas celulares transfectadas con cada uno de los plásmidos (pMCV1.4-zfcrp1-7) o incubadas con los ssCRPs fueron infectadas con SVCV (multiplicidad 10⁻² o 10⁻³) a 4 °C. Dos horas post-infección, los sobrenadantes de las células infectadas fueron retirados para eliminar el virus no unido y se incubaron con medio RPMI 2 % FBS a 22 °C durante 20 h más. La infección de estas células fue evaluada por citometría de flujo y/o mediante el recuento de unidades formadoras de focos (ffu). Brevemente, las monocapas se fijaron con 4 % formaldehído (Sigma, F1635) durante 20 min y fueron incubadas con el anticuerpo policlonal anti-SVCV (BioX Diagnostics SA, Bélgica) y el anticuerpo secundario de cabra marcado con Alexa Fluor® 488 que reconoce IgG de ratón (ThermoFisher). Posteriormente se contaron los focos de infección mediante microscopía de fluorescencia para determinar el número de ffu. Alternativamente, la células de estas monocapas fueron suspendidas con tripsina y analizadas por BD FACS Canto II apparatus (BD Biosciences). El porcentaje de células infectadas fue calculado utilizando la siguiente fórmula: 100 x nº células con fluorescencia por encima del umbral / nº células por pocillo. Los resultados finales se expresan como porcentaje de neutralización mediante la fórmula: 100-100 x (nº células tratadas con CRP e infectadas / nº células control infectadas). Cada uno de estos ensayos fue realizado al menos tres veces y por triplicado.

Durante estos ensayos se utilizaron dos líneas celulares: EPC para determinar el efecto de la transfección de pMCV1.4-zfcrps sobre la infección vírica y tanto EPC como ZF4 para estudiar el efecto de los ssCRPs. La incubación de las EPC con los distintos ssCRPs se realizó de cinco maneras: 2 o 20 h antes de la inoculación, al mismo tiempo que la inoculación y durante 2 o 20 h después de la adsorción. No obstante, como el tratamiento con mejores resultados fue la incubación 2 h antes de la infección, las incubaciones en ZF4 se realizaron exclusivamente de esa manera.

13.2. Ensayos de neutralización *in vivo*

Por otra parte, para estudiar el efecto de las zfCRPs sobre la infección con SVCV *in vivo*, se microinyectaron embriones de pez cebra en estado de una sola célula con 150 pg de

las construcciones pMCV1.4-*gfp*/zfcrp2-5 siguiendo la metodología descrita anteriormente [205]. Tres días después, las larvas resultantes de esas microinyecciones se anestesiaron e infectaron, utilizando también el sistema de microinyección, con SVCV (10^4 pfu) o PBS. La infección fue monitorizada durante siete días y los resultados se representaron como supervivencia acumulada utilizando la siguiente fórmula: $100 - 100 \times (\text{nº peces muertos inyectados con pMCV1.4-zfcrp2-5} / \text{nº peces muertos inyectados con pMCV1.4- gfp})$.

13.3. Ensayos de neutralización con ssCRPs empobrecidos (deplet-ssCRPs)

Para demostrar que la actividad antiviral de los ssCRPs se debe a las zfCRPs en lugar de a otros compuestos derivados de EPC, las zfCRPs fueron retiradas de los ssCRPs al incubar los sobrenadantes con 25-hidroxcolesterol (25-HOC) inmovilizado en fase sólida. Se utilizó el 25-HOC por ser un lípido por el que la mayoría de las zfCRPs muestran niveles altos de afinidad, como se describe en la P3. Brevemente, los pocillos de las placas de 96 pocillos Maxisorb (Nunc, Roskilde, Dinamarca) se recubrieron en sequedad con $100 \mu\text{M}$ de 25-HOC disuelto en etanol y se mantuvieron secos hasta su uso. Después de tres lavados con PBS, se agregaron los ssCRPs diluidos 4 veces y se incubaron durante 2 h. Finalmente, los sobrenadantes empobrecidos (deplet-ssCRPs) se recogieron y fueron utilizados para realizar ensayos de neutralización *in vitro* como los que se describen en la sección 13.1.

13.4. Ensayos de neutralización con LPS

Para estudiar las interferencias producidas por las posibles contaminaciones de LPS de *E. coli* en los plásmidos purificados, se realizó un ensayo de neutralización como el descrito en la sección 13.1. En este ensayo, las monocapas de EPC se incubaron con concentraciones crecientes de LPS (20 a 500 ng por pocillo) de dos cepas bacterianas (*E.coli* O55B5 y 0111:B4). Estas concentraciones fueron mayores a las que pueden estar presentes en nuestras transfecciones según las instrucciones del fabricante.

14. ENSAYOS DE ACTIVIDAD ANTIVIRAL DE LAS zfCRPs

Con el objetivo de determinar el mecanismo por el cual las zfCRPs tienen actividad antiviral, se estudió la influencia de las zfCRPs: a) en la unión del virus a la célula, b) en el proceso de fusión de la membrana vírica con los endosomas, c) en la secreción de moléculas antivirales al medio celular, d) en las etapas tempranas después de la adsorción de SVCV, e)

MATERIAL Y MÉTODOS

en la inducción del sistema de interferón y f) en la regulación de la autofagia (descrita en la sección 20).

14.1. Ensayos para determinar la inhibición de la unión del virus a la célula

Para estudiar si las zfCRPs inhiben la unión de partículas de SVCV a las potenciales células huéspedes, las monocapas de EPC fueron incubadas con SVCV (multiplicidad de infección, MOI 1) en ausencia (ssGFP) o presencia de zfCRP1-7 (ssCRPs) sólo durante el período de adsorción (2 h a 4 °C), para permitir la unión del virus pero no su endocitosis. Posteriormente, las células se lavaron tres veces con medio RPMI 2 % FBS para eliminar el virus sin unir. Las diferencias en la unión del virus a las potenciales células huéspedes por el tratamiento con ssCRPs se estimaron por la medida mediante RT-qPCR del gen que codifica la proteína N de SVCV.

14.2. Ensayos de fusión mediada por la proteína G de SVCV

Para evaluar el efecto de los ssCRPs sobre la capacidad de fusión de membranas de la proteína G de SVCV, monocapas de EPC sembradas en placas de 96 pocillos se infectaron con SVCV (MOI 10²). Tras 20 h, los medios celulares se eliminaron de las células infectadas, que se lavaron tres veces con medio RPMI 2 % FBS. Posteriormente, las células se trataron con ssCRP o ssGFP durante 2 h a 22 °C. Después de otros tres lavados, la conformación de fusión de membrana de la proteína G de SVCV se indujo mediante la incubación de las monocapas celulares con medios de fusión (pH 6) durante 30 min a 22 °C. Luego las células se lavaron de nuevo tres veces y se incubaron nuevamente con medio a pH 7,5 durante 2 h a 22 °C. Finalmente estas células fueron fijadas con metanol frío (-20 °C) durante 15 min, se secaron al aire y se tiñeron con Giemsa (5 mg/mL en PBS). Los sincitios resultantes de la fusión de células adyacentes se contaron y fotografiaron en el microscopio óptico. El porcentaje de sincitios se calculó mediante la fórmula: 100 x nº sincitios en monocapas tratadas con ssCRPs / nº sincitios en monocapas tratadas con ssGFP. Se realizaron tres ensayos diferentes por triplicado. Los resultados se muestran como media y desviación estándar (s.d.).

14.3. Actividad de los sobrenadantes condicionados por el tratamiento con ssCRPs

Para producir medios condicionados destinados a evaluar si las zfCRPs inducen la secreción de factores antivirales en las células tratadas, las monocapas de EPC se incubaron durante 2 h a 22 °C con ssCRPs. Tras tres lavados, los ssCRPs se reemplazaron con medio RPMI 10 % FBS y se incubaron durante 24 h más a 22 °C. Finalmente, estos sobrenadantes se recogieron y se utilizaron para hacer ensayos de neutralización *in vitro* como se describe en la sección 13.1.

14.4. Determinación de los niveles de replicación de SVCV *in vitro* en etapas tempranas después de la adsorción

Para determinar si las zfCRPs afectan a la replicación de SVCV en etapas tempranas después de la adsorción, las monocapas de EPC y ZF4 se incubaron con una mezcla que contenía ssCRP2-6 a partes iguales (mix-CRP) durante 2 h a 22 °C. A continuación, las células se lavaron tres veces con medio RPMI 2 % FBS y se inocularon a 4 °C con SVCV (MOI 0,01) durante 2 h más. Despues de otros tres lavados, se agregaron nuevos medios y las monocapas se incubaron a 22 °C. Las células infectadas se recolectaron 0, 1, 2, 3, 4 y 5 h post-adsorción para analizar los niveles de replicación viral midiendo la expresión génica de *n* y *g* de SVCV por RT-qPCR.

14.5. Análisis de la capacidad de los ssCRPs para inducir el sistema de interferón

Para evaluar si las zfCRPs estaban afectando el sistema de interferón (IFN) a nivel transcripcional, las células EPC se trataron con ssCRP durante 2 h a 22 °C. Tras este periodo, las monocapas se lavaron tres veces y se recogieron muestras a las 20 h. Con estas muestras se analizó la regulación transcripcional de *mx* (ISG) mediante RT-qPCR. En las monocapas de ZF4, la medida de expresión génica de *mx* no fue sólo a las 20 h, también se realizó a 1, 2, 3, 4 y 5 horas post-tratamiento con la mixCRPs. A estos tiempos también se analizó la expresión de *ifnphi1* e *ifnphi2* en estas últimas muestras.

15. EVALUACIÓN DEL PAPEL DE LA IL6 EN LA INDUCCIÓN DE zfcrps

Para probar los efectos de IL6 en la expresión de *crp1-7*, se microinyectaron 2 nL de PBS que contenían 150 pg de pMCV1.4 o pMCV1.4-*il6* en embriones de una sola célula,

MATERIAL Y MÉTODOS

como se describe en la sección 13.2. Tres días después, se extrajo el ARN de grupos de tres larvas y se midieron los niveles de tránscritos de *zfcrp1-7* por RT-qPCR como se describe en la sección 10.

16. PREDICCIONES *IN SILICO*

16.1. Estructuras tridimensionales de las zfCRPs

La predicción de las estructuras tridimensionales de zfCRP1-7 se realizó mediante el servidor de homología SWISS-MODEL (<https://swissmodel.expasy.org/interactive>) [206-208]. Este servidor compara la secuencia de aminoácidos de la proteína diana (zfCRP) con otras secuencias proteicas de su base de datos e identifica la mejor plantilla para modelar su estructura. En este caso, la plantilla seleccionada por modelado automático fue la correspondiente a la zfCRP5 en presencia y ausencia de Ca²⁺(4PBP.pdb y 4PBO.pdb) [105].

16.2. Energías libres de unión de las zfCRPs a lípidos de membrana

La energía libre de unión (ΔG) de las zfCRPs a los diferentes lípidos se calculó utilizando AutoDock Vina [209] incluido en el paquete del programa PyRx [210]. Para la comparación de algunos datos experimentales, los valores de la constante de inhibición (Ki) fueron calculados a partir de los valores de ΔG mediante la fórmula: $Ki = \exp ([\Delta G * 1000] / [R * T])$ ($R = 1,98$ cal/mol, y $T=298$ °C) [211]. Las estructuras predichas se visualizaron en PyRx y/o PyMOL (<https://www.pymol.org/>).

17. ESTUDIO DE LA UNIÓN DE zfCRPs A LÍPIDOS

17.1. Unión en fase sólida

La unión de CRP1-7 (rCRPs y ssCRPs) a los lípidos se analizó en placas de 96 pocillos (Nunc, Maxisorb) modificando los métodos descritos anteriormente [212]. En primer lugar, en cada uno de los pocillos se inmovilizaron diferentes concentraciones de lípidos disueltos en etanol, que se dejaron secar hasta que estuvieron listos para su uso. Posteriormente, las placas se lavaron con 0,1 M de borato de sodio y 1 mM de CaCl₂ (pH 8) y se incubaron durante 2 h con 0,5 µg de rCRPs o ssCRP1-7 (diluidos 10 veces en el mismo tampón). Tras otro lavado, las zfCRPs unidas a los lípidos se detectaron mediante el anticuerpo anti-p3 e IgG anti-conejo de cabra conjugado con peroxidasa. Los niveles de

sustrato coloreado (o-fenilenodiamina, OPD) se midieron mediante espectrofotometría como se describió anteriormente [213, 214].

17.2. Análisis de secuencias de péptidos superpuestas (*Pepscan*)

Para evaluar el sitio de unión de las zfCRPs al 25-HOC, se realizaron ensayos de unión entre 25-HOC y péptidos sintéticos/*pepscan* (Quiron Mimotopes, Victoria, Australia) procedentes de la secuencia de zfCRP5. Estos péptidos de 15-mer se superponen 5 aminoácidos y tienen agregada una molécula de biotina en el amino terminal. Los ensayos de unión se realizaron siguiendo el protocolo descrito anteriormente. Brevemente, durante 60 min se incubaron 0,05 µg de cada péptido con 2 µg de 25-HOC inmovilizado previamente en las placas. Esta unión fue posteriormente detectada por la incubación durante 30 min de estreptavidina conjugada con peroxidasa y espectrofotometría.

Para predecir estas uniones *in silico*, los péptidos *pepscan* de CRP5 modelados con mejores valores por el programa Mobyle (<http://mobyle.rpbs.univ-parisdiderot.fr/cgi-bin/portal.py#forms::PEP-FOLD>) [215] se enfrentaron a todas las conformaciones posibles pronosticadas para 25-HOC.

18. EVALUACIÓN DEL EFECTO DE LA METIL- β -CICLODEXTRINA (M β CD) Y EL COLESTEROL (CH) SOBRE LA INFECCIÓN DE SVCV

Las monocapas de EPC tratadas durante 2 h con diferentes concentraciones (0–8 mM) de M β CD se incubaron con SVCV (MOI 10⁻²) durante 24 h (sección 13). El número de células infectadas se estimó por citometría de flujo tras su detección con el anticuerpo monoclonal anti-SVCV (BioX Diagnostics SA, Bélgica) y la IgG anti-ratón de cabra marcada con fluoresceína. Los resultados se expresaron como el porcentaje de infectividad de SVCV calculado por la siguiente fórmula: 100 × (ffu en tratamientos con M β CD / ffu en tratamientos sin M β CD). El efecto de 1 mM de M β CD y 0,5 y 1 mM de colesterol se analizó de manera similar. Además, en otro experimento se evaluó el efecto de 1 mM de M β CD con 0,5 o 1 mM de colesterol durante 2 horas a 22 °C.

Para analizar la viabilidad, las monocapas de EPC tratadas con M β CD (0–8 mM) se incubaron durante 3 h con 0,5 mg/mL bromuro de 3-(4,5-dimetiltiazol-2-il)-2,5-difeniltetrazol (MTT) diluido en un buffer a pH 7,4 (115 mM NaCl, 5 mM KCl, 1 mM KH₂PO₄, 1,2 mM MgSO₄, 2 mM CaCl₂ y 25 mM HEPES). La absorbancia medida a 570 nm

MATERIAL Y MÉTODOS

sirvió para calcular el porcentaje de viabilidad por la siguiente fórmula: $100 \times \text{absorbancia de células tratadas con M}\beta\text{CD} / \text{absorbancia de células no tratadas}$.

19. ANÁLISIS DEL EFECTO DEL 25-HOC SOBRE LA ACTIVIDAD ANTIVIRAL DE LAS zfCRPs

Para detectar los efectos de 25-HOC sobre la actividad de los ssCRP1-7 en la infección por SVCV, las monocapas de EPC se incubaron durante 20 h a 26 °C con ssCRP1-7 o ssGFP diluidos 4 veces en ausencia o presencia de 10 µM de 25-HOC. Tras el lavado del tratamiento, las células fueron infectadas con SVCV (MOI 0,01) durante 24 h y el número de células infectadas fue estimado por citometría de flujo. Los resultados de la preincubación de 25-HOC y ssCRPs se expresaron como porcentajes relativos de infección \pm 25-HOC calculados por la siguiente fórmula, $100 \times (\text{porcentaje de células EPC infectadas preincubadas con ssCRPs + 25-HOC} / \text{porcentaje de células EPC infectadas preincubadas con ssCRPs - 25-HOC})$.

20. ENSAYOS PARA LA DETERMINACIÓN DEL PAPEL DE LAS zfCRPs, 25-HOC, M β CD Y CH SOBRE LA AUTOFAGIA

20.1. Inmunofluorescencias

La primera evaluación del efecto de las zfCRPs, el 25-HOC y la M β CD sobre la autofagia se realizó *in vitro*. Las monocapas de ZF4 cultivadas al 80 % de confluencia en placas de 24 pocillos con cubreobjetos de vidrio de 12 mm se trataron con los siguientes compuestos en medios de infección durante 4 h: cloroquina (CQ, 25 µM), 25-HOC (10 µg/mL, que incluye etanol al 2,5%), Ch (10 µg/mL, que incluye etanol al 2,5%), SVCV (MOI 1), mix-ssCRP, mix-ssCRP+25-HOC, mix-ssCRP+SVCV, M β CD (4 mM), M β CD+SVCV. También se incluyeron células tratadas con ssGFP. Despues del tratamiento, las células se lavaron tres veces con medios de infección y se fijaron con formalina al 2 % durante 15 minutos a 4 °C. Tras tres lavados con PBS, las células se bloquearon con BSA al 1 % y Triton X-100 al 0,5 % (Sigma) (tampón de bloqueo) en PBS durante 1 h, se lavaron de nuevo y luego se incubaron durante la noche a 4 °C con una dilución de 1:200 del anticuerpo monoclonal anti-LC3B de ratón (NanoTools Antikörper Technik, Alemania). Despues del lavado, las células se incubaron con el anticuerpo secundario de cabra marcado con Alexa Fluor®488 anti IgG de ratón (dilución 1:500 en tampón de bloqueo) durante 1 h a temperatura

ambiente, y los núcleos se tiñeron con una solución de 4,6-diamido-2-fenilindol (DAPI) (0,1 µg/mL) (Molecular Probes-Life Technologies, Reino Unido) para la localización nuclear. Finalmente, las muestras de células se lavaron tres veces y se montaron utilizando ProLong AntifadeReagents (Life Technologies). Las imágenes confocales se capturaron utilizando un microscopio confocal TSC SPE y el software LAS AF (todos de Leica).

20.2. Determinación de autofagosomas intracelulares

La cuantificación de los autofagosomas se llevó a cabo mediante el análisis de las imágenes de inmunofluorescencia con el software ImageJ v1.52a (US National Institutes of Health, Bethesda, MD, EE.UU.). Para ello, la fluorescencia derivada de FITC de cada imagen, que se había convertido previamente a escala de grises, se midió aplicando un umbral de 1,2 %, que excluía el fondo y seleccionaba los puntos marcados fluorescentemente. Los núcleos teñidos con DAPI se contaron manualmente. Para cada tratamiento se analizaron tres imágenes por réplica y se representó la cantidad de autofagosomas por célula en comparación con el control (células no tratadas). Los datos se representan como la media y s.d. de tres experimentos independientes.

20.3. Ensayos *in vivo*

Para evaluar los efectos de las zfCRPs en el proceso autófágico *in vivo*, tres grupos de cinco peces cebra adultos se inyectaron por vía intraperitoneal con 5 µL de ssGFP o mix-ssCRPs. Dos días post-inyección, los órganos linfoides (bazo, hígado y riñón anterior) de cada pez fueron extraídos individualmente y sumergidos en RNAlater (Ambion, Austin, EE.UU.) donde se mantuvieron a -70 °C hasta su uso. Los niveles de expresión de genes relacionados con la autófagia fueron evaluados mediante RTqPCR como se describe en la sección 10. Los niveles de expresión génica en peces inyectados con la mix-ssCRPs se representaron en relación con los obtenidos con la inyección de ssGFP.

El estudio del efecto de las zfCRPs en la autófagia *in vivo* también incluyó la evaluación de los cambios en la distribución tisular de LC3 en larvas de pez cebra transgénicos (GFP-Lc3) ocasionados por la inyección de pMCV1.4-zfcrp1-4-5/il6. Este ensayo consistió en la microinyección de grupos de 30 embriones en etapa unicelular con 2 nL de PBS que contenía 150 pg de pMCV1.4, pMCV1.4-zfcrp1-4-5 o pMCV1.4-il6. Posteriormente, las larvas resultantes de tres días se anestesiaron con una solución de MS-222 al 0,05 % y se fotografiaron en una lupa de fluorescencia (microscopio AZ100, Nikon).

MATERIAL Y MÉTODOS

20.4. Ensayos funcionales *in vitro*

Se utilizaron M β CD, 25-HOC y mix-ssCRPs como consecuencia de sus propiedades anti-SVCV; CQ, 3-MA y rapamicina como moduladores de autofagia y N-acetilcisteína (NAC) como reductor de ROS. Sus soluciones madre (40 mM M β CD en PBS; 0,4 mg/mL 25-HOC en etanol; 0,1 M CQ en H₂O; 0,6 M NAC en H₂O; 0,2 M 3-MA en H₂O y 2 mM rapamicina en dimetilsulfóxido, DMSO) se almacenaron a -20 °C hasta su uso.

Para determinar que la actividad antiviral de las zfCRPs, M β CD y 25-HOC es consecuencia de una regulación de la autofagia, los porcentajes de infección obtenidos con el tratamiento de las células con cada uno de estos tres compuestos se compararon con los obtenidos en presencia de 3-MA, CQ, rapamicina y NAC. Brevemente, las monocapas de EPC se incubaron con 3-MA (0,5 mM y un gradiente de 0-1 mM, 20 h), CQ (25 μ M, 30 min), rapamicina (25 μ M, 4 h) o NAC (1 mM, 20 h) a 28°C. Después del período de incubación, las células se lavaron con medio de infección tres veces y luego se trataron durante 20 horas a 22 °C con: ssGFP, mix-ssCRPs, 4 mM M β CD o 10 μ g/mL 25-HOC. Posteriormente, estas monocapas se lavaron tres veces con medio de infección y se infectaron con SVCV (MOI 10⁻³), como se describió en la sección 13, para la posterior determinación del número de focos de infección.

21. ANÁLISIS ESTADÍSTICO

Los resultados de supervivencia representados por las curvas de Kaplan-Meier fueron analizados estadísticamente mediante la prueba log-Rank (Mantel-Cox), utilizando la función de análisis de supervivencia correspondiente del paquete de software de computadora OriginPro 2017. Este análisis comparó la supervivencia de las larvas sobre-expresoras de *zfcrp* con las sobre-expresoras de *gfp*. Los resultados de *microarray*, RTqPCR y neutralización se representaron como la media y s.d. de al menos 3 experimentos independientes. Para determinar sus diferencias significativas, los datos correspondientes se analizaron con GraphPad Prism 7 utilizando el análisis estadístico más apropiado en función del diseño experimental. A menos que indique lo contrario, las diferencias entre dos muestras se analizaron mediante la prueba t de Student y las diferencias entre grupos utilizando ANOVA. Las diferencias fueron estadísticamente significativas (*, a) cuando p ≤0,05, (**, b) cuando p ≤0,01 y (***, c) cuando p ≤0,001.

RESULTADOS

RESULTADOS

1. DESCRIPCIÓN DE LOS NIVELES DE EXPRESIÓN DE LAS *zfcrps* TRAS DIFERENTES ESTÍMULOS

Comenzamos los estudios de caracterización de la actividad de las zfCRPs analizando la expresión de estas moléculas a nivel constitutivo y en respuesta a diferentes estímulos patogénicos. Se analizaron los niveles de transcripción basal por RT-qPCR de las siete isoformas de zfCRPs en un conjunto de tejidos: riñón anterior, hígado, piel, branquias, intestino, músculo y bazo. Los resultados mostraron que las isoformas más expresadas basalmente son la 3, 4 y 5; y las que menos, la 1, 6 y 7 (**Fig. 1A, anexo 1**). Asimismo, cada tejido presentó un patrón de expresión de *zfcrps* diferente, ya que mientras la expresión principal en bazo es de *zfcrp3-5*, en branquias es de *zfcrp4* (**Tabla 1, P2; Fig. 1A, anexo 1**). Para estudiar si los niveles y el patrón de distribución basal de *zfcrp1-7* cambiaban tras una infección vírica, se analizaron los tránscritos de estas isoformas en los mismos tejidos tras 2 y 5 dpi con SVCV. Estos resultados mostraron que las isoformas más expresadas tras la infección seguían siendo 3, 4 y 5, alcanzándose los niveles más altos a los 5 dpi, coincidiendo con una mayor expresión de *n-SVCV* en los tejidos estudiados (**Fig. 1B, anexo 1**). No obstante, el resto de isoformas también se modularon. Esta tendencia, ya observada a 2 dpi, fue mucho más evidente a 5 dpi, cuando los niveles de tránscritos de *zfcrps* 3-7 aumentaron en la mayoría de los tejidos estudiados (**Fig. 1C, anexo 1**). Sin embargo, no todas las isoformas sufrieron la misma regulación tras la infección ya que, aparte de sobre-expresiones, las isoformas 4 y 5 aparecieron reprimidas significativamente en branquias y piel, respectivamente, a 2 dpi. Una represión que no se observó en ninguna isoforma a 5 dpi, que es cuando mayor cantidad de virus se detecta, salvo en la *zfcrp1*. En este caso, excepto en el hígado, el órgano que menor cantidad de *n-SVCV* expresó, la *zfcrp1* aparece reprimida en todos los tejidos estudiados, aunque no significativamente (**Fig. 1C, anexo 1**).

La sobre-expresión de *zfcrp2-7* tras la infección con SVCV se comprobó mediante el análisis transcripcional por *microarray* de estas isoformas en los órganos linfoides (riñón anterior y bazo) y en las aletas y piel adyacente de peces infectados y supervivientes a la infección. Este análisis mostró que la expresión de *zfcrp4/zfcrp7* en órganos linfoides y la de *zfcrp2/zfcrp4/zfcrp5* en aletas (**Fig. 2A, P2**) aumentaba ligeramente a 2 dpi con SVCV, especialmente la expresión de *zfcrp5* en aletas (~7 veces). De manera similar, los órganos linfoides y las aletas de los peces supervivientes tras un mes de la infección con SVCV sobre-expresaban *zfcrp2-5* y *zfcrp2-6*, respectivamente (**Fig. 2B, P2**).

RESULTADOS

El perfil transcripcional de las *zfcrps* también se estudió tras la infección con VHSV mediante *microarray*. Los resultados mostraron que, al igual que la infección con SVCV, el VHSV aumentaba los niveles de tránscritos de *zfcrps* en órganos internos a tiempos cortos después de la infección (2 dpi, VHSV+) (**Fig. 1, P2, barras rojas**). No obstante, la expresión de *zfcrp2-6* aparecía reprimida en los órganos internos de los supervivientes a dos meses de la infección con VHSV antes (VHSVS) y después de la re-infección con VHSV (VHSVS+) (**Fig. 1, P2, barras amarillas**). Esta represión de la expresión de *zfcrps* en órganos internos también se observó en los mutantes *rag1-/-* (carentes de sistema inmune adaptativo), que presentan constitutivamente niveles de expresión de *zfcrps* menores que los observados en los peces *wild type* (**Fig. 3, P2**). No obstante, a diferencia de lo ocurrido tras la infección de los supervivientes a VHSV, la infección de los mutantes *rag1-/-* con SVCV aumentó la expresión de todas las isoformas de *zfcrp* salvo la 4 y la 7, de hecho, la expresión de *zfcrp4* siguió reprimida (**Fig. 3, P2**).

Aparte de la infección vírica, existen otros estímulos que pueden conducir a un aumento de la expresión de las *zfcrps*. Este es el caso de la infección bacteriana con *A. hydrophila* y *V. fluvialis* que, de acuerdo con los resultados de *microarray*, a 5 meses post-infección aumenta la expresión de *zfcrp2-6* en los órganos internos de los peces (**Fig. 1, P2, barras azules**). Asimismo, la sobre-expresión de *il6* en larvas de pez cebra, debido a la microinyección de pMCV1.4-*zfil6* en estado embrionario de una sola célula, indujo la expresión de *zfcrp4-5* (**Fig. 6B, P2**). Estos resultados sugieren: **a)** que al igual que las CRPs de mamíferos, las zfCRPs podrían tener actividad antibacteriana, **b)** que la *il6*, el mayor inductor de la síntesis de CRP en mamíferos [216], también es responsable de la estimulación de algunas isoformas de zfCRPs y **c)** que algunas zfCRPs podrían comportarse como proteínas de fase aguda ya que la IL6 está involucrada en la activación de la respuesta inflamatoria aguda frente a la infección vírica [217, 218].

Con el fin de determinar si las zfCRPs actuaban como proteínas de fase aguda, se realizó un análisis proteómico para evaluar los niveles de CRP en el plasma sanguíneo de peces cebra infectados con SVCV a diferentes tiempos. Los resultados de este estudio revelaron un aumento significativo de todas las zfCRPs (~1,5-3 veces) salvo de la CRP7 a 24 hpi, siendo este aumento mayor para las isoformas 2 y 5. Asimismo, a 48 hpi sólo había más CRP2 en los peces infectados que en los peces control. Tras 5 dpi, los niveles de todas las zfCRPs eran inferiores a los observados a tiempo 0 (**Fig. 4, P2**).

2. EVALUACIÓN DE LA ACTIVIDAD ANTIVIRAL DE LAS zfCRPs

El aumento de tránscritos de zfCRPs tras infecciones víricas sugiere una función antiviral de estas proteínas. Para evaluar esta actividad, en la presente tesis se utilizaron: **a)** células transfectadas con plásmidos de expresión (pMCV1.4-*zfcrp1-7*); **b)** células tratadas con sobrenadantes enriquecidos con zfCRPs (ssCRPs) procedentes de células EPC transfectadas con los pMCV1.4-*zfcrp1-7*, ya que las zfCRPs son proteínas que se secretan al medio y **c)** proteínas recombinantes producidas en insecto (rCRPs). Sin embargo, como las rCRPs no mostraron ni actividad antibacteriana ni antiviral, probablemente por la ausencia de modificaciones post-traduccionales esenciales para su actividad como se ha visto en los ssCRPs (**Fig. 6D, P3**), finalmente su uso se limitó a control en los ensayos de caracterización de los ssCRPs y de afinidad a lípidos.

2.1. Caracterización de los sobrenadantes enriquecidos con zfCRPs (ssCRPs)

Previamente a la evaluación de las actividades de las zfCRPs, se realizó una caracterización de los ssCRPs. Esta caracterización incluyó: **a)** la cuantificación de tránscritos de *zfcrp* por RT-qPCR en células transfectadas con pMCV1.4-*zfcrp1-7*, **b)** la detección de zfCRPs en los ssCRP por *western-blot* y *dot-blot* y **c)** la determinación del estado de oligomerización de las zfCRPs presentes en los ssCRPs.

La cuantificación de tránscritos de *zfcrp* por RT-qPCR en las células transfectadas con pMCV1.4-*zfcrp1-7* demostró la sobre-expresión de todas las isoformas de *zfcrp* con respecto a las células transfectadas con pMCV1.4-*gfp*. Asimismo, como los niveles de expresión fueron similares para todas las isoformas, la eficiencia de transfección de cada una de ellas se consideró comparable (**Fig. S1A, P2**). Una vez comprobada la transfección de todas las *zfcrps*, se procedió a la identificación de cada una de las isoformas en los ssCRPs. Los ensayos de *western blot* detectaron todas las isoformas salvo la 1 (**Fig. 6D, P3**). No obstante, como esta isoforma sí estaba sobre-expresada en las células transfectadas con pMCV1.4-*zfcrp1* de las que procedían los ssCRPs, la no localización de CRP1 fue asociada a la incapacidad de detección de esta isoforma por el anticuerpo utilizado. Esta hipótesis concuerda con el hecho de que el anticuerpo utilizado (anti-p3) identifique una secuencia (¹³⁰SGGTVVVLGQDPDSYVGSF¹⁴⁷) muy conservada en todas las zfCRPs salvo en la 1 que presenta 7 sustituciones (¹²⁹PQGTALLGQDPDKLLGDFE¹⁴⁷). La zfCRP1 fue finalmente identificada por *dot blot* utilizando un anticuerpo diferente (anti-p2) que reconoce otra secuencia también muy conservada entre las zfCRPs (¹⁸⁹DWDTIEYDVTGN²⁰⁰) (**Fig. S1B, P2**).

RESULTADOS

Estos estudios no sólo demostraron la presencia de zfCRPs en los ssCRPs que se utilizarán a lo largo de esta tesis, también revelaron cambios en la masa molecular esperada (~25 kDa) para las zfCRPs. Estos cambios incluyeron tanto incrementos en CRP4, CRP6 y CRP7 como reducciones en CRP2 y CRP3 (**Fig. 6D, P3**).

Los estudios realizados para conocer el estado de oligomerización de las rCRPs y de las zfCRPs presentes en los ssCRPs se llevaron a cabo mediante electroforesis en gel de poliacrilamida (PAGE). Como las condiciones nativas de esta técnica excluyen el dodecilsulfato sódico (SDS), no se pudo determinar el peso molecular de las CRPs con precisión. Sin embargo, las diferencias observadas entre los pesos moleculares de las rCRPs, que coincidían con la predicción bioinformática de la estructura tridimensional de las zfCRPs, dieron una idea de las posibles conformaciones de las proteínas con las que estábamos trabajando.

En ausencia de SDS, la migración de las proteínas sometidas a un campo eléctrico depende de su carga y no de su peso molecular. Por ello, rCRP5 y rCRP7, que tienen el mismo punto isoeléctrico (PI=4,6), presentan un peso molecular aparente diferente al de rCRP2 que tiene un PI mayor (6,35) (**Fig. 6A izquierda, P3**). Sin embargo, la comparación de la migración de estas tres proteínas tras un tratamiento breve en condiciones desnaturalizantes (calor, SDS y β -mercaptoetanol) reveló tamaños más grandes para rCRP2 y rCRP5 que para rCRP7 (**Fig. 6A derecha, P3**). Aun así, no se pudo estimar el peso molecular de las rCRPs dado que estas condiciones siguen siendo imprecisas al excluir el SDS del tampón.

La migración de las rCRPs bajo condiciones nativas (sin calor, sin SDS, sin β -mercaptoetanol) pero con la inclusión de SDS en los tampones mostró diferentes bandas a ~75, ~50 y ~25 kDa, que se interpretaron como trímeros, dímeros y monómeros de zfCRP, respectivamente (**Fig. 6B izquierda, P3**). Sin embargo, en estas condiciones, cuando las proteínas fueron sometidas a un tratamiento desnaturalizante breve, el número de monómeros aumentó, especialmente en el caso de rCRP7 que no mostró bandas con pesos moleculares superiores a 25 kDa (**Fig. 6B derecha, P3**). Finalmente, sólo en condiciones completamente desnaturalizantes las tres rCRPs mostraron un peso molecular similar (~25 kDa) (**Fig. 6A derecha, P3**), a diferencia de las zfCRPs presentes en los ssCRPs que se detectaron como monómeros en todos los casos (condiciones nativas, desnaturalizantes breves y completamente desnaturalizantes) (**Fig. 6C, P3**).

Todos estos resultados parecen indicar **a)** que mientras rCRP2 y rCRP5 existen en equilibrio entre trímeros, dímeros y monómeros, rCRP7 tiende a formar exclusivamente monómeros y **b)** que las zfCRPs son secretadas al medio de las células EPC transfectadas principalmente como monómeros. Estos resultados concuerdan con las predicciones tridimensionales de las estructuras de las zfCRPs realizadas mediante SWISS-MODEL, que revelan la estructura de todas las isoformas de CRP como monómeros, salvo la de la CRP2 y la del 97,8% de las variantes transcripcionales de CRP5, que se modelan como trímeros (**Tabla 2, P3**).

2.2. Actividad antiviral de las zfCRPs

La evaluación de las propiedades antivirales de las zfCRPs se realizó en primer lugar *in vitro*, en la línea celular EPC y utilizando SVCV, uno de los virus cuya infección incrementaba los niveles de tránscritos de *zfcrps* en los diferentes tejidos de pez cebra. Estos experimentos demostraron que tanto la transfección de las células con pMCV1.4-*zfcrp2-7* como su tratamiento con ssCRP2-7 (previo a la infección) neutralizaban la infección de SVCV (**Fig. 5, P2**). Con el objetivo de identificar la etapa del ciclo viral en la que los ssCRPs ejercían la actividad neutralizante, y si tal actividad era consecuencia de una interacción directa con las partículas víricas, los ssCRPs fueron introducidos en diferentes puntos críticos del ciclo vírico de SVCV: antes, durante y después de la adsorción del virus (**diagramas Fig. 1, P4**). Cuando las células (**Fig. 1A, P4**) o el virus (**Fig. 1B, P4**) fueron tratados con los ssCRPs antes de la adsorción, se observaron actividades inhibitorias significativas (47,1-76,2 %) en todos los casos a excepción de los tratamientos con ssCRP1 (**Fig. 1A-B, P4**) y el tratamiento de 2 h de SVCV con ssCRP7 (**Fig. 1B, P4**). Los tratamientos que se limitaron a la adsorción también mostraron porcentajes de neutralización altos, que fueron significativos en el caso de las isoformas 2, 4 y 5 ($55,6 \pm 11,8\%$, $54,2 \pm 6,2\%$ y $46,6 \pm 16,3\%$, respectivamente) (**Fig. 1C, P4**) y similares, salvo en el caso de los ssCRP3/6/7, a los obtenidos tras la incubación de los ssCRPs con SVCV previamente a la infección (**Fig. 1B, P4**). Este resultado demostró la baja intervención de la interacción directa de los ssCRPs sobre las partículas víricas. Por otro lado, al contrario de lo ocurrido en los tratamientos previos a la adsorción, la duración del tratamiento sí afectó a la actividad inhibitoria de los ssCRP2-7 cuando fueron administrados en etapas posteriores a la adsorción. El efecto neutralizante aumentó significativamente cuando los tratamientos duraron 20 h (52,3-84,2 %) en comparación con los tratamientos de 2 h (12,1-27,7 %), que no inducían una neutralización significativa (**Fig. 1D, P4**).

RESULTADOS

Para comprobar que la actividad antiviral de los sobrenadantes se debía realmente a las zfCRPs y no al efecto de los lipopolisacáridos de *E. coli* remanentes en las preparaciones de los plásmidos, se comprobó si la incubación de LPS durante 2 h en las monocapas de EPC tenía efecto antiviral. Los resultados muestran que el LPS no neutralizó la infección de SVCV a la mayor concentración utilizada (500 ng/100 μ l) (**Fig. S2, P2**), que fue ~1000 veces más alta que la esperada en los plásmidos de acuerdo con la estimación del fabricante del kit de purificación.

Asimismo se verificó que todos los ssCRPs, a excepción de los ssCRP7, perdían capacidad neutralizante cuando las zfCRPs eran retiradas del medio por unión a 25-hidroxicolesiterol (25-HOC) en fase sólida (**Fig. S1, P4**), un lípido por el que las zfCRPs presentan alta afinidad ($\Delta G \sim -9$ Kcal/mol) (**Fig. 2, P3**). A nivel individual, tras la unión a 25-HOC, los ssCRP3/5 redujeron su capacidad antiviral hasta niveles de neutralización no significativos y los ssCRP2/4/6 mantuvieron una actividad neutralizante pero significativamente menor a sus controles no tratados con 25-HOC (**Fig. S1, P4**).

Una vez comprobada que la actividad antiviral observada *in vitro* era al menos en parte consecuencia de las zfCRPs, con el objetivo de constatar esta actividad *in vivo*, se microinyectaron 150 pg de plásmidos pMCV1.4-zfcrp2-5 en embriones de pez cebra en estado de una sola célula. Tres días después, cada larva eclosionada fue infectada con 10⁴ pfu de SVCV también por microinyección y sus mortalidades fueron monitorizadas diariamente durante 7 días. Las supervivencias acumuladas obtenidas fueron mayores en los grupos de peces injectados con los plásmidos pMCV1.4-zfcrp2-5 (~ 18, 12, 24 y 32 %, respectivamente) que en los injectados con pMCV1.4-gfp (0 %) (**Fig. 6A, P2**). Estos resultados corroboraron que las zfCRPs ofrecían protección frente al desafío con SVCV.

Las evidencias presentadas en los apartados 1 y 2 de esta sección apuntan a una actividad antiviral de las zfCRPs. Pese a que la actividad antibacteriana de las CRPs está ampliamente descrita, ésta es la primera vez que se describe una actividad antiviral *in vitro* e *in vivo* de esta proteína. Debido al carácter novedoso de este descubrimiento, los dos siguientes apartados de la tesis se centran en esclarecer el mecanismo de acción por el cual las zfCRPs protegen frente a la infección por SVCV.

3. ANÁLISIS DE LA AFINIDAD DE LAS zfCRPs A LÍPIDOS

Los resultados descritos en el apartado anterior definen la incubación de las monocapas de EPC con los ssCRPs durante 2 h antes de la infección como el tratamiento óptimo para inhibir la infección vírica. Este resultado sugiere que las zfCRPs actúan sobre las células para inhibir alguno de los pasos del proceso de entrada del virus. Dado que esta inhibición podría estar mediada por la afinidad de las zfCRPs a lípidos de membrana, como se ha reportado anteriormente con la hCRP [164, 219], se realizaron estudios para analizar la afinidad de las zfCRPs a diferentes lípidos. Entre los diferentes lípidos se incluyó el colesterol debido a la preferencia de determinados rabdovirus por las balsas lipídicas (*lipid rafts*) para su entrada [220].

En primer lugar se realizó una predicción de las energías libres de unión (ΔG) de zfCRP1-7 a una selección de lípidos que incluía, entre otros, la PC y el colesterol (Ch) debido a su interacción con la hCRP [111, 221-223]. Curiosamente, las menores ΔG fueron predichas para la unión de CRPs a Ch (ΔG de ~-7,5 a -9 Kcal/mol) mientras que las mayores, fueron para la unión a PC (ΔG de ~-4 a -5 Kcal/mol) (Fig. 1A, P3), el ligando prototípico de las CRPs de mamíferos [216]. Estos resultados no sólo revelan una alta afinidad de las zfCRPs a los Chs, también predicen una independencia de Ca^{2+} en esta unión ya que los valores de ΔG no mejoran en presencia de este catión (Tabla S1, P3).

Dado que las predicciones mostraban una alta afinidad de las zfCRPs por el Ch, los siguientes estudios centraron sus esfuerzos en predecir la energía libre de unión de las zfCRPs a un conjunto de 26 compuestos fisiológicos estructuralmente relacionados con el Ch. En este caso, las menores ΔG fueron obtenidas con los hidroxicoles (entre -7,5 y -9,3 Kcal/mol) independientemente de la presencia o no de Ca^{2+} (Fig. 2 y Tabla S2, P3). La unión de las zfCRPs a los hidroxicoles fue comprobada *in vitro* mediante ELISA. En estos ensayos de unión, se compararon las afinidades de las zfCRPs a la PC, el Ch y el 25-hidroxicoles (25-HOC), un hidroxicoles cuya actividad antiviral ha sido descrita previamente [205] y, por tanto, podría estar relacionado con la actividad antiviral de las zfCRPs. Los primeros ensayos de unión se realizaron con las rCRPs y, tras verificar que las rCRPs presentaban mayor afinidad por el Ch y por el 25-HOC que por la PC (Fig. 3A, P3), se comprobó si los distintos ssCRPs también se unían al 25-HOC. Estos últimos resultados mostraron que los ssCRPs se unen al 25-HOC con diferentes perfiles dependientes de concentración. Concretamente, el ssCRP1 y el ssCRP7 fueron en este sentido el más y el menos activo, respectivamente, a las concentraciones más bajas de 25-HOC analizadas (<10

RESULTADOS

μM). Por otro lado, a las concentraciones más altas estudiadas, la afinidad por el 25-HOC fue similar para todas las isoformas (**Fig. 3B** y **Tabla S4, P3**).

Para ampliar el conocimiento de la unión de las zfCRPs al 25-HOC, se intentó identificar la región de las zfCRPs responsable de esta unión mediante la evaluación de la interacción de péptidos de 15 aa de CRP5 con 25-HOC en fase sólida (*pepscan*). Esta aproximación identificó cuatro posibles regiones de unión a 25-HOC entre los aa ~30-50, 70-90, 110-150 y 170-190 (**Fig. 4A, línea negra, P3**), que coincidieron con las posiciones predichas *in silico* (**Fig. 4A, línea azul, P3**). De estas cuatro regiones identificadas, sólo la de la posición 30-50 estaba en una región similar a la del péptido 35-47 identificado previamente en hCRP como el principal dominio de unión a Ch [224]. Finalmente, se utilizó el software PyMol para localizar la interacción de 25-HOC con las estructuras tridimensionales de zfCRP1-7. Estos estudios revelaron un acoplamiento del 25-HOC a la superficie de la estructura CRP5 con ΔG entre -7,5 y -8,4 Kcal/mol (algunas de las posiciones de contacto son T41, E48, R71, F84, F85, S117) (**Fig. 4B, CRP5, P3**). Por el contrario, el 25-HOC se unió a otras regiones en el resto de las isoformas con ΔG entre -8,6 y -9,1 Kcal/mol (algunas de las posiciones de contacto para CRP1 son R113, S115, G153, E154, Y161 y E206) (**Fig. 4B, CRP1, P3**). Tanto los valores de ΔG obtenidos como las ubicaciones de acoplamiento para mCRP5 y tCRP5 fueron similares (**Tabla S5, P3**).

Hasta ahora se ha comprobado que las zfCRPs se unen con mayor afinidad a los Chs que al resto de lípidos. Sin embargo, para que esta interacción sea el desencadenante de la neutralización del SVCV tendría que **a)** impedir la entrada del virus a la célula (*binding*) o **b)** inducir una respuesta inmune capaz de inhibir la infección. Se ha descrito que algunos virus envueltos necesitan interaccionar con las balsas lipídicas de la superficie celular para entrar de manera eficiente en la célula [224, 225]; si este fuese el caso del SVCV, la unión de las zfCRPs al colesterol presente en las balsas lipídicas como consecuencia de la preincubación de las células con los ssCRPs, podría estar impidiendo la posterior unión del SVCV a la célula y, por tanto, la infección. Por ello, los siguientes ensayos consistieron en determinar la posible función del Ch en la infección del SVCV.

El secuestro del Ch mediante la incubación de las monocapas de EPC con concentraciones crecientes de metil- β -cyclodextrina (M β CD) (0,5 a 8 mM) durante 2 h disminuyó un 80 % la infectividad del SVCV (**Fig. 1B, P3**). Este resultado confirma la necesidad de Ch en las membranas celulares para la infección de SVCV y, por tanto, sugiere que las zfCRPs podrían estar interfiriendo en el *binding* del SVCV a la célula.

Por otra parte, como se ha demostrado una actividad independiente contra el SVCV tanto del 25-HOC [205] como de las zfCRPs y una alta afinidad de las zfCRPs por este hidroxicolesterol, se quiso comprobar el efecto de la combinación de ambos tratamientos. Los resultados mostraron que el efecto anti-SVCV del 25-HOC era mejor en presencia de ssCRPs (**Fig. 5, P3**). La combinación de 25-HOC con todas las isoformas de zfCRPs redujo significativamente la infección de SVCV en comparación con sus tratamientos por separado. Concretamente la combinación con las isoformas 4, 5 y 7 redujo la infección a más de la mitad.

4. DETERMINACIÓN DEL MECANISMO ANTIVIRAL DE LAS zfCRPs

El último objetivo de esta tesis es determinar el mecanismo por el cual las zfCRPs protegen frente a la infección por SVCV. Los resultados procedentes de la introducción de los ssCRPs en las diferentes fases del ciclo de replicación de SVCV revelaron que el efecto de los ssCRPs se producía en alguna etapa temprana (**Fig. 1, P4**). Las etapas iniciales del ciclo de replicación de los rabdovirus comprenden, secuencialmente: a) la unión de la proteína G de la superficie de los rabdovirus a un receptor celular de membrana (*binding*), b) la internalización por endocitosis y c) la fusión de la membrana vírica con los endosomas del huésped para liberar el genoma vírico al citoplasma [226].

Debido a la alta afinidad de las zfCRPs por el Ch y a la necesidad de Ch en las membranas celulares para que la infección de SVCV sea posible, la primera hipótesis que se barajó fue la interferencia de los ssCRPs con la entrada (procesos de *binding* y fusión) del virus. Sin embargo, la incubación de las células con SVCV (MOI 1) junto con cualquier ssCRP durante el periodo de adsorción (2 h a 4 °C) no modificó la cantidad de partículas víricas unidas a la superficie celular, cuantificadas a partir del número copias del gen *n*-SVCV por RT-qPCR (**Fig. 2A, P4**). Asimismo, en general, los ssCRPs tampoco modificaron la capacidad de fusión dependiente de pH de la proteína G, como refleja la ausencia de cambios en la cantidad de sincitios inducidos en las células infectadas. Sólo el ssCRP7 redujo la capacidad de fusión de la proteína G en ~20 % (**Fig. 2B, P4**).

Aunque estos últimos ensayos demuestran que los ssCRPs no alteran la entrada del virus (**Fig. 2A-B, P4**), el seguimiento de la infección durante las primeras horas post-adsorción evidencia que el pretratamiento de las células durante 2 h con una mezcla de ssCRPs reduce la transcripción de la *n* y *g* de SVCV, cuantificadas por RT-qPCR, a las 4 h post-adsorción (**Fig. 2C, P4**). Por tanto, los ssCRPs inhiben la infección de SVCV en una

RESULTADOS

etapa temprana de la replicación del virus. Considerando este resultado, se procedió a comprobar una segunda hipótesis: si la incubación de los ssCRPs era capaz de inducir en la célula una respuesta inmune antiviral. Esta respuesta inmune podría ser del sistema de interferón, una de las principales frente a virus [227, 228]. Sin embargo, la incubación de las monocapas de EPC con los ssCRPs durante 2 h no aumentó los niveles de tránscritos de *mx* (gen estimulado por interferón) cuantificados por RT-qPCR a las 20 h post-retirada del tratamiento (**Fig. 2D, P4**). Del mismo modo, la incubación con ssCRPs tampoco indujo la secreción de ningún factor antiviral al medio, ya que los medios condicionados procedentes de células tratadas con ssCRP1-7 no confirieron actividad antiviral a otras células (**Fig. 2E, P4**).

Hasta ahora, todos los ensayos se han realizado en EPC, una línea celular muy empleada en la investigación de enfermedades de peces [229] y susceptible a SVCV [230]. No obstante, como las CRPs con las que se hicieron las construcciones son de pez cebra y existe una mayor disponibilidad de herramientas moleculares para esta especie, se empezó a trabajar con una línea celular procedente de este organismo, la ZF4. Los ensayos antivirales con los ssCRPs en ZF4 demostraron que la incubación de las monocapas durante 2 h antes de la infección con cualquier ssCRPs (salvo ssCRP1 y ssCRP6) o la mezcla de todos ellos (mix-ssCRPs, que no incluye ssCRP1 ni ssCRP7) neutralizaba el SVCV (**Fig. 3A, P4**).

El análisis de la progresión de la replicación vírica en ZF4 en las etapas tempranas posteriores a la adsorción (**Fig. 3B, P4**) mostró un perfil análogo al observado anteriormente en EPC (**Fig. 2C, P4**), es decir, inhibiciones significativas de ≥ 2 veces a partir de 4 h post-adsorción. Además, en consonancia con los datos obtenidos en EPC, la mix-ssCRPs tampoco activó la respuesta de IFN en ZF4, ya que el análisis transcripcional reveló una reducción significativa de los niveles de *mxa* desde el inicio ($t=0$ h) del tratamiento de las células durante 2 h ($p < 0,01$) y de los niveles de *mxe* a 4 h post-tratamiento ($p < 0,05$) (**Fig. 3C, P4**). Los niveles de tránscritos de los genes que codifican zfIFN β 1 y 2 también se analizaron en esta línea celular. No obstante, pese a aparecer diferencias a partir de la 5^o hora post-tratamiento (**Fig. S2, P4**), los niveles de tránscritos de *ifn* no alcanzaron aumentos >2 veces y, por tanto, no se consideraron representativos de esta respuesta, ni causantes de la protección antiviral observada, ya que los niveles de expresión de estos genes suelen ser mucho mayores, de hasta más de 1000 veces [231].

La neutralización de la replicación de SVCV observada a partir de la 4^a hora post-adsorción debe ser consecuencia de la activación de algún otro mecanismo celular. Como se ha descrito que algunos rabdovirus como SVCV, VHSV y SHVV (*Snakehead vesiculovirus*)

modulan la autofagia [232, 233], se decidió comprobar si la neutralización generada por los ssCRPs involucraba la regulación de este mecanismo. En este sentido, la expresión de tránscritos obtenida tras el tratamiento de 2 h de las células con la mix-ssCRPs reveló la estimulación algunos genes relevantes en este proceso. Particularmente, el tratamiento con la mix-ssCRPs moduló los niveles de *wipi1* (> 2 veces a 2 h), de *ambra1* ($> 2,5$ veces a 2 h) y de *lc3a* (1,5-2 veces a 3-5 h) (Fig. 3D, P4). Estos niveles transcripcionales comenzaron a estabilizarse a las 5 h post-tratamiento y se re-establecieron completamente a las 20 h, excepto en el caso de *lc3a* que mostró una reducción significativa (~2 veces) (Fig. 3D, P4). Esta misma modulación se observó en tejidos relevantes del sistema inmune (bazo, hígado y riñón anterior) de peces cebra inyectados i.p. con la mix-ssCRPs a 2 días post-inyección (Fig. 3E, P4).

Adicionalmente al estudio transcripcional, la modulación de la autofagia se analizó a nivel proteico. En circunstancias normales LC3B-I se distribuye uniformemente en las células, por lo que aparece un patrón difuso, pero cuando se activa la autofagia, LC3B-I se convierte en LC3B-II y forma agregados. Por tanto, para establecer si existe o no una regulación de la autofagia como consecuencia del tratamiento con la mix-ssCRPs, la cuantificación de estos agregados es determinante. Los resultados de la cuantificación de puntos de LC3 (en verde) mostraron que el tratamiento de las células con la mix-ssCRPs aumentaba de manera significativa el número de autofagosomas ($2,3 \pm 0,6$ veces) (Fig. 4A, P4), al igual que el tratamiento con CQ (Fig. 6A, P4). Conviene recordar que la CQ es un agente inhibidor de la autofagia que actúa bloqueando la fusión del autofagosoma con el lisosoma, lo cual se refleja en una acumulación de vesículas marcadas con LC3 [234].

La regulación de la autofagia producida por las zfCRPs también se estudió *in vivo* a nivel proteico. Para ello se visualizó la expresión de Lc3 en larvas de pez cebra transgénico con expresión de GFP-Lc3 que fueron microinyectadas, en etapa embrionaria de una sola célula, con pMCV1.4-zfcrp1/4/5 o pMCV1.4-zfil6. Las imágenes mostraron que la sobreexpresión recombinante de *zfcrps* aumentaba la fluorescencia de las larvas, especialmente en el saco vitelino (Fig. 4B, P4). Entre los genes de *zfcrps* analizados, la sobreexpresión de *zfcrp5* indujo más este efecto; sin embargo, la sobreexpresión de *zfil6* (citoquina estimuladora de la expresión de *crps*) causó incluso una fluorescencia mayor. En estos dos casos también se pudo detectar una mayor agregación de Lc3 definiendo los ganglios de la raíz dorsal (Fig. 4B, P4).

Todos los resultados anteriores sugieren que las zfCRPs son capaces de inducir un estado antiviral como consecuencia de la regulación de la autofagia. Sin embargo, si

RESULTADOS

la infección con SVCV activa la autofagia como describen otros autores [71, 232, 235], estos resultados no son tan fáciles de interpretar. Por ello, también se analizó la acumulación de agregados de LC3 *in vitro* en respuesta a SVCV en presencia y ausencia de la mix-ssCRPs (**Fig. 5A, P4**). De acuerdo con nuestros resultados, el tratamiento de las células ZF4 con SVCV (MOI 1) durante 4 h no moduló el flujo autofágico ($0,7 \pm 0,1$ veces) en comparación con las células control tratadas con ssGFP ($1,0 \pm 0,3$ veces). Sin embargo, este mismo tratamiento en combinación con la mix-ssCRPs sí aumentó significativamente la formación de autofagosomas ($2,6 \pm 1,1$ veces, $p < 0,05$). Este último aumento fue similar al obtenido al tratar las células con la mix-ssCRPs sola ($2,3 \pm 0,6$) (**Fig. 4A, P4**).

El análisis transcripcional *in vitro* en las etapas tempranas de la infección (0-5 h post-adsorción) reveló que, en comparación con los resultados obtenidos con la mix-ssCRPs sola (**Fig. 3D, P4**), la adición del virus retrasaba 2 h la modulación transcripcional de genes relacionados con la autofagia provocada por la mix-ssCRPs (**Fig 5B, P4**). No obstante, este retraso transcripcional aumentó significativamente los niveles de transcripción de *wipi1* ($3,5 \pm 1,1$ veces a las 4 h y $4,9 \pm 1,1$ veces a las 5 h) y *atg5* ($4,0 \pm 0,6$ veces a las 5 h) en comparación con los obtenidos tras el tratamiento con la mix-ssCRPs sola. En el caso de *lc3a*, sus niveles ya fueron significativos a las 3 h post-adsorción ($1,9 \pm 0,6$ veces) y permanecieron altos hasta el final del periodo analizado ($2,0 \pm 0,3$ veces a las 4 h; $2,4 \pm 0,2$ veces a las 5 h).

En consonancia con estos resultados, en las células infectadas con SVCV en ausencia de la mix-ssCRPs no se observó ningún incremento transcripcional a ningún tiempo post-adsorción estudiado (0-5 h) sino que por el contrario, se observaron reducciones significativas en la expresión de *wipi1* y *lc3a* a 0 h (~2 veces) (**Fig. S4, P4**).

Como se explica más detalladamente en la discusión, aunque los resultados transcripcionales obtenidos podrían sugerir que las zfCRPs estuviesen induciendo la autofagia, los estudios funcionales revelan lo contrario. En este contexto, la **Fig. 5C, P4** muestra que el tratamiento de las células ZF4 con 3-MA, un bloqueador de la autofagia [236], previo a la infección inhibe la replicación de SVCV, alcanzando los máximos niveles de neutralización ($87,4 \pm 1,6\%$) a la mayor concentración utilizada (1 mM durante 20 h). Por tanto, nuestros resultados confirman la necesidad del proceso autofágico para la replicación de SVCV. Para confirmar que los ssCRPs ejercen un efecto inhibitorio sobre la autofagia, se realizaron ensayos con ssCRPs en combinación con algunos moduladores de la autofagia: bloqueadores como 3-MA y CQ y activadores como la rapamicina. Como se había

demostrado anteriormente (**Fig. 5C, P4**), el tratamiento con los bloqueadores neutralizó la infectividad de SVCV, siendo esta neutralización mayor en combinación con la mix-ssCRPs (**Fig. 5D, P4**). Por otro lado, el tratamiento con rapamicina no sólo favoreció la replicación del virus, sino que también revirtió parte del efecto neutralizante de la mix-ssCRPs (~20 %) (**Fig. 5D, P4**).

5. IMPLICACIÓN DEL COLESTEROL EN LA ACCIÓN ANTIVIRAL DE LAS zfCRPs.

Dada la relación funcional de las zfCRPs con la M β CD (ambas unen Ch) y con el 25-HOC (sus actividades antivirales son sumatorias) y tras comprobar que la inhibición de la autofagia estaba implicada en el mecanismo antiviral de las zfCRPs, se estudió si la actividad antiviral de estos dos compuestos también era consecuencia de un bloqueo de este mecanismo. Este estudio siguió la misma línea experimental que los realizados para determinar el mecanismo antiviral de las zfCRPs. Como muestra la **Fig. 6B, P4**, el análisis de la distribución de LC3 en ZF4 en respuesta al tratamiento durante 4 h con 25-HOC (10 μ g/mL) o M β CD (4 mM) no reveló acumulación de autofagosomas en comparación con las células control ($0,9 \pm 0,2$ veces para 25-HOC y $1,2 \pm 0,2$ veces para M β CD). No obstante, cuando estos tratamientos eran aplicados en combinación con la mix-ssCRPs, la cuantificación de autofagosomas aumentaba significativamente en comparación con cualquiera de los tratamientos individuales ($16,1 \pm 2,8$ veces para 25-HOC + mix-ssCRPs y $7,3 \pm 1,4$ veces para M β CD + mix-ssCRPs). Asimismo, los ensayos de neutralización de SVCV realizados con 25-HOC o M β CD en combinación con los reguladores de autofagia mostraron: **a**) que las combinaciones de ambos compuestos con cualquier bloqueador (3-MA o CQ) aumentaban la actividad antiviral y **b**) que las combinaciones con el inductor (rapamicina) revertían la neutralización (**Fig. 6C, P4**). El tratamiento con NAC, un secuestrador de ROS, pese a no afectar a la replicación de SVCV, revirtió significativamente la neutralización ejercida tanto por la mix-ssCRPs como por el 25-HOC y la M β CD (~50%) (**Fig. 6D, P4**).

Pensando que el efecto antiviral de estos compuestos podría ser consecuencia de un desequilibrio en la concentración de Ch celular, se comprobó si la adición de Ch ($C_{27}H_{46}O$) también regulaba la autofagia. El tratamiento de las monocapas de ZF4 con 10 μ g/mL de Ch indujo significativamente la acumulación de agregados de LC3 (**Fig. S5A, P4**). Asimismo, el tratamiento de ZF4 con 0,5 o 1 mM de Ch durante 2 h neutralizó la infección con SVCV. Esta

RESULTADOS

neutralización se redujo cuando el tratamiento de Ch se realizó en combinación con 0,5 mM de M β CD, su agente secuestrante (**Fig. S5B, P4**).



DISCUSIÓN

DISCUSIÓN

1. REGULACIÓN DE LA EXPRESIÓN GÉNICA DE LAS PENTRAXINAS CORTAS DE PECES ANTE DIFERENTES ESTÍMULOS

Basándonos en nuestros resultados, las siete isoformas de *zfcrps* se expresan constitutivamente en todos los tejidos estudiados, demostrando una producción extrahepática generalizada de *crps* en peces, que también parece ocurrir en menor medida en mamíferos [237]. Esta expresión, al igual que en otras especies de peces como la carpa [100], el salmón (*Salmo salar*) [144], el pez pico rayado (*Oplegnathus fasciatus*) [169] y el lenguado (*Cynoglossus semilaevis*) [238], sigue un patrón específico de tejido. En el caso del pez cebra, los mayores niveles de tránscritos de pentraxinas cortas se encuentran en branquias, como también se ha descrito en lenguado [238]; en riñón, como en el pez pico rayado[169] y en bazo, como se observa tanto en el pez roca coreano [149] como en lenguado[239]. Estos resultados aumentan la relevancia en la expresión de *crps*, en peces con respecto a mamíferos, de tejidos que funcionan como principales órganos linfoides [240] o forman parte del sistema inmune de mucosas de peces teleósteos [241].

La exposición de los peces cebra a diferentes patógenos virales provoca un cambio en el patrón constitutivo de expresión de las isoformas de *zfcrps*. De acuerdo con los datos obtenidos por RT-qPCR y *microarray*, la infección con rabdovirus (SVCV y VHSV) aumenta la expresión tisular de las *zfcrps*, al menos, durante el primer mes post-infección. Esta tendencia, que no se observa en *zfcrp1* tras la infección con SVCV/VHSV ni en *zfcrp5/7* tras la infección con VHSV, se ha encontrado también en el hígado del pez pico rayado tras 3 dpi con RSIV [169] y en los órganos internos (riñón, bazo e hígado) de lenguado tras 1-7 dpi con megalocitovirus [238]. Sorprendentemente, la expresión de *zfcrps* aumentó más en las aletas y la piel adyacente que en los órganos internos de peces cebra adultos infectados con SVCV a 2 días y 1 mes post-infección [171]. La piel forma parte del sistema inmune de mucosas de los teleósteos [241, 242], por tanto, el hecho de que tras una infección vírica las *zfcrps* se sobre-expresen preferentemente en este tejido sugiere un papel de estas proteínas en la defensa antiviral de los tejidos linfoides asociados a mucosas (MALT). En este sentido, se ha identificado CRP en el moco de las branquias y de la piel del salmón infectado con el parásito *Neoparamoeba perurans* [243].

El cambio de expresión como consecuencia de la infección por rabdovirus que sufre cada una de las isofomas de *zfcrp* es diferente. De hecho, a 2 dpi con SVCV algunos tejidos

DISCUSIÓN

expresan preferencialmente unas isoformas, quedando otras reprimidas y, por tanto, haciendo que algunas isoformas sufran regulaciones diferentes en función del tejido. La regulación negativa de las pentraxinas cortas a tiempos cortos post-infección se ha comprobado también en otras especies: la expresión de *crp1* en hígado de carpa aparece reprimida a 1-5 dpi con CyHV-3 pero no a 14 dpi, cuando los niveles de *crp1* aumentan [158].

El análisis de los resultados de *microarray* reveló que los peces supervivientes a la infección con VHSV, a diferencia de los supervivientes a SVCV, tenían reprimida la expresión de las *zfcrps* en los órganos internos. Aunque este hallazgo fue explicado por una migración de las células del sistema inmune desde los órganos linfoides hasta los tejidos periféricos (sitio de entrada del virus) [171], todavía no se ha descrito ningún tipo celular sobreexpresor de *crps* en peces que permita explicar esto. A falta de esta información, proponemos que las marcas epigenéticas que definen la accesibilidad de la maquinaria de transcripción a los promotores de las *zfcrps* son diferentes en función del patógeno que las origina [244] y, por tanto, los supervivientes a VHSV pueden tener marcas inhibitorias en lugar de activadoras como se ha descrito para SVCV [173].

El aumento de la expresión de las *zfcrps* tras la infección con SVCV ocurre incluso en los órganos linfoides de los peces mutantes *rag1*-/- que parten con un estado inmunológico en los órganos internos inferior al de los peces *wild type*. Este aumento de expresión tras la infección vírica, dependiente de isoforma y de tejido, sugiere que las *zfcrps* tengan un papel en la respuesta inmune inducida por virus con diferentes aportaciones en función de la isoforma y del tejido. El aumento de la expresión de genes que codifican proteínas antivirales tras la infección con SVCV ha sido descrito en varios estudios tanto *in vitro* como *in vivo*. Entre los diferentes ejemplos: *mx*, *viperin*, *ifn* [245], *β-defensina* [175] y *trim32* [246].

A parte de la exposición a virus, la infección bacteriana también aumenta la expresión de todas las *zfcrps* (salvo la 1 y la 7) en los órganos linfoides de los peces cebra. Sin embargo este aumento, que también se ha descrito en los órganos linfoides del pez pico rayado [169] y del lenguado [238], no tiene lugar ni en el hígado del salmón tras 24 hpi con *A. salmonicida* [144], ni en el de la trucha [247] durante los primeros 28 dpi con *Yersina ruckeri*. Estas observaciones sugieren: **a)** un papel secundario del hígado en la producción de las pentraxinas cortas de los peces y **b)** una protección temprana a patógenos específico de especie como la observada en tres tipos de salmones (*Salmo salar*, *Oncorhynchus keta* y *Oncorhynchus gorbuscha*) tras la infección con *Lepeophtheirus salmonis* [248].

El cambio de expresión de las *zfcfps* tras la exposición a bacterias es muy similar al observado tras la infección con VHSV, a excepción de la isoforma *zfcfp5*, que parece tener una respuesta dependiente de patógeno ya que su expresión aumenta tras la exposición a SVCV o bacterias, pero no tras la exposición a VHSV. La especificidad de algunas isoformas de zfCRPs por ciertos patógenos podría explicar: **a)** la falta de modulación de la expresión de *zfcfp1* bajo los estímulos estudiados y **b)** la sobreexpresión de *zfcfp7* tras la infección con SVCV pero no con VHSV o bacterias. Por ello, no se descarta que otros estímulos, como la infección por parásitos, pudieran modular la expresión de las *zfcfp1/7*.

El aumento de expresión de *zfcfp4-5* en las larvas que sobre-expresan *il6* sugiere que el incremento de expresión de estas isoformas tras la infección sea mediado por la expresión de esta citoquina, que a su vez, es la responsable de aumentar los niveles de pCRP circulante en humanos [216]. Este hallazgo concuerda con el incremento de la expresión de *il6* descrito en carpa [249], lenguado olivo (*Paralichthys olivaceus*) [250] y lenguado senegalés (*Solea senegalensis*) [251] pocas horas después de la infección vírica, así como en trucha tras la exposición a LPS [252]. No obstante, los altos niveles de expresión de *il6* presentes en las especies de salmón resistentes a *L. salmonis* (coho y sockeye) no cursan con niveles elevados de expresión de *sap* o *crp* [253]. Sin embargo, como *L. salmonis* es un parásito, la función de la *il6* en la respuesta antiparasitaria no tiene porque ser la misma que en la respuesta antibacteriana o antiviral y, por tanto, este resultado no contradice el nuestro.

Las APPs son secretadas en respuesta a citoquinas proinflamatorias como la IL6 [254], por ello no sorprendió que las zfCRPs aumentasen sus niveles en sangre tras la infección vírica. Por el contrario, la escasa magnitud de este aumento sí fue inesperada, ya que mientras la CRP humana aumenta sus niveles en sangre ~1000 veces después de la infección bacteriana [99], los niveles de zfCRPs sólo se incrementaron entre ~1,5 y 3 veces tras la infección con SVCV. No obstante, esta subida en los niveles de CRPs, pequeña en comparación con la observada en humanos, ya ha sido descrita en otras especies de peces donde las pentraxinas cortas son consideradas APP [154, 255, 256]. Las CRPs son consideradas APP positivas en muchas especies de peces como el pez gato americano (*Ictalurus punctatus*) [156], el pez roca coreano [149] y la carpa [158]. Sin embargo, no lo son en otros peces como el bacalao (*Gadus morhua*) [159].

Para determinar si las zfCRPs también se comportan como proteínas de fase aguda en pez cebra, se midieron las concentraciones de las 7 isoformas de zfCRPs en la sangre de peces control e infectados. Este método posibilitó la clasificación de todas las zfCRPs salvo la CRP7 como proteínas de fase aguda. Como el cambio en los niveles de APPs refleja la

DISCUSIÓN

presencia y la intensidad de la inflamación durante una infección o lesión, el conocimiento de las principales APP de cada especie de pez es importante para el pronóstico de enfermedades virales, bacterianas y parasíticas presentes en acuicultura [257]. Además, como los vertebrados inferiores dependen en gran medida de la inmunidad innata en la protección contra patógenos, pensamos que las APP podrían tener un papel más crítico en la respuesta inmune proinflamatoria que en los vertebrados superiores. Como consecuencia de esta dependencia de la inmunidad innata, el abanico de APPs podría ser superior en peces que en mamíferos. En este sentido, se necesitan más estudios para determinar: **a)** si las zfCRPs son las principales APP en pez cebra y **b)** cuál es el estímulo que permite la secreción de las zfCRP2/3/6/7 tras una infección.

2. ACTIVIDAD ANTIVIRAL DE LAS zfCRPs

Nuestros trabajos son los primeros en describir que las zfCRPs neutralizan la infección de SVCV. Hasta ahora, la única actividad antiviral descrita asociada a las pentraxinas era la actividad anti-Influenza A de la SAP [258] y la PTX3 humanas [259]. Sin embargo, mientras la actividad antiviral de estas pentraxinas se debe a un efecto directo sobre el virus [259], la inhibición observada tras el tratamiento de las células previamente a la infección indica que la actividad antiviral de las zfCRPs, a excepción de la isoforma 6, es consecuencia de una interacción con la célula. Este efecto se ha reportado también para otros antivirales. Por ejemplo, la proteína VIPERINA (*virus inhibitory protein, endoplasmic reticulum [ER]-associated, IFN-inducible*) suprime la replicación de SVCV *in vitro* facilitando la producción de IFN1 e ISGs a través de la activación de RIG-I, IRF3 e IRF7 [260].

La ausencia de actividad antiviral de la zfCRP1 en la mayoría de los ensayos fue explicada porque es la única isoforma sin péptido señal de acuerdo con las predicciones *in silico*. Teniendo en cuenta la carencia de péptido señal, pensamos que su detección por *dot-blot* en los ssCRP1 es debido a su liberación desde las células muertas durante la transfección. Esta hipótesis fue propuesta anteriormente para explicar la actividad antiviral de los interferones intracelulares (iIFN) que carecen de péptido señal [261].

Los resultados obtenidos al añadir los ssCRPs en diferentes estadíos del ciclo viral mostraron que la protección conferida por estas moléculas es muy rápida, ya que se observan inhibiciones incluso en los tratamientos post-adsorción. Este resultado está en consonancia con el obtenido en el examen del curso de la infección de SVCV *in vitro*, que mostró que el pre-tratamiento con ssCRP reducía la carga viral ya a 4 h, lo que también

sugiere que dicha inhibición se produce en una etapa temprana del ciclo de replicación viral. De todas formas, aunque en este estudio se haya profundizado más en esta línea, con los datos obtenidos no se puede descartar que también puedan producirse efectos inhibitorios en las etapas de salida del ciclo de replicación viral.

La actividad antiviral de las zfCRPs fue demostrada *in vitro* en dos líneas celulares procedentes de especies diferentes de ciprínido (EPC y ZF4), sugiriendo que esta actividad no es específica de especie. Además, la mayor supervivencia de las larvas sobre-expresoras de *zfcfps* a infecciones con SVCV confirmó esta actividad *in vivo*. Este último resultado mostró que algunas proteínas del sistema inmune innato pueden actuar como inhibidores naturales de virus, limitando el crecimiento y la propagación de éste durante las primeras etapas de infección antes de la inducción de las respuestas inmunes adaptativas.

Las modificaciones post-transcripcionales (PTMs) tienen gran impacto en la función de algunas proteínas. Tanto es así que una misma proteína puede tener funciones diferentes dependiendo de las PTMs que sufra [262]. En el caso de las zfCRPs, la zfCRP5 recombinante producida en insecto, cuyo peso molecular experimental coincide con el teórico, no presenta actividad antiviral ni antibacteriana (resultados pendientes de publicación). Sin embargo, los ssCRPs cuyas zfCRPs tienen un peso molecular experimental ligeramente diferente al teórico, sí presentan dicha actividad. Se piensa que estas pequeñas diferencias en el peso molecular son consecuencia de PTMs. Como las PTMs dependen de enzimas presentes en el retículo endoplasmático y en el aparato de Golgi de la célula del huésped eucariota, es lógico que la expresión de *zfcfps* en diferentes sistemas (insecto y células de pez), con diferentes medios de cultivo y diferentes eficiencias [263], pueda afectar las PTMs sufridas por las zfCRPs.

Entre las posibles PTMs sufridas por las zfCRPs, es muy probable que los aumentos de masa molecular sean debidos a glicosilaciones, como revelan las predicciones derivadas de los análisis bioinformáticos (resultados pendientes de publicación). Además, como se ha descrito una heterogeneidad de glicosilación en las pentraxinas cortas de algunos peces [255], esta PTM podría explicar las múltiples bandas que revelan los SDS-PAGE realizados durante esta tesis para una única zfCRP. Por otra parte, el peso molecular de algunas zfCRPs determinado experimentalmente es menor que el teórico. Esta reducción de peso molecular podría explicarse por una proteólisis entre los aminoácidos 159 y 181, que generaría péptidos con pesos moleculares entre 17,9 y 20,3 kDa. En este sentido se ha reportado que las proteasas derivadas de neutrófilos humanos son capaces de digerir la CRP humana y formar

DISCUSIÓN

péptidos similares a la tuftsin (un péptido producido por el clivaje del dominio Fc de la cadena pesada de la inmunoglobulina G) con potente actividad inmunomoduladora [264].

3. RECONOCIMIENTO DE LIGANDOS POR LAS zfCRPs

Dado que no se ha realizado una clasificación basada en la afinidad a ligandos, no se sabe con seguridad si las zfCRPs son CRPs o SAPs. El análisis de afinidad a moléculas lipídicas *in silico* predijo energías libres de unión ligeramente menores para PC, el ligando prototípico de la hCRP [216], que para el ligando principal de la hSAP, la PE [77, 101]. No obstante, como estas diferencias fueron mínimas y sólo observadas en presencia de Ca²⁺ no se pueden extraer conclusiones concretas en este aspecto.

De acuerdo con los experimentos *in silico* e *in vitro*, el lípido con mayor afinidad por las zfCRPs es el colesterol. La unión de la hCRP y la hSAP a colesterol ya ha sido descrita por otros autores [221] como consecuencia de la realización de estudios para comprender la acumulación específica de hCRP y hSAP en las lesiones ateroscleróticas [265]. Sin embargo, dicha unión a colesterol, al contrario de la observada con las zfCRPs, sí que es dependiente de Ca²⁺ [221]. La unión a lípidos independiente de Ca²⁺ observada en las zfCRPs está en consonancia con la actividad antiviral de estas proteínas a bajas concentraciones de Ca²⁺ (0,42 mM, en el medio de los ssCRPs). Actividad que no mejora a concentraciones más altas (1 mM). Si suponemos que la actividad antiviral de las zfCRPs se inicia con el reconocimiento de lípidos en la superficie de las células infectadas, es lógico que si la actividad antiviral es independiente de este catión, la unión de las zfCRPs a estos lípidos también lo sea.

Las diferentes afinidades de cada una de las isoformas de zfCRPs por cada lípido (Ch, 25-HOC y PC), podría explicar diferencias funcionales, así como diferentes estados de oligomerización. Sin embargo, sólo se ha podido demostrar estados monoméricos en los sobrenadantes. Esto puede deberse a la baja concentración de Ca²⁺ en los medios de los ssCRPs, ya que ha sido descrito que la estructura de las pentraxinas de peces cambia en función de la presencia/ausencia de Ca²⁺, tendiendo a la formación de oligómeros en los tampones que contienen Ca²⁺ [255].

4. EVALUACIÓN DE LA CAPACIDAD BLOQUEADORA DE LA ENTRADA DEL VIRUS

Los resultados obtenidos tras el tratamiento de las células con M β CD demostraron la necesidad de la integridad de las balsas lipídicas, dominios de membrana ricos en colesterol y esfingolípidos, en las membranas celulares para la infección por SVCV. Este papel de las balsas lipídicas en la infección ha sido previamente descrito para otros virus envueltos como Influeza A [266-268], Sendai [269], el virus del sarampión [270, 271] y el virus de la enfermedad Newcastle [272-274]. Como la unión de la hCRP a las balsas lipídicas ya ha sido descrita [275] y nuestros resultados muestran bajas energías libres de unión a la interacción zfCRP-Ch, pensamos que las zfCRPs podrían estar interaccionando con las balsas lipídicas de manera que estuviesen impidiendo la entrada del virus por competición. Sin embargo, el tratamiento de las células con ssCRPs 2 h antes de la infección no afectó a la unión del virus a la célula. Asimismo, los ssCRP1-6 no inhibieron los sincitios generados por el proceso de fusión de membranas inducido por el virus, otra etapa importante en la fase de entrada del virus; a excepción del tratamiento con ssCRP7 que sí redujo el proceso de fusión. Este último resultado estuvo en consonancia con los ensayos de *binding* realizados mediante ELISA, que demuestran una mayor afinidad de la CRP7 por el colesterol con respecto al resto de isoformas estudiadas. Esta alta afinidad podría estar inhibiendo parte de la fusión vírica, no obstante, no explicaría la totalidad de la neutralización observada, sugiriendo que la zfCRP7 utiliza múltiples mecanismos para inhibir la infección de SVCV. La actividad antiviral a través de la modulación de múltiples mecanismos se ha observado en otras proteínas del sistema inmune innato como las TRIM de los mamíferos, que restringen al virus directamente, modulan la señal inmune y, además, regulan la autofagia [276]. Asimismo, la contribución de las balsas lipídicas en el proceso de fusión ha sido sugerida anteriormente por otros autores en virus como varicela-zoster [277] y el virus linfotrópico de células T humanas [278].

5. REGULACIÓN DE MECANISMOS CON ACCIÓN ANTIVIRAL

5.1. Sistema de interferón

El sistema de interferón es una estrategia muy utilizada por los vertebrados inferiores para establecer un estado antiviral [279] a través de la inducción de unas moléculas efectoras, codificadas por los genes estimulados por interferón (ISGs), que limitan

DISCUSIÓN

la capacidad de replicación de los virus [280]. Sin embargo, la activación de este sistema como mecanismo antiviral de las zfCRPs fue descartado tras comprobar que tanto la incubación de EPC como la de ZF4 con ssCRPs no inducía la expresión de *mx*, sino que por el contrario, la inhibía. La Mx es la ISG mejor estudiada dentro de la ruta de IFN en peces [280], es inducida tanto por IFN tipo I como por IFN tipo II [281] y el análisis de sus niveles de expresión es utilizado para determinar la activación del sistema de interferón [282-284]. Asimismo, esta no es la primera vez que se reporta la inhibición del sistema de interferón por la CRP: se describió un aumento significativo de la expresión de IFN tipo I y de *isg15* al silenciar la expresión de *crp* con siRNA en células de hepatocarcinoma [285]. Los resultados de expresión de *mx* en células tratadas con ssCRPs estuvieron en consonancia con la carencia de actividad de los medios condicionados procedentes de células EPC tratadas con ssCRP.

5.2. La regulación de la autofagia como mecanismo de defensa antiviral

La regulación de la muerte celular es una respuesta importante del huésped para combatir la infección vírica. Dentro de los diferentes tipos de muerte celular observadas en peces tras la infección se incluyen: apoptosis, necroptosis, piroptosis y autofagia [286-289]. En este sentido, en esta tesis hemos encontrado evidencias de que SVCV necesita que el proceso autófágico esté activo para replicar, como ha sido descrito para muchos otros virus [290-293]. De hecho, existen trabajos previos que relacionan la infección de SVCV con la activación de la autofagia [71, 232, 235]. No obstante, mientras esta activación fue interpretada en algunos casos como un mecanismo regulador negativo de la replicación del virus [232, 235], en otros, en consonancia con este estudio, fue interpretado como un mecanismo requerido por el virus para realizar su ciclo de replicación [71]. La autofagia es un tema reciente de estudio, de hecho, el verdadero mecanismo de algunos bloqueadores como la CQ no ha sido desvelado hasta hace muy poco [234]. Por tanto, cabe la posibilidad de la existencia de interpretaciones erróneas en los estudios pioneros.

En este trabajo los ensayos de bloqueo químico de la autofagia se llevaron a cabo no sólo con 3-MA sino también con CQ. Este bloqueo reveló una disminución de la replicación de SVCV que mejoró cuando el tratamiento se realizó en combinación con la mix-ssCRPs, M β CD o 25-HOC. Este resultado, junto con la disminución de la neutralización al combinar cada uno de estos tres compuestos con rapamicina, mostró que la neutralización de SVCV *in vitro* producida por el tratamiento de las células con la mix-ssCRPs, M β CD o 25-HOC es consecuencia de un bloqueo de la autofagia o de algún elemento común entre la autofagia y la vía de endocitosis viral. En este sentido, ya se han descrito casos en los que estas dos vías

convergen como consecuencia de la fusión de los autofagosomas con los endosomas que contienen a los virus. Esta fusión da lugar a unas estructuras llamadas anfisomas [294-296]. Además, como nuestros resultados fueron acompañados por una acumulación de autofagosomas cuando las células eran tratadas con alguno de estos tres compuestos, planteamos la hipótesis de que dicho bloqueo se produce en una etapa tardía, como la fusión del autofagosoma o endosoma intermedio o anfisoma con el lisosoma [292], tal y como ocurre al tratar las células con CQ [234, 297, 298] o con L-asparagina [294].

Teniendo en cuenta que los lisosomas son vulnerables al estrés oxidativo [299], con el fin de comprender el mecanismo por el cual las zfCRPs, 25-HOC y M β CD bloquean la fusión del autofagosoma, endosoma o anfisoma con el lisosoma, se analizó la posible implicación de las ROS en este proceso. Los resultados mostraron una reducción significativa del efecto antiviral de los tres compuestos tras el tratamiento con NAC (reductor de estrés oxidativo [290]) y, en consecuencia, se estableció una relación directa entre el aumento de ROS y el bloqueo de la autofagia. Esta relación ha sido descrita para otros bloqueadores de la autofagia [297]. En cuanto a las implicaciones de estos en la replicación de SVCV, un aumento en la concentración de ROS incrementa el pH en los lisosomas evitando tanto la fusión del lisosoma con el autofagosoma [297] como el cambio conformacional de la proteína G de SVCV. Sin el cambio conformacional de la G, las partículas víricas son incapaces de entrar en el citoplasma del huésped [226, 300].

La capacidad de las zfCRPs de bloquear la autofagia explica no sólo la actividad anti-SVCV sino también la disminución de la expresión de *mx* en las células tratadas con la mix-ssCRPs. De hecho, ha sido descrito que la inducción de la actividad antiviral del sistema de interferón es sensible al pH de los lisosomas o endosomas y, por ello, la actividad de IFN se ve afectada por ejemplo en presencia de CQ [301].

Esta tesis aporta además evidencias *in vivo* que apoyan las conclusiones obtenidas *in vitro*: **a)** la inyección i.p. de la mix-ssCRPs en peces cebra adultos aumenta los niveles de tránscritos de un conjunto de genes implicados en la autofagia y **b)** la sobre-expresión de *zfcrps* en larvas de pez cebra transgénico con expresión de GFP-Lc3 cambia el patrón de fluorescencia tisular. El cambio de patrón de fluorescencia en las larvas transgénicas GFP-Lc3 ha sido demostrado anteriormente al modificar los niveles de autofagia de estas larvas con el tratamiento de bloqueadores como la CQ [302] y de activadores como la rapamicina [235].

DISCUSIÓN

Esta no es la primera vez que se describe que una molécula del sistema inmune innato, a la que se le asigna otra función diferente a la antiviral, modula la autofagia para inhibir la infección de un virus. Ejemplo de ello es que el péptido antimicrobiano NK-lysina, que posee actividad directa contra bacterias, hongos y parásitos, es capaz de inhibir la replicación del VHSV en los eritrocitos de rodaballo (*Scophthalmus maximus*) activando la autofagia [205].

Por otra parte, la autofagia ha sido recientemente descrita como un mecanismo importante en la generación de memoria del sistema inmune innato [303]. Por tanto, la persistencia de los cambios de expresión de las zfCRPs en los peces supervivientes a las infecciones víricas (tras 1 mes) y bacterianas (tras 5 meses) podría estar indicando un papel importante de esta familia multigénica en la inmunidad entrenada. Esto explicaría por qué los promotores de las zfCRPs presentan marcas epigenéticas tras la infección con SVCV [173].

6. INFLUENCIA DE LOS LÍPIDOS EN LA ACTIVIDAD ANTIVIRAL DE LAS zfCRPs

El mecanismo por el cual los inhibidores de la autofagia (zfCRPs, M β CD y 25-HOC) aumentan los niveles de ROS intracelulares no está todavía claro. Sin embargo, teniendo en cuenta el contenido de NAPDH oxidasa (enzimas generadoras de ROS) en las balsas lipídicas [304], una posible explicación podría ser que el secuestro del colesterol de membrana indujese la formación de ROS [305]. Esta hipótesis explicaría el bloqueo de la autofagia dependiente de ROS observado tras el tratamiento de las células con zfCRPs y M β CD, ya que su alta afinidad por Ch podría alterar las balsas lipídicas de membrana. En esta línea, se ha descrito que la mCRP humana induce la generación de ROS en células mononucleares de sangre periférica (PBMC) como consecuencia de su unión a balsas lipídicas [128].

Además, dado que tanto el 25-HOC como el Ch ejercen un efecto muy parecido sobre la autofagia y la replicación de SVCV, en esta tesis sugerimos que cualquier desequilibrio en el contenido de colesterol de las membranas celulares, lo que incluye también el desafío lipídico exógeno, reduce la eficacia de estos procesos (la autofagia y la endocitosis del virus) o su probable efecto convergente (**Fig. 7, P4**). En este sentido, otros estudios han demostrado la incapacidad de la autofagia para adaptarse a una carga lipídica exógena tanto *in vitro* como *in vivo*: a) el tratamiento de hepatocitos con lípidos reduce la co-

localización de LD (gotas de lípidos) con LAMP1 (proteína de membrana asociada a lisosoma 1) y b) el aumento de grasas en la dieta de los ratones disminuye notablemente el número de autofagosomas que contienen LD [306].

El 25-HOC pertenece a la familia de los oxisteroles, que son derivados de la oxidación del colesterol que contienen un grupo hidroxilo, epóxido o cetona en el núcleo del esterol y/o un grupo hidroxilo en la cadena lateral [307]. Entre las múltiples funciones fisiológicas de algunos oxisteroles específicos, como el 25-HOC [308-312] y el 27-hidroxicolestrol (27-HOC) [313], se encuentra la capacidad de inhibir infecciones víricas. El 25-HOC inhibe la replicación de SVCV *in vitro*, en la línea celular EPC (en este trabajo) y, en ZF4 [205]. En estudios precedentes, se ha demostrado que el tratamiento de las células con 25-HOC antes de la infección con virus envueltos bloquea la fusión de la membrana vírica con la celular al inducir cambios (expansiones y agregaciones) en la última [312]. Este hecho, lejos de contradecir, encaja con el modelo que proponemos (**Fig. 7, P4**) ya que, como se discutió anteriormente, la generación de ROS aumenta el pH lisosomal reduciendo su capacidad de fusión con autofagosomas y endosomas. Este bloqueo se traduce en la limitación de la capacidad de fusión dependiente de pH de la proteína G del SVCV, o de otras proteínas fusogénicas de otros virus que también requieran un pH ácido, evitando la liberación del genoma vírico al citoplasma.

La capacidad de inhibición del proceso autófágico podría ser exclusiva del 25-HOC dentro del grupo de los oxisteroles ya que el 24S-hidroxicolestrol (24S-HOC) [314, 315], el 7-ketocolesterol (7KC), el 7 β -hidroxicolestrol (7 β -HOC) [315] y el 27-HOC [316] activan la autófagia en lugar de inhibirla. No obstante, más estudios son necesarios en este sentido y, sobre todo, en relación con la replicación vírica.

CONCLUSIONES

CONCLUSIONES

1. Las zfCRPs tienen actividad protectora frente a la infección del SVCV tanto *in vitro*, en células EPC y ZF4, como *in vivo*, en larvas de pez cebra.
2. Los colesteroles, y de entre ellos el 25-HOC, son los lípidos por los que las zfCRPs presentan mayor afinidad, lo que las sugiere como secuestradoras de este tipo de moléculas.
3. La perturbación del nivel de colesterol en las balsas lipídicas producida por el tratamiento con zfCRPs, M β CD o 25-HOC podría ser el desencadenante de la neutralización de la infección de SVCV con estos tratamientos.
4. El SVCV requiere la maquinaria autofágica o algunos de sus componentes para su replicación en las células huésped.
5. El efecto anti-SVCV producido por zfCRPs, M β CD o 25-HOC es consecuencia de un bloqueo de la autofagia o de la ruta de endocitosis del virus, a través de la inhibición de la etapa de fusión del autofagosoma, anfisoma o endosoma con el lisosoma.
6. El bloqueo de la autofagia producido por zfCRPs, M β CD o 25-HOC parece ser consecuencia de la estimulación de la generación de ROS.



BIBLIOGRAFÍA

1. Goldszmid RS, Trinchieri G. The price of immunity. *Nature immunology*. 2012;13(10):932.
2. Grubbs H, Whitten R. Physiology, Active Immunity. StatPearls [Internet]: StatPearls Publishing; 2018.
3. Andrade VM, Stevenson M. Host and viral factors influencing interplay between the macrophage and hiv-1. *Journal of Neuroimmune Pharmacology*. 2018;1:11.
4. Boyer Z, Palmer S. Targeting immune checkpoint molecules to eliminate latent HIV. *Frontiers in Immunology*. 2018;9:2339.
5. Dhama K, Karthik K, Khandia R, Chakraborty S, Munjal A, Latheef SK, et al. Advances in Designing and Developing vaccines, Drugs, and Therapies to Counter ebola virus. *Frontiers in immunology*. 2018;9:1803.
6. Parvizpour S, Razmara J, Omidi Y. Breast cancer vaccination comes to age: impacts of bioinformatics. *BioImpacts: BI*. 2018;8(3):223.
7. Del Giudice G, Rappuoli R, Didierlaurent AM, editors. Correlates of adjuvanticity: A review on adjuvants in licensed vaccines. *Seminars in immunology*; 2018: Elsevier.
8. Harandi AM, editor Systems analysis of human vaccine adjuvants. *Seminars in immunology*; 2018: Elsevier.
9. Niwa R, Satoh M. The current status and prospects of antibody engineering for therapeutic use: focus on glycoengineering technology. *Journal of pharmaceutical sciences*. 2015;104(3):930-41.
10. Panowski S, Bhakta S, Raab H, Polakis P, Junutula JR, editors. Site-specific antibody drug conjugates for cancer therapy. *mabs*; 2014: Taylor & Francis.
11. Benvenuto LJ, Anderson MR, Arcasoy SM. New frontiers in immunosuppression. *Journal of Thoracic Disease*. 2018;10(5):3141-55.
12. Danforth K, Granich R, Wiedeman D, Baxi S, Padian N. Global Mortality and Morbidity of HIV/AIDS. *Disease Control Priorities, (Volume 6): Major Infectious Diseases*. 2017.
13. Pollett S, Melendrez M, Berry IM, Duchêne S, Salje H, Cummings D, et al. Understanding dengue virus evolution to support epidemic surveillance and counter-measure development. *Infection, Genetics and Evolution*. 2018.
14. Okafor CN, Finnigan NA. Malaria (*Plasmodium Ovale*). StatPearls [Internet]: StatPearls Publishing; 2018.
15. Netea MG, Joosten LA, Latz E, Mills KH, Natoli G, Stunnenberg HG, et al. Trained immunity: a program of innate immune memory in health and disease. *Science*. 2016;352(6284):aaf1098.
16. Netea MG, van der Meer JW. Trained immunity: an ancient way of remembering. *Cell host & microbe*. 2017;21(3):297-300.
17. Italiani P, Boraschi D. New insights into tissue macrophages: from their origin to the development of memory. *Immune network*. 2015;15(4):167-76.
18. Chabalgoity J, Pereira M, Rial A. Inmunidad contra los agentes infecciosos. Temas de Bacteriología y Virología Médica 2a ed Uruguay: FEFMUR. 2006:99-114.
19. Cronkite DA, Strutt TM. The Regulation of Inflammation by Innate and Adaptive Lymphocytes. *Journal of Immunology Research*. 2018;2018.
20. Daigo K, Inforzato A, Barajon I, Garlanda C, Bottazzi B, Meri S, et al. Pentraxins in the activation and regulation of innate immunity. *Immunological reviews*. 2016;274(1):202-17.
21. Vijay K. Toll-like receptors in immunity and inflammatory diseases: past, present, and future. *International immunopharmacology*. 2018;59:391-412.

BIBLIOGRAFÍA

22. Mesa-Villanueva M, Patiño P. Receptores tipo Toll: entre el reconocimiento de lo no propio infeccioso y las señales endógenas de peligro. Inmunología (1987). 2006;25(2):115-30.
23. Tassia MG, Whelan NV, Halanych KM. Toll-like receptor pathway evolution in deuterostomes. Proceedings of the National Academy of Sciences. 2017;114(27):7055-60.
24. Abdulkhaleq L, Assi M, Abdullah R, Zamri-Saad M, Taufiq-Yap Y, Hezmee M. The crucial roles of inflammatory mediators in inflammation: A review. Veterinary world. 2018;11(5):627.
25. Buchmann K. Evolution of innate immunity: clues from invertebrates via fish to mammals. Frontiers in immunology. 2014;5:459.
26. Lewis KL, Del Cid N, Traver D. Perspectives on antigen presenting cells in zebrafish. Developmental & Comparative Immunology. 2014;46(1):63-73.
27. ten Broeke T, Wubbolts R, Stoorvogel W. MHC class II antigen presentation by dendritic cells regulated through endosomal sorting. Cold Spring Harbor perspectives in biology. 2013;5(12):a016873.
28. Sun JC, Lanier LL. Is there natural killer cell memory and can it be harnessed by vaccination? NK cell memory and immunization strategies against infectious diseases and cancer. Cold Spring Harbor perspectives in biology. 2018;10(10):a029538.
29. Rauta PR, Nayak B, Das S. Immune system and immune responses in fish and their role in comparative immunity study: a model for higher organisms. Immunology letters. 2012;148(1):23-33.
30. Gourbal B, Pinaud S, Beckers GJ, Van Der Meer JW, Conrath U, Netea MG. Innate immune memory: An evolutionary perspective. Immunological reviews. 2018;283(1):21-40.
31. Mourits VP, Wijkmans JC, Joosten LA, Netea MG. Trained immunity as a novel therapeutic strategy. Current Opinion in Pharmacology. 2018;41:52-8.
32. de Bree CL, Koeken VA, Joosten LA, Aaby P, Benn CS, van Crevel R, et al., editors. Non-specific effects of vaccines: Current evidence and potential implications. Seminars in immunology; 2018: Elsevier.
33. Pradeu T, Du Pasquier L. Immunological memory: What's in a name? Immunological reviews. 2018;283(1):7-20.
34. Dominguez-Andres J, Netea MG. Long-term reprogramming of the innate immune system. Journal of leukocyte biology. 2018.
35. Rojo-Cembreros AH, Ibarra-Castro L, Martínez-Brown JM. Immunostimulation and trained immunity in marine fish larvae. Fish & shellfish immunology. 2018.
36. Cassone A. The Case for an Expanded Concept of Trained Immunity. mBio. 2018;9(3):e00570-18.
37. Rusek P, Wala M, Druszczyńska M, Fol M. Infectious agents as stimuli of trained innate immunity. International journal of molecular sciences. 2018;19(2):456.
38. Zhang Z, Chi H, Dalmo RA. Trained innate immunity of fish is a viable approach in larval aquaculture. Frontiers in Immunology. 2019;10.
39. Melillo D, Marino R, Italiani P, Boraschi D. Innate Immune Memory in Invertebrate Metazoans: A Critical Appraisal. Frontiers in immunology. 2018;9.
40. Norouzitallab P, Baruah K, Biswas P, Vanrompay D, Bossier P. Probing the phenomenon of trained immunity in invertebrates during a transgenerational study, using brine shrimp *Artemia* as a model system. Scientific reports. 2016;6:21166.
41. Barski A, Cuddapah S, Cui K, Roh T-Y, Schones DE, Wang Z, et al. High-resolution profiling of histone methylations in the human genome. Cell. 2007;129(4):823-37.
42. Medzhitov R, Horng T. Transcriptional control of the inflammatory response. Nature Reviews Immunology. 2009;9(10):692.
43. Wei G, Wei L, Zhu J, Zang C, Hu-Li J, Yao Z, et al. Global mapping of H3K4me3 and H3K27me3 reveals specificity and plasticity in lineage fate determination of differentiating CD4+ T cells. Immunity. 2009;30(1):155-67.

44. Sánchez-Ramón S, Conejero L, Netea MG, Sancho D, Palomares O, Subiza JL. Trained immunity-based vaccines: a new paradigm for the development of broad-spectrum anti-infectious formulations. *Frontiers in immunology*. 2018;9.
45. Quintin J, Cheng S-C, van der Meer JW, Netea MG. Innate immune memory: towards a better understanding of host defense mechanisms. *Current opinion in immunology*. 2014;29:1-7.
46. Netea MG. Training innate immunity: the changing concept of immunological memory in innate host defence. *European journal of clinical investigation*. 2013;43(8):881-4.
47. Gardiner CM, Mills KH, editors. *The cells that mediate innate immune memory and their functional significance in inflammatory and infectious diseases*. Seminars in immunology; 2016: Elsevier.
48. Saiz ML, Rocha-Perugini V, Sánchez-Madrid F. Tetraspanins as organizers of antigen-presenting cell function. *Frontiers in immunology*. 2018;9.
49. Platt AM, Randolph GJ. Dendritic cell migration through the lymphatic vasculature to lymph nodes. *Advances in immunology*. 120: Elsevier; 2013. p. 51-68.
50. Esche C, Stellato C, Beck LA. Chemokines: key players in innate and adaptive immunity. *Journal of Investigative Dermatology*. 2005;125(4):615-28.
51. Petri B, Sanz M-J. Neutrophil chemotaxis. *Cell and tissue research*. 2018;1-12.
52. Nourshargh S, Alon R. Leukocyte migration into inflamed tissues. *Immunity*. 2014;41(5):694-707.
53. Gasque P. Complement: a unique innate immune sensor for danger signals. *Molecular immunology*. 2004;41(11):1089-98.
54. Lidani KC, Bavia L, Ambrosio AR, de Messias-Reason IJ. The complement system: a prey of Trypanosoma cruzi. *Frontiers in microbiology*. 2017;8:607.
55. Giang J, Seelen MA, van Doorn M, Prens EP, Damman JD. Complement activation in inflammatory skin diseases. *Frontiers in immunology*. 2018;9:639.
56. Mödinger Y, Teixeira G, Neidlinger-Wilke C, Ignatius A. Role of the Complement System in the Response to Orthopedic Biomaterials. *International journal of molecular sciences*. 2018;19(11):3367.
57. Qian M, Fang X, Wang X. Autophagy and inflammation. *Clinical and translational medicine*. 2017;6(1):24.
58. Paulus GL, Xavier RJ. Autophagy and checkpoints for intracellular pathogen defense. *Current opinion in gastroenterology*. 2015;31(1):14.
59. Puleston DJ, Simon AK. Autophagy in the immune system. *Immunology*. 2014;141(1):1-8.
60. Cadwell K. Crosstalk between autophagy and inflammatory signalling pathways: balancing defence and homeostasis. *Nature Reviews Immunology*. 2016;16(11):661.
61. Kinsella RL, Nehls EM, Stallings CL. Roles for autophagy proteins in immunity and host defense. *Veterinary pathology*. 2018;55(3):366-73.
62. Gomes LC, Dikic I. Autophagy in antimicrobial immunity. *Molecular cell*. 2014;54(2):224-33.
63. Kaur J, Debnath J. Autophagy at the crossroads of catabolism and anabolism. *Nature reviews Molecular cell biology*. 2015;16(8):461.
64. Bah A, Vergne I. Macrophage Autophagy and Bacterial Infections. *Frontiers in immunology*. 2017;8:1483.
65. Kohler LJ, Roy CR. Autophagic targeting and avoidance in intracellular bacterial infections. *Current opinion in microbiology*. 2017;35:36-41.
66. Rathinam VA, Fitzgerald KA. Inflamasome complexes: emerging mechanisms and effector functions. *Cell*. 2016;165(4):792-800.

BIBLIOGRAFÍA

67. Delgado M, Singh S, De Haro S, Master S, Ponpuak M, Dinkins C, et al. Autophagy and pattern recognition receptors in innate immunity. *Immunological reviews*. 2009;227(1):189-202.
68. Fattah EA, Bhattacharya A, Herron A, Safdar Z, Eissa NT. Critical role for IL-18 in spontaneous lung inflammation caused by autophagy deficiency. *The Journal of Immunology*. 2015;194(11):5407-16.
69. Netea-Maier RT, Plantinga TS, van de Veerdonk FL, Smit JW, Netea MG. Modulation of inflammation by autophagy: consequences for human disease. *Autophagy*. 2016;12(2):245-60.
70. Lee HK, Lund JM, Ramanathan B, Mizushima N, Iwasaki A. Autophagy-dependent viral recognition by plasmacytoid dendritic cells. *Science*. 2007;315(5817):1398-401.
71. Liu L, Zhu B, Wu S, Lin L, Liu G, Zhou Y, et al. Spring viraemia of carp virus induces autophagy for necessary viral replication. *Cellular microbiology*. 2015;17(4):595-605.
72. Golconda U, Sobonya R, Klotz S. Do Pentraxins Bind to Fungi in Invasive Human Gastrointestinal Candidiasis? *Journal of Fungi*. 2018;4(3):111.
73. Garlanda C, Bottazzi B, Salvatori G, De Santis R, Cotena A, Deban L, et al. Pentraxins in innate immunity and inflammation. *Innate Immunity to Pulmonary Infection*. 2007:80-91.
74. Roumenina LT, Ruseva MM, Zlatarova A, Ghai R, Kolev M, Olova N, et al. Interaction of C1q with IgG1, C-reactive protein and pentraxin 3: mutational studies using recombinant globular head modules of human C1q A, B, and C chains. *Biochemistry*. 2006;45(13):4093-104.
75. Doni A, Garlanda C, Mantovani A, editors. Innate immunity, hemostasis and matrix remodeling: PTX3 as a link. *Seminars in immunology*; 2016: Elsevier.
76. Ma YJ, Lee BL, Garred P. An overview of the synergy and crosstalk between pentraxins and collectins/ficolins: their functional relevance in complement activation. *Experimental & molecular medicine*. 2017;49(4):e320.
77. Mantovani A, Valentino S, Gentile S, Inforzato A, Bottazzi B, Garlanda C. The long pentraxin PTX3: a paradigm for humoral pattern recognition molecules. *Annals of the New York Academy of Sciences*. 2013;1285(1):1-14.
78. Richter K, Sagawe S, Hecker A, Küllmar M, Askevold I, Damm J, et al. C-reactive protein stimulates nicotinic acetylcholine receptors to control ATP-mediated monocytic inflammasome activation. *Frontiers in immunology*. 2018;9.
79. Boehm T, Swann JB. Origin and evolution of adaptive immunity. *Annu Rev Anim Biosci*. 2014;2(1):259-83.
80. Wilson AB. MHC and adaptive immunity in teleost fishes. *Immunogenetics*. 2017;69(8-9):521-8.
81. Marrack P, Scott-Browne JP, Dai S, Gapin L, Kappler JW. Evolutionarily conserved amino acids that control TCR-MHC interaction. *Annu Rev Immunol*. 2008;26:171-203.
82. Edholm E-S, Grayfer L, Robert J. Evolution of nonclassical MHC-dependent invariant T cells. *Cellular and molecular life sciences*. 2014;71(24):4763-80.
83. Edholm E-S, Banach M, Robert J. Evolution of innate-like T cells and their selection by MHC class I-like molecules. *Immunogenetics*. 2016;68(8):525-36.
84. Rangarajan S, Mariuzza RA. T cell receptor bias for MHC: co-evolution or co-receptors? *Cellular and molecular life sciences*. 2014;71(16):3059-68.
85. Bengten E, Wilson M, Miller N, Clem L, Pilström L, Warr G. Immunoglobulin isotypes: structure, function, and genetics. *Origin and Evolution of the Vertebrate Immune System*: Springer; 2000. p. 189-219.
86. Flajnik MF, Kasahara M. Origin and evolution of the adaptive immune system: genetic events and selective pressures. *Nature Reviews Genetics*. 2010;11(1):47.
87. Anelli T, Van Anken E. Missing links in antibody assembly control. *International journal of cell biology*. 2013;2013.

88. Jackson D, Elsawa S. Factors regulating immunoglobulin production by normal and disease-associated plasma cells. *Biomolecules*. 2015;5(1):20-40.
89. Ollila J, Vihtinen M. B cells. *The international journal of biochemistry & cell biology*. 2005;37(3):518-23.
90. Flajnik MF. A cold-blooded view of adaptive immunity. *Nature Reviews Immunology*. 2018;1.
91. Flajnik MF. Re-evaluation of the immunological Big Bang. *Current Biology*. 2014;24(21):R1060-R5.
92. Patel B, Banerjee R, Samanta M, Das S. Diversity of Immunoglobulin (Ig) Isotypes and the Role of Activation-Induced Cytidine Deaminase (AID) in Fish. *Molecular biotechnology*. 2018;60:435-53.
93. Gauthier ME, Du Pasquier L, Degnan BM. The genome of the sponge Amphimedon queenslandica provides new perspectives into the origin of Toll-like and interleukin 1 receptor pathways. *Evolution & development*. 2010;12(5):519-33.
94. Kawai T, Akira S. Signaling to NF- κ B by Toll-like receptors. *Trends in molecular medicine*. 2007;13(11):460-9.
95. Vanha-aho L-M, Valanne S, Rämet M. Cytokines in *Drosophila* immunity. *Immunology letters*. 2016;170:42-51.
96. Stein M-P, Mold C, Du Clos TW. C-reactive protein binding to murine leukocytes requires Fc γ receptors. *The Journal of Immunology*. 2000;164(3):1514-20.
97. Zhang L, Liu S-H, Wright TT, Shen Z-Y, Li H-Y, Zhu W, et al. C-reactive protein directly suppresses Th1 cell differentiation and alleviates experimental autoimmune encephalomyelitis. *The Journal of Immunology*. 2015;1402909.
98. Lu J, Marjon KD, Mold C, Du Clos TW, Sun PD. Pentraxins and Fc receptors. *Immunological reviews*. 2012;250(1):230-8.
99. Bottazzi B, Inforzato A, Messa M, Barbagallo M, Magrini E, Garlanda C, et al. The pentraxins PTX3 and SAP in innate immunity, regulation of inflammation and tissue remodelling. *Journal of hepatology*. 2016;64(6):1416-27.
100. Falco A, Cartwright JR, Wiegertjes GF, Hoole D. Molecular characterization and expression analysis of two new C-reactive protein genes from common carp (*Cyprinus carpio*). *Developmental & Comparative Immunology*. 2012;37(1):127-38.
101. Du Clos TW. Pentraxins: structure, function, and role in inflammation. *ISRN inflammation*. 2013;2013.
102. Daigo K, Mantovani A, Bottazzi B. The yin-yang of long pentraxin PTX3 in inflammation and immunity. *Immunology letters*. 2014;161(1):38-43.
103. McFadyen J, Kiefer J, Loseff-Silver J, Braig D, Potempa LA, Eisenhardt SU, et al. Dissociation of C-reactive protein localizes and amplifies inflammation: Evidence for a direct biological role of CRP and its conformational changes. *Frontiers in immunology*. 2018;9:1351.
104. Lin L, Liu T-Y. Isolation and characterization of C-reactive protein (CRP) cDNA and genomic DNA from *Xenopus laevis*. A species representing an intermediate stage in CRP evolution. *Journal of Biological Chemistry*. 1993;268(9):6809-15.
105. Chen R, Qi J, Yuan H, Wu Y, Hu W, Xia C. Crystal structures for short-chain pentraxin from zebrafish demonstrate a cyclic trimer with new recognition and effector faces. *Journal of structural biology*. 2015;189(3):259-68.
106. Iwaki D, Osaki T, Mizunoe Y, Wai SN, Iwanaga S, Kawabata Si. Functional and structural diversities of C-reactive proteins present in horseshoe crab hemolymph plasma. *European journal of biochemistry*. 1999;264(2):314-26.
107. Shrive AK, Burns I, Chou H-T, Stahlberg H, Armstrong PB, Greenhough TJ. Crystal structures of Limulus SAP-like pentraxin reveal two molecular aggregations. *Journal of molecular biology*. 2009;386(5):1240-54.

BIBLIOGRAFÍA

108. Lu J, Marjon KD, Marnell LL, Wang R, Mold C, Du Clos TW, et al. Recognition and functional activation of the human IgA receptor (Fc α RI) by C-reactive protein. *Proceedings of the National Academy of Sciences*. 2011;201018369.
109. Narkates AJ, Volanakis JE. C-reactive protein binding specificities: artificial and natural phospholipid bilayers. *Annals of the New York Academy of Sciences*. 1982;389(1):172-82.
110. Thiele J, Zeller J, Bannasch H, Stark G, Peter K, Eisenhardt S. Targeting C-reactive protein in inflammatory disease by preventing conformational changes. *Mediators of inflammation*. 2015;2015.
111. Agrawal A, Shrive AK, Greenhough TJ, Volanakis JE. Topology and structure of the C1q-binding site on C-reactive protein. *The Journal of Immunology*. 2001;166(6):3998-4004.
112. Agrawal A, Simpson MJ, Black S, Carey MP, Samols D. A C-reactive protein mutant that does not bind to phosphocholine and pneumococcal C-polysaccharide. *The Journal of Immunology*. 2002;169(6):3217-22.
113. Gulhar R, Jialal I. Physiology, Acute Phase Reactants. StatPearls [Internet]; StatPearls Publishing; 2018.
114. Boncler M, Watała C. Regulation of cell function by isoforms of C-reactive protein: a comparative analysis. *Acta Biochimica Polonica*. 2009;56(1):17-31.
115. Di Napoli M, Slevin M, Popa-Wagner A, Singh P, Lattanzi S, Divani AA. Monomeric C-reactive protein and cerebral hemorrhage: from bench to bedside. *Frontiers in immunology*. 2018;9.
116. Adukauskienė D, Čiginskienė A, Adukauskaitė A, Pentiokienė D, Šlapikas R, Čeponienė I. Clinical relevance of high sensitivity C-reactive protein in cardiology. *Medicina*. 2016;52(1):1-10.
117. Ridker PM. A test in context: high-sensitivity C-reactive protein. *Journal of the American College of Cardiology*. 2016;67(6):712-23.
118. Ocaklı B, Tuncay E, Gungor S, Sertbas M, Adiguzel N, Irmak I, et al. Inflammatory Markers in Patients Using Domiciliary Non-invasive Mechanical Ventilation: C Reactive Protein, Procalcitonin, Neutrophil Lymphocyte Ratio. *Frontiers in public health*. 2018;6.
119. Sack GH. Serum amyloid A-a review. *Molecular Medicine*. 2018;24(1):46.
120. Black S, Kushner I, Samols D. C-reactive protein. *Journal of Biological Chemistry*. 2004;279(47):48487-90.
121. Trial J, Potempa LA, Entman ML. The role of C-reactive protein in innate and acquired inflammation: new perspectives. *Inflammation and cell signaling*. 2016;3(2).
122. Singh SK, Suresh MV, Hammond Jr DJ, Rusiñol AE, Potempa LA, Agrawal A. Binding of the monomeric form of C-reactive protein to enzymatically-modified low-density lipoprotein: effects of phosphoethanolamine. *Clinica Chimica Acta*. 2009;406(1-2):151-5.
123. Caprio V, Badimon L, Di Napoli M, Fang W-H, Ferris GR, Guo B, et al. pCRP-mCRP dissociation mechanisms as potential targets for the development of small-molecule anti-inflammatory therapeutics. *Frontiers in Immunology*. 2018;9.
124. Badimon L, Peña E, Arderiu G, Padró T, Slevin M, Vilahur G, et al. C-reactive protein in atherosclerosis and angiogenesis. *Frontiers in immunology*. 2018;9:430.
125. Fujita M, Takada YK, Izumiya Y, Takada Y. The binding of monomeric C-reactive protein (mCRP) to Integrins $\alpha v\beta 3$ and $\alpha 4\beta 1$ is related to its pro-inflammatory action. *PLoS One*. 2014;9(4):e93738.
126. Molins B, Fuentes-Prior P, Adán A, Antón R, Arostegui JI, Yagüe J, et al. Complement factor H binding of monomeric C-reactive protein downregulates proinflammatory activity and is impaired with at risk polymorphic CFH variants. *Scientific reports*. 2016;6:22889.

127. Mihlan M, Blom AM, Kupreishvili K, Lauer N, Stelzner K, Bergström F, et al. Monomeric C-reactive protein modulates classic complement activation on necrotic cells. *The FASEB Journal*. 2011;25(12):4198-210.
128. Thiele JR, Zeller J, Kiefer J, Braig D, Kreuzaler S, Lenz Y, et al. A conformational change in C-reactive protein enhances leukocyte recruitment and reactive oxygen species generation in ischemia/reperfusion injury. *Frontiers in immunology*. 2018;9:675.
129. Sproston NR, Ashworth JJ. Role of C-Reactive Protein at Sites of inflammation and infection. *Frontiers in immunology*. 2018;9.
130. Bansal T, Pandey A, Deepa D, Asthana AK. C-reactive protein (CRP) and its association with periodontal disease: a brief review. *Journal of clinical and diagnostic research: JCDR*. 2014;8(7):ZE21.
131. Peltola H. C-reactive protein for rapid monitoring of infections of the central nervous system. *The Lancet*. 1982;319(8279):980-3.
132. Agrawal A. CRP after 2004. *Molecular immunology*. 2005;42(8):927-30.
133. Kishore U, Ghai R, Greenhough TJ, Shrive AK, Bonifati DM, Gadjeva MG, et al. Structural and functional anatomy of the globular domain of complement protein C1q. *Immunology letters*. 2004;95(2):113-28.
134. Mukerji R, Mirza S, Roche AM, Widener RW, Croney CM, Rhee D-K, et al. Pneumococcal surface protein A inhibits complement deposition on the pneumococcal surface by competing with the binding of C-reactive protein to cell-surface phosphocholine. *The Journal of Immunology*. 2012;120:1967.
135. Thomas-Rudolph D, Du Clos TW, Snapper CM, Mold C. C-reactive protein enhances immunity to *Streptococcus pneumoniae* by targeting uptake to Fc γ R on dendritic cells. *The Journal of Immunology*. 2007;178(11):7283-91.
136. Ng PM, Le Saux A, Lee CM, Tan NS, Lu J, Thiel S, et al. C-reactive protein collaborates with plasma lectins to boost immune response against bacteria. *The EMBO journal*. 2007;26(14):3431-40.
137. Marnell LL, Mold C, Volzer MA, Burlingame RW, Du Clos T. C-reactive protein binds to Fc gamma RI in transfected COS cells. *The Journal of Immunology*. 1995;155(4):2185-93.
138. Bharadwaj D, Stein M-P, Volzer M, Mold C, Du Clos TW. The major receptor for C-reactive protein on leukocytes is Fc γ receptor II. *Journal of Experimental Medicine*. 1999;190(4):585-90.
139. Tron K, Manolov DE, Röcker C, Kächele M, Torzewski J, Nienhaus GU. C-reactive protein specifically binds to Fc γ receptor type I on a macrophage-like cell line. *European journal of immunology*. 2008;38(5):1414-22.
140. Kindmark C-O. Stimulating effect of C-reactive protein on phagocytosis of various species of pathogenic bacteria. *Clinical and experimental immunology*. 1971;8(6):941.
141. Mold C, Baca R, Du Clos TW. Serum amyloid P component and C-reactive protein opsonize apoptotic cells for phagocytosis through Fc γ receptors. *Journal of autoimmunity*. 2002;19(3):147-54.
142. Garlanda C, Bottazzi B, Bastone A, Mantovani A. Pentraxins at the crossroads between innate immunity, inflammation, matrix deposition, and female fertility. *Annu Rev Immunol*. 2005;23:337-66.
143. Pepys M, Baltz M, Gomer K, Davies A, Doenhoff M. Serum amyloid P-component is an acute-phase reactant in the mouse. *Nature*. 1979;278(5701):259-61.
144. Lee P, Bird S, Zou J, Martin S. Phylogeny and expression analysis of C-reactive protein (CRP) and serum amyloid-P (SAP) like genes reveal two distinct groups in fish. *Fish & shellfish immunology*. 2017;65:42-51.

BIBLIOGRAFÍA

145. Behrens A-J, Duke RM, Petralia LM, Harvey DJ, Lehoux S, Magnelli PE, et al. Glycosylation profiling of dog serum reveals differences compared to human serum. *Glycobiology*. 2018;28(11):825-31.
146. Bose R, Bhattacharya S. C-reactive protein in the hemolymph of *Achatina fulica*: interrelationship with sex steroids and metallothionein. *Comparative Biochemistry and Physiology Part A: Molecular & Integrative Physiology*. 2000;125(4):485-95.
147. Tan SS, Ng PM, Ho B, Ding JL. The antimicrobial properties of C-reactive protein (CRP). *Journal of endotoxin research*. 2005;11(4):249-56.
148. Hoover GJ, El-Mowafi A, Simko E, Kocal TE, Ferguson HW, Hayes MA. Plasma proteins of rainbow trout (*Oncorhynchus mykiss*) isolated by binding to lipopolysaccharide from *Aeromonas salmonicida*. *Comparative Biochemistry and physiology part B: biochemistry and molecular biology*. 1998;120(3):559-69.
149. Elvitigala DAS, Wan Q, Kim HC, Lee J. Identification of a C-reactive protein like homologue from black rockfish (*Sebastes schlegelii*) evidencing its potent anti-microbial properties at molecular level. *Developmental & Comparative Immunology*. 2015;53(1):169-78.
150. Mukherjee S, Barman S, Sarkar S, Mandal NC, Bhattacharya S. Anti-bacterial activity of *Achatina* CRP and its mechanism of action. 2014.
151. Harrington JM, Chou H-T, Gutsmann T, Gelhaus C, Stahlberg H, Leippe M, et al. Membrane activity of a C-reactive protein. *FEBS letters*. 2009;583(6):1001-5.
152. Pathak A, Agrawal A. Evolution of C-reactive protein. *Frontiers in Immunology*. 2019;10:943.
153. Lund V, Olafsen JA. A comparative study of pentraxin-like proteins in different fish species. *Developmental & Comparative Immunology*. 1998;22(2):185-94.
154. Lund V, Olafsen JA. Changes in serum concentration of a serum amyloid P-like pentraxin in Atlantic salmon, *Salmo salar* L., during infection and inflammation. *Developmental & Comparative Immunology*. 1999;23(1):61-70.
155. Talbot AT, Pottinger TG, Smith TJ, Cairns MT. Acute phase gene expression in rainbow trout (*Oncorhynchus mykiss*) after exposure to a confinement stressor: a comparison of pooled and individual data. *Fish & shellfish immunology*. 2009;27(2):309-17.
156. Szalai AJ, Norcum M, Bly J, Clem L. Isolation of an acute-phase phosphorylcholine-reactive pentraxin from channel catfish (*Ictalurus punctatus*). *Comparative biochemistry and physiology B, Comparative biochemistry*. 1992;102(3):535-43.
157. MacCarthy EM, Burns I, Irnazarow I, Polwart A, Greenhough TJ, Shrive AK, et al. Serum CRP-like protein profile in common carp *Cyprinus carpio* challenged with *Aeromonas hydrophila* and *Escherichia coli* lipopolysaccharide. *Developmental & Comparative Immunology*. 2008;32(11):1281-9.
158. Pionnier N, Adamek M, Miest JJ, Harris SJ, Matras M, Rakus KŁ, et al. C-reactive protein and complement as acute phase reactants in common carp *Cyprinus carpio* during CyHV-3 infection. *Diseases of aquatic organisms*. 2014;109(3):187-99.
159. Magnadottir B, Audunsdottir SS, Bragason BT, Gisladottir B, Jonsson ZO, Gudmundsdottir S. The acute phase response of Atlantic cod (*Gadus morhua*): humoral and cellular response. *Fish & shellfish immunology*. 2011;30(4-5):1124-30.
160. Magnadóttir B, Hayes P, Gísladóttir B, Bragason BP, Hristova M, Nicholas AP, et al. Pentraxins CRP-I and CRP-II are post-translationally deiminated and differ in tissue specificity in cod (*Gadus morhua* L.) ontogeny. *Developmental & Comparative Immunology*. 2018;87:1-11.
161. Gisladottir B, Gudmundsdottir S, Brown L, Jonsson ZO, Magnadottir B. Isolation of two C-reactive protein homologues from cod (*Gadus morhua* L.) serum. *Fish & Shellfish Immunology*. 2009;26(2):210-9.

162. Cray C. Acute phase proteins in animals. *Progress in molecular biology and translational science.* 105: Elsevier; 2012. p. 113-50.
163. Ansar W, Ghosh S. C-reactive protein and the biology of disease. *Immunologic research.* 2013;56(1):131-42.
164. Pepys MB, Hirschfield GM. C-reactive protein: a critical update. *The Journal of clinical investigation.* 2003;111(12):1805-12.
165. Pionnier N, Falco A, Miest JJ, Shrive AK, Hoole D. Feeding common carp *Cyprinus carpio* with β -glucan supplemented diet stimulates C-reactive protein and complement immune acute phase responses following PAMPs injection. *Fish & shellfish immunology.* 2014;39(2):285-95.
166. Pionnier N, Falco A, Miest J, Frost P, Irnazarow I, Shrive A, et al. Dietary beta-glucan stimulate complement and C-reactive protein acute phase responses in common carp (*Cyprinus carpio*) during an *Aeromonas salmonicida* infection. *Fish Shellfish Immunol.* 2013;34(3):819-31. doi: 10.1016/j.fsi.2012.12.017. PubMed PMID: 23291104.
167. MacCarthy EM, Burns I, Irnazarow I, Polwart A, Greenhough TJ, Shrive AK, et al. Serum CRP-like protein profile in common carp *Cyprinus carpio* challenged with *Aeromonas hydrophila* and *Escherichia coli* lipopolysaccharide. *Dev Comp Immunol.* 2008;32(11):1281-9. doi: 10.1016/j.dci.2008.04.004. PubMed PMID: 18538390.
168. Pionnier N, Adamek M, Miest JJ, Harris SJ, Matras M, Rakus KL, et al. C-reactive protein and complement as acute phase reactants in common carp *Cyprinus carpio* during CyHV-3 infection. *Dis Aquat Organ.* 2014;109(3):187-99. doi: 10.3354/dao02727. PubMed PMID: 24991845.
169. Choi K-M, Shim SH, An CM, Nam B-H, Jeong J-M, Kim J-W, et al. Functional characterisation and expression analysis of recombinant serum amyloid P isoform 1 (RbSAP1) from rock bream (*Oplegnathus fasciatus*). *Fish & shellfish immunology.* 2015;45(2):277-85.
170. Hwang SD, Bae JS, Jo DH, Kim KI, Cho MY, Jee BY, et al. Gene expression and functional characterization of serum amyloid P component 2 in rock bream, *Oplegnathus fasciatus*. *Fish Shellfish Immunol.* 2015;47(1):521-7. doi: 10.1016/j.fsi.2015.09.048. PubMed PMID: 26455663.
171. Bello-Perez M, Falco A, Medina-Gali R, Pereiro P, Encinar JA, Novoa B, et al. Neutralization of viral infectivity by zebrafish c-reactive protein isoforms. *Molecular immunology.* 2017;91:145-55.
172. Estepa A, Coll J. Innate multigene family memories are implicated in the viral-survivor zebrafish phenotype. *PloS one.* 2015;10(8):e0135483.
173. Medina-Gali R, Belló-Pérez M, Martínez-López A, Falcó A, Ortega-Villaizán M, Encinar JA, et al. Chromatin immunoprecipitation and high throughput sequencing of SVCV-infected zebrafish reveals novel epigenetic histone methylation patterns involved in antiviral immune response. *Fish & shellfish immunology.* 2018;82:514-21.
174. Ballesteros NA, Saint-Jean SS, Encinas PA, Perez-Prieto SI, Coll JM. Oral immunization of rainbow trout to infectious pancreatic necrosis virus (Ipnv) induces different immune gene expression profiles in head kidney and pyloric ceca. *Fish Shellfish Immunol.* 2012;33(2):174-85. doi: 10.1016/j.fsi.2012.03.016. PubMed PMID: 22521628.
175. García-Valtanen P, Martínez-López A, López-Muñoz A, Bello-Perez M, Medina-Gali RM, Ortega-Villaizán MdM, et al. Zebra fish lacking adaptive immunity acquire an antiviral alert state characterized by upregulated gene expression of apoptosis, multigene families, and interferon-related genes. *Frontiers in immunology.* 2017;8:121.
176. Valério E, Chaves S, Tenreiro R. Diversity and impact of prokaryotic toxins on aquatic environments: a review. *Toxins.* 2010;2(10):2359-410.

BIBLIOGRAFÍA

177. Gozlan RE, Peeler EJ, Longshaw M, St-Hilaire S, Feist SW. Effect of microbial pathogens on the diversity of aquatic populations, notably in Europe. *Microbes and Infection*. 2006;8(5):1358-64.
178. Yoder JA, Nielsen ME, Amemiya CT, Litman GW. Zebrafish as an immunological model system. *Microbes and Infection*. 2002;4(14):1469-78.
179. Crim MJ, Riley LK. Viral diseases in zebrafish: what is known and unknown. *ILAR journal*. 2012;53(2):135-43.
180. Novoa B, Figueras A. Zebrafish: model for the study of inflammation and the innate immune response to infectious diseases. *Current Topics in Innate Immunity II*: Springer; 2012. p. 253-75.
181. H Meijer A, P Spaink H. Host-pathogen interactions made transparent with the zebrafish model. *Current drug targets*. 2011;12(7):1000-17.
182. Iwanami N. Zebrafish as a model for understanding the evolution of the vertebrate immune system and human primary immunodeficiency. *Experimental hematology*. 2014;42(8):697-706.
183. Trede NS, Langenau DM, Traver D, Look AT, Zon LI. The use of zebrafish to understand immunity. *Immunity*. 2004;20(4):367-79.
184. Rembold M, Lahiri K, Foulkes NS, Wittbrodt J. Transgenesis in fish: efficient selection of transgenic fish by co-injection with a fluorescent reporter construct. *Nature protocols*. 2006;1(3):1133.
185. Torraça V, Mostowy S. Zebrafish infection: from pathogenesis to cell biology. *Trends in cell biology*. 2017.
186. Varela M, Figueras A, Novoa B. Modelling viral infections using zebrafish: innate immune response and antiviral research. *Antiviral research*. 2017;139:59-68.
187. Sun G, Li H, Wang Y, Zhang B, Zhang S. Zebrafish complement factor H and its related genes: identification, evolution, and expression. *Functional & integrative genomics*. 2010;10(4):577-87.
188. Brugman S. The zebrafish as a model to study intestinal inflammation. *Developmental & Comparative Immunology*. 2016;64:82-92.
189. Gabor KA, Goody MF, Mowle WK, Breitbach ME, Gratacap RL, Witten PE, et al. Influenza A virus infection in zebrafish recapitulates mammalian infection and sensitivity to anti-influenza drug treatment. *Disease models & mechanisms*. 2014;7(11):1227-37.
190. Hoffmann B, Beer M, Schütze H, Mettenleiter T. Fish rhabdoviruses: molecular epidemiology and evolution. *The World of Rhabdoviruses*: Springer; 2005. p. 81-117.
191. Snow M. The contribution of molecular epidemiology to the understanding and control of viral diseases of salmonid aquaculture. *Veterinary research*. 2011;42(1):56.
192. Purcell MK, Laing KJ, Winton JR. Immunity to fish rhabdoviruses. *Viruses*. 2012;4(1):140-66.
193. Ashraf U, Lu Y, Lin L, Yuan J, Wang M, Liu X. Spring viraemia of carp virus: recent advances. *Journal of General Virology*. 2016;97(5):1037-51.
194. Shao L, Zhao J, Zhang H. Spring viraemia of carp virus enters grass carp ovary cells via clathrin-mediated endocytosis and macropinocytosis. *Journal of General Virology*. 2016;97(11):2824-36.
195. Bearzotti M, Delmas B, Lamoureux A, Loustau A-M, Chilmonczyk S, Bremont M. Fish rhabdovirus cell entry is mediated by fibronectin. *Journal of virology*. 1999;73(9):7703-9.
196. Liu H, Liu Y, Liu S, Pang D-W, Xiao G. Clathrin-mediated endocytosis in living host cells visualized through quantum dot labeling of infectious hematopoietic necrosis virus. *Journal of virology*. 2011;85(13):6252-62.
197. Collet B. Innate immune responses of salmonid fish to viral infections. *Developmental & Comparative Immunology*. 2014;43(2):160-73.

198. Liu Z, Teng Y, Liu H, Jiang Y, Xie X, Li H, et al. Simultaneous detection of three fish rhabdoviruses using multiplex real-time quantitative RT-PCR assay. *Journal of virological methods*. 2008;149(1):103-9.
199. Balmer BF, Getchell RG, Powers RL, Lee J, Zhang T, Jung ME, et al. Broad-spectrum antiviral JL122 blocks infection and inhibits transmission of aquatic rhabdoviruses. *Virology*. 2018;525:143-9.
200. Ortega-Villaizan M, Chico V, Martinez-Lopez A, Garcia-Valtanen P, Coll J, Estepa A. Development of new therapeutical/adjuvant molecules by pepscan mapping of autophagy and IFN inducing determinants of rhabdoviral G proteins. *Molecular immunology*. 2016;70:118-24.
201. Sanders GE, Batts WN, Winton JR. Susceptibility of zebrafish (*Danio rerio*) to a model pathogen, spring viremia of carp virus. *Comparative medicine*. 2003;53(5):514-21.
202. Ahne W, Bjorklund H, Essbauer S, Fijan N, Kurath G, Winton J. Spring viremia of carp (SVC). *Diseases of aquatic organisms*. 2002;52(3):261-72.
203. Livak KJ, Schmittgen TD. Analysis of relative gene expression data using real-time quantitative PCR and the 2- $\Delta\Delta CT$ method. *methods*. 2001;25(4):402-8.
204. Encinas P, Garcia-Valtanen P, Chinchilla B, Gomez-Casado E, Estepa A, Coll J. Identification of multipath genes differentially expressed in pathway-targeted microarrays in zebrafish infected and surviving spring viremia carp virus (SVCV) suggest preventive drug candidates. *PLoS One*. 2013;8(9):e73553.
205. Pereiro P, Forn-Cuní G, Dios S, Coll J, Figueras A, Novoa B. Interferon-independent antiviral activity of 25-hydroxycholesterol in a teleost fish. *Antiviral research*. 2017;145:146-59.
206. Biasini M, Bienert S, Waterhouse A, Arnold K, Studer G, Schmidt T, et al. SWISS-MODEL: modelling protein tertiary and quaternary structure using evolutionary information. *Nucleic acids research*. 2014;42(W1):W252-W8.
207. Arnold K, Bordoli L, Kopp J, Schwede T. The SWISS-MODEL workspace: a web-based environment for protein structure homology modelling. *Bioinformatics*. 2006;22(2):195-201.
208. Guex N, Peitsch MC. SWISS-MODEL and the Swiss-Pdb Viewer: an environment for comparative protein modeling. *electrophoresis*. 1997;18(15):2714-23.
209. Trott O, Olson AJ. AutoDock Vina: improving the speed and accuracy of docking with a new scoring function, efficient optimization, and multithreading. *Journal of computational chemistry*. 2010;31(2):455-61.
210. Dallakyan S, Olson AJ. Small-molecule library screening by docking with PyRx. *Chemical Biology*: Springer; 2015. p. 243-50.
211. Shityakov S, Förster C. In silico predictive model to determine vector-mediated transport properties for the blood-brain barrier choline transporter. *Advances and applications in bioinformatics and chemistry: AACBC*. 2014;7:23.
212. Bíró A, Cervenák L, Balogh A, Lőrincz A, Uray K, Horváth A, et al. Novel anti-cholesterol monoclonal immunoglobulin G antibodies as probes and potential modulators of membrane raft-dependent immune functions. *Journal of lipid research*. 2007;48(1):19-29.
213. Torrent F, Villena A, Lee P, Fuchs W, Bergmann S, Coll J. The amino-terminal domain of ORF149 of koi herpesvirus is preferentially targeted by IgM from carp populations surviving infection. *Archives of virology*. 2016;161(10):2653-65.
214. Coll JM. herpesvirus infection induces both specific and heterologous antiviral antibodies in carp. *Frontiers in immunology*. 2018;9:39.
215. Néron B, Ménager H, Maufrais C, Joly N, Maupetit J, Letort S, et al. Mobyle: a new full web bioinformatics framework. *Bioinformatics*. 2009;25(22):3005-11.

BIBLIOGRAFÍA

216. Du Clos TW, Mold C. Pentraxins (CRP, SAP) in the process of complement activation and clearance of apoptotic bodies through Fc_y receptors. *Current opinion in organ transplantation.* 2011;16(1):15.
217. Paludan SR. Requirements for the induction of interleukin-6 by herpes simplex virus-infected leukocytes. *Journal of virology.* 2001;75(17):8008-15.
218. Wang J, Wang Q, Han T, Li Y-K, Zhu S-L, Ao F, et al. Soluble interleukin-6 receptor is elevated during influenza A virus infection and mediates the IL-6 and IL-32 inflammatory cytokine burst. *Cellular & molecular immunology.* 2015;12(5):633.
219. Goda T, Miyahara Y. Calcium-independent binding of human C-reactive protein to lysophosphatidylcholine in supported planar phospholipid monolayers. *Acta biomaterialia.* 2017;48:206-14.
220. Wang W, Fu Y, Zu Y, Wu N, Reichling J, Efferth T. Lipid rafts play an important role in the vesicular stomatitis virus life cycle. *Archives of virology.* 2009;154(4):595-600.
221. Pilely K, Fumagalli S, Rosbjerg A, Genster N, Skjoedt M-O, Perego C, et al. c-reactive Protein Binds to cholesterol crystals and co-localizes with the Terminal complement complex in human atherosclerotic Plaques. *Frontiers in immunology.* 2017;8:1040.
222. Taskinen S, Hyvönen M, Kovanen PT, Meri S, Pentikäinen MO. C-reactive protein binds to the 3 β -OH group of cholesterol in LDL particles. *Biochemical and biophysical research communications.* 2005;329(4):1208-16.
223. Thompson D, Pepys MB, Wood SP. The physiological structure of human C-reactive protein and its complex with phosphocholine. *Structure.* 1999;7(2):169-77.
224. Wang M-Y, Ji S-R, Bai C-J, El Kebir D, Li H-Y, Shi J-M, et al. A redox switch in C-reactive protein modulates activation of endothelial cells. *The FASEB Journal.* 2011;25(9):3186-96.
225. Clemente R, De Parseval A, Perez M, Juan C. Borna disease virus requires cholesterol in both cellular membrane and viral envelope for efficient cell entry. *Journal of virology.* 2009;83(6):2655-62.
226. Pöhlmann S, Simmons G. *Viral entry into host cells:* Springer; 2013.
227. Langevin C, Aleksejeva E, Passoni G, Palha N, Levraud J-P, Boudinot P. The antiviral innate immune response in fish: evolution and conservation of the IFN system. *Journal of molecular biology.* 2013;425(24):4904-20.
228. Zhang Y, Gui J. Fish interferon response and its molecular regulation: a review. *Sheng wu gong cheng xue bao= Chinese journal of biotechnology.* 2011;27(5):675-83.
229. Zou PF, Nie P. *Zebrafish as a Model for the Study of Host-Virus Interactions.* Innate Antiviral Immunity: Springer; 2017. p. 57-78.
230. Yuan J, Yang Y, Nie H, Li L, Gu W, Lin L, et al. Transcriptome analysis of epithelioma papulosum cyprini cells after SVCV infection. *BMC genomics.* 2014;15(1):935.
231. Zou J, Gorgoglione B, Taylor NG, Summathad T, Lee P-T, Panigrahi A, et al. Salmonids have an extraordinary complex type I IFN system: characterization of the IFN locus in rainbow trout *Oncorhynchus mykiss* reveals two novel IFN subgroups. *The Journal of Immunology.* 2014;193(5):2273-86.
232. García-Valtanen P, Ortega-Villaizán MdM, Martínez-López A, Medina-Gali R, Pérez L, Mackenzie S, et al. Autophagy-inducing peptides from mammalian VSV and fish VHSV rhabdoviral G glycoproteins (G) as models for the development of new therapeutic molecules. *Autophagy.* 2014;10(9):1666-80.
233. Wang Y, Chen N, Hegazy AM, Liu X, Wu Z, Liu X, et al. Autophagy induced by snakehead fish vesiculovirus inhibited its replication in SSN-1 cell line. *Fish & shellfish immunology.* 2016;55:415-22.
234. Mauthe M, Orhon I, Rocchi C, Zhou X, Luhr M, Hijlkema K-J, et al. Chloroquine inhibits autophagic flux by decreasing autophagosome-lysosome fusion. *Autophagy.* 2018;14(8):1435-55.

235. Espín-Palazón R, Martínez-López A, Roca FJ, López-Muñoz A, Tyrkalska SD, Candel S, et al. TNF α impairs rhabdoviral clearance by inhibiting the host autophagic antiviral response. *PLoS pathogens*. 2016;12(6):e1005699.
236. Vinod V, Padmakrishnan C, Vijayan B, Gopala S. 'How can I halt thee?'The puzzles involved in autophagic inhibition. *Pharmacological research*. 2014;82:1-8.
237. Murphy TM, Baum LL, Beaman KD. Extrahepatic transcription of human C-reactive protein. *Journal of Experimental Medicine*. 1991;173(2):495-8.
238. Wang T, Sun L. CsSAP, a teleost serum amyloid P component, interacts with bacteria, promotes phagocytosis, and enhances host resistance against bacterial and viral infection. *Developmental & Comparative Immunology*. 2016;55:12-20.
239. Li M-f, Chen C, Li J, Sun L. The C-reactive protein of tongue sole *Cynoglossus semilaevis* is an acute phase protein that interacts with bacterial pathogens and stimulates the antibacterial activity of peripheral blood leukocytes. *Fish & shellfish immunology*. 2013;34(2):623-31.
240. Zapata A, Diez B, Cejalvo T, Gutierrez-de Frias C, Cortes A. Ontogeny of the immune system of fish. *Fish & shellfish immunology*. 2006;20(2):126-36.
241. Salinas I. The mucosal immune system of teleost fish. *Biology*. 2015;4(3):525-39.
242. Tarnawska M, Augustyniak M, Łaszczycyca P, Migula P, Irnazarow I, Krzyżowski M, et al. Immune response of juvenile common carp (*Cyprinus carpio* L.) exposed to a mixture of sewage chemicals. *Fish & shellfish immunology*. 2019.
243. Valdenegro-Vega VA, Crosbie P, Bridle A, Leef M, Wilson R, Nowak BF. Differentially expressed proteins in gill and skin mucus of Atlantic salmon (*Salmo salar*) affected by amoebic gill disease. *Fish & shellfish immunology*. 2014;40(1):69-77.
244. Bierne H, Hamon M, Cossart P. Epigenetics and bacterial infections. *Cold Spring Harbor perspectives in medicine*. 2012;2(12):a010272.
245. Gong X-Y, Zhang Q-M, Gui J-F, Zhang Y-B. SVCV infection triggers fish IFN response through RLR signaling pathway. *Fish & shellfish immunology*. 2019;86:1058-63.
246. Wang Y, Li Z, Lu Y, Hu G, Lin L, Zeng L, et al. Molecular characterization, tissue distribution and expression, and potential antiviral effects of TRIM32 in the Common Carp (*Cyprinus carpio*). *International journal of molecular sciences*. 2016;17(10):1693.
247. Raida MK, Buchmann K. Innate immune response in rainbow trout (*Oncorhynchus mykiss*) against primary and secondary infections with *Yersinia ruckeri* O1. *Developmental & Comparative Immunology*. 2009;33(1):35-45.
248. Braden LM, Barker DE, Koop BF, Jones SR. Comparative defense-associated responses in salmon skin elicited by the ectoparasite *Lepeophtheirus salmonis*. *Comparative Biochemistry and Physiology Part D: Genomics and Proteomics*. 2012;7(2):100-9.
249. Wei X, Li XZ, Zheng X, Jia P, Wang J, Yang X, et al. Toll-like receptors and interferon associated immune factors responses to spring viraemia of carp virus infection in common carp (*Cyprinus carpio*). *Fish & shellfish immunology*. 2016;55:568-76.
250. Nam B-H. Molecular cloning and characterisation of the flounder (*Paralichthys olivaceus*) interleukin-6 gene. *Fish Shellfish Immunol*. 2007;23:231-6.
251. Carballo C, Castro D, Borrego JJ, Manchado M. Gene expression profiles associated with lymphocystis disease virus (LCDV) in experimentally infected Senegalese sole (*Solea senegalensis*). *Fish & shellfish immunology*. 2017;66:129-39.
252. Iliev DB, Castellana B, MacKenzie S, Planas JV, Goetz FW. Cloning and expression analysis of an IL-6 homolog in rainbow trout (*Oncorhynchus mykiss*). *Molecular immunology*. 2007;44(7):1803-7.
253. Braden LM, Barker DE, Koop BF, Jones SR. Differential modulation of resistance biomarkers in skin of juvenile and mature pink salmon, *Oncorhynchus gorbuscha* by the salmon louse, *Lepeophtheirus salmonis*. *Fish & shellfish immunology*. 2015;47(1):7-14.

BIBLIOGRAFÍA

254. Karsten A, Rice C. c-Reactive protein levels as a biomarker of inflammation and stress in the Atlantic sharpnose shark (*Rhizoprionodon terraenovae*) from three southeastern USA estuaries. *Marine environmental research*. 2004;58(2-5):747-51.
255. Giang DTH, Van Driessche E, Vandenberghe I, Devreese B, Beeckmans S. Isolation and characterization of SAP and CRP, two pentraxins from *Pangasianodon* (*Pangasius*) hypophthalmus. *Fish & shellfish immunology*. 2010;28(5-6):743-53.
256. Winkelhake JL, Vodicnik MJ, Taylor JL. Induction in rainbow trout of an acute phase (C-reactive) protein by chemicals of environmental concern. *Comparative biochemistry and physiology C, Comparative pharmacology and toxicology*. 1983;74(1):55-8.
257. Roy S, Kumar V, Kumar V, Behera B. Acute Phase Proteins and their Potential Role as an Indicator for Fish Health and in Diagnosis of Fish Diseases. *Protein and peptide letters*. 2017;24(1):78-89.
258. Job ER, Bottazzi B, Gilbertson B, Edenborough KM, Brown LE, Mantovani A, et al. Serum amyloid P is a sialylated glycoprotein inhibitor of influenza A viruses. *PLoS One*. 2013;8(3):e59623.
259. Reading PC, Bozza S, Gilbertson B, Tate M, Moretti S, Job ER, et al. Antiviral activity of the long chain pentraxin PTX3 against influenza viruses. *The Journal of Immunology*. 2008;180(5):3391-8.
260. Wang F, Jiao H, Liu W, Chen B, Wang Y, Chen B, et al. The antiviral mechanism of viperin and its splice variant in spring viremia of carp virus infected fathead minnow cells. *Fish & shellfish immunology*. 2018.
261. Chang M-X, Zou J, Nie P, Huang B, Yu Z, Collet B, et al. Intracellular interferons in fish: a unique means to combat viral infection. *PLoS pathogens*. 2013;9(11):e1003736.
262. Jungblut PR, Holzhütter HG, Apweiler R, Schlüter H. The speciation of the proteome. *Chemistry Central Journal*. 2008;2(1):16.
263. Werner RG, Kopp K, Schlueter M. Glycosylation of therapeutic proteins in different production systems. *Acta Paediatrica*. 2007;96:17-22.
264. Robey F, Ohura K, Futaki S, Fujii N, Yajima H, Goldman N, et al. Proteolysis of human C-reactive protein produces peptides with potent immunomodulating activity. *Journal of Biological Chemistry*. 1987;262(15):7053-7.
265. Song Z, Cai L, Guo L, Tsukamoto Y, Yutani C, Li X-A. Accumulation and expression of serum amyloid P component in human atherosclerotic lesions. *Atherosclerosis*. 2010;211(1):90-5.
266. Leser GP, Lamb RA. Influenza virus assembly and budding in raft-derived microdomains: a quantitative analysis of the surface distribution of HA, NA and M2 proteins. *Virology*. 2005;342(2):215-27.
267. Scheiffele P, Rietveld A, Wilk T, Simons K. Influenza viruses select ordered lipid domains during budding from the plasma membrane. *Journal of Biological Chemistry*. 1999;274(4):2038-44.
268. Takeda M, Leser GP, Russell CJ, Lamb RA. Influenza virus hemagglutinin concentrates in lipid raft microdomains for efficient viral fusion. *Proceedings of the National Academy of Sciences*. 2003;100(25):14610-7.
269. Ali A, Nayak DP. Assembly of Sendai virus: M protein interacts with F and HN proteins and with the cytoplasmic tail and transmembrane domain of F protein. *Virology*. 2000;276(2):289-303.
270. Manié SN, Debreyne S, Vincent S, Gerlier D. Measles virus structural components are enriched into lipid raft microdomains: a potential cellular location for virus assembly. *Journal of virology*. 2000;74(1):305-11.
271. Vincent S, Gerlier D, Manié SN. Measles virus assembly within membrane rafts. *Journal of virology*. 2000;74(21):9911-5.

272. Dolganiuc V, McGinnes L, Luna EJ, Morrison TG. Role of the cytoplasmic domain of the Newcastle disease virus fusion protein in association with lipid rafts. *Journal of virology*. 2003;77(24):12968-79.
273. Laliberte JP, McGinnes LW, Peeples ME, Morrison TG. Integrity of membrane lipid rafts is necessary for the ordered assembly and release of infectious Newcastle disease virus particles. *Journal of virology*. 2006;80(21):10652-62.
274. Laliberte JP, McGinnes LW, Morrison TG. Incorporation of functional HN-F glycoprotein-containing complexes into newcastle disease virus is dependent on cholesterol and membrane lipid raft integrity. *Journal of virology*. 2007;81(19):10636-48.
275. Ji S-R, Ma L, Bai C-J, Shi J-M, Li H-Y, Potempa LA, et al. Monomeric C-reactive protein activates endothelial cells via interaction with lipid raft microdomains. *The FASEB Journal*. 2009;23(6):1806-16.
276. Langevin C, Levraud J-P, Boudinot P. Fish antiviral tripartite motif (TRIM) proteins. *Fish & shellfish immunology*. 2019;86:724-33.
277. Hambleton S, Steinberg S, Gershon M, Gershon A. Cholesterol dependence of varicella-zoster virion entry into target cells. *Journal of virology*. 2007;81(14):7548-58.
278. Niyogi K, Hildreth JE. Characterization of new syncytium-inhibiting monoclonal antibodies implicates lipid rafts in human T-cell leukemia virus type 1 syncytium formation. *Journal of virology*. 2001;75(16):7351-61.
279. Ke F, Zhang Q-Y. Aquatic animal viruses mediated immune evasion in their host. *Fish & shellfish immunology*. 2018.
280. Poynter SJ, DeWitte-Orr SJ. Fish interferon-stimulated genes: the antiviral effectors. *Developmental & Comparative Immunology*. 2016;65:218-25.
281. Zou J, Secombes CJ. Teleost fish interferons and their role in immunity. *Developmental & Comparative Immunology*. 2011;35(12):1376-87.
282. Jurado MT, García-Valtanen P, Estepa A, Perez L. Antiviral activity produced by an IPNV-carrier EPC cell culture confers resistance to VHSV infection. *Veterinary microbiology*. 2013;166(3):412-8.
283. Nombela I, Puente-Marin S, Chico V, Villena AJ, Carracedo B, Ciordia S, et al. Identification of diverse defense mechanisms in rainbow trout red blood cells in response to halted replication of VHS virus. *F1000Research*. 2017;6.
284. Parreño R, Torres S, Almagro L, Belló-Pérez M, Estepa A, Perez L. Induction of viral interference by IPNV-carrier cells on target cells: A cell co-culture study. *Fish & shellfish immunology*. 2016;58:483-9.
285. She S, Xiang Y, Yang M, Ding X, Liu X, Ma L, et al. C-reactive protein is a biomarker of AFP-negative HBV-related hepatocellular carcinoma. *International journal of oncology*. 2015;47(2):543-54.
286. Berryman S, Brooks E, Burman A, Hawes P, Roberts R, Netherton C, et al. FMDV induces autophagosomes during cell entry via a class III PI3K-independent pathway. *Journal of virology*. 2012;JVI. 00846-12.
287. Delgado MA, Elmaoued RA, Davis AS, Kyei G, Deretic V. Toll-like receptors control autophagy. *The EMBO journal*. 2008;27(7):1110-21.
288. Shoji-Kawata S, Levine B. Autophagy, antiviral immunity, and viral countermeasures. *Biochimica et Biophysica Acta (BBA)-Molecular Cell Research*. 2009;1793(9):1478-84.
289. Yang Y, Jiang G, Zhang P, Fan J. Programmed cell death and its role in inflammation. *Military Medical Research*. 2015;2(1):12.
290. Li M, Li J, Zeng R, Yang J, Liu J, Zhang Z, et al. Respiratory syncytial virus replication is promoted by autophagy-mediated inhibition of apoptosis. *Journal of virology*. 2018;92(8):e02193-17.

BIBLIOGRAFÍA

291. Kim JY, Wang L, Lee J, Ou J-hJ. Hepatitis C virus induces the localization of lipid rafts to autophagosomes for its RNA replication. *Journal of virology*. 2017;91(20):e00541-17.
292. Peng J, Zhu S, Hu L, Ye P, Wang Y, Tian Q, et al. Wild-type rabies virus induces autophagy in human and mouse neuroblastoma cell lines. *Autophagy*. 2016;12(10):1704-20. doi: 10.1080/15548627.2016.1196315. PubMed PMID: 27463027; PubMed Central PMCID: PMC5079669.
293. Tu Z, Gong W, Zhang Y, Feng Y, Liu Y, Tu C. Inhibition of Rabies Virus by 1, 2, 3, 4, 6-Penta-O-galloyl- β -d-Glucose Involves mTOR-Dependent Autophagy. *Viruses*. 2018;10(4):201.
294. Khakpoor A, Panyasrivanit M, Wikan N, Smith DR. A role for autophagolysosomes in dengue virus 3 production in HepG2 cells. *Journal of General Virology*. 2009;90(5):1093-103.
295. Hurwitz SN, Cheerathodi MR, Nkosi D, York SB, Meckes DG. Tetraspanin CD63 bridges autophagic and endosomal processes to regulate exosomal secretion and intracellular signaling of Epstein-Barr virus LMP1. *Journal of virology*. 2018;92(5):e01969-17.
296. Panyasrivanit M, Khakpoor A, Wikan N, Smith DR. Co-localization of constituents of the dengue virus translation and replication machinery with amphisomes. *Journal of General Virology*. 2009;90(2):448-56.
297. Zheng K, Li Y, Wang S, Wang X, Liao C, Hu X, et al. Inhibition of autophagosome-lysosome fusion by ginsenoside Ro via the ESR2-NCF1-ROS pathway sensitizes esophageal cancer cells to 5-fluorouracil-induced cell death via the CHEK1-mediated DNA damage checkpoint. *Autophagy*. 2016;12(9):1593-613.
298. Redmann M, Benavides GA, Berryhill TF, Wani WY, Ouyang X, Johnson MS, et al. Inhibition of autophagy with bafilomycin and chloroquine decreases mitochondrial quality and bioenergetic function in primary neurons. *Redox biology*. 2017;11:73-81.
299. Terman A, Kurz T, Gustafsson B, Brunk U. Lysosomal labilization. *IUBMB life*. 2006;58(9):531-9.
300. Le Blanc I, Luyet P-P, Pons V, Ferguson C, Emans N, Petiot A, et al. Endosome-to-cytosol transport of viral nucleocapsids. *Nature cell biology*. 2005;7(7):653.
301. Chelbi-Alix M, Thang MN. Chloroquine impairs the interferon-induced antiviral state without affecting the 2', 5'-oligoadenylate synthetase. *Journal of Biological Chemistry*. 1985;260(13):7960-4.
302. Cui J, Sim TH-F, Gong Z, Shen H-M. Generation of transgenic zebrafish with liver-specific expression of EGFP-Lc3: a new *in vivo* model for investigation of liver autophagy. *Biochemical and biophysical research communications*. 2012;422(2):268-73.
303. Buffen K, Oosting M, Quintin J, Ng A, Kleinnijenhuis J, Kumar V, et al. Autophagy controls BCG-induced trained immunity and the response to intravesical BCG therapy for bladder cancer. *PLoS pathogens*. 2014;10(10):e1004485.
304. Lee S-J, Jung YH, Kim JS, Lee HJ, Lee SH, Lee K-H, et al. A *Vibrio vulnificus* VvpM induces IL-1 β production coupled with necrotic macrophage death via distinct spatial targeting by ANXA2. *Frontiers in cellular and infection microbiology*. 2017;7:352.
305. Hsu SP, Kuo JS, Chiang H-C, Wang H-E, Wang Y-S, Huang C-C, et al. Temozolomide, sirolimus and chloroquine is a new therapeutic combination that synergizes to disrupt lysosomal function and cholesterol homeostasis in GBM cells. *Oncotarget*. 2018;9(6):6883.
306. Singh R, Kaushik S, Wang Y, Xiang Y, Novak I, Komatsu M, et al. Autophagy regulates lipid metabolism. *Nature*. 2009;458(7242):1131.
307. Lembo D, Cagno V, Civra A, Poli G. Oxysterols: an emerging class of broad spectrum antiviral effectors. *Molecular aspects of medicine*. 2016;49:23-30.

308. Li C, Deng Y-Q, Wang S, Ma F, Aliyari R, Huang X-Y, et al. 25-Hydroxycholesterol protects host against Zika virus infection and its associated microcephaly in a mouse model. *Immunity*. 2017;46(3):446-56.
309. Li C, Sun L, Lin H, Qin Z, Tu J, Li J, et al. Glutamine starvation inhibits snakehead vesiculovirus replication via inducing autophagy associated with the disturbance of endogenous glutathione pool. *Fish & shellfish immunology*. 2019;86:1044-52.
310. Shawli GT, Adeyemi OO, Stonehouse NJ, Herod MR. The Oxysterol 25-Hydroxycholesterol Inhibits Replication of Murine Norovirus. *Viruses*. 2019;11(2):97.
311. Shrivastava-Ranjan P, Bergeron É, Chakrabarti AK, Albariño CG, Flint M, Nichol ST, et al. 25-Hydroxycholesterol inhibition of Lassa virus infection through aberrant GP1 glycosylation. *MBio*. 2016;7(6):e01808-16.
312. Liu S-Y, Aliyari R, Chikere K, Li G, Marsden MD, Smith JK, et al. Interferon-inducible cholesterol-25-hydroxylase broadly inhibits viral entry by production of 25-hydroxycholesterol. *Immunity*. 2013;38(1):92-105.
313. Civra A, Francese R, Gamba P, Testa G, Cagno V, Poli G, et al. 25-Hydroxycholesterol and 27-hydroxycholesterol inhibit human rotavirus infection by sequestering viral particles into late endosomes. *Redox biology*. 2018;19:318-30.
314. Noguchi N, Urano Y, Takabe W, Saito Y. New aspects of 24 (S)-hydroxycholesterol in modulating neuronal cell death. *Free Radical Biology and Medicine*. 2015;87:366-72.
315. Nury T, Zarrouk A, Mackrill JJ, Samadi M, Durand P, Riedinger J-M, et al. Induction of oxiapoptophagy on 158N murine oligodendrocytes treated by 7-ketosterol-, 7 β -hydroxycholesterol-, or 24 (S)-hydroxycholesterol: Protective effects of α -tocopherol and docosahexaenoic acid (DHA; C22: 6 n-3). *Steroids*. 2015;99:194-203.
316. Vurusانer B, Gargiulo S, Testa G, Gamba P, Leonarduzzi G, Poli G, et al. The role of autophagy in survival response induced by 27-hydroxycholesterol in human promonocytic cells. *Redox biology*. 2018.



COMPENDIO DE PUBLICACIONES

PUBLICACIÓN 1

TÍTULO: Structure and functionalities of the human c-reactive protein compared to the zebrafish multigene family of c-reactive-like proteins

COAUTORES: Melissa Belló Pérez, Alberto Falcó Graciá, Regla María Medina Gali, Jose Antonio Encinar Hidalgo, Beatriz Novoa García, Luis Pérez García-Estañ, Amparo Estepa Pérez, Julio Coll Morales.

REVISTA: Developmental and Comparative Immunology

doi: 10.1016/j.dci.2016.12.001

Volumen 69, Abril 2017, Páginas 33-40

Structure and functionalities of the human c-reactive protein compared to the zebrafish multigene family of c-reactive-like proteins

short title: Comparative zebrafish CRP-like proteins

7

8

11

¹² ¹³ ¹ Instituto Nacional Investigación y Tecnología Agrarias y Alimentarias, Dpto. Biotecnología. INIA. Madrid, Spain.

15 ²Universidad Miguel Hernández, UMH-IBMC, 03202 Elche, Spain

16 ³ Instituto de Investigaciones Marinas, CSIC, Vigo, España

17

18 Keywords: multi-gene family; pentraxins; c-reactive protein; zebrafish; structure; function

19

20 * Corresponding author
21
22 Email addresses:
23 MB, melissa.bello@goumh.umh.es
24 AF, alber.falco@umh.es
25 RM, reglita2000@yahoo.com
26 JA, jant.encinar@goumh.umh.es
27 BN, beatriznovoa@iim.csic.es
28 LP, luis.perez@umh.es
29 JC, juliocoll@inia.es
30

31

32

33

34 **Abstract**

35 Because of the recent discovery of multiple c-reactive protein (*crp*)-like genes in zebrafish (*Danio rerio*) with
36 predicted heterogeneous phospholipid-binding amino acid sequences and heterogeneous transcript expression
37 levels in viral survivors and adaptive-deficient mutants, zebrafish constitute an attractive new model for
38 exploring the evolution of these protein's functions, including their possible participation in fish trained
39 immunity. Circulating human CRP belongs to the short pentraxin family of oligomeric proteins that are
40 characteristic of early acute-phase innate responses and is widely used as a clinical inflammation marker. In
41 contrast to pentameric human CRP (pCRP), zebrafish CRPs are trimeric (tCRP); however monomeric CRP
42 (mCRP) conformations may also be generated when associated with cellular membranes as occurs in
43 humans. Compared to human CRP, zebrafish CRP-like proteins show homologous amino acid sequence
44 stretches that are consistent with, although not yet demonstrated, cysteine-dependent redox switches,
45 calcium-binding spots, phosphocholine-binding pockets, C1q-binding domains, regions interacting with
46 immunoglobulin Fc receptors (FcR), unique mCRP epitopes, mCRP binding peptides to cholesterol-enriched
47 rafts, protease target sites, and/or binding sites to monocyte, macrophage, neutrophils, platelets and/or
48 endothelial cells. Amino acid variations among the zebrafish CRP-like multiprotein family and derived
49 isoforms in these stretches suggest that functional heterogeneity best fits the wide variety of aquatic
50 pathogens. As occurs in humans, phospholipid-tagged tCRP-like multiproteins might also influence local
51 inflammation and induce innate immune responses; however, in addition, different zebrafish tCRP-like
52 proteins and/or isoforms might fine tune new still unknown functions. The information reviewed here could
53 be of value for future studies not only to comparative but also medical immunologists and/or fisheries
54 sectors. This review also introduces some novel speculations for future studies.

55

56

57

58 **1. The human CRP short-pentraxin family**

59 Human c-reactive protein (CRP) belongs to a family of short-chain pentraxins that share > 50 %
60 amino acid identity and some structural/functional features with the serum amyloid P component (SAP)
61 (Woo et al., 1985). Blood circulating human CRP shows a pentameric (pCRP) cyclic symmetry which is
62 formed by monomers of ~ 200 amino acids (~ 23 KDa) (Shrive et al., 1996). Other minority conformations
63 such as mild-acidic-pH pentamers (Hammond et al., 2010) or decamers and tissue-associated monomers
64 (mCRP), have also been described (Wu et al., 2015).

65 CRP is a part of the innate response and is released mainly from the liver into the blood, triggered by
66 any cellular damage produced by an injury and/or disease to affect systemic/local inflammation and help in
67 pathogen neutralization (Zhang et al., 2010). CRP as a part of the acute-phase response increases its basal
68 plasma level 2-3 orders of magnitude (i.e., from 1-5 to 500-1000 µg per ml) hours after the inflammatory
69 signals are generated (Bottazzi et al., 2016; Du Clos, 2013; Vilahur and Badimon, 2015). Therefore it has
70 been widely used as a biomarker for inflammation (Pepys et al., 2006).

71 Human pCRP is arranged in flat pentamers with one face showing Ca⁺⁺-dependent phospholipid-head
72 recognition and the other face being responsible for most of their biological effects. After binding ~1 mM
73 Ca⁺⁺, pCRP recognizes membrane exposed phospholipid-head ligands primarily containing
74 phosphorylcholine heads with µM affinities, while pSAP preferentially binds phosphorylethanolamine heads
75 (Du Clos and Mold, 2011). The Ca⁺⁺-dependent binding of pCRP to phospholipid heads, triggers binding to
76 C1q (activating the classical complement pathway) and immunoglobulin Fc receptors (FcR) (activating
77 phagocytosis) (Bang et al., 2005; Du Clos and Mold, 2011; Inforzato et al., 2013; Vilahur and Badimon,
78 2015). After the discovery of different monomeric CRP (mCRP) conformations, the list of ligands has
79 expanded (Li et al., 2016; Wu et al., 2015), as conformational changes control not only local inflammation
80 but also many different innate immune responses (Wang et al., 2011; Wu et al., 2015) (further details are
81 discussed later in section 5).

82 CRP-like proteins are found from arthropods to mammals (Bottazzi et al., 2016; Vilahur and
83 Badimon, 2015), including lower vertebrates such as teleost fish (MacCarthy et al., 2008, Pionnier et al.,

84 2014, Pionnier et al., 2013). However, CRP proteins have been mostly studied in humans because of their
85 clinical implications. In this work, we will compare the unique properties of the human *crp* gene /CRP
86 protein with those of the zebrafish *crp*/CRP multi-gene/multi-protein family with respect to their sequences,
87 protein structure and biological functionalities.

88 **2. The CRP-like multi-gene family in zebrafish**

89 One of the zebrafish CRP-like recombinant protein members (similar to CRP5) has a similar
90 backbone structure to human CRP but crystallizes as a trimer with only 32 % amino acid identity (Chen et
91 al., 2015). In sharp contrast to human and other fish CRP-like proteins, 7 different *crp* loci (coding for
92 CRP1-7) were detected in chromosome 24 of the zebrafish (*Danio rerio*) genome (Falco et al.,
93 2012). Furthermore, zebrafish *crp5* expresses 79 different transcript variants suggesting the existence
94 of at least 5 different isoforms of this particular gene (GenBank UniGene accession numbers
95 Dr.124528-Dr.162306)(Chen et al., 2015). In addition, mRNA transcripts identified as 4 *sap*-like
96 genes in earlier home-designed microarrays (Encinas et al., 2013; Encinas et al., 2010; Estepa and Coll,
97 2015) have now been confirmed to be isoforms of *crp2* and *crp5* in most recent genome releases (not
98 shown). Caution is necessary when assigning *crp/sap* identities based only on their sequences, especially
99 when searching for orthologous sequences from other species such as human CRP, because of their high
100 similarity. Classification is best based on affinity or ligand-binding functionality rather than sequence (i.e.,
101 human CRP preferentially binds phosphocholine while SAP binds phosphoethanolamine, and other
102 molecules could have other preferences) (Du Clos and Mold, 2011). Although it is likely that there might be
103 more *crp*-like genes and/or isoforms in zebrafish, carp and/or other fish (Fujiki et al., 2001), their complete
104 identification must wait for further sequencing advances of their corresponding genomes and/or transcripts.
105 The existence of a *crp*-like multi-gene family rather than a unique gene could offer an alternative
106 repertoire of anti-pathogen responses for primitive vertebrates such as fish that have a limited
107 adaptive immune response (i.e., lack of IgG). However, the corresponding zebrafish CRP-like multi-
108 protein function(s) and regulation(s) remain largely unexplored.

109 Zebrafish is a suitable model for studying evolutionary immunology since it has been
110 used not only for modelling other vertebrates due to its important resources for genetic and
111 developmental studies but also for modelling many infectious diseases affecting fish
112 (Chinchilla et al., 2015; Lopez-Munoz et al., 2010; Novoa et al., 2006; Rowe et al., 2014;
113 Sanders et al., 2003) and humans (Goody et al., 2014). In addition, transcriptomic data showing
114 differentially modulated *crp1-7* multi-gene has been reported in zebrafish surviving rhabdoviral
115 infections such as VHSV (Estepa and Coll, 2015), or SVCV (Encinas et al., 2013), bacterial
116 infections (Estepa and Coll, 2015) and/or adaptive-immune deficient zebrafish (Garcia-Valtanen et al.,
117 2016). Some of these results will be discussed in more detail in section 6.

118 **3. Comparative amino acid sequences of human CRP and zebrafish CRP-like proteins**

119 A sequence alignment of the known CRP proteins from various species revealed CRP-like protein
120 sequences from fish clustered together in a phylogenetic tree, while those from mammals formed a
121 distinct clade and *Limulus* was out grouped (Falco et al., 2012). Both ³⁶Cys and ⁹⁷Cys and the cholesterol-
122 binding sequence (residues 35 to 47) were well conserved throughout evolution (Table 1), suggesting that at
123 least some of their functions (to be discussed in section 5), such as redox switching or interactions with
124 cholesterol-enriched rafts, might be similar (Chen et al., 2015; Wang et al., 2011). A high degree of
125 conservation was also observed when comparing the protein hydrophobicity profiles between human CRP
126 and zebrafish CRP-like proteins (see Figure 1A for CRP5 and not shown). In addition to the two cysteine
127 residues, the locations of Ca⁺⁺-binding and putative phospholipid-binding pockets were highly conserved
128 (Figure 1B, Table 1). Variation of amino acid residues among zebrafish CRP1-7 showed a conserved 26-39
129 amino acid stretch around ³⁶Cys suggesting a common structural/functional requirement (possibly a
130 cholesterol-binding sequence). The highest variations were found around the putative phospholipid-binding
131 pocket (residues 70-86) and the C-terminal region (residues 180-206), suggesting different possible
132 specificities for ligand binding (Figure 1B, Table 1).

133 **4. Tridimensional structures of human CRP and zebrafish CRP-like proteins**

134 The X-ray derived structures of crystallized human CRP are pentameric (Shrive et al., 1996).

135 Circular dichroism, infrared spectroscopy and/or immunochemistry suggest Ca⁺⁺-dependent reversible small
136 conformational changes (Ramadan et al., 2002; Wu et al., 2015). Furthermore, in the presence of Ca⁺⁺ the
137 pCRP structures become resistant to heat or urea denaturation, mercaptoethanol and/or proteolysis (Black et
138 al., 2003; Coll, 1988). In sharp contrast, the X-ray structures of zebrafish CRP-like proteins were trimeric
139 (tCRP), with a small central pore of ~ 16.8 Å compared to human pCRP, which is ~ 47 Å. Small Ca⁺⁺-
140 dependent conformational changes were also shown for one of the zebrafish tCRP-like proteins (Chen et al.,
141 2015) but no Ca⁺⁺-dependent or any other cation-dependent binding specificities have been reported to date.

142 Each human CRP monomer binds 2 molecules of Ca⁺⁺ at a binding site for the negatively charged
143 phosphate moiety of phospholipid ligand heads. The loss of Ca⁺⁺ results in a highly charged negative surface
144 of the Ca⁺⁺-binding loop (Figure 1A, green squares) activating binding to ligands such as polycations (i.e.,
145 polyLys). The major significant change between Ca⁺⁺-depleted and Ca⁺⁺-bound human CRP occurs in the
146 Ca⁺⁺-binding loop (amino acids 138-150) (Figure 1A, blue squares), which are disordered and mobile in the
147 absence of Ca⁺⁺, and refold in the presence of Ca⁺⁺ to protect the ¹⁴⁵Asn-¹⁴⁷Glu site (Figure 1A red triangles)
148 from proteolytic attack (Kinoshita et al., 1992).

149 The location of the highest amino acid sequence variations (Figure 1B, Table 1) and homology
150 docking-modelling (Chen et al., 2015) of the phospholipid pockets of different zebrafish CRP-like proteins,
151 suggest that different specificities for phospholipid head binding might exist for each of them. However, to
152 date there is no experimental evidence that could confirm these indirect observations.

153 Accumulating evidence, however, confirms that human CRP has two forms, pentameric serum-
154 circulating CRP (pCRP) and monomeric tissue-associated CRP (mCRP)(Wu et al., 2015). The mCRP might
155 be induced *in vivo* by interactions between pCRP and cholesterol-enriched lipid rafts in the membranes of
156 damaged cells (Wang et al., 2011) (further discussed in section 5) or direct biosynthesis from macrophages
157 (Ciubotaru et al., 2005). *In vitro* the pCRP to mCRP has been induced in the absence of Ca⁺⁺ (presence of
158 EDTA) with urea, low-pH or low-salt buffers (Potempa et al., 1983; Taylor and van den Berg, 2007).

159 The conversion of human pCRP to mCRP is required for an additional conformational change, due
160 to reduction of the intra-monomer ³⁶Cys-⁹⁷Cys disulfide bond as detected by its slower migration in SDS-
161 denaturing gel electrophoresis and/or specific monoclonal antibodies (Wang et al., 2011). Reducing agents
162 such as DTT, GSH, Cys or mercaptoethanol can reduce mCRP but not pCRP, since the disulfide bond is
163 protected inside the pentameric structure (Shrive et al., 1996). Once reduced, spontaneous re-oxidation of
164 mCRP that could complicate the interpretation of the results, can be prevented by treatment with *N*-
165 ethylmaleimide or, alternatively, by substituting the two Cys for Ala in recombinant CRP (Ji et al., 2007;
166 Potempa et al., 2015). The reduction affects some of the human mCRP biological functions (Wang et al.,
167 2011; Wu et al., 2015), but no X-ray structures have been yet reported for non-reduced or reduced
168 conformations to date.

169 Therefore, the participation of every possible conformation of CRP (pCRP, mCRP and/or reduced
170 mCRP) should be correctly determined before drawing any valid experimental conclusions. In addition, the
171 fact that most commercially available anti-CRP antibodies recognize both pCRP and mCRP (Schwedler et
172 al., 2006), complicates the interpretation of previous and/or future studies. Similar concerns will apply to
173 research on zebrafish CRP-like proteins although there is no evidence that the tCRP to mCRP conversion
174 also occurs in any zebrafish CRPs.

175 **5. Biological functions of CRP**

176 The presence and some functions of CRP-like (Bayne and Gerwick, 2001; Bayne et al., 2001) and
177 SAP-like (Hwang et al., 2015; Wang and Sun, 2016) proteins have been described in several fish but not in
178 the zebrafish CRP multi-protein family. Several biological functions which might be expected to be found
179 in the zebrafish CRP multi-proteins will be briefly discussed here.

180 **5.1. Inflammation biomarker of CRP circulating levels.** Human local tissue injuries cause (even
181 hours later) the release of pro-inflammatory signals such as IL6, IL1 β and TNF α , which distribute throughout
182 the body and induce the liver to synthesize and release pCRP to the blood. The participation of these earliest
183 signals has raised some possibilities for the clinical control of pCRP blood levels to reduce excessive tissue
184 damage using antibodies directed against pro-inflammatory signaling molecules. Three examples of such

185 antibodies are Tocilizumab (anti-human IL6R), Rilonacept (anti-human IL1R), and Certolizumab (anti-
186 TNF-alpha) (www.drugbank.ca accession numbers DB06372, DB06273 and DB08904, respectively). In
187 contrast, similar fish studies are very scarce (Bayne and Gerwick, 2001; Bayne et al., 2001). Nevertheless,
188 the analysis of differential expression data of transcription factors present in previous zebrafish microarray
189 studies (Estepa and Coll, 2015), might help to identify some of the regulation of the *crp1-7* promoters in
190 zebrafish surviving viral diseases.

191 **5.2. Ca⁺⁺-dependent recognition of exposed phospholipid heads.** The similar relative locations
192 and partial amino acid identities between the amino acid stretches in human and zebrafish CRP involved
193 binding Ca⁺⁺ (residues 60-61, 138-140, and 147-150 in human CRP) and phosphocholine (17-mer peptide
194 47-63 and residues 68, 76, 138, 140, and 150 in human CRP) (Table 1) strongly suggested that similar
195 functionalities exist in both human and zebrafish monomers. However, Ca⁺⁺-dependent binding to exposed
196 membrane phosphocholine *in silico* modelled with different zebrafish CRP-like monomers identified
197 different binding pocket geometries for the different CRPs (Chen et al., 2015). Preliminary extension of
198 similar *in silico* binding energy data to different phospholipid heads has also shown heterogeneity among
199 the different zebrafish CRP-like proteins (not shown) and requires further refinement studies. Validation of
200 such *in silico* data can be performed by ELISA using solid-phases coated with different phospholipid-heads
201 (Martinez and Coll, 1987; Martinez and Coll, 1988) or CRP pepscans (Garcia-Valtanen et al., 2014) as
202 presently being attempted (results not shown). In addition, interactions of zebrafish CRP-like conformations
203 (tCRP, mCRP, reduced-mCRP) could not only be studied by ELISA/pepscan methods but also with fish
204 cells and/or model membranes. Infected fish cells might offer a new exciting exploration subject for PCR-
205 like bindings because VHSV infection induced translocation/exposure of cellular phosphatidylserine heads
206 (Estepa et al., 2001).

207 **5.3. Binding to C1q and complement components.** Once human pCRP binds phospholipid-head exposed
208 targets, it binds C1q to activate the classical complement pathway (Agrawal et al., 2001; Agrawal and
209 Volanakis, 1994; Gaboriaud et al., 2003; Thompson et al., 1999). The binding of human CRP to apoptotic
210 cells in damaged tissues in a Ca⁺⁺-dependent manner affects not only complement but also innate immune

responses. Thus, CRP-“marking” of apoptotic cells increased the classical pathway of complement activation but protected the cells from assembly of the terminal complement components avoiding excessive tissue damage. Furthermore, apoptotic cells “marked” with CRP enhanced their opsonisation and phagocytosis by anti-inflammatory TGF β - activated macrophages. The anti-inflammatory effects of CRP required C1q and factor H. However, reduction of the disulfide bridge enhanced the interaction of mCRP with C1q (Wu et al., 2015), a novel interaction which is much less studied. All the above observations demonstrate that CRP and some complement components act in concert to promote non-inflammatory clearance of apoptotic cells (Gershov et al., 2000). The similar relative locations and partial amino acid identities in 5 different stretches involved in human CRP binding to C1q (residues 38, 88, 112-114, 158, 175-176) strongly suggest similar functionalities might exist in pCRP and tCRP (Table 1). C1q and other complement components have been identified in zebrafish (Boshra et al., 2006), and most recently the crystal structure of one of the globular domains of zebrafish C1q which might be implicated in CRP-binding was elucidated (Yuan et al., 2016). However, how the different tCRP-like proteins from zebrafish might recognize and interact with C1q could only be modelled until more experimental data will be available.

5.4. Binding to immunoglobulin Fc. Once human CRP binds phospholipid-head exposed targets, binds to Fc transmembrane immunoglobulin receptors (FcR) present in most human haematopoietic cells, enhancing FcR $^+$ leukocyte phagocytosis of bacteria (Kindmark, 1971). Each pCRP bound one specific FcR molecule (Lu et al., 2012), two monomers participating in the binding (Lu et al., 2008) (PDB entries 1F2Q and 1QVZ for Fc ϵ RI and Fc γ RI, respectively). For instance, human pCRP binds to Fc γ RIIa (*cd32*) and Fc γ RI (*cd64*) while mCRP binds to FcRIIb (Wu et al., 2015). Internalization of CRP-FcR caused immunosuppression in macrophages, suggesting that CRP/FcR complexes might also protect against excessive inflammation (Marjon et al., 2009). However, none of those described human Fc receptors were IgM-specific, while IgM is the primary fish immunoglobulin. In addition, only polymeric immunoglobulin (*pig*) receptor (*pigr*) genes have been identified in zebrafish (Zhang et al., 2010). Transcript levels of *pig* genes were down-regulated after infection with Snakehead rhabdovirus, suggesting that viral infection may suppress them (Kortum et al., 2014), but there are few other reports on interactions of fish tCRP-like proteins with FcRs (Bayne and

237 Gerwick, 2001; Bayne et al., 2001; Lu et al., 2012) and none with mCRP conformations (Li et al., 2016).

238 In this context, it will be of interest to study CRP-like/FcR interactions in zebrafish *rag1*^{-/-} mutants lacking
239 IgM and expression of transcripts of *pig/pigr* in microarray studies.

240 **5.5. Changing conformations after binding to cholesterol-enriched lipid rafts.** The most important
241 human CRP peptide implicated in cholesterol-enriched lipid raft binding (residues 35-47) is found in a
242 similar relative location with 38.4 % partial amino acid identity in zebrafish CRP-like molecules (Table 1
243 shows correspondences between human and zebrafish CRP5). Similarly, the main stretches participating in
244 human mCRP interactions to form pCRP could also be found in CRP5 (Table 1, residues 40-45, 91-94, 109-
245 119, 167-175 in human CRP). Both findings suggest that human and zebrafish CRPs may use similar
246 mechanisms for CRP cholesterol-induced conformations. The Ca⁺⁺-dependent binding of human CRP to
247 damaged cell membranes enhances the pCRP dissociation to mCRP (Ji et al., 2007). The pCRP dissociation
248 could be due to interactions with hydrophobic cholesterol-enriched lipid rafts as shown by mimicking with
249 model membranes made with cholesterol, phosphatidylcholine and sphingomyelin (Potempa et al., 2015;
250 Wang et al., 2011). Furthermore, evidence is accumulating that the changes in the pCRP conformation
251 further alter its biological effects (Wu et al., 2015). In human CRP, this generates an expanded list of not
252 only those well-known interactions such as C1q/Fc but also with new ligands such as LDL, fibronectin,
253 collagen (Li et al., 2016) and/or many other possibilities which have not yet been identified.

254 **5.6. *In vivo* reduction of the ³⁶Cys switch.** The relative locations of the two Cys residues present in each of
255 the CRP monomers were highly conserved in human and all zebrafish CRP-like molecules (residues 36 and
256 97 or 36 and 98). After losing the pentameric symmetry, the human mCRP intra-monomer disulfide bridge
257 acts as a redox-sensitive switch whose reduction might be required for the expression of further pro-
258 inflammatory effects (Wang et al., 2011). *In vivo* interactions of pCRP with cholesterol-enriched lipid rafts
259 not only activates the conversion to mCRP but also the reduction of the ³⁶Cys (Li et al., 2016; Wang et al.,
260 2011). Since human mCRP promotes recruitment of thioredoxin (Trx)-rich monocytes/macrophages
261 (Eisenhardt et al., 2009a), Trx might be responsible for the ~1000-fold enhancement of the disulfide
262 reduction rate compared to chemical reagents (Wang et al., 2011). In this respect, immunohistochemical

263 studies with specific MAbs detected mCRP rather than pCRP in human atherosclerotic plaques (Eisenhardt
264 et al., 2009a; Eisenhardt et al., 2009b; Eisenhardt et al., 2009c). Reduced mCRP has also been associated
265 with enhanced binding to LDL (Ji et al., 2006b), further activation of complement (Ji et al., 2006a; Wang et
266 al., 2011) and stimulation of innate immune responses of endothelial cells (Heuertz et al., 2005; Ji et al.,
267 2009). While there are no similar confirmatory studies made yet on this recently described phenomenon on
268 any zebrafish tCRP-like molecules, it is probable that their Cys behave in similarly despite being in a trimer.

269 **5.7. Cellular interactions.** Little is known about how the changes in the recently described human pCRP
270 conformations may affect cellular responses. Furthermore, while there are many studies on the effects of
271 human CRP on different cells and cellular lines, the results are sometimes contradictory and in any case
272 difficult to interpret. Very often, the CRP preparations used for the experimentation could not be completely
273 characterized (i.e., composition of pCRP, mCRP, reduced-mCRP) at the time the experiments were made.
274 Nevertheless, recent evidence suggests that the effects of human mCRP are mostly pro-inflammatory,
275 through the interaction with monocyte/macrophages, neutrophils, platelets, and/or endothelial cells (Khireiss
276 et al., 2004, 2005; Wu et al., 2015). No studies have been yet made with any zebrafish tCRP-like molecules
277 but if the corresponding recombinant proteins can be purified and their preparations characterized, protease
278 digestion (Coll, 1988), pepscan mapping (Chico et al., 2010; Li et al., 2016) and specific cellular assays
279 (Garcia-Valtanen et al., 2014) could be then applied to map possible heterogeneous cellular functionalities.

280 **6. Do zebrafish CRP-like genes belong to some of the molecules recently implicated in
281 "Trained Immunity"?**

282 Recent evidence reveals that vertebrate innate immunity has a stronger and more rapid response to a
283 second pathogen exposure, two characteristic properties of classical adaptive immune memory responses
284 (Netea et al., 2016), constituting the so-called trained immunity (Netea et al., 2011). Because of their
285 primitive immunological system among vertebrates (i.e., immunological memories showing only shorter lag-
286 time rather than higher level responses, no IgG switch, no IgM maturation, mucosal IgT, phagocytic B-cells,
287 etc.), fish offers a suitable model in which to study immune evolution (Bengten and Wilson, 2015; Sunyer,
288 2013). A first observation suggesting different functions for the fish *crp*-like genes and/or isoforms, was

289 their tissue expression heterogeneity in carp (Falco et al., 2012). Confirming this possibility,
290 transcriptional microarray and RTqPCR profiles of zebrafish lymphoid organs, showed that *crp1-6*-
291 transcripts (except *crp7*), were down-regulated in survivors to viral haemorrhagic septicemia virus (VHSV)
292 before and after VHSV re-infection, while they remain mostly un-modulated shortly after the first VHSV
293 infection (except *crp7*) (Figure 2). Furthermore, only *crp2*, *crp5* and *crp6* transcript levels increased when
294 survivors were re-infected (compare the corresponding open and hatched yellow bars with * in Figure 2).
295 Down-regulation of most *crp*-like genes in VHSV survivors before and after re-infection was a surprising
296 finding that might reflect a rapid cell migration to the viral entry sites. Nevertheless, these observations
297 were the first description of *crp*-like transcript bacterial responses in viral-infected fish (Estepa and Coll,
298 2015). The expression heterogeneity of *crp*-like genes was confirmed in zebrafish *rag1*^{-/-} mutants
299 defective in V(D)J recombination in IgM and T-cell receptor genes (Garcia-Valtanen et al., 2016).
300 Transcript upregulation of a unique trout *crp*-like gene was also induced by oral DNA-vaccination to virus
301 (Ballesteros et al., 2012), confirming the importance of CRP-like proteins in fish immunization to viruses.
302 Because, some of the mammalian orthologous to fish multi-gene families (i.e., *nitr*) were linked to long-term
303 NK-cells in mammalian trained immune memory (Martin-Fontech et al., 2004), the analogous *crp*-like
304 family might also be responsible for similar purposes. As further discussed in previously published (Estepa
305 and Coll, 2015) and submitted work (Garcia-Valtanen et al., 2016), because of its heterologous expression
306 within microarray data and the existence of multiple genes and/or transcript isoforms similar to in the *nitr*
307 family, zebrafish tCRP-like molecules might be one of the novel actors of trained immunity in fish.
308

309

7. Conclusions

310 None of the novel aspects of the functionality of human mCRP molecules have been studied in
311 zebrafish. It is unknown whether zebrafish tCRP-like molecules behave as serum acute-phase proteins,
312 although this has been observed in other fish (Bayne and Gerwick, 2001; Bayne et al., 2001) and preliminary
313 experiments using viral-infected zebrafish (unpublished). In addition to the different binding specificities of
314 the different CRP1-7 and its transcript variants, because of the possible co-existence of different CRPs in the

315 same cell, the generation of heterologous tCRP may further increase its potential functionalities. The
316 sequence diversity of the *crp*-like genes combined with their possible different phospholipid-binding
317 affinities and the possibility of heterologous tCRP, suggests this gene family could mimic a limited antibody
318 repertoire. The heterogeneous transcript expression demonstrated after a viral infection, in viral survivors and
319 in the absence of any adaptive immunological system confirms this idea. Human *crp/sap* might be coded by
320 unique genes as a minimal remnant of phylogenetically earlier *crp*-like gene families which were more
321 important when antibodies were not fully developed given their capacity to recognize a wide variety of
322 ligands. Therefore, *crp*-like gene families might constitute an ancient link between innate and adaptive
323 immune responses.

324 Further studies on how the zebrafish tCRP-like molecules and any of their transcript variants and/or
325 protein conformations affect binding specificities and/or functionalities could help the understanding of
326 immune evolution and improve prevention methods against diseases, including vaccines, adjuvants and
327 other biotechnological tools. However, since most functional studies will have to use recombinant fish CRP-
328 like proteins, caution with both LPS contamination (Pepys et al., 2005) and conformation composition should
329 be carefully taken for a correct interpretation of future results.

330

331 Acknowledgements

332 Special thanks are due to the co-author Dr. Amparo Estepa, who recently passed away, who
333 contributed to the initial ideas and financing behind this work. Thanks are also due to Paula Perez Gonzalez
334 for her analysis of zebrafish CRP-like protein alignments. This work was supported by INIA project
335 RTA2013-00008-00-00, CICYT project AGL2014-51773-C3, and AGL2014-53190 REDC of the Ministerio de
336 Economía y Competitividad of Spain.

337
338
339
340
341
342
343

344
345
346
347
348

Table 1
Some reported activities of amino acid sequences and/or peptides from human and zebrafish CRP

Activity	human amino acid sequence zebrafish amino acid sequence
Redox switch	³⁶ C + ⁹⁷ C ³⁶ C + ⁹⁸ C
pCRP Ca ⁺⁺ main contacts	⁶⁰ D N ⁶¹ + ¹³⁸ E <u>QD</u> ¹⁴⁰ + ¹⁴⁷ E <u>G</u> S <u>Q</u> ¹⁵⁰ ⁶⁰ D E ⁶¹ + ¹³⁹ <u>D</u> P <u>D</u> ¹⁴¹ + ¹⁴⁸ <u>D</u> V <u>D</u> <u>Q</u> ¹⁵¹
pCRP phosphocholine binding peptide & sites	⁴⁷ R GYSI <u>F</u> S <u>Y</u> A <u>T</u> KR <u>Q</u> DNEI ⁶³ + ⁶⁸ S + ⁷⁶ T + ¹³⁸ E + ¹⁴⁰ D + ¹⁴⁹ S ⁴⁷ R E <u>V</u> I <u>L</u> F <u>A</u> <u>Y</u> <u>Y</u> T <u>P</u> D <u>V</u> <u>D</u> E <u>L</u> N ⁶³ + ⁶⁷ <u>E</u> + ⁷⁵ <u>Y</u> + ¹³⁹ <u>D</u> + ¹⁴¹ D + ¹⁵² S
C1q binding	³⁸ H + ⁸⁸ E + ¹¹² D <u>G</u> <u>K</u> ¹¹⁴ + ¹⁵⁸ N + ¹⁷⁵ Y <u>L</u> ¹⁷⁶ ³⁸ R + ⁸⁹ P + ¹¹³ <u>D</u> G <u>R</u> ¹¹⁵ + ¹⁵⁹ <u>N</u> + ¹⁷⁶ <u>Y</u> <u>Y</u> ¹⁷⁷
mCRP binding to Ch, C1q, LDL, fibronectin, collagen	³⁵ V C <u>L</u> H <u>F</u> T <u>E</u> <u>L</u> S <u>S</u> T <u>R</u> ⁴⁷ ³⁵ L C <u>M</u> R <u>V</u> <u>A</u> <u>T</u> <u>E</u> <u>L</u> <u>P</u> <u>L</u> D <u>R</u> ⁴⁷
Implicated in mCRP-mCRP interactions	⁴⁰ Y <u>T</u> <u>E</u> <u>L</u> <u>S</u> <u>S</u> ⁴⁵ + ⁹¹ vAPV ⁹⁴ + ¹⁰⁹ F W <u>V</u> <u>D</u> <u>G</u> <u>K</u> P <u>R</u> V <u>R</u> <u>K</u> ¹¹⁹ + ¹⁶⁷ S <u>P</u> <u>D</u> <u>E</u> <u>I</u> <u>N</u> <u>T</u> <u>I</u> Y ¹⁷⁵ ⁴⁰ <u>A</u> <u>T</u> <u>E</u> <u>L</u> <u>P</u> ⁴⁵ + ⁹¹ <u>S</u> <u>T</u> <u>L</u> <u>Q</u> ⁹⁴ + ¹¹⁰ F W <u>M</u> D <u>G</u> <u>R</u> <u>R</u> <u>S</u> <u>L</u> <u>H</u> <u>Q</u> ¹²⁰ + ¹⁶⁸ S <u>S</u> <u>A</u> <u>Q</u> <u>I</u> <u>K</u> <u>A</u> <u>V</u> Y ¹⁷⁶
Unique mCRP epitope	²⁰¹ G <u>E</u> <u>V</u> <u>F</u> <u>T</u> K <u>P</u> ²⁰⁷ ²⁰⁵ <u>G</u> <u>N</u> <u>V</u> <u>L</u> <u>V</u> <u>V</u> <u>P</u> ²¹¹
Protease sensitive sequence	¹⁴⁵ N <u>F</u> <u>E</u> ¹⁴⁷ ¹⁴⁶ <u>S</u> <u>F</u> <u>D</u> ¹⁴⁸
Highest amino acid variations on zebrafish CRP-like sequences	⁷⁰ D <u>I</u> <u>G</u> <u>Y</u> <u>S</u> <u>F</u> <u>T</u> V <u>G</u> <u>G</u> -- <u>S</u> <u>E</u> <u>I</u> <u>L</u> <u>F</u> <u>E</u> <u>V</u> ⁸⁶ ⁶⁹ <u>D</u> <u>G</u> <u>R</u> <u>V</u> S <u>L</u> <u>Y</u> <u>I</u> <u>Q</u> <u>S</u> <u>S</u> <u>K</u> <u>D</u> <u>A</u> <u>F</u> <u>F</u> <u>R</u> <u>L</u> ⁸⁷
Lowest amino acid variations on zebrafish CRP-like sequences	¹⁸ S <u>Y</u> <u>V</u> <u>S</u> <u>L</u> <u>K</u> <u>A</u> <u>P</u> <u>L</u> <u>T</u> <u>K</u> <u>P</u> L <u>K</u> <u>A</u> <u>F</u> <u>T</u> <u>V</u> <u>C</u> <u>L</u> <u>H</u> ³⁹ ¹⁸ <u>S</u> <u>Y</u> <u>V</u> <u>K</u> <u>L</u> <u>Y</u> <u>P</u> <u>E</u> <u>K</u> <u>P</u> <u>L</u> <u>S</u> <u>L</u> <u>S</u> <u>A</u> <u>F</u> <u>T</u> <u>L</u> <u>C</u> <u>M</u> <u>R</u> ³⁹

349
350
351
352
353
354
355
356
357
358

Human CRP sequence 1GNH.pdb and zebrafish CRP5 sequence from Protein Bank accession number 4PBP.pdb (GenBank accession number JF772178.1) were aligned and numerated without the signal peptides as reported before (Chen et al., 2015; Shrive et al., 1996). Compiled from several published data (Chen et al., 2015; Li et al., 2016; Shrive et al., 1996; Wang et al., 2011; Wu et al., 2015; Ying et al., 1989) and this work. **Bold**, identical amino acids between human CRP and zebrafish CRP5. **Underlined**, location of amino acid variations among different zebrafish CRP-like 1-7 molecules.

359 **Figure 1. Hydrophobicity map (A) and variability (B) of human and zebrafish CRP amino acid**
360 **sequences.** A) The hydrophobicity map of human and zebrafish CRP (accession numbers 1GNH and 4PBP
361 from the RCSB PDB Protein Data Bank at <http://www.rcsb.org/pdb/home/home.do>, respectively) were
362 derived using Clone Manager vs9 software. The crystalized zebrafish CRP 4PBP (GenBank accession
363 number JF772178.1)(Chen et al., 2011) is highly similar to CRP5 (Falco et al., 2012). The numbering
364 correspond to the amino acid sequences without their signal peptide. **Black line**, human CRP. **Red line**,
365 zebrafish CRP. **Black circles**, location of cysteines (³⁶Cys and ⁹⁷Cys). **Green squares**, amino acids involved
366 in human pCRP-Ca⁺⁺ binding. **Open squares**, amino acids involved in the intermolecular monomer (mCRP)
367 to mCRP interactions to form pCRP. **Red triangles**, protease sensitive sequence. **Blue squares**, amino acids
368 involved in ligand (PC)-CRP-binding. **Blue circles**, predominant epitope (197-202) expressed only in mCRP
369 but imbedded in the inter-monomer regions in pCRP (Wu et al., 2015). **Black squares**, amino acids involved
370 in C1q-binding (Chen et al., 2015; Shrive et al., 1996). **Open triangles**, sequence implicated in the binding to
371 cholesterol-enriched lipid rafts (residues 35-47) mediating mCRP insertion and signalling (Wu et al., 2015).
372 **B)** Number of different amino acids per position in zebrafish CRP1-7 gene derived proteins (accesion
373 numbers XM_693995, BC097160, BC154042, BC115188, BC121777, BC162745, BC150371,
374 respectively)(Falco et al., 2012).

375

376 **Figure 2. Example of heterogenous differential expression profiles of individual *crp* gene transcripts**
377 **from zebrafish surviving VHSV infections.** Adult zebrafish were infected by VHSV and some of them
378 analysed 2 days later. Survivors were maintained during 6 months and analysed before and after being re-
379 infected with VHSV 2 days later. For the analysis, zebrafish lymphoid organs (head kidney + spleens) were
380 harvested, their RNA extracted, fluorescently labelled and hybridized to zebrafish *crp1-7* probes in a home-
381 designed microarray. The transcript differential expression was calculated for each *crp* gene using the
382 following formula: fluorescence of each VHSV-infected replicate / mean fluorescences from non-infected
383 replicates (n=4 zebrafish pools of 5 fish per pool). Means and standard deviations were then obtained for
384 each gene to remove outliers and calculate final folds.. **Open bars**, 2-days after VHSV infection. **Yellow**
385 **open bars**, 6 month survivors after 2 consecutive VHSV infections. **Yellow hatched bars**, 6 month
386 survivors, 2 days after being re-infected. **Red horizontal hatched line**, 1- fold thresholds. **Folds>1**, up-
387 regulated. **Folds<1**, down-regulated *, significantly different from non-re-infected VHSV survivors (yellow
388 open bars) at the p<0.05 level (Student T). Re-drawn from previously published data using unique 60-mer
389 probes from zebrafish CRP1-7 mRNA (accesion numbers XM_693995, BC097160, BC154042, BC115188,
390 BC121777, BC162745, BC150371, respectively)(Estepa and Coll, 2015).

391

392

393 **References**

394

- 395 Agrawal, A., Shrive, A.K., Greenhough, T.J., Volanakis, J.E., 2001. Topology and structure of the C1q-
396 binding site on C-reactive protein. *J Immunol* 166, 3998-4004.
- 397 Agrawal, A., Volanakis, J.E., 1994. Probing the C1q-binding site on human C-reactive protein by site-
398 directed mutagenesis. *J Immunol* 152, 5404-5410.
- 399 Ballesteros, N.A., Rodríguez Saint-Jean, S.S., Perez-Prieto, S.I., Coll, J.M., 2012. Trout oral VP2 DNA
400 vaccination mimics transcriptional responses occurring after infection with infectious pancreatic necrosis
401 virus (IPNV). *Fish & Shellfish Immunology* 33, 1249-1257.
- 402 Bang, R., Marnell, L., Mold, C., Stein, M.P., Clos, K.T., Chivington-Buck, C., Clos, T.W., 2005. Analysis of
403 binding sites in human C-reactive protein for Fc $\{\gamma\}$ RI, Fc $\{\gamma\}$ RIIA, and C1q by site-directed
404 mutagenesis. *J Biol Chem* 280, 25095-25102.
- 405 Bayne, C.J., Gerwick, L., 2001. The acute phase response and innate immunity of fish. *Dev Comp Immunol*
406 25, 725-743.
- 407 Bayne, C.J., Gerwick, L., Fujiki, K., Nakao, M., Yano, T., 2001. Immune-relevant (including acute phase)
408 genes identified in the livers of rainbow trout, *Oncorhynchus mykiss*, by means of suppression subtractive
409 hybridization. *Dev Comp Immunol* 25, 205-217.
- 410 Bengten, E., Wilson, M., 2015. Antibody Repertoires in Fish. *Results Probl Cell Differ* 57, 193-234.
- 411 Black, S., Agrawal, A., Samols, D., 2003. The phosphocholine and the polycation-binding sites on rabbit C-
412 reactive protein are structurally and functionally distinct. *Mol Immunol* 39, 1045-1054.
- 413 Boshra, H., Li, J., Sunyer, J.O., 2006. Recent advances on the complement system of teleost fish. *Fish*
414 *Shellfish Immunol* 20, 239-262.
- 415 Bottazzi, B., Inforzato, A., Messa, M., Barbagallo, M., Magrini, E., Garlanda, C., Mantovani, A., 2016. The
416 pentraxins PTX3 and SAP in innate immunity, regulation of inflammation and tissue remodelling. *J Hepatol*
417 64, 1416-1427.
- 418 Ciubotaru, I., Potempa, L.A., Wander, R.C., 2005. Production of modified C-reactive protein in U937-
419 derived macrophages. *Exp Biol Med (Maywood)* 230, 762-770.
- 420 Coll, J.M., 1988. Immunochemical recognition of the binding of C-reactive protein to solid-phase
421 phosphorylethanalamide. *Revista Española Fisiología* 44, 45-55.
- 422 Chen, R., Qi, J., Yao, S., Pan, X., Gao, F., Xia, C., 2011. Expression, crystallization and preliminary
423 crystallographic analysis of C-reactive protein from zebrafish. *Acta Crystallogr Sect F Struct Biol Cryst*
424 *Commun* 67, 1633-1636.
- 425 Chen, R., Qi, J., Yuan, H., Wu, Y., Hu, W., Xia, C., 2015. Crystal structures for short-chain pentraxin from
426 zebrafish demonstrate a cyclic trimer with new recognition and effector faces. *J Struct Biol* 189, 259-268.
- 427 Chico, V., Martinez-Lopez, A., Ortega-Villaizan, M., Falco, A., Perez, L., Coll, J.M., Estepa, A., 2010.
428 Pepscan Mapping of Viral Hemorrhagic Septicemia Virus Glycoprotein G Major Lineal Determinants
429 Implicated in Triggering Host Cell Antiviral Responses Mediated by Type I Interferon. *Journal Virology* 84,
430 7140-7150.
- 431 Chinchilla, B., Encinas, P., Estepa, A., Coll, J.M., Gomez-Casado, E., 2015. Transcriptome analysis of
432 rainbow trout in response to non-virion (NV) protein of viral haemorrhagic septicaemia virus (VHSV). *Appl*
433 *Microbiol Biotechnol* 99, 1827-1843.
- 434 Du Clos, T.W., 2013. Pentraxins: structure, function, and role in inflammation. *ISRN Inflamm* 2013, 379040.
- 435 Du Clos, T.W., Mold, C., 2011. Pentraxins (CRP, SAP) in the process of complement activation and
436 clearance of apoptotic bodies through Fcgamma receptors. *Curr Opin Organ Transplant* 16, 15-20.
- 437 Eisenhardt, S.U., Habersberger, J., Murphy, A., Chen, Y.C., Woppard, K.J., Bassler, N., Qian, H., von Zur
438 Muhlen, C., Hagemeyer, C.E., Ahrens, I., Chin-Dusting, J., Bobik, A., Peter, K., 2009a. Dissociation of
439 pentameric to monomeric C-reactive protein on activated platelets localizes inflammation to atherosclerotic
440 plaques. *Circ Res* 105, 128-137.
- 441 Eisenhardt, S.U., Habersberger, J., Peter, K., 2009b. Monomeric C-reactive protein generation on activated
442 platelets: the missing link between inflammation and atherothrombotic risk. *Trends Cardiovasc Med* 19, 232-
443 237.

- 444 Eisenhardt, S.U., Thiele, J.R., Bannasch, H., Stark, G.B., Peter, K., 2009c. C-reactive protein: how
445 conformational changes influence inflammatory properties. *Cell Cycle* 8, 3885-3892.
- 446 Encinas, P., Garcia-Valtanen, P., Chinchilla, B., Gomez-Casado, E., Estepa, A., Coll, J., 2013. Identification
447 of multipath genes differentially expressed in pathway-targeted microarrays in zebrafish infected and
448 surviving spring viremia carp virus (SVCV) suggest preventive drug candidates. *PLoS One* 8, e73553.
- 449 Encinas, P., Rodriguez-Milla, M.A., Novoa, B., Estepa, A., Figueiras, A., Coll, J.M., 2010. Zebrafish fin
450 immune responses during high mortality infections with viral haemorrhagic septicemia rhabdovirus. A
451 proteomic and transcriptomic approach. *BMC Genomics* 11, 518-534.
- 452 Estepa, A., Coll, J.M., 2015. Innate multigene family memories are implicated in the viral-survivor zebrafish
453 phenotype. *Plos One* 10, e0135483.
- 454 Estepa, A.M., Rocha, A.I., Mas, V., Perez, L., Encinar, J.A., Nunez, E., Fernandez, A., Ros, J.M.G.,
455 Gavilanes, F., Coll, J.M., 2001. A protein G fragment from the Salmonid viral hemorrhagic septicemia
456 rhabdovirus induces cell-to-cell fusion and membrane phosphatidylserine translocation at low pH. *Journal of*
457 *Biological Chemistry* 276, 46268-46275.
- 458 Falco, A., Cartwright, J.R., Wiegertjes, G.F., Hoole, D., 2012. Molecular characterization and expression
459 analysis of two new C-reactive protein genes from common carp (*Cyprinus carpio*). *Dev Comp Immunol* 37,
460 127-138.
- 461 Fujiki, K., Bayne, C.J., Shin, D.H., Nakao, M., Yano, T., 2001. Molecular cloning of carp (*Cyprinus carpio*)
462 C-type lectin and pentraxin by use of suppression subtractive hybridisation. *Fish Shellfish Immunol* 11, 275-
463 279.
- 464 Gaboriaud, C., Juanhuix, J., Gruez, A., Lacroix, M., Darnault, C., Pignol, D., Verger, D., Fontecilla-Camps,
465 J.C., Arlaud, G.J., 2003. The crystal structure of the globular head of complement protein C1q provides a
466 basis for its versatile recognition properties. *J Biol Chem* 278, 46974-46982.
- 467 Garcia-Valtanen, P., Martinez-Lopez, A., Lopez-Muñoz, A., Bello-Perez, M., Medina-Gali, R.M., Ortega-
468 Villaizan, M., Figueiras, A., Mulero, V., Novoa, B., Estepa, A., Coll, J., 2016. Zebrafish lacking adaptive
469 responses acquire an alert state characterized by trained immunity-like memories in interferons, apoptosis
470 and multi-gene families submitted.
- 471 Garcia-Valtanen, P., Ortega-Villaizan Mdel, M., Martinez-Lopez, A., Medina-Gali, R., Perez, L., Mackenzie,
472 S., Figueiras, A., Coll, J.M., Estepa, A., 2014. Autophagy-inducing peptides from mammalian VSV and fish
473 VHSV rhabdoviral G glycoproteins (G) as models for the development of new therapeutic molecules.
474 *Autophagy* 10, 1666-1680.
- 475 Gershov, D., Kim, S., Brot, N., Elkon, K.B., 2000. C-Reactive protein binds to apoptotic cells, protects the
476 cells from assembly of the terminal complement components, and sustains an antiinflammatory innate
477 immune response: implications for systemic autoimmunity. *J Exp Med* 192, 1353-1364.
- 478 Goody, M.F., Sullivan, C., Kim, C.H., 2014. Studying the immune response to human viral infections using
479 zebrafish. *Dev Comp Immunol* 46, 84-95.
- 480 Hammond, D.J., Jr., Singh, S.K., Thompson, J.A., Beeler, B.W., Rusinol, A.E., Pangburn, M.K., Potempa,
481 L.A., Agrawal, A., 2010. Identification of acidic pH-dependent ligands of pentameric C-reactive protein. *J*
482 *Biol Chem* 285, 36235-36244.
- 483 Heuertz, R.M., Schneider, G.P., Potempa, L.A., Webster, R.O., 2005. Native and modified C-reactive protein
484 bind different receptors on human neutrophils. *Int J Biochem Cell Biol* 37, 320-335.
- 485 Hwang, S.D., Bae, J.S., Jo, D.H., Kim, K.I., Cho, M.Y., Jee, B.Y., Park, M.A., Park, C.I., 2015. Gene
486 expression and functional characterization of serum amyloid P component 2 in rock bream, *Oplegnathus*
487 *fasciatus*. *Fish Shellfish Immunol* 47, 521-527.
- 488 Inforzato, A., Doni, A., Barajon, I., Leone, R., Garlanda, C., Bottazzi, B., Mantovani, A., 2013. PTX3 as a
489 paradigm for the interaction of pentraxins with the complement system. *Semin Immunol* 25, 79-85.
- 490 Ji, S.R., Ma, L., Bai, C.J., Shi, J.M., Li, H.Y., Potempa, L.A., Filep, J.G., Zhao, J., Wu, Y., 2009. Monomeric
491 C-reactive protein activates endothelial cells via interaction with lipid raft microdomains. *FASEB J* 23, 1806-
492 1816.

- 493 Ji, S.R., Wu, Y., Potempa, L.A., Liang, Y.H., Zhao, J., 2006a. Effect of modified C-reactive protein on
 494 complement activation: a possible complement regulatory role of modified or monomeric C-reactive protein
 495 in atherosclerotic lesions. *Arterioscler Thromb Vasc Biol* 26, 935-941.
- 496 Ji, S.R., Wu, Y., Potempa, L.A., Qiu, Q., Zhao, J., 2006b. Interactions of C-reactive protein with low-density
 497 lipoproteins: implications for an active role of modified C-reactive protein in atherosclerosis. *Int J Biochem
 498 Cell Biol* 38, 648-661.
- 499 Ji, S.R., Wu, Y., Zhu, L., Potempa, L.A., Sheng, F.L., Lu, W., Zhao, J., 2007. Cell membranes and liposomes
 500 dissociate C-reactive protein (CRP) to form a new, biologically active structural intermediate: mCRP(m).
 501 *FASEB J* 21, 284-294.
- 502 Khreiss, T., Jozsef, L., Potempa, L.A., Filep, J.G., 2004. Conformational rearrangement in C-reactive protein
 503 is required for proinflammatory actions on human endothelial cells. *Circulation* 109, 2016-2022.
- 504 Khreiss, T., Jozsef, L., Potempa, L.A., Filep, J.G., 2005. Loss of pentameric symmetry in C-reactive protein
 505 induces interleukin-8 secretion through peroxynitrite signaling in human neutrophils. *Circ Res* 97, 690-697.
- 506 Kindmark, C.O., 1971. Stimulating effect of C-reactive protein on phagocytosis of various species of
 507 pathogenic bacteria. *Clin Exp Immunol* 8, 941-948.
- 508 Kinoshita, C.M., Gewurz, A.T., Siegel, J.N., Ying, S.C., Hugli, T.E., Coe, J.E., Gupta, R.K., Huckman, R.,
 509 Gewurz, H., 1992. A protease-sensitive site in the proposed Ca(2+)-binding region of human serum amyloid
 510 P component and other pentraxins. *Protein Sci* 1, 700-709.
- 511 Kortum, A.N., Rodriguez-Nunez, I., Yang, J., Shim, J., Runft, D., O'Driscoll, M.L., Haire, R.N., Cannon,
 512 J.P., Turner, P.M., Litman, R.T., Kim, C.H., Neely, M.N., Litman, G.W., Yoder, J.A., 2014. Differential
 513 expression and ligand binding indicate alternative functions for zebrafish polymeric immunoglobulin
 514 receptor (pIgR) and a family of pIgR-like (PIGRL) proteins. *Immunogenetics* 66, 267-279.
- 515 Li, H.Y., Wang, J., Meng, F., Jia, Z.K., Su, Y., Bai, Q.F., Lv, L.L., Ma, F.R., Potempa, L.A., Yan, Y.B., Ji,
 516 S.R., Wu, Y., 2016. An Intrinsically Disordered Motif Mediates Diverse Actions of Monomeric C-reactive
 517 Protein. *J Biol Chem* 291, 8795-8804.
- 518 Lopez-Munoz, A., Roca, F.J., Sepulcre, M.P., Meseguer, J., Mulero, V., 2010. Zebrafish larvae are unable to
 519 mount a protective antiviral response against waterborne infection by spring viremia of carp virus.
 520 *Developmental Comparative Immunology* 34, 546-552.
- 521 Lu, J., Marjon, K.D., Mold, C., Du Clos, T.W., Sun, P.D., 2012. Pentraxins and Fc receptors. *Immunol Rev*
 522 250, 230-238.
- 523 Lu, J., Marnell, L.L., Marjon, K.D., Mold, C., Du Clos, T.W., Sun, P.D., 2008. Structural recognition and
 524 functional activation of FcgammaR by innate pentraxins. *Nature* 456, 989-992.
- 525 Marjon, K.D., Marnell, L.L., Mold, C., Du Clos, T.W., 2009. Macrophages activated by C-reactive protein
 526 through Fc gamma RI transfer suppression of immune thrombocytopenia. *J Immunol* 182, 1397-1403.
- 527 Martinez, J., Coll, J.M., 1987. Preliminary clinical studies of C-reactive protein quantified by enzyme-
 528 immunoassay. *Clinical Chemistry* 33, 2185-2190.
- 529 Martinez, J.A., Coll, J.M., 1988. Selection and performance of monoclonal anti-C-reactive protein in ELISA
 530 quantitative assay. *Clinica chimica acta; international journal of clinical chemistry* 176, 123-132.
- 531 Netea, M.G., 2013. Training innate immunity: the changing concept of immunological memory in innate host
 532 defence. *Eur J Clin Invest* 43, 881-884.
- 533 Netea, M.G., Joosten, L.A., Latz, E., Mills, K.H., Natoli, G., Stunnenberg, H.G., O'Neill, L.A., Xavier, R.J.,
 534 2016. Trained immunity: A program of innate immune memory in health and disease. *Science* 352, aaf1098.
- 535 Netea, M.G., Quintin, J., van der Meer, J.W., 2011. Trained immunity: a memory for innate host defense.
 536 *Cell Host Microbe* 9, 355-361.
- 537 Novoa, B., Romero, A., Mulero, V., Rodriguez, I., Fernandez, I., Figueras, A., 2006. Zebrafish (*Danio rerio*)
 538 as a model for the study of vaccination against viral haemorrhagic septicemia virus (VHSV). *Vaccine* 24,
 539 5806-5816.
- 540 Pepys, M.B., Hawkins, P.N., Kahan, M.C., Tennent, G.A., Gallimore, J.R., Graham, D., Sabin, C.A.,
 541 Zychlinsky, A., de Diego, J., 2005. Proinflammatory effects of bacterial recombinant human C-reactive
 542 protein are caused by contamination with bacterial products, not by C-reactive protein itself. *Circ Res* 97,
 543 e97-103.

- 544 Pepys, M.B., Hirschfield, G.M., Tennent, G.A., Gallimore, J.R., Kahan, M.C., Bellotti, V., Hawkins, P.N.,
545 Myers, R.M., Smith, M.D., Polara, A., Cobb, A.J., Ley, S.V., Aquilina, J.A., Robinson, C.V., Sharif, I., Gray,
546 G.A., Sabin, C.A., Jenvey, M.C., Kolstoe, S.E., Thompson, D., Wood, S.P., 2006. Targeting C-reactive
547 protein for the treatment of cardiovascular disease. *Nature* 440, 1217-1221.
- 548 Potempa, L.A., Maldonado, B.A., Laurent, P., Zemel, E.S., Gewurz, H., 1983. Antigenic, electrophoretic and
549 binding alterations of human C-reactive protein modified selectively in the absence of calcium. *Mol Immunol*
550 20, 1165-1175.
- 551 Potempa, L.A., Yao, Z.Y., Ji, S.R., Filep, J.G., Wu, Y., 2015. Solubilization and purification of recombinant
552 modified C-reactive protein from inclusion bodies using reversible anhydride modification. *Biophys Rep* 1,
553 18-33.
- 554 Ramadan, M.A., Shrive, A.K., Holden, D., Myles, D.A., Volanakis, J.E., DeLucas, L.J., Greenhough, T.J.,
555 2002. The three-dimensional structure of calcium-depleted human C-reactive protein from perfectly twinned
556 crystals. *Acta Crystallogr D Biol Crystallogr* 58, 992-1001.
- 557 Rowe, H.M., Withey, J.H., Neely, M.N., 2014. Zebrafish as a model for zoonotic aquatic pathogens. *Dev
558 Comp Immunol* 46, 96-107.
- 559 Sanders, G.E., Batts, W.N., Winton, J.R., 2003. Susceptibility of zebrafish (*Danio rerio*) to a model pathogen,
560 spring viremia of carp virus. *Comp Med* 53, 514-521.
- 561 Schwedler, S.B., Filep, J.G., Galle, J., Wanner, C., Potempa, L.A., 2006. C-reactive protein: a family of
562 proteins to regulate cardiovascular function. *Am J Kidney Dis* 47, 212-222.
- 563 Shrive, A.K., Cheetham, G.M., Holden, D., Myles, D.A., Turnell, W.G., Volanakis, J.E., Pepys, M.B.,
564 Bloomer, A.C., Greenhough, T.J., 1996. Three dimensional structure of human C-reactive protein. *Nat Struct
565 Biol* 3, 346-354.
- 566 Sunyer, J.O., 2013. Fishing for mammalian paradigms in the teleost immune system. *Nat Immunol* 14, 320-
567 326.
- 568 Taylor, K.E., van den Berg, C.W., 2007. Structural and functional comparison of native pentameric,
569 denatured monomeric and biotinylated C-reactive protein. *Immunology* 120, 404-411.
- 570 Thompson, D., Pepys, M.B., Wood, S.P., 1999. The physiological structure of human C-reactive protein and
571 its complex with phosphocholine. *Structure* 7, 169-177.
- 572 Vilahur, G., Badimon, L., 2015. Biological actions of pentraxins. *Vascul Pharmacol* 73, 38-44.
- 573 Wang, M.Y., Ji, S.R., Bai, C.J., El Kebir, D., Li, H.Y., Shi, J.M., Zhu, W., Costantino, S., Zhou, H.H.,
574 Potempa, L.A., Zhao, J., Filep, J.G., Wu, Y., 2011. A redox switch in C-reactive protein modulates activation
575 of endothelial cells. *FASEB J* 25, 3186-3196.
- 576 Wang, T., Sun, L., 2016. CsSAP, a teleost serum amyloid P component, interacts with bacteria, promotes
577 phagocytosis, and enhances host resistance against bacterial and viral infection. *Dev Comp Immunol* 55, 12-
578 20.
- 579 Woo, P., Korenberg, J.R., Whitehead, A.S., 1985. Characterization of genomic and complementary DNA
580 sequence of human C-reactive protein, and comparison with the complementary DNA sequence of serum
581 amyloid P component. *J Biol Chem* 260, 13384-13388.
- 582 Wu, Y., Potempa, L.A., El Kebir, D., Filep, J.G., 2015. C-reactive protein and inflammation: conformational
583 changes affect function. *Biol Chem* 396, 1181-1197.
- 584 Ying, S.C., Gewurz, H., Kinoshita, C.M., Potempa, L.A., Siegel, J.N., 1989. Identification and partial
585 characterization of multiple native and neoantigenic epitopes of human C-reactive protein by using
586 monoclonal antibodies. *J Immunol* 143, 221-228.
- 587 Yuan, H., Chen, R., Tariq, M., Liu, Y., Sun, Y., Xia, C., 2016. Crystal structure of zebrafish complement
588 1qA globular domain. *Protein Sci* 25, 1883-1889.
- 589 Zhang, Y.A., Salinas, I., Li, J., Parra, D., Bjork, S., Xu, Z., LaPatra, S.E., Bartholomew, J., Sunyer, J.O.,
590 2010. IgT, a primitive immunoglobulin class specialized in mucosal immunity. *Nat Immunol* 11, 827-835.
- 591

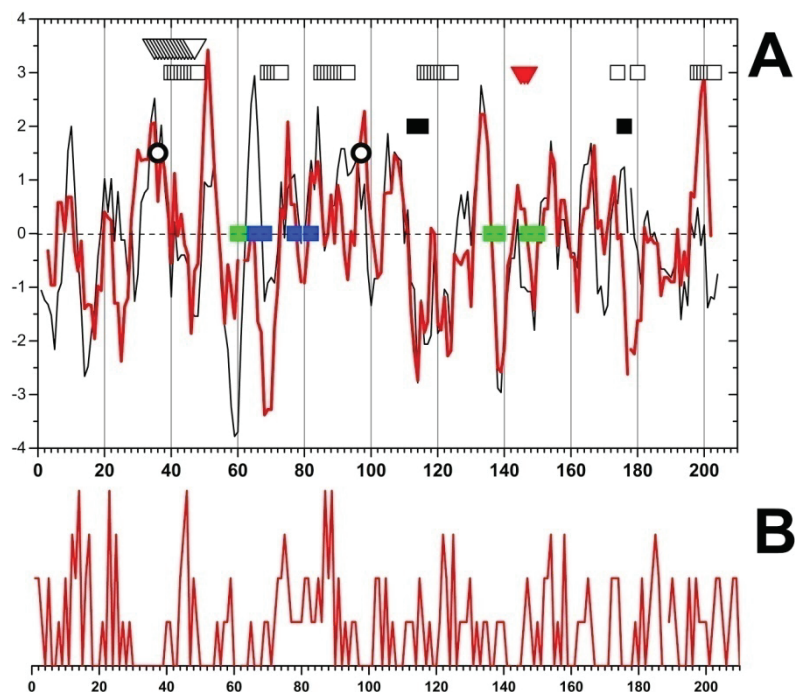


Figure 1.

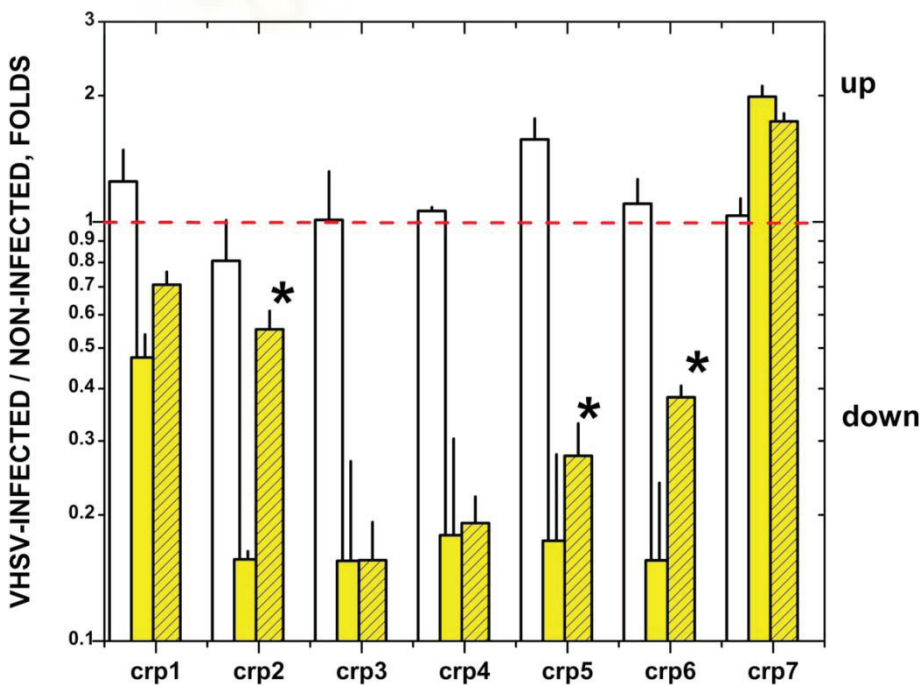


Figure 2.

PUBLICACIÓN 2

TÍTULO: Neutralization of viral infectivity by zebrafish c-reactive protein isoforms

COAUTORES: Melissa Belló Pérez, Alberto Falcó Graciá, Regla María Medina Gali, Patricia Pereiro González, Jose Antonio Encinar Hidalgo, Beatriz Novoa García, Luis Perez García-Estañ, Julio Coll Morales.

REVISTA: Molecular immunology

doi: 10.1016/j.molimm.2017.09.005

Volumen 91, Noviembre 2017, Páginas 145-155

1

2

3

4

5

6

NEUTRALIZATION OF VIRAL INFECTIVITY BY ZEBRAFISH C-REACTIVE PROTEIN ISOFORMS

7

8

Melissa Bello-Perez², Alberto Falco², Regla Medina-Gali², Patricia Pereiro³, Jose Antonio Encinar², Beatriz Novoa³, Luis Perez², Julio Coll^{1*}.

9

10

11

12

13

14

15

16

17

18

19

20

21

22

23

24

25

26

27

28

29

30

31

32

33

¹ Instituto Nacional Investigaciones y Tecnologías Agrarias y Alimentarias, Dpto. Biotecnología. INIA. Madrid, Spain.

² Instituto de Biología Molecular y Celular, Universidad Miguel Hernández (IBMC-UMH). Elche, Spain .

³ Investigaciones Marinas.CSIC. Vigo, Spain

* Corresponding author

Email addresses:

MB, melissa.bello@goumh.umh.es

AF, alber.falco@umh.es

RM, reglita2000@yahoo.com

PP, patriciapereiro@iim.csic.es

JA, jant.encinar@goumh.umh.es

BN, beatriznovoa@iim.csic.es

LP, luis.perez@umh.es

JC, juliocoll@inia.es

34 **Abstract**

35 This work explores the unexpected *in vivo* and *in vitro* anti-viral functions of the seven c-reactive protein
36 (*crp1-7*) genes of zebrafish (*Danio rerio*). First results showed heterogeneous *crp1-7* transcript levels in
37 healthy wild-type zebrafish tissues and organs and how those levels heterogeneously changed not only after
38 bacterial but also after viral infections, including those in adaptive immunity-deficient *rag1*^{-/-} mutants. As
39 shown by microarray hybridization and proteomic techniques, *crp2/CRP2* and *crp5/CRP5*
40 transcripts/proteins were among the most modulated during *in vivo* viral infection situations including the
41 highest responses in the absence of adaptive immunity. In contrast *crp1/CRP1/* and *crp7/CRP7* very often
42 remained unmodulated. All evidences suggested that zebrafish *crp2-6/CRP2-6* may have *in vivo* anti-viral
43 activities in addition to their well known anti-bacterial and/or physiological functions in mammals.
44 Confirming those expectations, *in vitro* neutralization and *in vivo* protection against spring viremia carp virus
45 (SVCV) infections were demonstrated by *crp2-6/CRP2-6* using *crp1-7* transfected and/or CRP1-7-enriched
46 supernatant-treated fish cells and *crp2-5*-injected one-cell stage embryo eggs, respectively. All these findings
47 discovered a *crp1-7/CRP1-7* primitive anti-viral functional diversity. These findings may help to study similar
48 functions on the one-gene-coded human CRP, which is widely used as a clinical biomarker for bacterial
49 infections, tissue inflammation and coronary heart diseases.

50

51

52

53

54

55

56

57

58

59

60 1. Introduction

61 Widely used as a general biomarker for bacterial infection and inflammation during many decades,
62 circulating human pentameric CRP (pCRP) has been found recently within atherosclerotic lesions and might
63 be used as a new biomarker for cardiovascular diseases (Shrivastava et al., 2015). Correlation between
64 infections and cardiovascular heart diseases has been demonstrated not only for bacteria but also for several
65 viral infections (Adinolfi et al., 2014; McKibben et al., 2016; Voulgaris and Sevastianos, 2016; Wu et al.,
66 2016). Furthermore, although pCRP was initially discovered during acute-phase responses to bacterial
67 infections increasing their circulating levels from <10 to >500 mg/l, intermediate concentrations of 10-50
68 mg/l were also detected during viral infections (Shah et al., 2015), suggesting that pCRP may have also anti-
69 viral function(s). At this respect, viral infections induce human interferon alpha that represses the *crp*
70 promoter, suggesting also pCRP antiviral effects (Enocsson et al., 2009). Nevertheless and despite pCRP
71 being one of the most investigated risk biomarker molecule in the human cardiovascular field, and an
72 important component of the anti-bacterial innate responses (Vilahur and Badimon, 2015), to our knowledge,
73 there is no evidence yet that pCRP has any antiviral function.

74 In contrast to the one-gene *crp* of humans, zebrafish (*Danio rerio*) has 7 *crp* genes, from *crp1* to *crp7*
75 (here simplified as *crp1-7* or CRP1-7 for their derived proteins). Amino acid variations among CRP1-7
76 proteins were mostly found in both their Ca⁺⁺-dependent phospholipid-binding pocket and conformational-
77 domain sequences (Bello et al., 2017; Chen et al., 2015; Falco et al., 2012). By offering an easy-to-screen *in*
78 *vivo* system for novel therapeutic molecules, zebrafish supplies a suitable model to explore CRP lipid-
79 binding properties and conformation-dependent functionalities related to cardiovascular heart diseases
80 including viral infections. Zebrafish is a well known model for heart development and function (Genge et al.,
81 2016; Lu et al., 2016; Pitto et al., 2011) and a well known target for several fish rhabdoviruses (Encinas et
82 al., 2013; Estepa and Coll, 2015a; Garcia-Valtanen et al., 2017; Varela et al., 2016). In this context, we have
83 first explored *crp1-7/CRP1-7* transcript/protein levels during several zebrafish viral infection situations and
84 then designed several *in vitro/in vivo* strategies to explore *crp1-7/CRP1-7* implication on viral infections.

85 Zebrafish CRP1-7 are made of protein monomers of ~ 200 amino acids (~23 kDa)(Chen et al.,
86 2015; Falco et al., 2012). According to its proposed 3D structure, CRP5 is a trimeric Ca^{++} -dependent
87 phospholipid-binding protein (tCRP) rather than a pentameric molecule (pCRP) as in humans (Chen et al.,
88 2015). It is not yet known whether all the rest of zebrafish CRP isoforms are also trimeric (Bello et al., 2017)
89 and/or whether they all have similar functionalities than human pCRP. For instance, although C1q (a known
90 ligand of pCRP) have been identified in zebrafish (Boshra et al., 2006), fish have only IgM and one class of
91 polymeric immunoglobulin receptor (PIGR)(Zhang et al., 2010) (other IgG receptors bind C1q-pCRP
92 complexes). There have been no reports on interactions between CRP1-7 and zebrafish C1q or PIGR (Lu et
93 al., 2012). Therefore, the possible human analogous functions of the CRP1-7 isoforms remain
94 unknown.

95 Human and zebrafish CRPs showed a high degree of conservation, including the location of their
96 two cysteine residues, and similarities between the amino acid sequences involved in their Ca^{++} -dependent
97 ligand-binding pockets. Such conservation suggested similar functions in human pCRP and zebrafish tCRPs
98 (Bello et al., 2017; Chen et al., 2015). On the other hand, the variations of amino acids around the ligand-
99 binding pockets of zebrafish CRPs, suggested different ligand-binding specificities, which may be
100 hypothetically explained by the need to target a wide pathogen diversity such as that found in aquatic
101 environments (Bello et al., 2017). Previous preliminary data showing modulation of zebrafish *crp*-pathways
102 during viral infections (Estepa and Coll, 2015a; Garcia-Valtanen et al., 2017) or trout *crp* upregulation
103 during oral vaccination against virus (Ballesteros et al., 2012), suggested that zebrafish *crp1-7/CRP1-7* may
104 have some anti-viral activities. Because all the above mentioned reasons, we have further studied possible
105 relations between zebrafish individual *crp1-7/CRP1-7* and viral infections.

106 As zebrafish viral infection models we mainly chose two rhabdoviruses to which zebrafish is
107 susceptible, the Spring Viremia Carp Virus (SVCV) (Lopez-Munoz et al., 2010; Sanders et al., 2003), and
108 the Viral Haemorrhagic Septicemia Virus (VHSV) (Novoa et al., 2006). Rhabdoviruses penetrate into the
109 fish body via their fins (Harmache et al., 2006). The progress of infection becomes externally associated with
110 exophthalmia, abdominal distension, and petechial haemorrhages in fins and gills 3 to 6 days after

111 penetration. A few days later, the most important fish internal lymphoid organs such as head kidney and
112 spleen become also affected (Ahne et al., 2002; Ashraf et al., 2016). Mortalities are highest ~ 15 days after
113 the beginning of infection (Encinas et al., 2013; Encinas et al., 2010).

114 To detect possible variations on *crp1-7*/CRP1-7 expression, we have explored several zebrafish
115 infection situations. Thus, among the viral infection situations chosen, short-term (infection) and long-term
116 responses (survival) were studied after infection with VHSV (Encinas et al., 2010; Estepa and Coll,
117 2015b) and SVCV (Encinas et al., 2013). Bacterial infections were also studied because of the
118 well known anti-bacterial pCRP responses on humans (Kindmark, 1971). Since resistance to viral
119 infections in both fish and mammals depends both on innate and adaptive responses (i.e., neutralizing IgM
120 antibodies in fish and both IgM/IgG antibodies in mammals), fish rely more heavily in innate than in
121 adaptive responses to fight viral infections (Sunyer, 2013; Sunyer et al., 1998). To explore the importance
122 of *crp1-7* innate responses in the presence and absence of adaptive immunity, we studied
123 adaptive immunity-deficient zebrafish *rag1*^{-/-} mutants, which have no antibodies nor T-cell receptors and
124 whose responses to viral infections have been studied recently (Garcia-Valtanen et al., 2017). Results showed
125 heterogeneous *crp1-7* transcriptional profiles in all the above mentioned infection situations including higher
126 responses in the absence of adaptive immunity, all results suggesting heterogeneous *crp1-7* anti-viral
127 responses. Confirming those expectations, *in vitro* neutralization and *in vivo* protection of SVCV infection
128 were found for the first time to be induced by the different zebrafish *crp1-7*/CRP1-7 isoforms. In addition to
129 its possible implications to prevent and/or to treat human cardiovascular/viral diseases, this knowledge and
130 future studies on their mechanism(s) of action may help to understand primitive vertebrate CRP diversity and
131 how it may have evolved to humans. It also could be applied to improve prevention methods for viral
132 infection in farmed fish.

133

134

135

136 **2. Material and methods**

137 **2.1. Zebrafish (*Danio rerio*)**

138 Adult XL wild type zebrafish of 700-900 mg of body weight (3-4 cm in length) were obtained
139 from a local pet shop (Aquarium Madrid, Madrid, Spain). Zebrafish of 6 months of age (~ 500 mg of body
140 weight) with truncated-inactivated recombinant activation gene (*rag1*^{-/-}) and their corresponding wild-type
141 *rag1*^{+/+} counterparts were originally obtained from David Raible's fish facility at the University of
142 Washington (USA) and raised, maintained, and characterized as described before (Garcia-Valtanen et al.,
143 2017). Zebrafish were maintained at 24-28 °C in 30 l aquaria with tap-dechlorinated carbon-filtered
144 water with 1 g of CaCl₂, 1 g of NaHCO₃ and 0.5 g of Instant Ocean sea salts added to water resulting in a
145 conductivity of 200-300 µS and pH of 7.8-8.2. The aquaria were provided with biological filters and fish
146 fed daily with a commercial feed diet (Vipan Bio-Vip, Sera, Heisenberg, Germany). Previously to the
147 viral infection challenge, fish were acclimatized for 2 weeks to the corresponding optimal viral replication
148 temperatures.

149 **2.2. Fish cell culture**

150 The *epithelioma papulosum cyprinid* (EPC) cells from the fathead minnow fish (*Pimephales promelas*)
151 were obtained from the American Type Culture Collection (ATCC, Manassas, Vi, USA, code number CRL-
152 2872). EPC cell monolayers were grown at 28 °C in a 5 % CO₂ atmosphere in RPMI-1640 Dutch modified
153 culture medium (Gibco, UK) supplemented with 20 mM HEPES, 10 % fetal bovine serum, FBS (Sigma, St.
154 Louis, USA), 1 mM piruvate, 2 mM glutamine, 50 µg/ml of gentamicin (Gibco) and 2 µg/ml of fungizone.

155 **2.3. *In vitro* infections with viral haemorrhagic septicemia virus (VHSV) and spring viremia carp
156 virus (SVCV)**

157 The fish *novirhabdovirus* viral haemorrhagic septicemia virus (VHSV) strain 07.71 (accession number
158 AJ233396) isolated from rainbow trout *Oncorhynchus mykiss* (LeBerre et al., 1977) and the rhabdovirus Spring
159 Viremia Carp Virus (SVCV) isolate 56/70 from carp *Cyprinus carpio* (Fijan et al., 1971), recently renamed
160 *Carp Sprivivirus* (ICTV, 2015), were used for *in vitro* and *in vivo* infections. VHSV or SVCV were
161 replicated in EPC cell monolayers at 14 °C (Estepa and Coll, 2015a) or at 22 °C (Garcia-Valtanen et al.,

162 2017), respectively, in the cell culture media described above except for 2 % FBS (infection media) and
163 absence of the CO₂ atmosphere. Supernatants from VHSV or SVCV-infected EPC cell monolayers were
164 clarified by centrifugation at 4000 g for 30 min and kept at -80 °C. *In vitro* viral infections were performed by 2
165 h adsorption of the viral supernatants to the EPC cell monolayers, followed by washing the unbound viruses
166 with infection media and incubation at their respective optimal replication temperatures during 24 h. The
167 infected EPC cell monolayers were fixed and viral titers assayed by the *in vitro* by the focus forming units
168 (ffu) assay as described before (Chinchilla et al., 2013b).

169 **2.4. *In vivo* infections of adult zebrafish with VHSV, SVCV and bacteria**

170 The procedures used for infecting zebrafish with VHSV or SVCV viruses were described before.
171 Briefly, zebrafish were acclimatized to 14 °C for VHSV infection or to 22 °C for SVCV infection
172 during 2 weeks and infected for 2 h by bath immersion in cell culture supernatants containing 10⁷ ffu /ml
173 of VHSV (Estepa and Coll, 2015a) or 10⁴ ffu/ml of SVCV(Garcia-Valtanen et al., 2017), respectively.
174 Parallel, non-infected zebrafish were mock-infected with cell culture medium to calculate
175 differential expression folds. Zebrafish infected at short times with rhabdoviruses were
176 euthanized 2-days after infection. Zebrafish surviving rhabdovirus infections were euthanized 2 months
177 after last infection of 2 consecutive VHSV infections, (Estepa and Coll, 2015a) or 1 month after SVCV
178 infection (Encinas et al., 2013). Zebrafish surviving a chronic infection with *Aeromonas hydrophila* and
179 *Vibrio fluvialis* as identified by the Microbiological Service of the Fundación Hospital Alarcon (Madrid
180 Spain), were euthanized ~ 5 months after the first deaths were detected (Estepa and Coll, 2015a).

181 **2.5. Harvest of lymphoid organs, fin tissues, and blood plasma from virally infected zebrafish.** For
182 microarray and RTqPCR studies, head kidney and spleen (lymphoid organs) and/or fin tissues were
183 harvested and pooled from 3 zebrafish for each biological replica. Harvested samples for
184 microarray/RTqPCR analysis were kept in RNAlater (Qiagen) at -70 °C until used. For the proteomic
185 studies, anesthetized zebrafish were bled by cutting the final end of their tails. Blood was collected
186 in 100 µl of sterilized anticoagulant media (0.64 g sodium citrate, 0.15 g EDTA, 0.9 g sodium
187 chloride per 100 ml of water containing 50 mg per ml of gentamicin) at 4 °C. Diluted blood was

188 immediately centrifuged at 1000 g for 3 min to obtain plasma. Plasma were kept frozen at -70 °C until
189 used.

190 **2.6. Ethic statement on zebrafish handling**

191 Zebrafish were handled following National and European guidelines. In addition, specific zebrafish
192 protocols were locally approved by the Ethics Committee (authorization CEEA 2011/022) following the
193 National Guidelines for type III experimentation (Annex X, permission RD53/2013). All personnel
194 implicated in the handling of zebrafish obtained the special C National permission for training in animal
195 experimentation. To record for health and behavior, the VHSV- or SVCV-infected fish were daily monitored 2-
196 4 times. To minimize suffering (Huang et al., 2010), fish showing external haemorrhages and/or abnormal
197 swimming behavior (endpoint criteria) were immediately euthanized by immersion in iced water (5 parts ice/1
198 part water, 0-4° C) for 10 min and then exposed to an overdose of methanesulfonate 3-aminobenzoic acid ethyl
199 ester (MS222, 300 mg/l) for > 10 min after cessation of opercular movement ("Guidelines for Use of Zebrafish
200 in the NIH Intramural Research Program", <http://oacu.od.nih.gov/ARAC/documents/Zebrafish.pdf>). No fish
201 died before meeting the endpoint criteria. MS222 at 90 mg/l was used to anesthetized the fish while obtaining
202 blood. The fish were then euthanized by an overdose of MS222 to extract lymphoid organs and/or fin tissues.

203 **2.7. RNA isolation from zebrafish tissues/organs and EPC cell monolayers**

204 For RTqPCR tissues/organs analysis, RNA from different external tissues (fin, gill, gut) and internal
205 organs (muscle, head kidney, spleen, liver) of healthy adult zebrafish were extracted and pooled from 4
206 individual zebrafish to obtain enough RNA. All tissues/organs were carefully dissected under a binocular
207 loupe for each individual zebrafish by trained personnel. Tissues were excised and pooled from dorsal,
208 ventral and caudal fins, while muscle was obtained from the tail part of the body and washed in PBS to avoid
209 possible contamination with internal organs. For microarray analysis, pooled head kidney and spleen
210 lymphoid organs or fins were pooled from 3-4 individual zebrafish for each biological replica to obtain
211 enough RNA for hybridization. The pooled tissues/organs were immediately immersed in RNAlater
212 (Ambion, Austin, USA) and maintained at 4 °C for 24 h before being frozen at -70 °C. RNA was extracted
213 from sonicated samples (1 min x 3 times at 40 W in ice) using a commercial RNA isolation kit (RNeasy kit,

214 Qiagen, Hilden, Germany) following manufacturer's instructions. For RTqPCR of EPC cell cultures, RNA
215 from the cell monolayers were similarly extracted by the same RNeasy kit used above without the sonication
216 step. Once purified, RNA concentrations were estimated by Nanodrop absorbances at 260 nm. The presence of
217 18 and 28 S RNA bands was confirmed by denatured RNA agar electrophoresis (Sigma, Che.Co, MS, USA).
218 Purified RNAs were stored at -70 °C until used.

219 **2.8. Estimation of relative expression of *crp1-7* transcripts by RTqPCR**

220 The 7 *crp* loci coding for 7 CRP isoform proteins, first identified in the CH211-234P6 linkage group
221 24 of the zebrafish (*Danio rerio*) genome (Falco et al., 2012), were used to define the 7 *crp1*/CRP1 to
222 *crp7*/CRP7 (*crp1-7*/CRP1-7) transcript/protein isoform sequences and their corresponding specific probes
223 and primers (Table S1). Reverse transcriptase quantitative polymerase chain reactions (RTqPCR) were
224 performed to estimate *crp1-7* transcript levels. For that, one microgram of purified RNA from each sample
225 was converted to its corresponding cDNA using RT from Moloney murine leukemia virus (Invitrogen) as
226 previously described (Falco et al., 2008). Quantitative PCR (qPCR) was then performed using the ABI
227 PRISM 7300 (Applied Biosystems, NJ, USA) with SYBR Green PCR master mix (Life Technologies,
228 United Kingdom). Reactions were prepared in 20 µl volume with 2 µl of cDNA, 900 nM of each forward and
229 reverse primers (Table S1) and 10 µL of SYBR Green PCR master mix. Non-template controls were included
230 for each isoform analysis. The cycling conditions were 95 °C for 10 min, followed by 40 cycles at 65 °C 1
231 min, 95 °C for 1 min. The relative gene expression values were obtained using the $2^{-\Delta\Delta Ct}$ method (Livak and
232 Schmittgen.T.D., 2001), by normalizing each *crp* gene expression value by the formula, expression of each
233 gene / expression of *eifla*.

234 **2.9. Microarray hybridization and differential expression data analysis**

235 Oligo probes of 60-mer and 80 ± 3 °C of melting temperature, specific for each of the zebrafish *crp1-7*
236 sequences were designed (Array Designer 4.3, Premier Biosoft Palo Alto CA, USA) from the mRNA GenBank
237 data base accession number sequences listed in Table S1 (accessed in 2013) as previously described (Estepa and
238 Coll, 2015a). The *crp1-7* oligo probes were included in the ID41401 and ID47562 home-designed immune-
239 focused zebrafish microarray Agilent's versions which were validated by RTqPCR in previous studies

240 (Encinas et al., 2013; Estepa and Coll, 2015a). Both microarray designs were deposited also in the Gene
241 Expression Omnibus (GEO) numbers GPL15747 and GPL17670, respectively. Extracted RNA samples
242 from zebrafish tissues/organs were amplified and fluorescently labeled from 2 µg of high quality RNA (50
243 µg/ml) and hybridized to the above described microarrays by Nimgenetics (Cantoblanco, Madrid, Spain) as
244 previously described (Encinas et al., 2013; Estepa and Coll, 2015a). Because genes previously classified as
245 *saps* (Encinas et al., 2013) were recently identified as isoform variants of *crp2* (*sap1/sap2*) or *crp5*
246 (*sap/sapp*) (Bello et al., 2017), their similar microarray expression data were included into the corresponding
247 *crp* calculations. Raw data were normalized by the sum of all microarray fluorescences and outliers removed
248 as described before in detail (Encinas et al., 2013; Estepa and Coll, 2015a). Raw and normalized data were
249 deposited at GEO's GSE57952 (VHSV-infected and VHSV- / bacterial-survivor zebrafish), GSE58205
250 (SVCV-infected wild type zebrafish) and GSE54096 (*rag1*-/- mutant zebrafish) (Encinas et al., 2013; Estepa
251 and Coll, 2015a; Garcia-Valtanen et al., 2017). Results were expressed in differential expression folds
252 calculated by the formula detailed in each of the corresponding Figure legends (Figures 1, 2 and 3).

253 **2.10. Proteomic analysis of CRP1-7 induced by SVCV infection in zebrafish plasma**

254 Adult zebrafish were infected with SVCV and their blood harvested after 0, 24, 48 and 120 h (5-
255 days). Blood was obtained from 3 biological replicas for each time point, 3 fish pooled per replica (total
256 amount of fish = 36). Red blood cells were immediately removed by centrifugation at 3000 g for 10 min at 4
257 °C. The resulting plasma samples were treated with 9 M urea, 2 M thiourea, 5% CHAPS (Dimethyl[3-(
258 propyl]. azaniumyl] propane-1-sulfonate), 2 mM TCEP (Tris(2-carboxyethyl)phosphine) and anti-protease
259 cocktail (Sigma-Aldrich, St.Louis, Mi, USA). The samples were then precipitated with methanol/chloroform,
260 quantified by the BCA assay (Pierce Protein Assay kit, Rockford, Il, USA) and digested with trypsin. The
261 resulting peptides were cleaned using a StageTip-C18 column and 1 µg of each cleaned sample separated by
262 liquid chromatography (LC) in a C-18 column employing a long gradient for elution to reduce hemoglobin-
263 derived peptides. Mass spectrophotometry (MS) was performed in a Triple-TOF 6600 (LC/LC-MS/MS)
264 Sciex apparatus (Framingham, MA, USA) at the Proteomic Facilities at the "Centro Nacional de
265 Biotecnología" (CNB, Cantoblanco, Madrid, Spain). The CRP1-7 protein accession numbers corresponding

266 to the peptide sequences obtained were identified using the MASCOT search engine against the UNIPROT
267 protein data base of zebrafish (*Danio rerio*). Only those CRP identified with more than 2 different peptides
268 were considered for further analysis. Automatic CRP1-7 identifications were confirmed by manual
269 comparison with sequences derived from mRNA accession numbers and/or blast against mRNA-derived
270 protein sequence data banks. There were 1 to 5 UNIPROT accession numbers identified for each CRP
271 isoform (Table S2) except for CRP6. The number of peptides, spectra counts, and peptide probability scores
272 were used for quantitation of each of the CRP accession numbers identified. The results were finally
273 normalized by the number of expected peptides per CRP1-7 using the emPAI method (Ishihama et al., 2005).
274 Folds were then calculated by the formula, emPAI values of each CRP accession number at different times /
275 emPAI mean value of each CRP accession number at time 0 (n=3).

276 **2.11. Preparation of pMCV1.4 plasmids coding for *crp1-7***

277 The pMCV1.4 plasmid was used for subcloning each of the *crp1-7* genes (accession numbers in Table
278 S1). The MCV1.4 promoter is a large immediate early cytomegalovirus promoter which includes a synthetic
279 intron to increase expression efficiency (Rocha et al., 2005). To obtain the plasmid constructs, the
280 corresponding mRNA-derived *crp1-7* sequences were flanked by HindIII and XhoI nucleotide sequences,
281 chemically synthesized, subcloned into pMCV1.4 and their resulting sequences confirmed by sequencing both
282 strands (Genscript, NJ, USA). The resulting pMCV1.4-*crp1-7* plasmid constructs were used to transform
283 *E.coli* DH5alpha by electroporation, amplified and isolated with the Endofree Plasmid Midi purification Kit
284 (Qiagen, Germany) according to the manufacturer's instructions. Maximal concentrations of contaminating
285 *E.coli* lipopolysaccharide (LPS) were estimated to be < 0.52 ng per 100 ng of purified plasmid according to
286 the manufacturer. Purified plasmid solutions were adjusted to 1 mg/ml of total DNA (260 nm absorbances)
287 which contained 80-100 % of plasmid DNA, as shown by agarose gel electrophoresis. Purified plasmids were
288 stored at -20 °C.

289 **2.12. Transfection of EPC cell monolayers with pMCV1.4-*crp1-7* and infection with Spring 290 Viremia Carp Virus (SVCV)**

291 EPC cell monolayers in 96-well plates (50000 EPC cells per well) in 100 µl of cell culture medium

292 were transfected with 100 ng of each of the pMCV1.4-*crp1-7* plasmids complexed with 0.3 µl of FuGENE
293 HD (Promega, Madison, WI, USA) for 24 h at 22 ° C. Under these conditions, the transfection efficiency as
294 determined by the percentage of fluorescent cells after transfection with pMCV1.4-*gfp* varied between 15 to 30
295 % (n=3 experiments). After transfection, the cell culture medium was removed, fresh medium added and 48 h
296 later transcript expression estimated by RTqPCR as described above. When appropriated, the transfected
297 EPC cell monolayers were infected with 50 focus forming units (ffu) of SVCV per well in 100 µl
298 (multiplicity of infection of 10⁻³) and incubated for viral adsorption for 2 h. Then the virus remaining in the
299 supernatants were removed, fresh medium added and infected cell monolayers incubated for 24 h.

300 **2.13. SVCV neutralization of pMCV1.4-*crp1-7* plasmid transfected EPC cells or of CRP1-7-
301 enriched supernatant-treated EPC cells.** To study possible interference of CRP1-7 with SVCV replication
302 in EPC cell monolayers, 2 types of *in vitro* micro-neutralization assays were performed. In the first type of
303 assays, the EPC cell monolayers were transfected with pMCV1.4-*crp1-7* plasmids and 3-days later infected
304 with SVCV as described above. The transcript expression levels relative to the *efl1a* gen expression after
305 transfection and before infection were similar for *crp1-7* (Figure S1 A). In the second type of assays, large
306 amounts of cell-free supernatants were obtained by transfecting EPC cell monolayers in multiple 96-wells
307 with pMCV1.4-*crp1-7* and harvesting them 3-days later. Because Western blotting was not sensitive enough
308 to detect the CRP presence in the supernatants, to concentrate CRP, 500 µl of supernatants had to be spotted
309 onto each spot of the nitrocellulose filters. The CRP content of the concentrated CRP1-7 were estimated with
310 anti-CRP rabbit antibodies raised against one of the most conserved carboxy-terminal amino acid stretches
311 among zebrafish CRP1-7 (¹⁸⁹DWDTIEYDVTGN) (GenScript, Piscataway, NJ, USA). To reduce
312 background, the anti-CRP antibodies contained in the rabbit sera were purified by affinity chromatography
313 on a mixture of DWDTIEYDVTGNGGGGGK / KKGGGGGGDWDTIEYDVTGN peptides coupled to
314 CNBr-activated Sepharose. Affinity-purified anti-CRP antibodies bound to the CRP-enriched supernatant
315 samples were detected with horseradish peroxidase labeled goat anti-rabbit immunoglobulins and ECL
316 (BioRad) (Figure S1 B). Further details of the method are given in the Figure S1 legend. To study the effects

317 of CRP1-7-enriched supernatants, 100 µl were added to EPC cell monolayers for 24 h, washed, and
318 monolayers infected with SVCV as indicated above.

319 In both types of assays, the number of infected EPC cells was determined by micro focus forming
320 units (ffu) (n=2 experiments) and flow cytometry (n=2 experiments). The number of ffu were estimated by
321 immunofluorescence of the fixed cell monolayers and staining with polyclonal anti-SVCV (BioX Diagnostics
322 SA, Jemelle, Belgium) and rhodamine labeled goat anti mouse immunoglobulins (GAM-TRITC). The results
323 were then expressed as percentage of neutralization calculated by the formula, 100 - (number of infected cells
324 in transfected or treated EPC cells / number of infected cells in non-transfected or non-treated EPC cells).

325 Flow cytometry was performed by the high throughput micro method (Chinchilla et al., 2013a). Briefly, SVCV-
326 infected cell monolayers were fixed with formaldehyde, permeabilized with digitonine and stained with anti-
327 SVCV (BioX Diagnostics SA, Jemelle, Belgium) and GAM-FITC. EPC cell suspensions were then obtained by
328 trypsin digestion to be analyzed in a BD FACS Canto II apparatus (Beckton Dickinson, San Agustin de
329 Guadalix, Madrid, Spain) provided with a high throughput sampler. The number of fluorescent cells (SVCV-
330 infected cells) over a threshold containing 95 % (mean + 2 standard deviations) of non-infected EPC cells
331 was first determined. SVCV-infected cell monolayer controls in the absence of any treatment showed 25-40
332 % of the EPC cells were infected depending on the experiment. The percentage of infected EPC cells was then
333 calculated using the formula: 100 x number of cells with fluorescences above the threshold / total number of
334 cells gated per well. The final results were expressed in % of neutralization by the formula: 100 - 100 x
335 percentage of transfected or supernatant-treated and infected cells / percentage of infected cells in control
336 cells. Because no significant differences were found between ffu and flow cytometry assays, their results
337 were pooled and means and standard deviations calculated (n=4).

338 To study possible interferences in the neutralization assays caused by *E.coli* LPS which could be
339 contaminating the plasmids purified by the Endofree Plasmid Midi purification Kit (Qiagen, Germany), LPS
340 from *E.coli* O55B5 and 0111:B4 strains (Sigma Che Co, St.Louis MS, USA) were added at different
341 concentrations (20-500 ng per well) to non-transfected EPC cell monolayers. Those concentrations were
342 higher than the estimated amounts which may be present when transfecting EPC cell monolayers with 100 ng

343 of plasmids per well (< 0.52 ng per 100 ng of plasmid). The LPS-treated EPC cell monolayers were then
344 infected with SVCV and finally assayed for neutralization by ffu (Figure S2).

345 **2.14. Injection of one-cell stage embryos with pMCV1.4-*crp2-5* or pMCV1.4-*il6* plasmids and**
346 **resistance of zebrafish larvae to SVCV infection or induction of *crp1-7* transcripts, respectively**

347 To test for CRP1-7 induced resistance to SVCV, one-cell stage of zebrafish embryos were
348 microinjected with 2 nl of phosphate buffered saline (PBS) containing 150 pg of pMCV1.4 plasmids coding
349 for green fluorescent protein (GFP) and CRP2-5, by following the methodology described before (Pereiro et
350 al., 2017). The microinjections were performed with pulled glass microcapillary pipettes (WPI, USA) and a
351 Narishige IM-30 micromanipulator under an stereo microscope SMZ800 (Nikon). To study the effects of
352 SVCV challenge, the resulting 3-day hatched larvae were anesthetized and 12 larvae per group were
353 microinjected into the duct of Cuvier to induce a systemic infection with 2 nl of PBS containing 10^4 pfu of
354 SVCV or only PBS per larvae. Results at each of the different times after infection were expressed in
355 cumulative survival calculated by the formula $100 - (100 \times \text{number of dead fish injected with pMCV1.4-gfp}$
356 or *crps*). A 64.5 % mortality was obtained in fish injected with the pMCV1.4-gfp control 7 days after
357 infection. Kaplan-Meier cumulative survival curves were analyzed for statistical significance with the log-
358 Rank (Mantel-Cox) test (Mantel, 1966) by comparing the survival of fish injected with pMCV1.4-*crps* to
359 those of pMCV1.4-gfp.

360 To test for the effects of IL6 on *crp1-7* expression, one-cell stage embryos were microinjected with 2
361 nl of PBS containing 150 pg of pMCV1.4 or pMCV1.4-*il6* plasmids as described above. Three-days later the
362 larvae were pooled ($n = 4$ groups of 3 pooled fish per group, total number of larvae per group = 12), RNA
363 extracted and *crp1-7* transcript levels evaluated by RTqPCR using the primers described in Table S1. Results
364 were expressed relative to *eifla* expression as calculated by the formula, $100 \times \text{crp1-7 expression per group} /$
365 *eifla* expression per group. Means and standard deviations were represented.

366 **2.15. Statistical analysis**

367 Survival results represented by Kaplan-Meier survival curves were analyzed for statistically
368 significance by the log-Rank (Mantel-Cox) test (Mantel, 1966) using the corresponding survival analysis

369 feature of the computer software package OriginPro 2017 (64 bit, sr1) by comparing the survival of fish
370 injected with pMCV1.4-*crps* to those of pMCV1.4-*gfp*, following previous reports (Pereiro et al., 2017).
371 Results of microarray hybridization, RTqPCR and microneutralization were represented in differential
372 expression folds or percentage of neutralization as the means ± standard deviation of n biological replicates.
373 To determine their significant differences, the corresponding data were analyzed with OriginPro 2017 using
374 Student's t-test. In the graphs, $p < 0.05$ significant differences were displayed as *.

375

376

377

378

379

380

381

382

383

384

385

386

387

388

389

390 **3. RESULTS**

391 **3.1. Levels of *crp1-7* transcripts were specific of tissues and organs in healthy adult zebrafish**

392 RNA from different external tissues (fin, gill, gut) and internal organs (muscle, head kidney, spleen,

393 liver) of healthy adult zebrafish was extracted to investigate by RTqPCR the distribution of *crp1-7* transcript

394 expression relative to the *eifla* gene using specific primers (Table S1). Results showed amplified products

395 corresponding to an average of 45.2 relative expression units for the 7 tissues and *crp1-7* isoforms. The *crp4*

396 / *crp6* in gills (Table 1A) and *crp3* / *crp5* in spleen (Table 1B) showed relative expressions ~3-6-fold higher

397 (range from 124 to 293 relative expression units) than the average, while the expression of *crp3* / *crp5* in

398 gills, *crp6* in gut, *crp4* in spleen and *crp2* / *crp3* / *crp4* in kidney were > 60 relative expression units (Table

399 1A, B in gray). On the contrary, *crp7* in all and *crp1* in some (fin, gut, spleen, liver) tissues/organs showed

400 10-50 lower expression levels than *crp2-6*. Each tissue/organ had a different distribution of constitutive *crp1-*

401 *7* expression levels when expressed in percentage of their total expression (Table 1C). For instance, *crp5* was

402 the most abundant in percentage in spleen and was present at relatively high levels in most tissues/organs

403 while *crp2* was most abundant in muscle / head kidney and *crp6* in gut / gill / liver (Table 1C). A similar

404 tissue/organ specificity was already described in common carp for its *crp1-2* isoforms (Falco et al., 2012).

405 The existence of tissue-specific distribution of *crp1-7* transcript levels suggested different functionalities

406 among the 7 zebrafish CRP isoforms. Therefore, to study whether or not the constitutive levels of *crp1-7*

407 transcripts in healthy zebrafish tissues/organs may change after infection, head kidney plus spleen (the most

408 important lymphoid internal organs) and fins (the easiest-to-obtain external tissue) were selected for further

409 experimentation.

410 **3.2. Zebrafish infected with VHSV or surviving VHSV/bacterial infections showed**

411 **heterogeneous changes in the differential expression of their *crp1-7* transcripts in lymphoid organs**

412 Hybridization values (fluorescent arbitrary units) and differential expression folds (infected *versus*

413 non-infected zebrafish) of *crp1-7* transcripts from lymphoid organs were explored by microarray

414 hybridization using a unique home-designed platform which included 7 *crp* (*crp1-7*) specific probes (Table

415 S1, Figure 1).

416 In all the infection/survival situations studied, the hybridization values varied from 1 to 30000
417 fluorescent arbitrary units. However, while the *crp2-6* values ranged from 1000 to 30000 units, all *crp1*
418 values ranged from 1 to 50 and those of *crp7* from 10 to 200 units (not shown). Therefore, the constitutive
419 expression levels of *crp1 / crp7* found in healthy zebrafish tissues/organs (Table 1) remained low after viral
420 or bacterial infections when compared to the rest of *crp2-6*.

421 When expressed as differential expression folds, the results showed that after VHSV-infection *crp2 /*
422 *crp3 / crp4 / crp6* were upregulated (2-5-fold), while *crp1 / crp5 / crp7* remained unmodulated (Figure 1,
423 positive red hatched bars). Similar results were obtained for bacterial survival, although their corresponding
424 upregulation levels were higher (Figure 1, positive blue bars). However, in bacterial survival, *crp5* was also
425 upregulated (Figure 1, positive *crp5* blue bar), suggesting that *crp5* responses may differentiate bacterial
426 from viral infections. The upregulation of zebrafish *crp2-6* isoforms resembled that of human pCRP after
427 bacterial infection/survival (Kindmark, 1971). In conclusion, the profile of zebrafish *crp1-7* modulation was
428 comparable between bacterial survival and viral infections, except for *crp5*.

429 In contrast to viral infection and bacterial survival, fish surviving VHSV infection (VHSV-survivors)
430 resulted in downregulated levels of *crp2-6* (Figure 1, negative yellow bars). The levels of *crp1 / crp 7*
431 remained unmodulated. After VHSV re-infection of the VHSV- survivors, the levels of *crp2 / crp3 / crp6*
432 increased but still remained downregulated (compare negative yellow empty with yellow hatched bars in
433 Figure 1).

434 **3.3. Fins showed higher differential expression levels of *crp2-6* than lymphoid organs after**
435 **SVCV-infection and in SVCV-survivors**

436 The *crp1-7* transcriptional profiles were comparatively studied in internal lymphoid organs and
437 external fin tissues. Differential expression folds showed that after SVCV-infection, only *crp4 /crp7* in
438 internal lymphoid organs were slightly upregulated (Figure 2A, white hatched bars), while in external fins,
439 *crp2 / crp4 / crp5* were upregulated, specially *crp5* (~ 7-fold) (Figure 2A, gray hatched bars). Similarly, in
440 SVCV-survivors, *crp2 /crp4 / crp5* in lymphoid organs were slightly upregulated (Figure 2B, white hatched

441 bars), while in fins, *crp2-6* increased their upregulation, specially *crp5* (>15-fold) (Figure 2B, gray
442 hatched bars).

443 **3.4. Lymphoid organs from adaptive-deficient *rag1*^{-/-} zebrafish mutants showed high levels of**
444 **differential expression of *crp1-6* when infected with SVCV**

445 To explore any possible relation between *crp* and adaptive immunity responses, the *crp1-7* responses
446 to viral infection (innate responses) were studied in the absence of adaptive immunity (*rag1*^{-/-} mutants) and
447 compared to wild type *rag1*^{+/+} mutants. In addition, *crp1-7* transcripts were analysed in lymphoid organs
448 from zebrafish *rag1*^{-/-} mutants without (mock infected) and after infection with SVCV. Results showed that
449 compared to wild type *rag1*^{+/+}, the *crp1-6* were 5-20-fold downregulated in *rag1*^{-/-} mutants (Figure 3,
450 negative empty bars). In sharp contrast, highly upregulated levels of *crp1-6* appeared 2-days after the *rag1*⁻
451 ^{-/-} mutants were infected with SVCV compared to mock-infected *rag1*^{-/-} mutants (Figure 3, positive hatched
452 bars), except for *crp4* which remained similarly downregulated in both cases (Figure 3, negative hatched
453 bar). The *crp2/crp5* showed the highest upregulated levels (~ 10 and 17-fold, respectively) in the absence of
454 adaptive immunity.

455 **3.5. Time course of CRP1-7 protein differential expression in zebrafish plasma after SVCV**
456 **infection**

457 To compare *crp1-7* transcript levels in lymphoid organs with CRP1-7 protein levels in blood after
458 SVCV infection, we followed the time course of different CRP UNIPROT accession numbers by double
459 liquid chromatography/mass spectrophotometry (LC/LC/MS/MS) in plasma samples from SVCV-infected
460 zebrafish. Because of the similarity of amino acid sequences among zebrafish CRP1-7 isoforms (Bello et
461 al., 2017), the CRP1-7 identifications derived from the tryptic peptide analysis should be taken with caution.
462 For instance, some of the peptides could not differentiate between CRP2 / CRP3, some peptides were
463 common to CRP2 and CRP6, and no unique CRP6 peptides could be detected. Despite those limitations,
464 after 24 h, the number of accession numbers and the differential expression folds were higher in several of
465 the CRP2 / CRP5 than in CRP3 / CRP4. After 48 h, only CRP2 showed one higher fold than all the rest of
466 CRPs which were similar or lower than their levels at time 0 (fold = 1) . After 120 h, all identified CRPs

467 were lower than their levels at time 0 (Figure 4). The evolution of all CRP plasma levels in zebrafish after
468 SVCV infection were similar to those reported in carp CRP after infection with herpesvirus (Pionnier et al.,
469 2014).

470 In conclusion, the *crp2*/CRP2 and *crp5*/CRP5 were among the most important isoforms participating
471 in zebrafish viral responses, as suggested by most of the results obtained from the tissue/organ-specificity of
472 *crp1-7* levels on healthy zebrafish (Table 1), the *crp1-7* expression in lymphoid organs of fish
473 infected/surviving VHSV/bacterial infections (Figure 1), the comparative studies of *crp1-7* transcripts from
474 organs/fins after SVCV infection (Figure 2), the *crp1-7* highest expression on adaptive-deficient mutants
475 infected with SVCV (Figure 3) and the plasma levels of CRP1-7 proteins after SVCV infection (Figure 4).
476 In contrast, *crp1*/CRP1 and *crp7*/CRP7 remained unmodulated in most of the infection situations mentioned
477 above. On the other hand, since all those *in vivo* *crp1-7*/CRP1-7 responses could be due to some interference
478 with viral replication, we next undertook a series of experiments focusing on neutralization assays.

479 **3.6. Fish cells transfected with pMCV1.4-*crp1-7* or treated with CRP1-7-enriched supernatants**
480 **neutralized SVCV**

481 To investigate possible interferences of zebrafish *crp1-7*/CRP1-7 with SVCV replication, *crp1-7*
482 mRNA sequences were cloned into the pMCV1.4 eukaryotic expression plasmid. Micro-neutralization assays
483 for SVCV infection were then performed after using two complementary strategies to deliver *crp1-7*/CRP1-7
484 to fish cells *in vitro*, **i**) transfection of EPC cell monolayers with pMCV1.4-*crp1-7* or **ii**) treatment of EPC
485 cell monolayers with CRP1-7-enriched supernatants obtained from pMCV1.4-*crp1-7*-transfected EPC cells.

486 To interpret possible differences of expression among the CRP isoforms, the efficiency of
487 transfection of each of the pMCV1.4-*crp1-7* plasmid constructs and the presence of each of the
488 corresponding CRP1-7 proteins in the supernatants were first studied by RTqPCR and dot-blot, respectively.
489 Results showed that no significative differences could be demonstrated between relative expression levels of
490 *crp1-7* transcripts in pMCV1.4-*crp1-7* transfected cells (Figure S1, A). On the other hand, despite their low
491 level of protein expression (i.e., when compared to CRP levels in zebrafish intraperitoneal ascites), prevented
492 any quantitative analysis, CRP1-7 were present in enriched supernatants from pMCV1.4-*crp1-7* transfected

493 cells (Figure S1, B). In contrast no stained spot could be obtained in supernatants from pMCV1.4-*gfp*
494 transfected cells (Figure S1, B, lane 8). On the other hand, since bacterial LPS traces contaminating the
495 pMCV1.4-*crp1-7* plasmid preparations could be causing also neutralization, LPS from *E.coli* were added to
496 the cells and neutralization measured. No neutralization effects on SVCV infectivity could be demonstrated
497 even at the highest LPS concentrations tested (~1000-fold higher than those expected to be present in the
498 plasmids) with any of the two different sources of LPS (Figure S2). In contrast, parallel assays with cells
499 transfected with pMCV1.4-*crp2 / crp5*, confirmed, once more, the neutralization of SVCV (Figure S2).
500 Therefore, only sequence and/or conformational differences among the CRP1-7 isoforms could be
501 responsible for inducing neutralization of SVCV.

502 Results showed that the SVCV neutralization profiles obtained by transfecting EPC cells with the
503 pMCV1.4-*crp1-7* plasmids were similar to those obtained by treating the cells with the CRP1-7-enriched
504 supernatants (Figure 5A and B, respectively). Thus, *crp2*/CRP2, *crp3* and *crp5*/CRP5 obtained maximal
505 neutralization values of ~ 65-75 % in both transfected and treated cells, respectively (Figure 5A and B).
506 Lower but significant neutralization percentages (~ 35-65 %) were obtained for CRP3, *crp4*/CRP4,
507 *crp6*/CRP6 and *crp7*/CRP7. In contrast, no neutralization was obtained when using *crp1*/CRP1 (< 7 %).

508 Co-transfections were used to study possible neutralization synergies among *crp1-7*/CRP1-7. Synergy
509 was defined as the increase in neutralization levels when co-transfected two (pMCV1.4-*crp^a* + pMCV1.4-
510 *crp^b*) rather than one pMCV1.4-*crp1-7* plasmid. To carry out co-transfections, the concentration of each
511 plasmid was reduced from 100 to 50 ng per well. When required, 50 ng per well of the pMCV1.4-*gfp*
512 plasmid were added to obtain the same final concentration of 100 ng of DNA per well (pMCV1.4-*crp* +
513 pMCV1.4-*gfp*). Results of several co-transfections with different combinations between two pMCV1.4-
514 *crp1-7* plasmids showed that the neutralization levels were always lower (Figure S3, hatched bars) than the
515 theoretical sum obtained when the plasmids were separately transfected (Figure S3, black horizontal bars).
516 These results suggested some kind of interferences rather than synergies at the transcript or at the protein
517 levels between *crp1-7*/CRP1-7 isoforms. Interferences could be due to the formation of neutralization-

518 inactive CRP heteropolymers, to *crp* transcriptional controls or to changes in viral specificity (since they
519 could still neutralize other viruses). Further work needs to be done to explore such possibilities.

520 In conclusion, all the above mentioned results suggested that zebrafish *crp2-7/CRP2-7* (all except
521 *crp1/CRP1*) neutralized SVCV *in vitro*.

522 **3.7. Microinjection of zebrafish embryos with pMCV1.4-*crp2-5* induced protection to SVCV
523 infection and injection of pMCV1.4-*il6* induced *crp4-5* transcripts**

524 To investigate whether or not the *in vitro* neutralization of SVCV by *crp1-7/CRP1-7* could be also
525 observed *in vivo*, selected pMCV1.4-*crp2-5* plasmids were microinjected into one-cell stage zebrafish
526 embryos. Three days later, the hatched larvae were challenged by microinjection of 10^4 pfu of SVCV per
527 larvae. The cumulative survivals obtained after 7 days of SVCV challenge for the fish injected with the
528 pMCV1.4-*crp2-5* plasmids were ~ 18, 12, 24 and 32 %, respectively (Figure 6A) in contrast to 0 % of those
529 injected with pMCV1.4-*gfp*.

530 Because mammalian *il6* is one of the major physiological inducers of CRP synthesis (Du Clos and
531 Mold, 2011), and IL6 was upregulated after mammalian viral infections (Paludan, 2001; Wang et al., 2015;
532 Xia et al., 2015), we tested also whether the microinjection of pMCV1.4-*il6* into zebrafish egg embryos
533 modulated *crp1-7* expression in the resulting larvae. Results showed that only *crp4-5* were upregulated in
534 larvae after injection of pMCV1.4-*il6* in zebrafish egg embryos (Figure 6B).

535

536

537

538

539

540

541

542 **4. DISCUSSION**

543 Several correlations and evidences for *in vitro* and *in vivo* viral neutralizing heterogeneous activities
544 of zebrafish CRP1-7 isoforms were presented here. Previous observations included correlations between
545 zebrafish CRP-related pathways and viral infections with either SVCV (Encinas et al., 2013) or VHSV
546 (Estepa and Coll, 2015a). On the other hand, the Ca⁺⁺-dependent phospholipid-binding pocket structures of
547 *in silico*-modelled CRP1-7 using the CRP5 3D X-ray structure as template, suggested the existence of a
548 functional heterogeneity (Chen et al., 2015). The present work characterized and extended those previous
549 observations to the different distributions of *crp1-7* transcripts in healthy tissues/organs and the
550 heterogeneous *crp1-7*/CRP1-7 responses during several *in vivo* viral infections. Unexpected evidences for
551 both *in vitro* neutralization and *in vivo* protection against viral infection of some but not all *crp1-7*/CRP1-7
552 isoforms were then demonstrated.

553 To our knowledge, this work is the first to report both *in vitro* neutralization and *in vivo* protection of
554 viral infection by any CRP. However, the corresponding mechanism(s) underlying these effects are not yet
555 known. Different CRP1-7 conformations (Braig et al., 2017; Eisenhardt et al., 2009a; Eisenhardt et al.,
556 2009b; Li et al., 2016; Wang et al., 2011; Wu et al., 2015), heterologous trimers (Bello et al., 2017),
557 interferences with low-pH induced rhabdoviral fusion (Estepa and Coll, 1996; Estepa et al., 2001), and/or
558 interactions of CRP1-7 carboxy-terminal domains (Potempa et al., 2015; Wang et al., 2011)(Li et al., 2016;
559 Wu et al., 2015) or derived peptides (El Kebir et al., 2011; Shephard et al., 1989; Yavin and Fridkin, 1998)
560 with lipid membranes including cholesterol-enriched lipid rafts, may offer possible mechanisms for the viral
561 neutralization by CRP1-7. Alternatively or simultaneously, *crp1-7*/CRP1-7 molecules could also
562 differentially interact with infected or uninfected cells to induce other yet unknown isoform-specific innate
563 immunity defenses. Future work should be focused on some of the above mentioned possibilities to find a
564 suitable explanation for the heterogeneous anti-viral activities induced by zebrafish *crp1-7*/CRP1-7.

565 The physiological mechanism through which the injection of pMCV1.4-*crp2-5* to egg embryos
566 induced protection of larvae against SVCV challenge is also unknown. Once translated into proteins and after
567 reaching the blood, it is supposed that the tested circulating CRP2-5 would be transported by the blood to

target SVCV and/or SVCV-infected cells. After binding to exposed phospholipid heads in SVCV-damaged cells, CRP could induce inflammatory stimulus (i.e., *il6*, *illb*). At this respect, it seems to be confirmatory that *crp5* was induced by injection of *il6*, a cytokine that upregulates circulating pCRP in humans (Du Clos and Mold, 2011) and is itself upregulated by viral infections (Paludan, 2001; Wang et al., 2015; Xia et al., 2015). Although nothing is known about zebrafish CRP1-7-ligand functionality, these isoforms may behave like in humans which bind C1q (increasing complement-aided cell lysis) and/or immunoglobulin FcR (increasing phagocytosis of tagged cells). On the other hand, cell migration from lymphoid organs to external tissues may explain downregulation of most *crp2-6* levels in survivors of viral infection and in *rag1*^{-/-} mutants. The higher upregulation of *crp2/crp3/crp5* in fins compared to that in lymphoid organs (*crp2-6*) after SVCV infection and in SVCV survivors may confirm that hypothesis. While these results correlate with the elevated numbers of leukocytes in *rag1*^{-/-} zebrafish external tissues (Garcia-Valtanen et al., 2017), the depletion of lymphoid organ IgM⁺ cells despite the presence of neutralizing antibodies in plasma from VHSV-survivor zebrafish (Estepa and Coll, 2015a), the trans endothelial leukocyte migration visually observed on zebrafish transparent larvae during viral infection (Varela et al., 2014) and/or the leukocyte cell migration during other zebrafish diseases (Deng and Huttenlocher, 2012), additional evidence should be provided to confirm cell migration when specific cellular reagents will become available for zebrafish. All these possible *in vivo* mechanisms remain to be investigated.

Despite the different experimental approaches, *crp2/CRP2* and *crp5/CRP5* were among the major actors in most anti-viral responses, while very often *crp1/CRP1* and *crp7/CRP7* remained unmodulated, and *crp3/CRP3*, *crp4/CRP4*, *crp6/CRP6* were only modulated in some cases. On the other hand, *in vitro* assays demonstrated that *crp2/CRP2* and *crp5/CRP5* neutralized SVCV infectivity to the highest extent. In addition, *in vivo* injection of pMCV1.4-*crp2-5* confirmed that *crp5/CRP5* was the most important contributor to survival of zebrafish larvae to SVCV challenge and one of the unique *crp/CRP* that together with *crp4/CRP4* could be induced by injection of *il6* (a well known inducer of pCRP synthesis in humans). The low participation of CRP1 (the only zebrafish CRP lacking signal peptide) in viral responses and neutralization, suggested the idea that CRP2-7 should be secreted to be efficient. However, since CRP1 levels were detected

594 also in CRP1-enriched supernatants, other explanation(s) may be possible. The lack of generation of CRP1
595 anti-viral peptides may offer an alternative explanation. Thus, because of the presence in CRP2-7 of a
596 protease-sensitive site (¹⁴⁶SFN or SFD) which is not totally conserved in CRP1 (¹⁴⁶DFE) (Bello et al.,
597 2017), such hypothetically neutralizing peptides may be derived from all CRPs except from CRP1. The lack
598 of differential expression of *crp7*/CRP7 has no similar possible explanations, since it has signal peptide,
599 identical protease site sequence than other CRPs and some anti-viral neutralization capacity. One possible
600 explanation for the absence of differential expression may be that *crp7*/CRP7 could be induced in response to
601 other pathogen infections (i.e., parasites?) and/or physiological conditions (i.e., other kind of tissue damage
602 or internal stimulus, etc). The different experimental approaches, different fish used for the experiments, and
603 confirmation of some results at 3 different laboratories, argue in favour of the existence of functional
604 heterogeneity among *crp1-7*/CRP1-7 isoforms.

605 Zebrafish might provide a suitable model for further *crp1-7*/CRP1-7 studies. For instance, ligand-
606 CRP1-7-binding specificities could be explored to define whether isoform heterogeneity may be related to a
607 wider anti-viral functionality in the aquatic environment.

608

609

610

611

612

613

614

615

616

617

618

619

620 **Table 1**621 **Levels of *crp1-7* transcripts in external tissues (A) and internal organs (B) of healthy adult zebrafish
622 and their distribution in percentages (C)**

623 Each of the total RNA from individual external tissues (**A**) or internal organs (**B**) from 4 adult zebrafish was
624 RTqPCR amplified using the *crp1-7* specific primers listed in Table S1. The relative gene expression values
625 were obtained using the $2^{-\Delta\Delta Ct}$ method. Each *crp1-7* gene expression value was normalized by the
626 corresponding *efl1a* value by the formula, expression of each gene / expression of *efl1a*. Means (**bold**) and
627 standard deviations (sd) were represented in the Tables A and B (n=4). **Gray boxes**, *crp* relative expression
628 levels > 60. *, *crp* relative expression levels > 120. C, Pie *crp1-7* distribution in percentages of the total *crp*
629 expression in each tissue/organ. **White pie**, *crp1*. **Green pie**, *crp2*. **Yellow pie**, *crp3*. **Dark-yellow pie**, *crp4*.
630 **Red pie**, *crp5*. **Blue pie**, *crp6*. **Gray pie**, *crp7*.

631

632 **Figure 1. Upregulated (positive bars) and downregulated (negative bars) *crp1-7* transcript profiles
633 from lymphoid organs from zebrafish infected with VHSV (red) and surviving VHSV- (yellow) or
634 bacterial-(blue) infections**

635 Fluorescence was assayed after hybridization of transcript samples from zebrafish organs to microarray *crp1-7*
636 probes. Raw and normalized data were deposited in GEO's bank at GSE57952 (Estepa and Coll, 2015a).
637 Differential expression folds (upregulated genes) were calculated by the formula, fluorescence of each gene
638 from infected fish / mean fluorescence of each gene from non (mock)-infected fish. The same fold data were
639 represented as the inverse folds and arbitrarily given a negative value (-1/folds) to best visualize the
640 downregulated genes (duplicated representation). Using this type of duplicated representation, both positive
641 (>1.5 fold) and negative (< 0.66 fold = 1/1.5 fold) bars appeared in the positive and negative Y axes in the
642 Figure. Outliers were removed and means and standard deviations represented (n=4 replicas, 3 fish pooled per
643 replica, total number of fish = 36). Only one of the \pm standard deviations were represented to increase clarity.
644 *, folds significantly > 1.5 (+, positive upregulated values) or < 0.66 (-, negative downregulated values)
645 thresholds at p < 0.05 (Student t-test). **Red dashed horizontal lines**, 1.5- and 0.66-fold thresholds. **Red**

646 **hatched bars**, 2-days after VHSV infection (VHSV+). **Open yellow bars**, 2-month VHSV-survivors
647 (VHSVS). **Hatched yellow bars**, 2- days after VHSV re-infected 2-month VHSV-survivors (VHSVS+). **Blue**
648 **bars**, 5-month *A. hydrophila*- and *V. fluvialis*-survivors (BACS).

649

650 **Figure 2. Upregulated (> 1 bars) and downregulated (< 1 bars) *crp1-7* transcript profiles from**
651 **lymphoid organs and fins from zebrafish infected with SVCV (A) or surviving SVCV infection (B)**
652 Mean differential expression folds and standard deviations were calculated as described in the legend of
653 Figure 1 and represented only in positive folds. Only one of the \pm standard deviations were represented to
654 increase clarity. Raw and normalized data were deposited in GEO's bank at GSE58205 (Encinas et al., 2013).
655 *, folds significatively > 1 or <1 at p < 0.05 (Student t-test). **A)** 2-days after SVCV-infection (n=3 replicas, 3
656 fish pooled per replica). **B)** 1-month SVCV-survivors (n=2 replicas, 3 fish pooled per replica). The total
657 number of fish was 15. **Red dashed horizontal line**, fold = 1. **Hatched white bars**, lymphoid organs.

658 **Hatched gray bars**, fin tissues.

659

660 **Figure 3. Upregulated (positive bars) and downregulated (negative bars) *crp1-7* transcript profiles**
661 **from lymphoid organs from *rag1*^{-/-} mutants before and after SVCV infection**
662 Differential expression folds and standard deviations were calculated by the formula, fluorescence of each
663 gene from *rag1*^{-/-} mutant fish / mean fluorescence of each gene from *rag1*^{+/+} fish (white bars) and
664 fluorescence of each gene from SVCV-infected *rag1*^{-/-} mutants / mean fluorescence of each gene from *rag1*^{-/-}
665 mutant fish (hatched gray bars). The upregulated and downregulated results were represented as the
666 duplicated representation explained in Figure 1. Raw and normalized data were deposited in GEO's bank at
667 GEO's GSE54096 (Garcia-Valtanen et al., 2017). *, folds significatively > 1.5 (+, positive upregulated values)
668 and < 0.66 (-, negative downregulated values) at p < 0.05 (Student t-test). **Red dashed horizontal lines**, 1.5-
669 and 0.66-fold thresholds. **White bars**, *rag1*^{-/-} versus *rag1*^{+/+} genotypes, n=2 replicas each, 3 fish pooled per
670 replica (*rag1*^{-/-} vs *rag1*^{+/+}). **Hatched gray bars**, 2-day SVCV-infected *rag1*^{-/-} phenotype versus 2-day mock-
671 infected *rag1*^{-/-} genotype, n=2 replicas each, 3 fish pooled per replica (+*rag1*^{-/-} vs *rag1*^{-/-}).

672

673 **Figure 4. Differential expression of CRP1-7 UNIPROT accession numbers in blood plasma from**
674 **SVCV-infected zebrafish.** Plasma was harvested from zebrafish infected with SVCV at different time points
675 (0, 24, 48 and 120 h). For the calculations, 3 biological replicas were analyzed per time point. Each replica
676 consisted in pools of 3 plasma (total number of fish = 36). Pooled plasma proteins for each replica were
677 digested with trypsin, the resulting peptides separated by LC and analysed in a Triple-TOF (LC-MS/MS)
678 apparatus. Table S2 shows that there were 1-5 UNIPROT accession numbers identified for each of the CRP1-
679 7 isoforms. After emPAI normalization, differential expression folds were calculated by the formula, emPAI
680 values of each UNIPROT accession number / emPAI mean value of the corresponding UNIPROT accession
681 number at time 0. **Open circles**, folds of each of the UNIPROT accession numbers detected in the 3 replicas
682 per time point. *, folds significatively > 1 at p < 0.05 (Student t-test). **Red dashed horizontal line**, 1-fold
683 threshold. CRP6 was not identified by any of the peptides obtained.

684

685 **Figure 5. Neutralization of SVCV in pMCV1.4-*crp1-7* plasmid-transfected EPC cells (A) or in CRP1-
686 7-enriched supernatant-treated EPC cells (B).**

687 **A) EPC cell monolayers transfected with pMCV1.4-*crp1-7* plasmids.** Cells were transfected with
688 pMCV1.4-*crp1-7* plasmids and incubated for 3 days before SVCV infection (3-day exposure to *crp1-7*). **B)**
689 **EPC cell monolayers treated with CRP1-7-enriched supernatants.** Cells were treated with CRP1-7-
690 enriched supernatants (obtained from pMCV1.4-*crp1-7* transfected EPC cells) during 24 h before SVCV
691 infection (1-day exposure to CRP1-7). To infect with SVCV, the transfected/treated cell monolayers were
692 incubated during 2 h with SVCV, washed and incubated during 24 h. The number of SVCV infected EPC
693 cells were then determined by ffu assays (n=2 experiments) or flow cytometry (n=2). Results from the 2
694 methods were pooled to calculate means and standard deviations (n=4). The results were expressed as
695 neutralization percentages calculated by the formula, 100 - (number of SVCV infected cells in transfected or
696 treated cells / number of SVCV infected cells in non-transfected or non-treated cells). *, statistically higher

697 than neutralization levels obtained from cells transfected with pMCV1.4 (no CRP-coding plasmid, *nccp*) or
698 treated with the corresponding supernatants (NCCP) at $p < 0.05$ (Student t-test).

699

700 **Figure 6. Study of the larvae from injected one-cell stage zebrafish embryos: injection of pMCV1.4-**
701 ***crp2-5* and survival after infection with SVCV (A), and injection of pMCV1.4-*il6* and induction of**
702 ***crp1-7* transcripts (B)**

703 A) Five groups of 30 one-cell stage embryo per group (total number =150) were intraperitoneally
704 microinjected with 2 nl of phosphate buffered saline (PBS) containing 150 pg of pMCV1.4 plasmids coding
705 for green fluorescent protein (GFP) or CRP2-5. Three days later, 12 hatched larvae per group were
706 microinjected into the duct of Cuvier to induce a systemic infection with 10^4 pfu of SVCV resulting in 64.5
707 % mortality for pMCV1.4-*gfp* injection after 7 days. Kaplan-Meier cumulative survival curves were
708 analyzed for statistical significance with a log-Rank (Mantel-Cox) test (Mantel, 1966) as described before
709 (Pereiro et al., 2017). *, Significative differences between survival of fish injected with pMCV1.4-*crps* and
710 those injected with pMCV1.4-*gfp* at the $p < 0.05$ level. **Black dotted line**, pMCV1.4-*gfp*. **Red line**, pMCV1.4-
711 *crp5*. **Black line**, pMCV1.4-*crp2*. **Blue line**, pMCV1.4-*crp3*. **Green line**, pMCV1.4-*crp4*. B) One-cell
712 stage embryos were intraperitoneally microinjected with 2 nl of PBS containing 150 pg of pMCV1.4 or
713 pMCV1.4-*il6* plasmids. Three-days later the corresponding larvae were pooled (n = 4 groups of 3 pooled fish
714 per group, total number of larvae per group = 12), RNA extracted and *crp1-7* transcript levels estimated by
715 RTqPCR using the primers described in Table S1. Results were expressed relative to *ef1a* as calculated by
716 the formula, $100 \times (\text{crp1-7 expression per group} / \text{ef1a expression per group})$. Means and standard deviations
717 were represented. *, statistically higher than the mortality levels obtained after transfection with the
718 pMCV1.4 plasmid at $p < 0.05$ (Student t-test). **Open bars**, injected with pMCV1.4. **Hatched bars**, injected
719 with pMCV1.4-*il6*.

720

721

722

861 **5. References**

- Adinolfi L. E., Zampino R., Restivo L., Lonardo A., Guerrera B., Marrone A., Nascimbeni F., Florio A. and Loria P. (2014) Chronic hepatitis C virus infection and atherosclerosis: clinical impact and mechanisms. *World J Gastroenterol* **20**, 3410-7.
- Ahne W., Bjorklund H. V., Essbauer S., Fijan N., Kurath G. and Winton J. R. (2002) Spring viremia of carp (SVC). *Diseases of Aquatic Organisms* **52**, 261-272.
- Ashraf U., Lu Y., Lin L., Yuan J., Wang M. and Liu X. (2016) The spring viremia of carp virus: recent advances. *J Gen Virol*.
- Ballesteros N. A., Saint-Jean S. S., Encinas P. A., Perez-Prieto S. I. and Coll J. M. (2012) Oral immunization of rainbow trout to infectious pancreatic necrosis virus (Ipnv) induces different immune gene expression profiles in head kidney and pyloric ceca. *Fish Shellfish Immunol* **33**, 174-85.
- Bello M., Falco A., Medina R., Encinar J. A., Novoa B., Perez L., Estepa A. and Coll J. (2017) Structure and functionalities of the human c-reactive protein compared to the zebrafish multigene family of c-reactive-like proteins. *Developmental & Comparative Immunology* **69**, 33-40.
- Boshra H., Li J. and Sunyer J. O. (2006) Recent advances on the complement system of teleost fish. *Fish Shellfish Immunol* **20**, 239-62.
- Braig D., Nero T. L., Koch H. G., Kaiser B., Wang X., Thiele J. R., Morton C. J., Zeller J., Kiefer J., Potempa L. A., Mellett N. A., Miles L. A., Du X. J., Meikle P. J., Huber-Lang M., Stark G. B., Parker M. W., Peter K. and Eisenhardt S. U. (2017) Transitional changes in the CRP structure lead to the exposure of proinflammatory binding sites. *Nat Commun* **8**, 14188.
- Chen R., Qi J., Yuan H., Wu Y., Hu W. and Xia C. (2015) Crystal structures for short-chain pentraxin from zebrafish demonstrate a cyclic trimer with new recognition and effector faces. *J Struct Biol* **189**, 259-68.
- Chinchilla B., Encinas P., Estepa A., Coll J. M. and Gomez-Casado E. (2013a) Optimization of fixed-permeabilized cell monolayers for high throughput micro-neutralizing antibody assays: Application to the zebrafish / viral haemorrhagic septicemia virus (VHSV) model. *Journal Virological Methods* **193**, 627-632.
- Chinchilla B., Gomez-Casado E., Encinas P., Falco A., Estepa A. and Coll J. (2013b) In vitro neutralization of viral haemorrhagic septicemia virus (VHSV) by plasma from immunized zebrafish *Zebrafish* **10**, 43-51.
- Deng Q. and Huttenlocher A. (2012) Leukocyte migration from a fish eye's view. *J Cell Sci* **125**, 3949-56.
- Du Clos T. W. and Mold C. (2011) Pentraxins (CRP, SAP) in the process of complement activation and clearance of apoptotic bodies through Fc gamma receptors. *Curr Opin Organ Transplant* **16**, 15-20.
- Eisenhardt S. U., Habersberger J., Murphy A., Chen Y. C., Woppard K. J., Bassler N., Qian H., von Zur Muhlen C., Hagemeyer C. E., Ahrens I., Chin-Dusting J., Bobik A. and Peter K. (2009a) Dissociation of pentameric to monomeric C-reactive protein on activated platelets localizes inflammation to atherosclerotic plaques. *Circ Res* **105**, 128-37.
- Eisenhardt S. U., Habersberger J. and Peter K. (2009b) Monomeric C-reactive protein generation on activated platelets: the missing link between inflammation and atherothrombotic risk. *Trends Cardiovasc Med* **19**, 232-7.
- El Kebir D., Zhang Y., Potempa L. A., Wu Y., Fournier A. and Filep J. G. (2011) C-reactive protein-derived peptide 201-206 inhibits neutrophil adhesion to endothelial cells and platelets through CD32. *J Leukoc Biol* **90**, 1167-75.
- Encinas P., Garcia-Valtanen P., Chinchilla B., Gomez-Casado E., Estepa A. and Coll J. (2013) Identification of multipath genes differentially expressed in pathway-targeted microarrays in zebrafish infected and surviving spring viremia carp virus (SVCV) suggest preventive drug candidates. *PLoS One* **8**, e73553.

- Encinas P., Rodriguez-Milla M. A., Novoa B., Estepa A., Figueras A. and Coll J. M. (2010) Zebrafish fin immune responses during high mortality infections with viral haemorrhagic septicemia rhabdovirus. A proteomic and transcriptomic approach. *BMC Genomics* **11**, 518-534.
- Enocsson H., Sjowall C., Skogh T., Eloranta M. L., Ronnblom L. and Wettero J. (2009) Interferon-alpha mediates suppression of C-reactive protein: explanation for muted C-reactive protein response in lupus flares? *Arthritis Rheum* **60**, 3755-60.
- Estepa A. and Coll J. (2015a) Innate Multigene Family Memories Are Implicated in the Viral-Survivor Zebrafish Phenotype. *PLoS One* **10**, e0135483.
- Estepa A. and Coll J. M. (1996) Pepscan mapping and fusion related properties of the major phosphatidylserine-binding domain of the glycoprotein of viral hemorrhagic septicemia virus, a salmonid rhabdovirus. *Virology* **216**, 60-70.
- Estepa A. and Coll J. M. (2015b) Innate multigene family memories are implicated in the viral-survivor zebrafish phenotype. *Plos One* **10**, e0135483.
- Estepa A. M., Rocha A. I., Mas V., Perez L., Encinar J. A., Nunez E., Fernandez A., Ros J. M. G., Gavilanes F. and Coll J. M. (2001) A protein G fragment from the Salmonid viral hemorrhagic septicemia rhabdovirus induces cell-to-cell fusion and membrane phosphatidylserine translocation at low pH. *Journal of Biological Chemistry* **276**, 46268-46275.
- Falco A., Cartwright J. R., Wiegeritjes G. F. and Hoole D. (2012) Molecular characterization and expression analysis of two new C-reactive protein genes from common carp (*Cyprinus carpio*). *Dev Comp Immunol* **37**, 127-38.
- Falco A., Chico V., Marroqui L., Perez L., Coll J. M. and Estepa A. (2008) Expression and antiviral activity of a beta-defensin-like peptide identified in the rainbow trout (*Oncorhynchus mykiss*) EST sequences. *Mol Immunol* **45**, 757-65.
- Fijan N., Petrinec Z., Sulimanovic D. and Zwillenberg L. O. (1971) Isolation of the viral causative agent from the acute form of infectious dropsy of carp. *Veterinary Archives* **41**, 125-138.
- Garcia-Valtanen P., Martinez-Lopez A., Lopez-Munoz A., Bello-Perez M., Medina-Gali R. M., Ortega-Villaizan M. D., Varela M., Figueras A., Mulero V., Novoa B., Estepa A. and Coll J. (2017) Zebra Fish Lacking Adaptive Immunity Acquire an Antiviral Alert State Characterized by Upregulated Gene Expression of Apoptosis, Multigene Families, and Interferon-Related Genes. *Front Immunol* **8**, 121.
- Genge C. E., Lin E., Lee L., Sheng X., Rayani K., Gunawan M., Stevens C. M., Li A. Y., Talab S. S., Claydon T. W., Hove-Madsen L. and Tibbits G. F. (2016) The Zebrafish Heart as a Model of Mammalian Cardiac Function. *Rev Physiol Biochem Pharmacol* **171**, 99-136.
- Harmache A., Leberre M., Droineau S., Giovannini M. and Bremont M. (2006) Bioluminescence Imaging of Live Infected Salmonids Reveals that the Fin Bases Are the Major Portal of Entry for Novirhabdovirus. *Journal Virology* **103**, 3655-3659.
- Huang W. C., Hsieh Y. S., Chen I. H., Wang C. H., Chang H. W., Yang C. C., Ku T. H., Yeh S. R. and Chuang Y. J. (2010) Combined use of MS-222 (tricaine) and isoflurane extends anesthesia time and minimizes cardiac rhythm side effects in adult zebrafish. *Zebrafish* **7**, 297-304.
- ICTV. (2015) Implementation of taxon-wide non-Latinized binomial species names in the family *Rhabdoviridae*. *Rhabdoviridae Study Group*, 9.
- Ishihama Y., Oda Y., Tabata T., Sato T., Nagasu T., Rappaport J. and Mann M. (2005) Exponentially modified protein abundance index (emPAI) for estimation of absolute protein amount in proteomics by the number of sequenced peptides per protein. *Mol Cell Proteomics* **4**, 1265-72.
- Kindmark C. O. (1971) Stimulating effect of C-reactive protein on phagocytosis of various species of pathogenic bacteria. *Clin Exp Immunol* **8**, 941-8.
- LeBerre M., De Kinkelin P. and Metzger A. (1977) Identification sérologique des rhabdovirus des salmonidés. *Bulletin Office International Epizooties* **87**, 391-393.
- Li H. Y., Wang J., Meng F., Jia Z. K., Su Y., Bai Q. F., Lv L. L., Ma F. R., Potempa L. A., Yan Y. B., Ji S. R. and Wu Y. (2016) An Intrinsically Disordered Motif Mediates Diverse Actions of Monomeric C-reactive Protein. *J Biol Chem* **291**, 8795-804.

- Livak K. L. and Schmittgen.T.D. (2001) Analysis of Relative Gene Expression Data Using Real-Time Quantitative PCR and the 2 - DDCT Method. *Methods* **25**, 402-408.
- Lopez-Munoz A., Roca F. J., Sepulcre M. P., Meseguer J. and Mulero V. (2010) Zebrafish larvae are unable to mount a protective antiviral response against waterborne infection by spring viremia of carp virus. *Developmental Comparative Immunology* **34**, 546-52.
- Lu F., Langenbacher A. D. and Chen J. N. (2016) Transcriptional Regulation of Heart Development in Zebrafish. *J Cardiovasc Dev Dis* **3**.
- Lu J., Marjon K. D., Mold C., Du Clos T. W. and Sun P. D. (2012) Pentraxins and Fc receptors. *Immunol Rev* **250**, 230-8.
- Mantel N. (1966) Evaluation of survival data and two new rank order statistics arising in its consideration. *Cancer Chemother Rep* **50**, 163-70.
- McKibben R. A., Haberlen S. A., Post W. S., Brown T. T., Budoff M., Witt M. D., Kingsley L. A., Palella F. J., Jr., Thio C. L. and Seaberg E. C. (2016) A Cross-sectional Study of the Association Between Chronic Hepatitis C Virus Infection and Subclinical Coronary Atherosclerosis Among Participants in the Multicenter AIDS Cohort Study. *J Infect Dis* **213**, 257-65.
- Novoa B., Romero A., Mulero V., Rodriguez I., Fernandez I. and Figueras A. (2006) Zebrafish (*Danio rerio*) as a model for the study of vaccination against viral haemorrhagic septicemia virus (VHSV). *Vaccine* **24**, 5806-5816.
- Paludan S. R. (2001) Requirements for the induction of interleukin-6 by herpes simplex virus-infected leukocytes. *J Virol* **75**, 8008-15.
- Pereiro P., Forn-Cuni G., Dios S., Coll J., Figueras A. and Novoa B. (2017) Interferon-independent antiviral activity of 25-hydroxycholesterol in a teleost fish. *Antiviral Res* **145**, 146-159.
- Pionnier N., Adamek M., Miest J. J., Harris S. J., Matras M., Rakus K. L., Irnazarow I. and Hoole D. (2014) C-reactive protein and complement as acute phase reactants in common carp *Cyprinus carpio* during CyHV-3 infection. *Dis Aquat Organ* **109**, 187-99.
- Pitto L., Chiavacci E., Burchielli S., Dolfi L., Zozzini E. T., Priami C., Cellerino A. and Cremisi F. (2011) Zebrafish as Model System for Studying the Transcription Factor/miRNA Regulative Network in Brain and Heart Development. *Journal of the American Association for Laboratory Animal Science* **50**, 743-743.
- Potempa L. A., Yao Z. Y., Ji S. R., Filep J. G. and Wu Y. (2015) Solubilization and purification of recombinant modified C-reactive protein from inclusion bodies using reversible anhydride modification. *Biophys Rep* **1**, 18-33.
- Rocha A., Ruiz S. and Coll J. M. (2005) Improvement of transfection efficiency of epithelioma papulosum cyprini carp cells by modification of their cell cycle and using an optimal promoter. *Marine Biotechnology* **6**, 401-410.
- Sanders G. E., Batts W. N. and Winton J. R. (2003) Susceptibility of zebrafish (*Danio rerio*) to a model pathogen, spring viremia of carp virus. *Comp Med* **53**, 514-521.
- Shah S., Ma Y., Scherzer R., Huhn G., French A. L., Plankey M., Peters M. G., Grunfeld C. and Tien P. C. (2015) Association of HIV, hepatitis C virus and liver fibrosis severity with interleukin-6 and C-reactive protein levels. *AIDS* **29**, 1325-33.
- Shephard E. G., Beer S. M., Anderson R., Strachan A. F., Nel A. E. and de Beer F. C. (1989) Generation of biologically active C-reactive protein peptides by a neutral protease on the membrane of phorbol myristate acetate-stimulated neutrophils. *J Immunol* **143**, 2974-81.
- Shrivastava A. K., Singh H. V., Raizada A. and Singh S. K. (2015) C-reactive protein, inflammation and coronary heart disease. *The Egyptian Heart Journal* **67**, 89-97.
- Sunyer J. O. (2013) Fishing for mammalian paradigms in the teleost immune system. *Nat Immunol* **14**, 320-6.
- Sunyer J. O., Zarkadis I. K. and Lambris J. D. (1998) Complement diversity: a mechanism for generating immune diversity? *Immunol Today* **19**, 519-23.
- Varela M., Figueras A. and Novoa B. (2016) Modelling viral infections using zebrafish: Innate immune response and antiviral research. *Antiviral Res* **139**, 59-68.

- Varela M., Romero A., Dios S., van der Vaart M., Figueras A., Meijer A. H. and Novoa B. (2014) Cellular visualization of macrophage pyroptosis and interleukin-1beta release in a viral hemorrhagic infection in zebrafish larvae. *J Virol* **88**, 12026-40.
- Vilahur G. and Badimon L. (2015) Biological actions of pentraxins. *Vascul Pharmacol* **73**, 38-44.
- Voulgaris T. and Sevastianos V. A. (2016) Atherosclerosis as Extrahepatic Manifestation of Chronic Infection with Hepatitis C Virus. *Hepat Res Treat* **2016**, 7629318.
- Wang J., Wang Q., Han T., Li Y. K., Zhu S. L., Ao F., Feng J., Jing M. Z., Wang L., Ye L. B. and Zhu Y. (2015) Soluble interleukin-6 receptor is elevated during influenza A virus infection and mediates the IL-6 and IL-32 inflammatory cytokine burst. *Cell Mol Immunol* **12**, 633-44.
- Wang M. Y., Ji S. R., Bai C. J., El Kebir D., Li H. Y., Shi J. M., Zhu W., Costantino S., Zhou H. H., Potempa L. A., Zhao J., Filep J. G. and Wu Y. (2011) A redox switch in C-reactive protein modulates activation of endothelial cells. *FASEB J* **25**, 3186-96.
- Wu Y., Potempa L. A., El Kebir D. and Filep J. G. (2015) C-reactive protein and inflammation: conformational changes affect function. *Biol Chem* **396**, 1181-97.
- Wu Y. P., Sun D. D., Wang Y., Liu W. and Yang J. (2016) Herpes Simplex Virus Type 1 and Type 2 Infection Increases Atherosclerosis Risk: Evidence Based on a Meta-Analysis. *Biomed Res Int* **2016**, 2630865.
- Xia C., Liu Y., Chen Z. and Zheng M. (2015) Involvement of Interleukin 6 in Hepatitis B Viral Infection. *Cell Physiol Biochem* **37**, 677-86.
- Yavin E. J. and Fridkin M. (1998) Peptides derived from human C-reactive protein inhibit the enzymatic activities of human leukocyte elastase and cathepsin G: use of overlapping peptide sequences to identify a unique inhibitor. *J Pept Res* **51**, 282-9.
- Zhang Y. A., Salinas I., Li J., Parra D., Bjork S., Xu Z., LaPatra S. E., Bartholomew J. and Sunyer J. O. (2010) IgT, a primitive immunoglobulin class specialized in mucosal immunity. *Nat Immunol* **11**, 827-35.

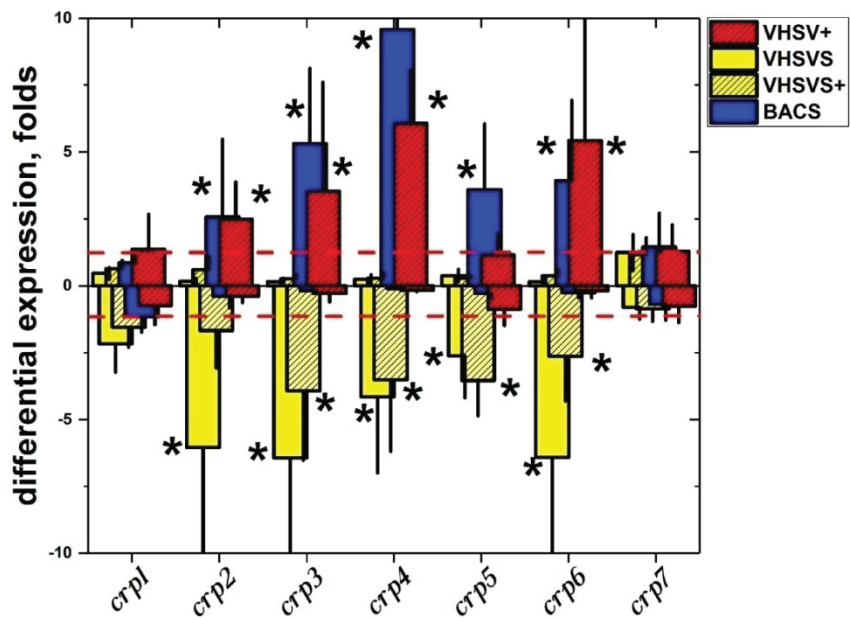


Figure 1.

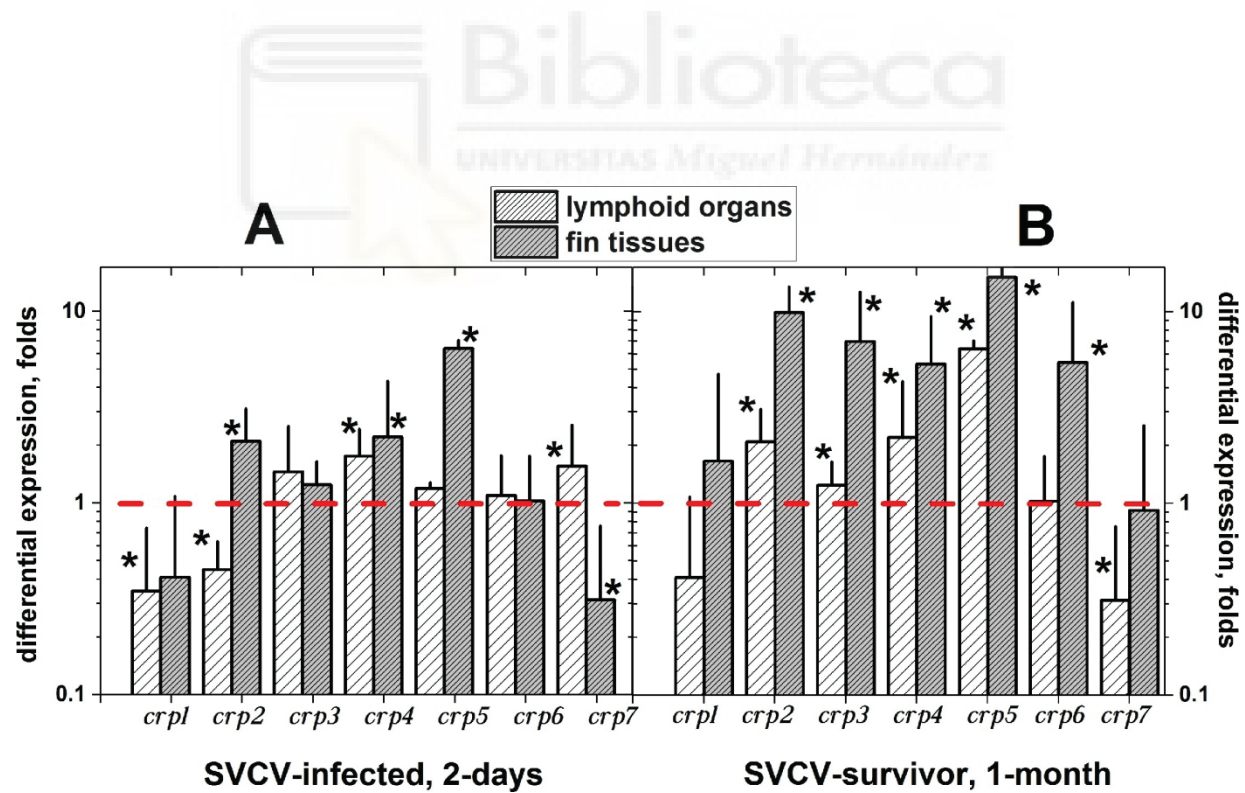


Figure 2.

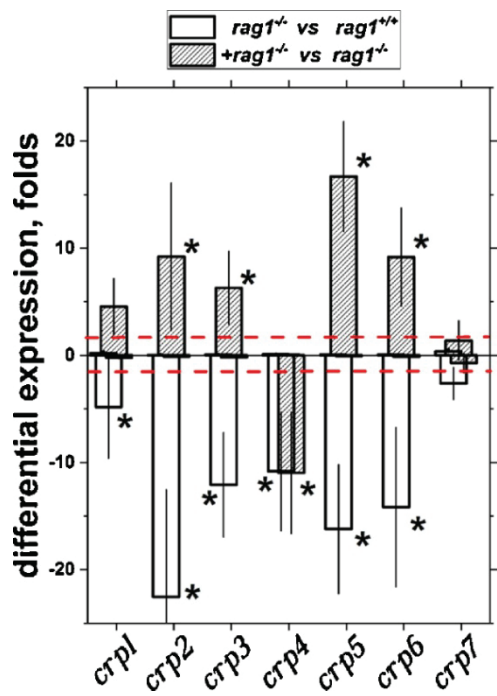


Figure 3.

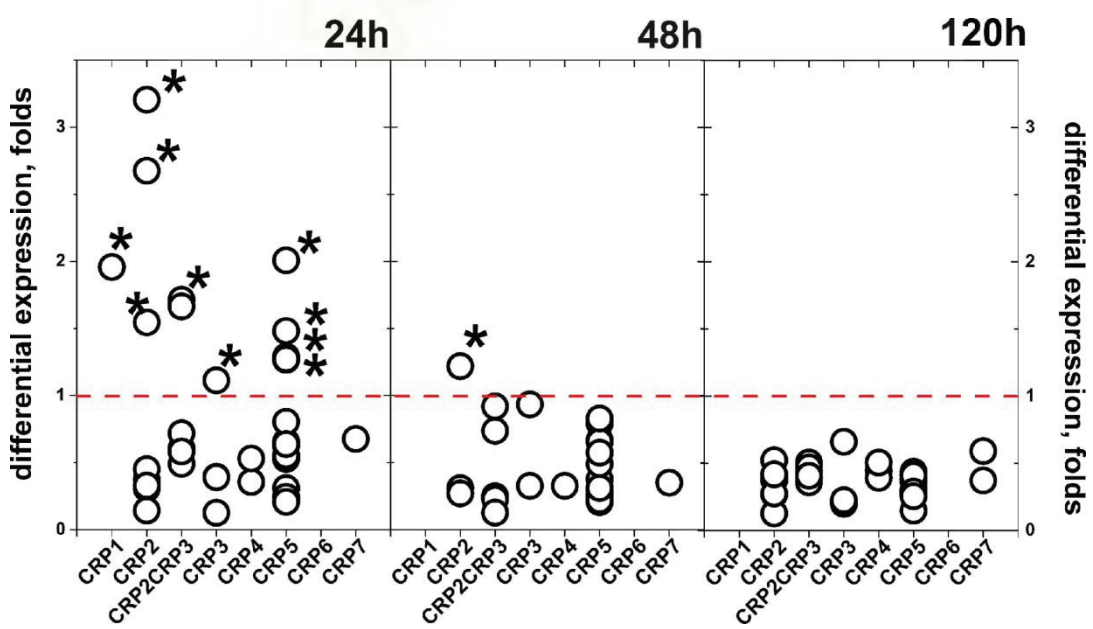


Figure 4.

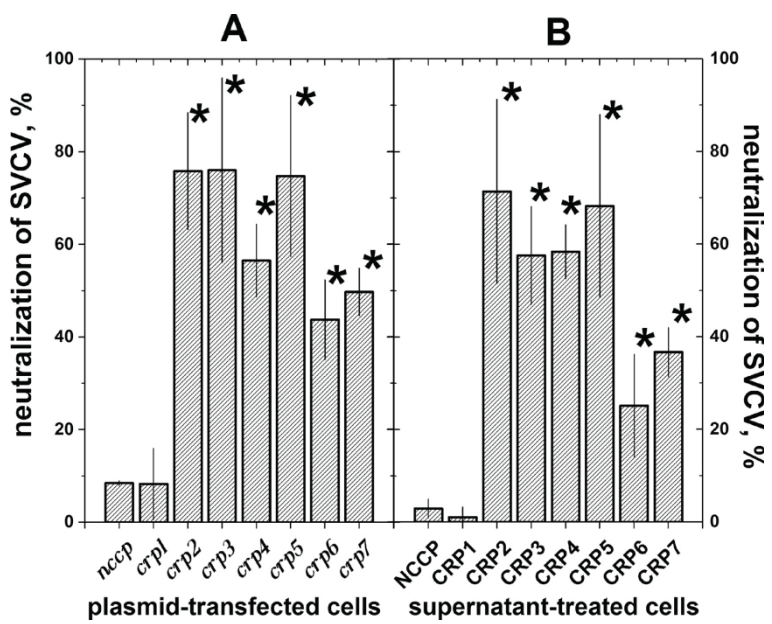


Figure 5.

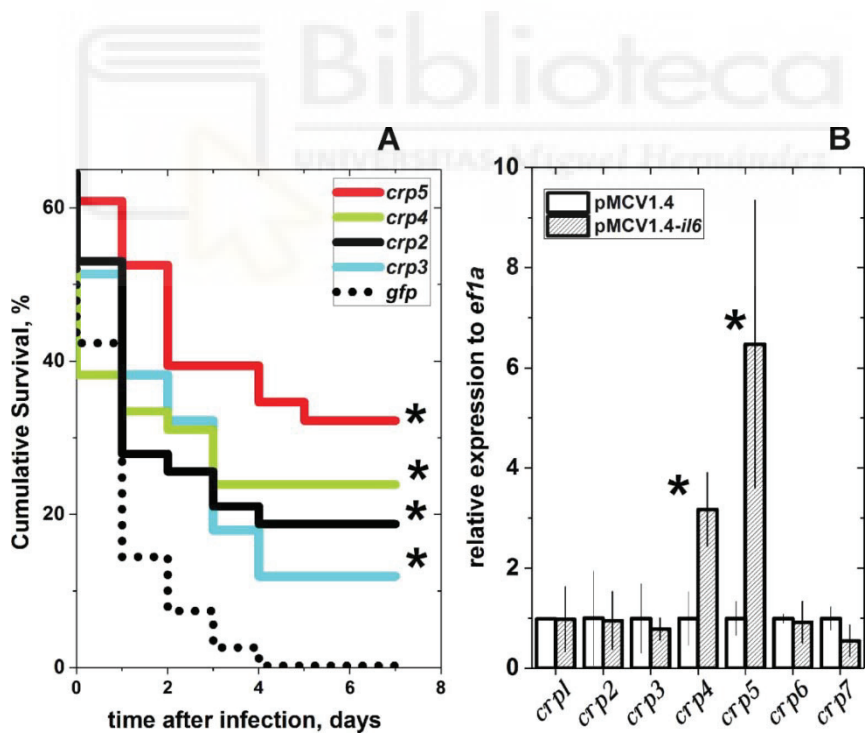
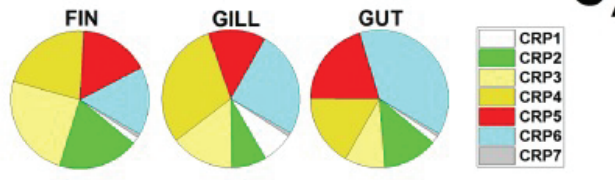


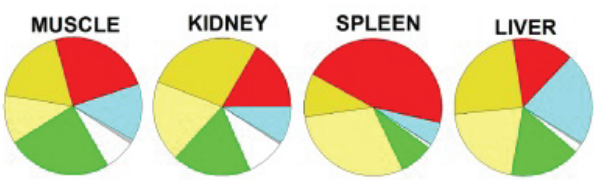
Figure 6.

A)Transcript levels of *crpI-7* in external tissues of healthy adult zebrafish

<i>crp</i>	Fin	±sd	Gill	±sd	Gut	±sd
<i>crp1</i>	2.7	1.5	36.9	3.1	3.0	1.4
<i>crp2</i>	29.5	9.4	40.2	12.6	21.6	10.1
<i>crp3</i>	38.5	17.9	73.7	30.1	15.9	1.2
<i>crp4</i>	33.7	18.0	*149.3	47.6	28.5	15.8
<i>crp5</i>	25.8	11.3	67.1	30.0	34.3	34.9
<i>crp6</i>	25.0	12.8	*124.0	65.4	64.2	26.4
<i>crp7</i>	1.3	1.0	4.5	2.0	1.3	0.7

C)**B)**Transcript levels of *crpI-7* in internal organs of healthy adult zebrafish

<i>crp</i>	Muscle	±sd	Head		Spleen	±sd	Liver	±sd
			kidney	±sd				
<i>crp1</i>	17.8	10.2	32.0	20.4	5.6	4.3	4.22	3.0
<i>crp2</i>	56.2	20.6	63.4	26.5	50.3	14.3	34.06	7.3
<i>crp3</i>	26.3	18.4	66.3	31.4	*191.8	109.0	42.74	7.4
<i>crp4</i>	42.2	21.9	95.1	16.9	65.9	12.4	50.01	21.0
<i>crp5</i>	55.3	57.4	57.4	46.7	*293.2	89.8	29.88	5.9
<i>crp6</i>	30.5	2.9	30.1	18.1	34.4	22.1	44.68	1.5
<i>crp7</i>	2.3	1.3	1.7	1.5	0.6	0.5	1.04	0.7

**Table 1.**

PUBLICACIÓN 3

TÍTULO: Hydroxycholesterol binds and enhances the anti-viral activities of zebrafish monomeric c-reactive protein isoforms.

COAUTORES: Melissa Belló Pérez, Alberto Falcó Graciá, Beatriz Novoa García, Luis Perez García-Estañ, Julio Coll Morales.

REVISTA: PLoS ONE

doi: [10.1371/journal.pone.0201509](https://doi.org/10.1371/journal.pone.0201509)

RESEARCH ARTICLE

Hydroxycholesterol binds and enhances the anti-viral activities of zebrafish monomeric c-reactive protein isoforms

Melissa Bello-Perez¹, Alberto Falco¹, Beatriz Novoa², Luis Perez¹✉, Julio Coll^{1,3*}

1 Instituto de Biología Molecular y Celular, Universidad Miguel Hernández (IBMC-UMH), Elche, Spain,

2 Institute of Marine Research (IIM), CSIC, Vigo, Spain, **3** Department of Biotechnology, Instituto Nacional Investigaciones y Tecnologías Agrarias y Alimentarias, INIA, Madrid, Spain

* These authors contributed equally to this work.

* juliocoll@inia.es



OPEN ACCESS

Citation: Bello-Perez M, Falco A, Novoa B, Perez L, Coll J (2019) Hydroxycholesterol binds and enhances the anti-viral activities of zebrafish monomeric c-reactive protein isoforms. PLoS ONE 14(1): e0201509. <https://doi.org/10.1371/journal.pone.0201509>

Editor: Keivan Zandi, Emory University, UNITED STATES

Received: July 13, 2018

Accepted: December 28, 2018

Published: January 17, 2019

Copyright: © 2019 Bello-Perez et al. This is an open access article distributed under the terms of the [Creative Commons Attribution License](#), which permits unrestricted use, distribution, and reproduction in any medium, provided the original author and source are credited.

Data Availability Statement: All relevant data are within the manuscript and its Supporting Information files.

Funding: Melissa Bello-Perez was financed by the Generalidad Valenciana, fellowship ACIF/2016. This work was supported by CICYT projects AGL2014-51773-C3-R and BIO2017-82851 of the Ministerio de Economía, Industria y Competitividad of Spain. The funders had no role in study design, data collection and analysis, decision to publish, or preparation of the manuscript.

Abstract

C-reactive proteins (CRPs) are among the faster acute-phase inflammation-responses proteins encoded by one gene (*hcrp*) in humans and seven genes (*crp1-7*) in zebrafish (*Danio rerio*) with importance in bacterial and viral infections. In this study, we described novel preferential bindings of 25-hydroxycholesterol (25HOCh) to CRP1-7 compared with other lipids and explored the antiviral effects of both 25HOCh and CRP1-7 against spring viremia carp virus (SVCV) infection in zebrafish. Both *in silico* and *in vitro* results confirmed the antiviral effect of 25HOCh and CRP1-7 interactions, thereby showing that the crosstalk between them differed among the zebrafish isoforms. The presence of oxidized cholesterols in human atherosclerotic plaques amplifies the importance that similar interactions may occur for vascular and/or neurodegenerative diseases during viral infections. In this context, the zebrafish model offers a genetic tool to further investigate these interactions.

Introduction

Previous studies have shown that, in contrast to a single gene-encoding human c-reactive protein (hCRP) [1], seven genes encode zebrafish (*Danio rerio*) CRP1-7 isoforms [2]. CRP molecules are present from invertebrates to vertebrates. In particular, hCRP is a crucial clinical biomarker for inflammation and most recently has been associated with relevant diseases such as those caused by cardiovascular and neurodegenerative disorders [3–5]. All circulating CRP molecules are planar oligomers of ~ 25 kDa monomers. While hCRP is pentameric (p-hCRP), zebrafish CRP5 crystallizes as trimers [6]. However, it is not yet known whether other CRP1-7 isoforms are trimeric and what are their prevalent physiological conformation(s), although some CRP1-7 isoform-dependent heterogeneous biological properties have been most recently described [6,7].

Planar p-hCRP molecules show opposite lipid-recognition and functional-effector faces [5]. It is well known that the recognition face mainly binds phosphocholine heads exposed at the surface of prokaryotic/eukaryotic membranes in a Ca⁺⁺ [8,9]- and phospholipase A₂ [10]-

Competing interests: The authors have declared that no competing interests exist.

Abbreviations: BSA, bovine serum albumin; CRP, C-reactive protein; Ig, immunoglobulin; kDa, kilo Daltons; MW, molecular weight; PAGE, polyacrylamide gel electrophoresis; PBS, phosphate-buffered saline; pfu, plaque forming units; SDS, sodium dodecyl sulfate; SVCV, spring viremia carp virus; VHSV, Viral haemorrhagic septicemia virus; EPC, *Epitheliooma papulosum cyprinid* cell line.

dependent manner when generated in damaged tissues [5]. Triggered by CRP- Ca^{++} -phosphocholine complexes, the functional-effector face binds C1q to activate the classical complement pathway, immunoglobulin Fc receptors to activate phagocytosis [11,12] and other ligands to activate multiple cellular functions [10]. To accomplish these various functions, hCRP shows at least 4 different conformations [5,13]: i) inactive serum-circulating p-hCRP, which is present in low concentrations in healthy humans, increasing 100- to 1000-fold after inflammation; ii) pro-inflammatory tissue-associated p-hCRP* [4]; iii) pro-inflammatory tissue-associated monomeric hCRP (m-hCRP) with wider ligand capacities which include cholesterol (Ch) [14–16] and iv) disulfide-reduced m-hCRP that activates lymphoid and many other cellular types [5,16–18]. Despite the different oligomeric structures of p-hCRP and t-CRP5 [6], their protein hydrophobic profiles, two cysteine residues per monomer, Ca^{++} -binding amino acid sequences and location of phosphocholine (PC)-binding pockets are highly conserved [19]. On the other hand, previous transcriptomic studies on *crp1-7* genes have demonstrated differential transcript expression in zebrafish tissues [2], in survivors of viral infection [20] and in mutants defective in adaptive immunity [21]. Additionally, unexpected *crp1-7*/CRP1-7 isoform-dependent anti-viral *in vitro* and *in vivo* activities have been described. In most of the above mentioned situations, *crp2*/CRP2 and *crp5*/CRP5 transcripts/proteins were the most modulated compared with *crp1*/CRP1 and *crp7*/CRP7. These recent findings revealed novel anti-viral CRP1-7 direct or indirect activities in zebrafish that, to our knowledge, have not been described yet for any CRP, including hCRP. Some of the similar properties mentioned above suggest analogous biological functions for p-hCRP and CRP1-7 [7]; however, whether the CRP1-7 isoforms physiologically exist as different oligomeric structures, conformations and/or become specialized in different ligand-binding or biological functions remains largely unexplored.

Widely used as a general biomarker for bacterial infection and inflammation during decades, circulating p-hCRP has been found recently within atherosclerotic lesions and was proposed as a biomarker for cardiovascular diseases [22]. Additionally, the correlation between infections and cardiovascular heart diseases in humans has been demonstrated not only for bacteria but also for several viral infections [23–26]. Thus, although circulating levels of p-hCRP were initially discovered as increasing from ~10 to >500 mg/l during acute-phase responses to bacterial infections, intermediate concentrations of 10–50 mg/l were detected also during viral infections [27], suggesting possible anti-viral function(s). Nevertheless and despite p-hCRP being one of the most investigated risk biomarker molecules in the human cardiovascular field, and an important component of the anti-bacterial innate response [9], to our knowledge, there is no evidence that p-hCRP or m-hCRP possesses antiviral function. The functional significance of the CRP oligomer-monomer conversion (and *viceversa*) need to be further clarified to evaluate new chemotherapeutic targets [10,28]. Zebrafish may offer a good genetic model to explore such physiological phenomena.

Using *in silico* and *in vitro* studies, we focused on the lipid-docking/binding, anti-viral activities and oligomeric forms of the zebrafish CRP1-7 isoforms and some of their transcript variants. We found that i) Ca^{++} -independent docking/binding of CRP1-7 to Ch was higher than that to other lipids, ii) HOChs were a preferential target for CRP1-7, iii) HOChs enhanced the anti-viral direct or indirect effects by zebrafish CRP1-7 in an isoform-dependent manner, and iv) CRP2/CRP5 and numerous CRP5 transcript variants have a stronger tendency to fold as trimers than other CRP-7 molecules.

Materials and methods

In silico docking predictions between zebrafish CRP1-7 and lipids

AutoDock Vina [29] included in the PyRx program package [30] was used to predict the Gibbs free-energy of docking (ΔG) of $60 \times 60 \times 60 \text{ \AA}$ grids surrounding the CRP1-7 molecules.

When required for comparison with the experimental data, the output ΔG energies were converted to constant inhibition (K_i) values in molar concentrations (M), using the formula $K_i = \exp([\Delta G \times 1000] / [R \times T])$ ($R = 1.98$ cal/mol, and $T = 298^\circ\text{C}$)^[31]. The predicted structures were visualized in PyRx and/or PyMOL (<https://www.pymol.org/>).

Cell culture in EPC cell monolayers

Epithelioma papulosum cyprinid (EPC) cells from fathead minnow fish (*Pimephales promelas*) were obtained from the American Type Culture Collection (ATCC, Manassas, VA, USA; code number CRL-2872). EPC cell monolayers were grown at 26°C in a 5% CO_2 atmosphere in RPMI-1640 Dutch modified cell culture medium supplemented with 20 mM HEPES, 10% fetal bovine serum, FBS (Sigma, St. Louis, USA), 1 mM pyruvate, 2 mM glutamine, 50 $\mu\text{g}/\text{ml}$ of gentamicin (Gibco) and 2 $\mu\text{g}/\text{ml}$ of fungizone [21].

Preparation of spring viremia of carp virus (SVCV)

The isolate 56/70 of spring viremia carp virus (SVCV) from carp *C. carpio* [32], recently renamed *Carp sprivivirus* [33], was replicated in EPC cell monolayers at 26°C , in the cell culture media described above except for 2% FBS and the absence of the CO_2 atmosphere. Supernatants from SVCV-infected EPC cell monolayers were clarified by centrifugation at 4000 g for 30 min and kept at -80°C [21].

Estimation of the effects of methyl-beta-cyclodextrin (MBCD) on SVCV infectivity

EPC cell monolayers treated for 2 h with different concentrations (0–8 mM) of MBCD were incubated with SVCV for 24 h and then were assayed for fluorescent focus-forming units (ffu) (see later). The results were expressed as the percentage of SVCV infectivity calculated by the following formula: $100 \times (\text{ffu treated with MBCD} / \text{ffu nontreated with MBCD})$. To assay for viability, EPC cell monolayers treated with MBCD as above were incubated with 0.5 mg/ml of 3-(4,5-dimethylthiazol-2-yl)-2,5-diphenyltetrazolium bromide (MTT) in a Krebs–Hensleit–HEPES buffer (115 mM NaCl, 5 mM KCl, 1 mM KH_2PO_4 , 1.2 mM MgSO_4 , 2 mM CaCl_2 , and 25 mM HEPES at pH 7.4) for 3 h, the absorbance at 570 nm was measured, and the percentage of viability was calculated by the following formula: absorbance of MBCD treated cells / absorbance of untreated cells. Means and standard deviations ($n = 2$) were interpolated and smoothed using the cubic B-spline method in Origin Pro 2017 (Northampton, MA, USA).

Construction of recombinant pRSET-CRP1-7 for *E.coli* expression

The corresponding mRNA sequences of the CRP1-7 proteins [7] were used for the design, construction and expression in *E.coli*. All the corresponding synthetic DNA sequences were cloned into the pRSET adding poly-histidine tails (polyH) at their C-terminal ends (GeneArt, Regensburg, Germany). The purified plasmids were then transfected into *E.coli* BL21(DE3) and grown at 37°C . The resulting recombinant bacteria from the pRSET-*crp1-7* constructs were induced with IPTG at 25°C . Gradient 4–20% polyacrylamide gel electrophoresis (PAGE) and Western blotting were used to detect CRP1-7 expression.

Construction of recombinant rCRP1, rCRP2, rCRP5, rCRP7 for insect expression

The mRNA sequences of CRP1, CRP2, CRP5 and CRP7 described previously [7], were used for the design, construction and expression in insect cells (GenScript, Piscataway, NJ, USA).

Briefly, target DNA containing the gp67 signal peptide + CRP1-7 + Flag (DYKDDDK) + 6 x polyHis sequences (construct size of ~ 3 Kbp) were synthesized and subcloned into the pFastBac1TM baculovirus transfer vector (Invitrogen). The pFastBac1 recombinants were transfected into DH10 BacTM-competent *E. coli* cells and bacmids prepared from selected *E. coli* clones. Next, recombinant baculoviruses were generated in *Spodoptera frugiperda* (Sf9) insect cells. For that, Sf9 cells cultured in Grace's insect media (Gibco BRL) with 10% foetal bovine serum, 3% nonessential amino acids and 20 µg/ml gentamicin at 28°C [34] were cotransfected with bacmids and baculovirus using Cellfectin II. The supernatants containing the recombinant baculoviruses were obtained 72 h posttransfection with titers of ~ 10⁷ pfu/ml.

For rCRP expression and purification, 500 ml of Sf9 cell supernatants were harvested 72 h postinfection and were dialyzed against 50 mM Tris, pH 8.0, 500 mM NaCl. The rCRP-containing medium was incubated with Flag or Ni⁺⁺ columns equilibrated with 50 mM Tris, 500 mM NaCl, 5% glycerol, pH 8.0, eluted with 200 µg/ml of the Flag peptide or 150 mM imidazole, dialyzed against equilibration buffer and kept at -20°C until ready for use. Purified rCRPs were loaded onto 8–20% SDS-polyacrylamide gels (BioRad), electrophoresed, and transferred to nitrocellulose membranes (Schleicher & Schuell) to detect specific tag epitopes. The membranes were blocked with phosphate buffered saline containing 0.05% Tween 20 and 4% skim milk, and then were incubated with anti-poly-H monoclonal antibody MAb (Sigma) for 1 h, followed by incubation with anti-mouse horseradish peroxidase-conjugated immunoglobulins (Sigma) and visualization with diaminobenzidine (DAB). The protein concentrations were determined using the bicinchoninic acid (BCA) method [35] and were confirmed by PAGE with BSA as the standard.

Production of rabbit antibodies to recognize zebrafish CRP1-7 isoforms

To detect CRP1-7 isoforms in lipid-binding assays and after PAGE by Western blotting, anti-CRP1-7 rabbit antibodies (GenScript, Piscataway, NJ, USA) were raised against 3 of the longest more conserved amino acid stretches such as peptide p1 (¹⁸SYVKLSPEKPLSLSAFTLC), peptide p2 (¹⁸⁹DWDTIEYDVTGN) and peptide p3 (¹²⁹RPGGTVLLGQDPDSYYVGSC). All p1, p2 and p3 were located at the CRP1-7 surface, as shown by PyMOL modelling of trimeric CRP5 ± Ca⁺⁺ (4PBP.pdb and 4PBO.pdb, respectively) [6] (data not shown). To reduce assay backgrounds, the anti-peptide antibodies were purified by affinity chromatography against the corresponding synthetic peptides coupled to CNBr-activated Sepharose. Only the affinity-purified anti-p3 antibodies bound purified insect-made rCRP2, rCRP5 and rCRP7 on Western blots under denaturing and nondenaturing conditions and recognized EPC cells transfected with pMCV1.4-*crp2-7* by immunofluorescence (data not shown).

Binding of CRP1-7 to solid-phase lipids

The binding of CRP1-7 to lipids was assayed in solid-phase 96-well plates (Nunc, Maxisorb) by modifying previously described methods [36]. The wells were coated to dryness with several concentrations of ethanol-dissolved lipids and were kept dried until ready for use. To assay for CRP1-7 binding, the plates were first washed with 0.1 M sodium borate, 1 mM CaCl₂ buffer, pH 8, and then 0.5 µg/well of rCRPs or 10-fold diluted ssCRP1-7 added in 50 µl of the same buffer and incubated for 60 min. After washing, bound CRP1-7 were detected with rabbit anti-p3 and peroxidase-labelled goat anti-rabbit IgG. Peroxidase was finally assayed with OPD as described previously [37,38]. The resulting data were interpolated and smoothed by the cubic B-spline method using Origin Pro 2017 (Northampton, MA, USA).

Binding of CRP5 pepscan peptides to solid-phase 25HOCh and docking predictions

A series of 15-mer peptides overlapping 5 amino acids of the CRP5 sequence was chemically synthesized by adding an amino-terminal biotin molecule (Chiron Mimotopes, Victoria, Australia). The synthetic pepscan peptides were diluted in distilled water to 4 mg/ml and were kept frozen until use.

To perform the binding experiments, 2 µg of 25HOCh was dissolved in 50 µl of ethanol and was dried into polystyrene wells of 96-well Nunc Maxisorb plates. After washing the plates with 0.1 M borate buffer pH 8, 1 mM CaCl₂, pepscan peptides (0.05 µg in 50 µl) were added to each of the wells and were incubated for 60 min. After washing, 1000-fold diluted horseradish-peroxidase-labelled streptavidin were added and incubated for 30 min. After the last wash, OPD was used to detect the amount of peroxidase as described previously [38].

To perform the *in silico* docking predictions, the best modelled CRP5 pepscan peptide sequences predicted in solution by the Mobyle program <http://mobyle.rpbs.univ-paris-diderot.fr/cgi-bin/portal.py#forms:PEP-FOLD> [39] were docked to all possible predicted conformations of 25HOCh. All the resulting docking data were interpolated and smoothed using the cubic B-spline method in Origin Pro 2017 (Northampton, MA, USA) and the data that best fitted pepscan binding were selected for representation. Validation of such strategy was confirmed by the high correlation obtained among similarly modeled VHSV G protein pepscan 15-mer peptides and previously published binding data to labeled phosphatidylserine [40] and phosphatidylinositol-bisphosphate [41] (data not shown).

Preparation of pMCV1.4 plasmids encoding *crp1-7*

Each of the chemically synthesized *crp1-7* and green fluorescent protein (*gfp*) genes was subcloned into the pMCV1.4 plasmid as described previously [7]. The resulting pMCV1.4-*crp1-7* and pMCV1.4-*gfp* plasmid constructs were used to transform *E.coli* DH5alpha, amplified and isolated using the Endofree Plasmid Midi purification Kit (Qiagen, Germany). Purified plasmid solutions containing 80–100% of plasmid DNA, as shown by agarose gel electrophoresis were stored at -20°C.

Preparation of CRP1-7-enriched supernatants

To produce ml amounts of CRP1-7-enriched supernatants (ssCRP1-7), 60% confluent EPC cell monolayers in 25 cm² bottles in 5 ml of cell culture medium were transfected with 5 µg of each of the pMCV1.4-*crp1-7* plasmids complexed with 15 µl of FuGENE HD (Promega, Madison, WI, USA) for 24 h at 22°C (transfection efficiency of 15.2–30.4%, n = 3 as estimated by transfection with pMCV1.4-*gfp*). After washing with fresh cell culture medium, the ssCRP1-7 were harvested 3-days later, the cell debris was eliminated by centrifugation, and the supernatants were sterilized by filtration through 0.2 µ filters and stored in aliquots at -80°C until ready for use [7].

SVCV infection of preincubated EPC cell monolayers with 25HOCh and ssCRP1-7

To detect the effects of 25HOCh and ssCRP1-7 (25HOCh + ssCRP1-7) on SVCV infection, the concentrations of 25HOCh, and ssCRP1-7, as well as the multiplicity of infection (m.o.i.) of SVCV were first optimized (data not shown). Optimal conditions were obtained when the EPC cell monolayers were pre-incubated with 100 µl of 4-fold diluted ssCRP1-7 or ssGFP in RPMI with 2% FBS in the absence or presence of 10 µM 25HOCH for 20 h at 26°C, the

monolayers were washed twice, and SVCV was added at 10^{-2} m.o.i. To estimate the extent of SVCV infection, the monolayers were incubated with SVCV for 2 h, washed, and incubated for 24 h at 26°C. The number of infected EPC cells was estimated by flow cytometry after staining with monoclonal anti-SVCV (BioX Diagnostics SA, Jemelle, Belgium) and fluorescein-labelled goat anti-mouse immunoglobulins as described previously [7]. The number of EPC infected cells varied from 29.6–39.7% or 9.9–20.1% ($n = 3$) after preincubation of the EPC cell monolayers with either 25HOCh or ssCRP1-7 alone, respectively. The results of preincubation with 25HOCh + ssCRP1-7 were expressed as relative percentages of infection \pm 25HOCh calculated by the following formula, $100 \times (\text{percentage of infected EPC cells preincubated with } 25\text{HOCh} + \text{CRP1-7}) / (\text{percentage of infected EPC cells preincubated in absence of } 25\text{HOCh and presence of CRP1-7})$.

In silico modeling of CRP1-7 tridimensional structures

To explore the CRP1-7 tridimensional structures, their protein sequences were automatically modelled (RMSD<0.3 Å) using the SWISS-MODEL homology server (<https://swissmodel.expasy.org/interactive>) [42–44]. The tridimensional structures of the target CRP1-7 sequences were predicted after pairwise comparison of the interfaces between the target and best template selected by the program. For each possible interface with > 10 residue-residue interactions, the QscoreOligomer score was calculated and averaged from all predicted interfaces [42,45]. The templates that resulted selected by automatic modeling corresponded to zebrafish CRP5 ± Ca++ (4PBP.pdb and 4PBO.pdb) [6] (RCSB data bank at <http://www.rcsb.org/pdb/home/home.do>).

Results

Preferential docking predictions of zebrafish CRP1-7 to Ch

To predict their docking ΔG energies to CRP1-7, the phosphocholine head (PC), other phospholipid heads [46–48] and cholesterol (Ch) [16] were selected because of their hCRP ligand properties. Interestingly, the results predicted the lowest ΔG (stronger binding) for Ch (ΔG ranges from -7.5 to -9 Kcal/mol) compared with phospholipid-heads (ΔG ranges from -4 to -5.5 Kcal/mol). The addition of a glycerol molecule to the phospholipid-heads did not change their predicted ΔG ([S1 Table](#)). The results also predicted that Ch docking energies were more Ca⁺⁺-independent than most other lipid-heads ([Fig 1A](#)) and predicted alternative docking locations for Ch and other lipid-heads (data not shown). These results were in contrast to the traditionally described phosphatidylcholine-binding preferences of hCRP [46–49]. Thus, although the Ch-binding properties of hCRP were described previously, their stronger binding energies were not [16]. Similar Ch-binding preferences were obtained by docking predictions made in parallel for hCRP and CRP1-7 ([S1 Table](#)).

Membrane Ch sequestration by methyl-beta-cyclodextrin reduces SVCV infection

To explore whether Ch could be implicated in SVCV infections, EPC cell monolayers were pretreated with methyl-beta-cyclodextrin (MBCD), a sequestering agent for membrane Ch [50]. Treatment with MBCD from 0.5 to 8 mM lowered the SVCV infectivity to ~ 20% ([Fig 1B](#), black line), while those concentrations exerted no significative effects on cell survival ([Fig 1B](#), blue dashed line). These results confirmed that the presence of Ch in the cell membranes was required for SVCV infectivity. Similar anti-viral activities of MBCD have been described, for instance, for poliovirus [51], pseudorabies [52], hepatitis [53], Sendai [54] and influenza

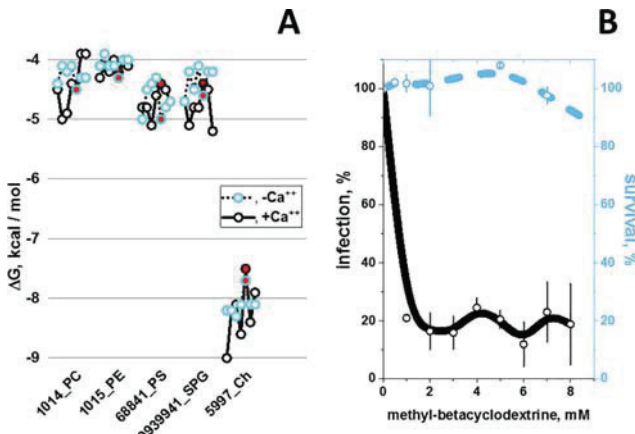


Fig 1. CRP1-7 preferential docking to Ch (A) and inhibition of SVCV infectivity by methyl-beta-cyclodextrin (MBCD) (B). **A)** Docking predictions to selected lipid-heads and Ch. CRP1-7 were SWISS-modeled using as templates CRP5 (GenBank accession number JF772178.1), 4PBP.pdb (+Ca⁺⁺) and 4PBO.pdb (-Ca⁺⁺) 3D-structures [6]. The structures were extracted from *.sdf from PubChem (<https://pubchem.ncbi.nlm.nih.gov/search/search.cgi>) and converted to *.pdbqt using the Babel program from the PyRx package [30]. PC, phosphocholine. PE, phosphoethanolamine. PS, phosphoserine. SPG, palmitoyl sphingomyelin. Ch, cholesterol. Numbers before the names, PubMed ID numbers. Blue open circles, consecutive CRP1-7 isoforms from left to right in the absence of Ca⁺⁺. Black open circles, consecutive CRP1-7 isoforms from left to right in the presence of Ca⁺⁺. Red circles, CRP5. Black lines, +Ca⁺⁺. Dot lines, -Ca⁺⁺. **B)** Effect of methyl-beta-cyclodextrin (MBCD) on SVCV infectivity. MBCD-treated EPC cell monolayers were incubated with SVCV for 24 h and were assayed for fff. The results were expressed as infectivity percentages calculated by the following formula, $100 \times (\text{fff treated with MBCD} / \text{fff nontreated with MBCD})$. To assay for viability, MBCD-treated EPC cell monolayers were incubated with MTT for 3 h, the absorbance at 570 nm was measured and the percentage of viability calculated using the following formula: absorbance of treated cells / absorbance of untreated cells. Open blue or black circles and their vertical lines, means and standard deviations ($n = 2$), respectively. The data were then interpolated and smoothed using the cubic B-spline method in Origin Pro 2017 (Northampton, MA, USA). Black line, SVCV infectivity. Blue dashed line, EPC cell monolayer viability.

<https://doi.org/10.1371/journal.pone.0201509.g001>

[50,55] viruses. Therefore, these results suggest that the Ch-CRP1-7 interaction may interfere with SVCV infectivity.

Because Ch-containing lipid rafts participate in interactions with hCRP [56], Ch is a key molecule involved in coronary diseases and Ch-related physiological compounds are highly diverse, an screening for other physiological Ch-related compounds was performed before studying any possible interactions among CRP1-7, Ch and viral infections.

Preferential predicted docking of zebrafish rCRPs to hydroxycholesterols (HOChs)

When 26 Ch-related physiological compounds were docked *in silico* to the modeled tridimensional structures of CRP1-7, stronger binding predictions (ΔG ranges between -7.5 to -9.3 Kcal/mol) were obtained for most of the hydroxy derivatives studied for CRP1-7 (Fig 2 and S2 Table). The ΔG values obtained in the absence or in the presence of Ca⁺⁺ were not significantly different (S2 Table). Most of the lowest ΔG values were obtained for CRP1, while CRP5 showed ~ 0.5–1 Kcal/mol higher ΔG than CRP1, depending on the Ch-related molecule. The most relevant results of these Ch-related docking predictions could be summarized as follows: i) water-soluble hydroxy Ch derivatives (HOChs) interacted with CRP1-7 within the lower ΔG ranges from -8.0 to -9 Kcal/mol; ii) among the HOChs, most of the lower ΔG values

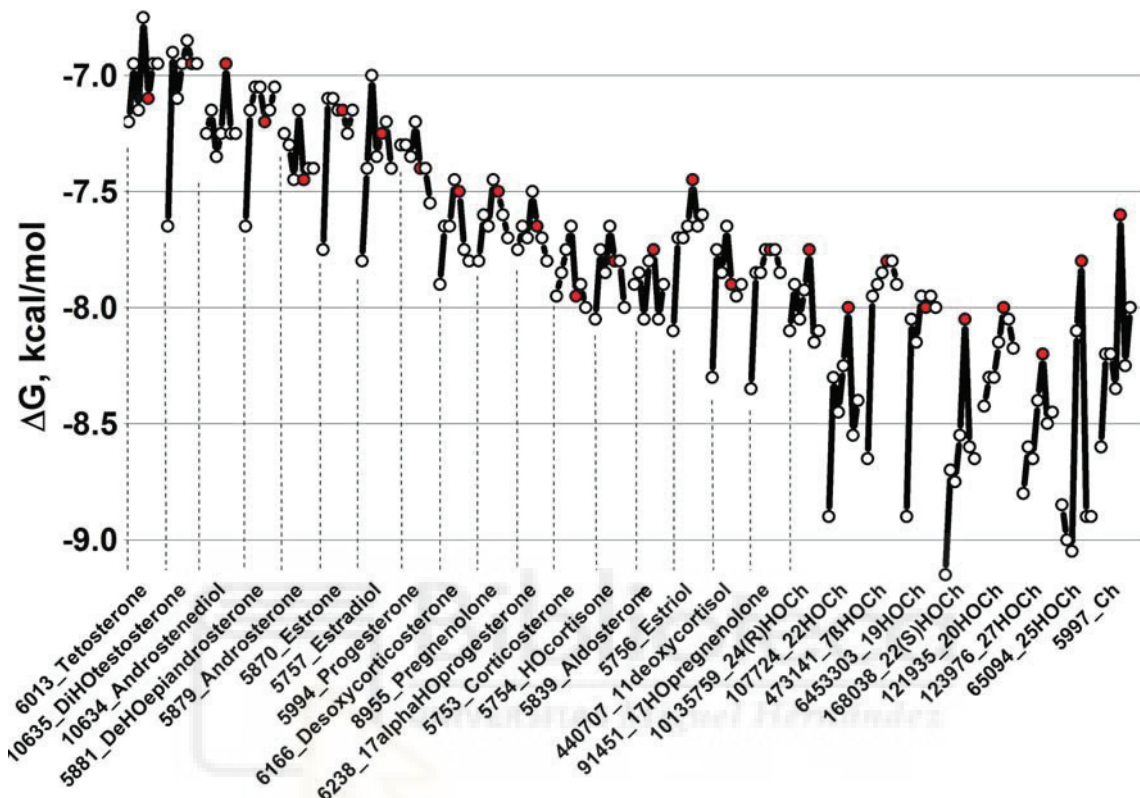


Fig 2. CRP1-7 docking predictions to several Ch-related physiological compounds. CRP1-7 models, Ch-related physiological molecules and ΔG predictions were obtained as described in the legend of Fig 1A. Because the predicted ΔG values in the absence or presence of Ca^{++} were similar (S2 Table), only the mean $\Delta Gs \pm \text{Ca}^{++}$ were represented. Open circles, consecutive CRP1-7 isoforms from left to right. Red circles, CRP5. Numbers before the names_, PubMed ID numbers. HO, hydroxy. Ch, cholesterol.

<https://doi.org/10.1371/journal.pone.0201509.g002>

corresponded to CRP1, while most of the highest ΔG values corresponded to CRP5; and **iii)** 25-hydroxycholesterol (25HOCh) was unique among all the studied HOChs because of their lowest ΔG values (~ -9 Kcal/mol). No previous reports on 25HOCh-CRP interactions could be found in the literature.

To explore the existence of other possible Ch-related compounds with still lower ΔG values that could be used as anti-inflammatory chemotherapeutic drugs, a library of 1093 Ch-related synthetic molecules was docked to modeled CRP1-7 tridimensional structures. The frequency distribution of the predicted ΔGs showed a distribution with a mean ± 3 standard deviations = -12 Kcal/mol (S3 Table). Twenty-one Ch-related nonphysiological or synthetic compounds showed the lowest ΔG values from -13.3 to -12 Kcal/mol (Table 1). Most of the new molecules identified contained deuterium, fluorine, bromine or chlorine atoms and 66.6% contained at least one hydroxy group per molecule. Therefore, some of these newly identified Ch-related derivatives could be further employed for drug applications and/or mechanistic studies in the

Table 1. Ch-related nonphysiological compounds with the best docking predictions to CRP1-7.

ID	Name	CRP	ΔG, Kcal/mol
71749935	M Progesterone-d3 Glucuronide	CRP5	-13.3
70626502	25-F-1α-HOCh	CRP1	-13.3
71749934	M Progesterone Glucuronide	CRP5	-13.3
70626891	diF-methyl-dodecahydro-cyclopentaphenanthrene	CRP1	-13.0
493972	F-11-HO-Methyl-DioxoPregnadien-Acetate	CRP5	-12.6
192154	triFlumedroxone Acetate	CRP5	-12.6
240767	Emetholone 17 Acetate	CRP5	-12.5
95574	F-16a,17-(isopropylidenedioxy) Corticosterone	CRP5	-12.5
71748935	20-HOCh-d7	CRP5	-12.4
21122966	6-HO-M Progesterone 17-Acetate	CRP5	-12.3
102276261	3-[(2-B-ethyl)Carbamoyl]Ch	CRP5	-12.3
71749110	HO-M Progesterone 17-Acetate	CRP5	-12.2
71748841	4-7 HOcholestene-d7	CRP1	-12.1
57357615	17-(Acetoxy)-C-(C-methyl)Pregnadienedione	CRP5	-12.1
126456352	24-HOCh-d4	CRP1	-12.1
71748930	4-HOCh-d7 4-Acetate	CRP5	-12.1
71315435	Cortexone M-d9	CRP1	-12.1
10476437	Flugestone 17-Acetate	CRP5	-12
71315435	Cortexone M-d9	CRP5	-12
71315434	Cortexone M-d8	CRP1	-12
71315434	Cortexone M-d8	CRP5	-12

Ch-related nonphysiological compound structures were retrieved from several libraries obtained from PubChem in a *.sdf format. To construct the library, 550 Chs, 314 colestens, 73 corticosterones, 41 dehydroepiandrosterones (DHEAs), 107 estriols, 99 pregnenolones, 196 progesterones and 107 HOChs were retrieved. Duplicated and extremely long molecules were eliminated from the total of 1487 *.sdf, resulting in a downsized library of 1093 *.pdbqt archives. After docking, the frequency distribution of ΔG showed two peaks with means at -11 and -7 Kcal/mol, respectively (S3 Table). Only Ch-related compounds with ΔG < -12 Kcal/mol (mean + 3 standard deviations) are shown. ID, PubMed number. HO, hydroxy. d, deuterium. F, fluoro-. C, chloro-. B, bromo. M, 17-acetyl-6,10,13-trimethyl-3-oxo-1,2,6,7,8,9,11,12,14,15,16,17-dodeca HOcyclopenta[a]phenanthren-16-yl acetate (medroxy).

<https://doi.org/10.1371/journal.pone.0201509.t001>

future. Next we tried to confirm some of the docking predictions mentioned above by solid-phase binding assays.

Binding of zebrafish rCRPs to hydroxycholesterols (HOChs), Ch and PC

Because of the recently described anti-viral activities of 25HOCh [57,58] and its highest predicted docking to CRP1-7, its binding was compared with Ch/PC (the former because it is the traditional ligand for hCRP). For the binding assays, we used polystyrene wells coated with the lipids [36]. Using 25HOCh to coat the solid-phase, the binding results confirmed the higher docking of rCRP5/rCRP7 to Ch/25HOCh than to PC (Fig 3A). The binding of rCRP7 to Ch/25HOCh was slightly higher than to rCRP2 or rCRP5 (Fig 3, rCRP2 and rCRP5). Whereas rCRP2/rCRP5 binding to Ch or PC were relatively low (Fig 3, rCRP2 and rCRP5). To complete the study, we explored all isoforms for binding to 25HOCh using supernatants from EPC cells transfected with pMCV.4-*crp1-7* (ssCRP1-7) as a source for CRP1-7. The results of these experiments showed different concentration-dependent profiles for different CRP1-7, with CRP1 being the most active at the lower 25HOCh concentrations assayed (<10 μM) (Fig 3B and S4 Table) confirming the docking predictions. On the other hand, although CRP7 showed slightly higher binding at >100 μM 25HOCh, similar values were obtained for all ssCRP1-7 at those higher concentrations. The binding of ssCRP1-7 to solid-phase 25HOCh showed relatively lower

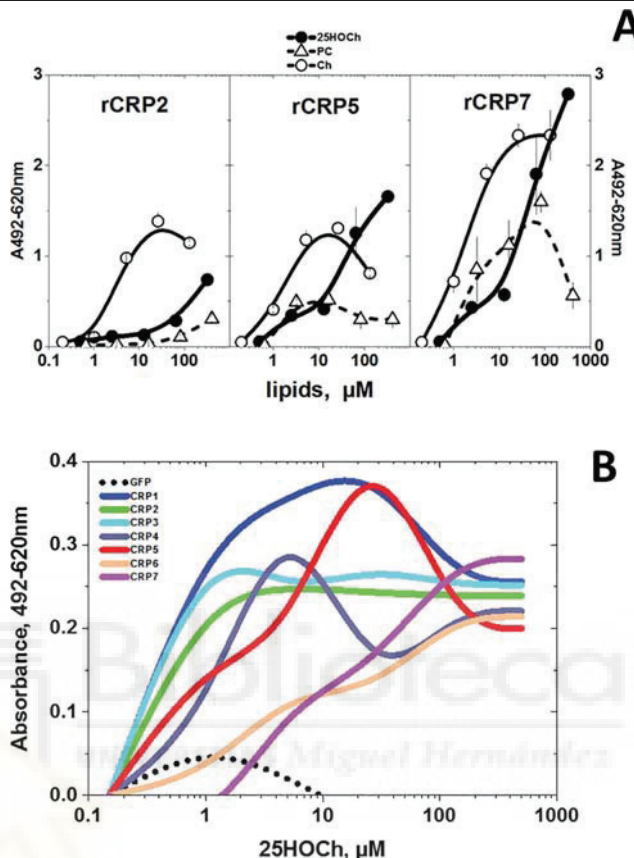


Fig 3. rCRP (A) and ssCRP1-7 (B) binding to solid-phase lipids. The binding of purified rCRPs and ssCRP1-7 to selected lipids was assayed by using 96-well plates coated to dryness with several lipid concentrations dissolved in ethanol. The lipid-coated plates were washed and were incubated with rCRP2 or ssCRP1-7 in borate buffer for 1 h in a 50 μ l volume. To detect bound rCRP or ssCRP1-7, rabbit anti-CRP p3 peptide, peroxidase-labeled goat anti-rabbit IgG and OPD were used as described previously [37,38]. The means and standard deviation from 2 independent experiments were represented. A) rCRP at 0.5 μ g/well in borate buffer. Open triangles, solid-phase phosphatidylcholine (PC). Open circles, solid-phase Ch. Black circles, solid-phase 25HOCh. B) ssCRP1-7 were 10-fold diluted in borate buffer. Results from one experiment out of three were interpolated and smoothed using the cubic B-spline method in Origin Pro 2017 (Northampton, MA, USA) (see data in S4 Table). Black points, supernatant from pMCV1.4-gfp transfected cells. Blue line, supernatant from pMCV1.4-crp1 transfected cells. Green line, supernatant from pMCV1.4-crp2 transfected cells. Light-blue line, supernatant from pMCV1.4-crp3 transfected cells. Gray line, supernatant from pMCV1.4-crp4 transfected cells. Red line, supernatant from pMCV1.4-crp5 transfected cells. Orange line, supernatant from pMCV1.4-crp6 transfected cells. Purple line, supernatant from pMCV1.4-crp7 transfected cells.

<https://doi.org/10.1371/journal.pone.0201509.g003>

values than that to rCRPs, most probably due to the lower CRP concentrations in the ssCRP1-7 (compare the ordinate values of Fig 3A and 3B).

Mapping of both binding and docking energies of CRP5 to 25HOCh

To further clarify 25HOCh binding to CRP1-7, we performed a pepscan approximation to map the interaction. Because m-hCRP, but not p-hCRP is the conformation that preferentially

binds Ch [16,17,59], some nonconformational motifs may conserve Ch-/25HOCh-binding activity and thus a pepscan may be used to map at least some conformation-independent binding. Therefore, we selected a pepscan to explore for possible non-conformational interactions of CRP5 with 25HOCh using both solid-phase binding assays and docking predictions.

For the peptide binding assays, each of the synthetically biotinylated 15-mer peptides derived from the CRP5 amino acid sequence was incubated with 25HOCh-coated solid-phases. The results showed maximal binding peaks at the ~ 30–50, 70–90, 110–150 and 170–190 amino acid positions (Fig 4A, black line). Similar peaks docked with minimal ΔG to 25HOCh (Fig 4A, blue line). Of the 25HOCh binding/docking peaks identified, only the 30–50 was in a similar region to that of the 35–47 peptide previously identified in hCRP as the main Ch-binding domain [16]. To locate the predicted interaction of 25HOCH with the CRP1-7 tridimensional structures we used PyMol. The 25HOCh docked at the CRP5 interface side with ΔG between -7.5 and -8.4 Kcal/mol (some of the contact positions at T41, E48, R71, F84, F85, S117) (Fig 4A, CRP5). By contrast, the 25HOCh docked at other CRP1-7 effector faces under the α-helix with ΔG between -8.6 and -9.1 Kcal/mol (some of the contact positions for CRP1 at R113, S115, G153, E154, Y161, and E206) (Fig 4B, CRP1). Similar ΔG values (S5 Table) and docking locations were predicted for m- or t-CRP5. Similar docking locations were predicted for 25HOCh and Ch for most CRP1-7 within ± ΔG > ~0.5 Kcal /mol (S5 Table).

Therefore, both the pepscan binding and docking predictions, confirmed the existence of an interaction between 25HOCh and CRP5, which most likely can be extended to all CRP1-7.

In vitro anti-SVCV effects caused by CRP1-7 in the presence of 25HOCh

Hydroxylated Chs (HOChs) are Ch oxidized derivatives with diverse biological activities, most of them correlating with inflammatory responses [60] similar to CRP. Among the HOChs, 25HOCh showed minimal ΔG docking predictions for CRP1-7 (-8 to -9 Kcal/mol, corresponding to concentrations between 1.35 and 0.35 μM) (Fig 3). Among their biological activities, 25HOCh has been related to viral infections [58,61], including the reduction of spring viremia carp virus (SVCV) infection in zebrafish [57]. Because of the Ch-dependence of SVCV infection (Fig 1B), the reduction of SVCV infection by zebrafish ssCRP1-7 [7] was chosen as an example of possible CRP1-7- HOChs interactions affecting the same biological function.

Because both 25HOCh [57] and CRP1-7 [7] have demonstrated their independent anti-SVCV activities, their concentrations were first independently titrated at different multiplicities of infection (m.o.i.) of SVCV to maximize the limits of detection when they were to be used together. Under those optimal conditions, the extent of SVCV infections obtained using ssCRP1-7 + 25HOCh (ssCRP1-7 + 25HOCh/ssCRP1-7 ratios) compared with 25HOCh (GFP + 25HOCh) were further reduced by 1.5 to 3-fold depending on the CRP1-7 isoform (Fig 5A). Similar results were obtained with rCRP5 and rCRP7 but not with rCRP2 (data not shown). The above results suggested that 25HOCh in the presence of CRP1-7 further enhanced the anti-viral effects caused by either 25HOCh or CRP1-7 alone. It is still too early to know the mechanisms implicated, because the interaction of 25HOCh with the L polymerase of SVCV [57], or inhibition of glycosylation by 25HOCh in other rhabdoviruses [62], may suggest that the binding of 25HOCh to some viral proteins cannot be excluded. Furthermore, other possible interactions among 25HOCh, CRP (direct effect) and/or other CRP-induced molecules (indirect effects) present in ssCRP1-7, may still explain the above mentioned antiviral effects.

To further explore any possible correlations among CRP1-7 tridimensional structures and 25HOCh binding or antiviral effects, we next studied whether different oligomeric forms were present in ssCRP1-7.

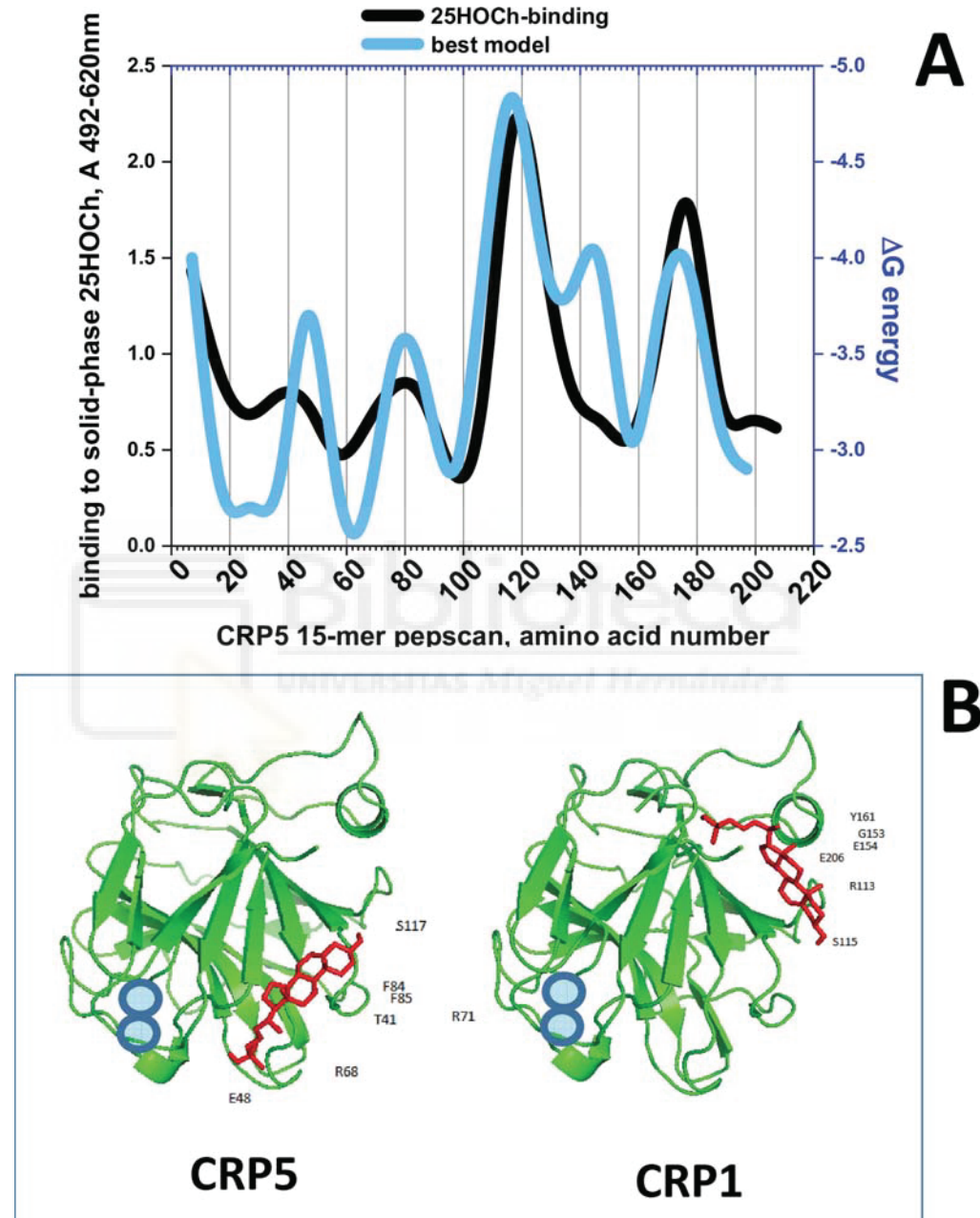


Fig 4. Solid-phase binding and docking predictions to 25HOCh of CRP5 pepscan peptides (A) and predicted best docking location (B). A) For the peptide-binding assays, a series of 15-mer peptides overlapping 5 amino acids from CRP5 was chemically synthesized by adding an amino-terminal biotin molecule. Solid-phases were coated with 2 µg per well of 25HOCh into polystyrene 96-well plates. The binding of 0.05 µg of

biotinylated pepscan peptides, detection with peroxidase-labeled streptavidin and staining with OPD were then performed. The means from 3 independent experiments were represented and standard deviations omitted for clarity (S5 Table). For the *in silico* docking predictions, the modeled pepscan peptides with the lowest energies were docked to several possible conformations of 25HOCh as described in the methods section. The docking energies that best fitted the binding data were then represented (S5 Table). **Black line**, peptide binding to 25HOCh. **Blue line**, predicted ΔG energy of peptide docking to 25HOCh. **B**) PyMOL representation of the lowest energy structures of CRP5 and CRP1 complexed to 25HOCh (the remaining CRP1-7 were similar). **Green**, CRP amino acid chains. **Red**, 25HOCh. **Blue circles**, Ca⁺⁺ atoms located at the PC-binding pocket [6].

<https://doi.org/10.1371/journal.pone.0201509.g004>

Insect-made rCRPs suggest their different oligomerization states

The *E.coli*-made zebrafish c-reactive protein CRP5 isoform (rCRP5) was crystallized as trimers (t-CRP5), as shown by X-ray studies [6]. However, it is not yet known whether trimers are the physiological form for the remaining CRP1-7 isoforms.

Our first attempts to characterize CRP1-7 isoforms included expression in *E.coli*. However, numerous experiments met with irreproducibility, expression failure, high CRP denaturation

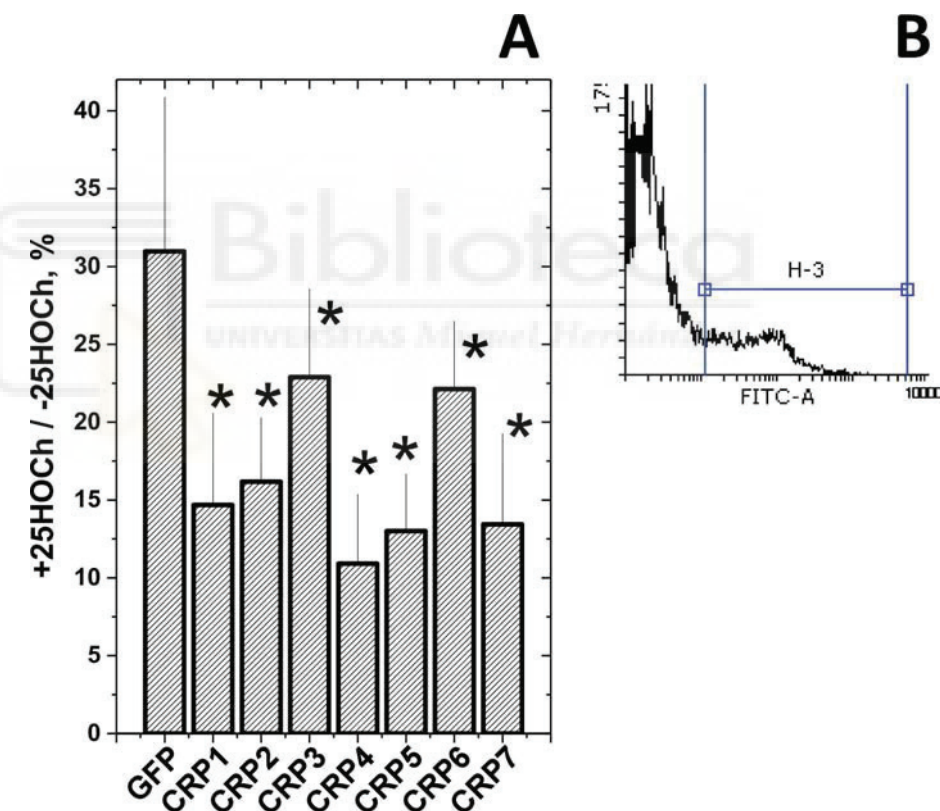


Fig 5. Anti-SVCV infectivity after treatment of EPC cell monolayers with 25HOCh and CRP1-7. **A)** EPC cell monolayers were incubated with 100 μl of ssGFP or ssCRP1-7 4-fold diluted in RPMI with 2% FBS ± 10 μM 25HOCh for 20 h at 26°C. After washing, 10⁻² m.o.i of SVCV were added and incubated for 24 h. After staining with anti-SVCV and fluorescein-labeled goat anti-mouse immunoglobulins [7], the number of fluorescent cells were estimated by flow cytometry. **B)** Representative aspects of histograms from nonfluorescent and fluorescent cells. The number of SVCV-infected EPC cells varied from 12.7 to 50.6% (n = 5), depending on the experiment. The results were expressed as relative infection percentages calculated by the following formula, 100 × (number of infected cells+25HOCh / number of infected cells -25HOCh). The means and standard deviations of a representative experiment were represented (n = 3). *, statistically < than cells transfected with ssGFP at p < 0.05 (Student's t-test).

<https://doi.org/10.1371/journal.pone.0201509.g005>

or low yields, despite the reduction of autoinduction and temperature, and/or recloning of the best-producing clones (data not shown). Most probably some of those results could be explained by the toxicity of the rCRPs to *E.coli*.

Alternatively, we explored the production of rCRP1/rCRP2/rCRP5/CRP7 in insect cells. The results showed that while insect-made rCRP2/rCRP5/rCRP7 could be expressed and purified by nondenaturing affinity chromatography, all attempts to purify rCRP1 were unsuccessful. Western blot analysis using anti-polyH antibodies indicated that although small amounts of rCRP1 were present, they were not retained by the affinity columns (data not shown), most likely due to polyH tail inaccessibility, perhaps because of a different conformation of rCRP1 compared with that of the other rCRPs.

Polyacrylamide gel electrophoresis (PAGE) in the absence of SDS in the buffers, treating the samples under nondenaturing conditions (no heat, no SDS, no β -mercaptoethanol and 1 mM CaCl₂), and Western blotting with anti-p3 antibodies, showed that rCRP2 (calculated isoelectric point IP of 6.35) banded at an apparent molecular weight > 100 kDa, while rCRP5 (IP 4.6) and rCRP7 (IP 4.6) banded at ~ 75 kDa (Fig 6A left). A brief (2 min) treatment of the rCRP samples under denaturing conditions, increased the migration of all rCRP, especially that of rCRP7 (Fig 6A right). Although, in the absence of SDS, the estimation of the molecular weights is not accurate, the results suggested larger sizes for rCRP2/rCRP5 than for rCRP7, according to previous electrophoretic data described for p-hCRP and m-hCRP [63].

By contrast, by applying PAGE in the presence of SDS in the buffers, samples under nondenaturing conditions and Western blotting, all the rCRP displayed similar bands that could be interpreted as residual amounts of trimers (~75 kDa), dimers (~50 kDa) and monomers (~25 kDa) (Fig 6B, left). The number of monomers increased when the samples were briefly treated (2 min) under denaturing conditions; especially for rCRP7, only monomers were detected (Fig 6B, middle). All rCRP became homogeneously monomeric (~25 kDa) when the samples were treated for longer (5 min) under denaturing conditions (Fig 6B, right). The slightly different positions of the monomeric forms could be due to differences in their glycosylation, although posttranscriptional deimidation has also been described in cod CRPs to cause electrophoretic heterogeneity [64].

The most likely explanation for all the above commented data suggest that, while insect-made rCRP2/rCRP5 may exist as an equilibrium among trimers, dimers and monomers, rCRP7 has a stronger tendency to form monomers.

Only monomeric CRP1-7 could be detected from enriched supernatants

Western blotting of ssCRP1-7 using anti-p3 antibodies, only detected CRP2-7 monomers of ~ 25 kDa with slightly different positions for each ssCRP2-7, with similar profiles under denaturing (Fig 6C, down), 20-fold lower SDS concentration (not shown)[65] and nondenaturing (data not shown) sample and buffer conditions. Similar CRP2-7 levels were present in ssCRP2-7 as shown using actin as an internal control marker (Fig 6C, up). In these experiments, it was not possible to detect the presence of any CRP1 band, most likely because of its lower concentration, because previous results have demonstrated its presence by dot-blot analysis when using concentrated ssCRP1 [7]. Therefore, most likely, all ssCRP1-7 were secreted from EPC transfected cells mainly as monomers. Tridimensional structure predictions were used to further explore these possibilities.

In silico predictions of CRP1-7 tridimensional structures

To obtain more data on the possible tridimensional structures of CRP1-7, their amino acid sequences were modeled using the SWISS-MODEL web program. Automatic modeling showed that only CRP2/CRP5 rendered trimers, while the remaining of the CRP1-7 only

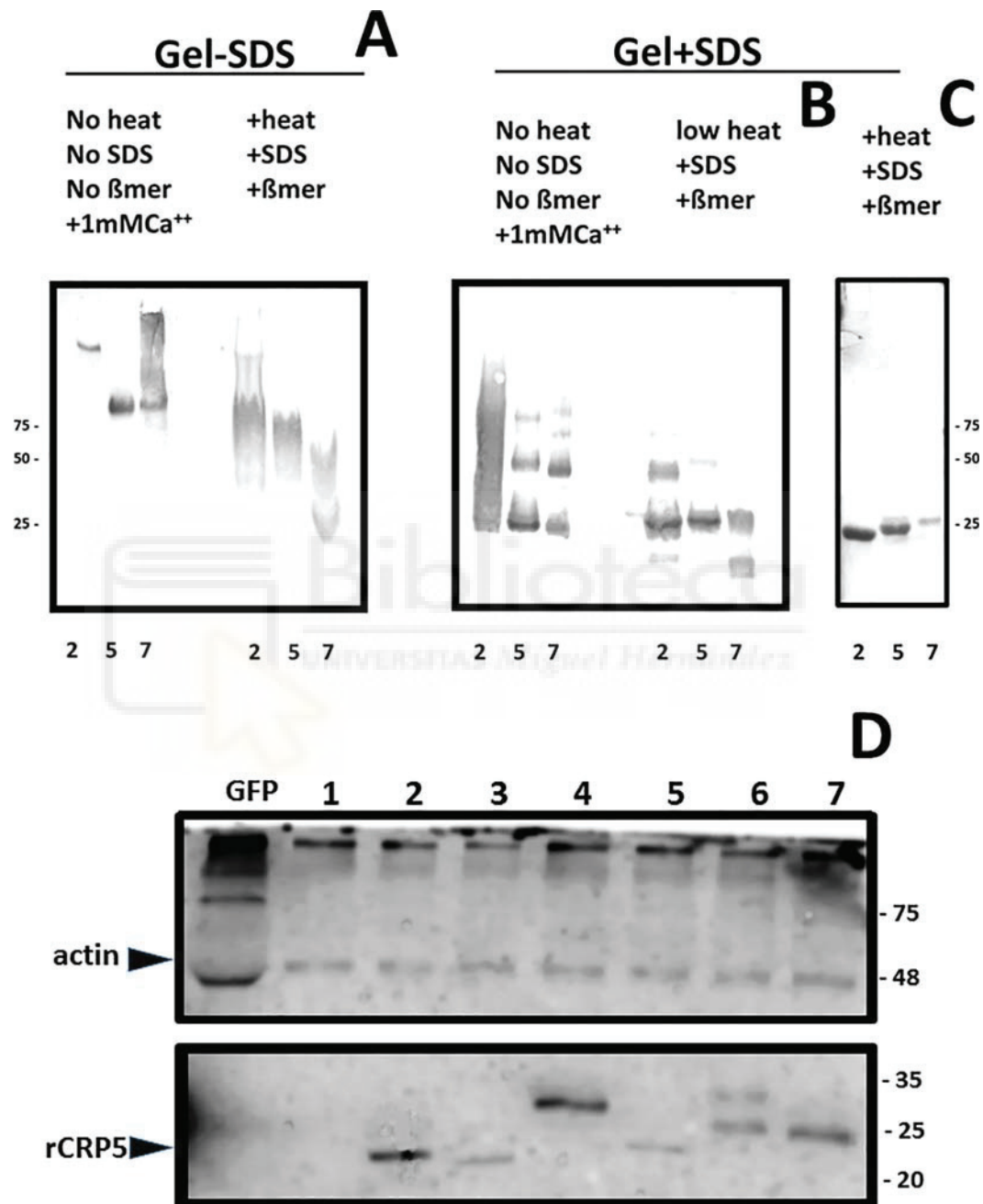


Fig 6. Polyacrylamide gel electrophoresis and Western blotting of rCRPs (A,B,C) and ssCRP1-7 (D). The insect-made affinity purified samples were electrophoresed in 4–20% gradient polyacrylamide gels. A) Samples of rCRPs prepared and electrophoresed in the absence of SDS in the buffers and stained

with Coomassie (nondenaturing conditions). **B)** Samples of rCRPs heated at 100°C in the presence of β-mercaptoethanol and SDS, electrophoresed in the presence of SDS in the buffers (denaturing conditions) and stained with Coomassie. **C)** Western blotting of the gel B transferred to nitrocellulose membranes, stained with anti-p3 antibody, peroxidase-labeled anti-rabbit and overexposed to diaminobenzidine (DAB) [37]. The ssCRP1-7 were electrophoresed in 15% polyacrylamide gels. **D)** Samples of ssCRP1-7 treated at 100°C in the presence of β-mercaptoethanol and SDS, electrophoresed in the presence of SDS in the buffers, transferred to nitrocellulose membranes, stained with anti-actin (up) or anti-p3 (down) antibody, peroxidase-labeled anti-rabbit IgG and developed by chemiluminescence [7]. Similar results were obtained with samples electrophoresed under nondenaturing conditions (data not shown). **Numbers around the gels**, molecular weight markers in kDa. **Up left arrow**, position recognized by anti-actin antibodies. **Down left arrow**, position of purified rCRP5 recognized by anti-p3 antibodies. The results are representative of at least 3 experiments.

<https://doi.org/10.1371/journal.pone.0201509.g006>

modeled as monomers (Table 2). These results could be explained because CRP2/CRP5 have differences in most of their modeling parameters, specially in their torsion-angle potentials, compared with the other CRP1-7 (Table 2). Because the existence of EST from zebrafish in the UniGene Bank classified as CRP5 transcript variants [6] offered another opportunity to test the reliability of the trimer/monomer predictions mentioned above, we explored these sequences by automatic modeling. The corresponding modeling results predicted that 97.8% of the 47 CRP5 longest variant sequences modelled as trimers such as CRP2/CRP5. The comparison of the CRP5 variant amino acid sequences demonstrated 2-3-times more variations downstream of position 200 than in the rest of the molecule (Fig 7, red). On the other hand, most amino acid variations among the CRP1-7 isoforms were in the PC-binding pockets or hCRP-homologous Ch-binding domain (Fig 7, blue or green rectangles, respectively). Therefore, these results predicted the tendency of CRP2, CRP5 and CRP5-transcript variants to oligomerize as trimers and prompted further studies about the biological significance of both CRP isoforms and variants.

Discussion

The PAGE/Western data and *in silico* predictions, together with the results of 25HOCh binding and enhancement of anti-SVCV effects by ssCRP1-7, may implicate more m-CRP1-7 rather than t-CRP1-7 in those biological functions. However, CRP1-7 may also physiologically exist as an equilibrium of trimers, dimers and monomers, as shown in the cases of CRP2/

Table 2. Parameter values of *in silico*-predicted CRP1-7 oligomeric structures.

isoform	Acc.number	Automatic SWISS prediction	QMEAN	Cβ	AA	SO	TO
CRP1	XM_693995.4	monomer	-0.55	-1.36	-1.03	-1.03	0.01
CRP2	BC097160	homotrimer	0.77	-1.64	-1.08	-0.92	1.19
CRP3	BC154042	monomer	0.01	-1.15	-1.15	-1.03	0.51
CRP4	BC115188	monomer	-1.81	-1.65	-1.95	-1.33	-1.07
CRP5	BC121777	homotrimer	1.42	-0.71	-0.89	-0.60	1.62
CRP5-	Dr.124528-	97.8%	1.12	-0.90	-0.99	-0.68	1.30
47 variants	Dr.162306	homotrimers	± 0.31	± 0.5	± 0.2	± 0.4	± 0.5
CRP6	BC162745	monomer	-0.45	-1.20	-1.17	-1.34	0.15
CRP7	BC150371	monomer	-0.42	-1.04	-1.22	-1.28	0.15

The CRP1-7 amino acid sequences [2] were modeled as tridimensional structures using the SWISS-MODEL server with automatic template selection. Additionally, 47 full-length CRP5 amino acid sequences were modeled from 73 zebrafish *crp5* EST variants (UniGene Dr.124528-Dr.162306) [6]. QMEAN, estimation of the total similarity to the template, comprising 4 individual Z-score parameters (Cβ, all-atom, solvation and torsion). The individual Z-scores compare the predicted tridimensional structures with the template as follows: **i**) Cβ atoms of three consecutive amino acids (Cβ), **ii**) all-atoms (AA), **iii**) solvation burial status of the residues (SO) and **iv**) torsion angle potentials (TO). Low QMEAN score values indicate low similarity to the template. High QMEAN score values indicate high similarity to the template. **Bold**, highest and/or lowest score values. **Gray**, CRP2/CRP5. The mean \pm standard deviation ($n = 47$) of the calculated score values of the CRP5-transcript variants were represented.

<https://doi.org/10.1371/journal.pone.0201509.t002>

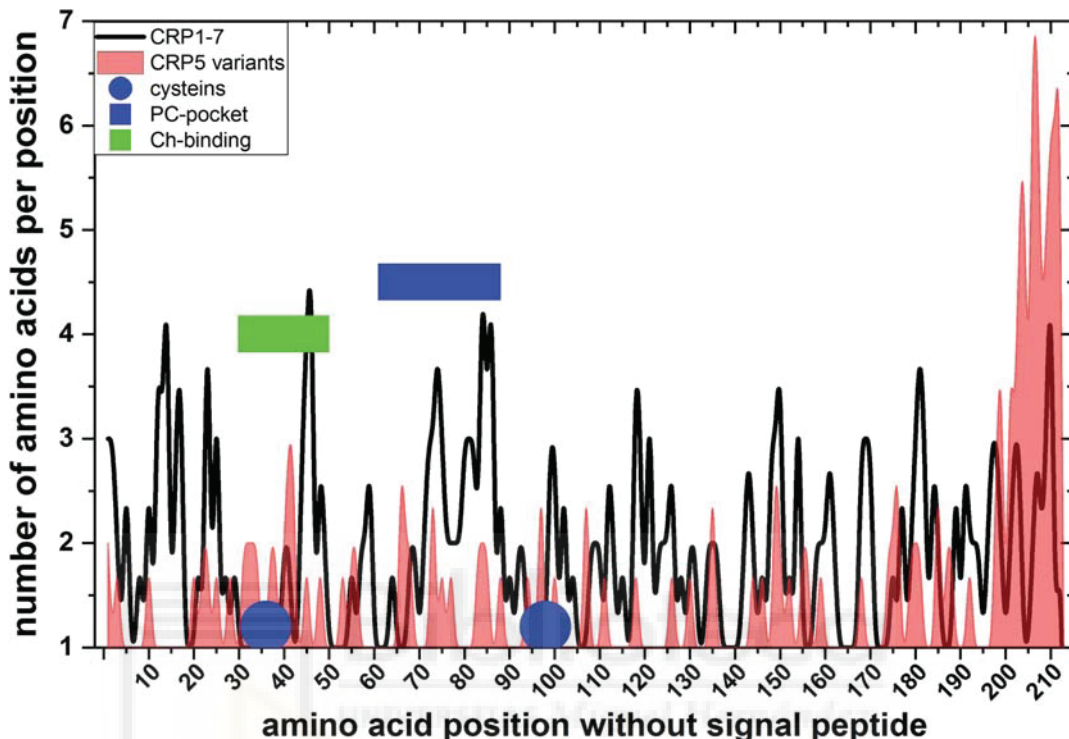


Fig 7. Alignment among EST-derived amino acid sequences of CRP5-transcript variants. Transcript variants corresponding to the zebrafish *crp5* gene were retrieved from 73 ESTs obtained from different zebrafish tissues (UniGene Dr.124528-Dr.162306) [6]. The corresponding ORFs > 100 amino acids translated by the Virtual Ribosome software (<http://www.cbs.dtu.dk/services/VirtualRibosome/>) were numbered without the signal peptide ('FKNL..in CRP5) and were aligned to CRP5 (BC121777). The number of different amino acids per position was represented. The raw data (S6 Table) were smoothed using the cubic B-spline method (Origin Pro 2017, Northampton, MA, USA). Blue circles, cysteines. Blue rectangle, PC-binding pocket of hCRP. Green rectangles, Ch-binding residues of hCRP [16]. Black line, number of amino acids per position of CRP1-7. Red profile, number of amino acids per position of CRP5 transcript variants.

<https://doi.org/10.1371/journal.pone.0201509.g007>

CRP5 and, to a lower extent CRP7. On the other hand, because m-hCRP can also be produced during *in vitro* manipulations, for instance, by treatments in the absence of Ca^{++} with urea, low-pH or low-salt buffers [65,66], the m-CRP1-7 detected in this work may have been produced by other *in vitro* manipulations (e.g., purification by affinity chromatography in the absence of Ca^{++} or transfection of EPC cells). We may also speculate that t-CRP1-7 or at least CRP2/CRP5 could preferentially exist in fish until an unknown stimulus triggers their conversion to m-CRP1-7 and/or *viceversa*. Similarly, circulating hCRP is pentameric (p-hCRP) [13] and converts to the monomeric form (m-hCRP) after interaction with any exposed phosphocholine heads and/or Ch-enriched lipid rafts of cellular membranes in damaged tissues [16,17,59,63]. It is tempting to speculate that t-CRP2/CRP5 may be functionally analogous to the circulating p-hCRP and m-CRP1-7 could be analogous to the converted m-hCRP. Alternatively, all zebrafish m-CRP1-7 may be synthesized *de novo* as monomers. We may also think of the possibility of heterologous CRP1-7 oligomers. However, any of these possibilities remains speculative until specific reagents could be developed to differentiate each of those isoforms.

Together, the above commented evidence shows that the oligomeric state of CRP1-7 isoforms fine tunes their lipid binding and, at least, some of their resulting heterogeneity of biological functionalities, as suggested previously [2,6,7]. Thus, previous transcriptomic studies on zebrafish *crp1-7* genes have demonstrated differential transcript expression throughout tissues [67], in survivors of VHSV infection [20] and in *rag1*^{-/-} mutants defective in adaptive immunity [21]. Additionally, unexpected isoform-dependent *in vitro* and *in vivo* anti-viral activities were recently described for zebrafish CRP1-7 [7], while similar activities have never been reported for hCRP, or for any other CRP. In all those studies, *crp2*/CRP2 and *crp5*/CRP5 transcripts/proteins were the most modulated during either bacterial and viral infections, correlating with the higher trimeric propensity of CRP2/CRP5 and in sharp contrast to *crp1*/CRP1 and *crp7*/CRP7 which had remained mostly unmodulated. These findings together with the preference of CRP1-7 for hydroxycholesterol derivatives shown in this work, revealed fish primitive anti-viral functional CRP1-7 diversity that may also be relevant to the single-gene-encoded hCRP.

The relevance of these explorations in the CRP1-7 lipid interactions with viral infection diseases may have important implications for human diseases. For instance, the abundance of oxidized Chs in human atherosclerotic plaques amplifies the impact that hCRP-Ch interactions may have for vascular diseases and neurodegenerative disorders during viral infections [58,68,69].

Supporting information

S1 Table. Docking predictions to selected lipid-heads and Ch. The CRP1-7 were SWISS-modeled using the 3D structures CRP5 (GenBank accession number JF772178.1), 4PBP.pdb (+Ca⁺⁺) and 4PBO.pdb (-Ca⁺⁺) as templates. The structures of the lipid heads and cholesterol were extracted from *.sdf from PubChem (<https://pubchem.ncbi.nlm.nih.gov/search/search.cgi>) and converted to *.pdbqt using the Babel program from the PyRx package. Dockings were performed with a grid of 50x50x50 Angstrom. **Yellow background**, data used to derive Fig 1A. (XLSX)

S2 Table. CRP1-7 docking predictions to several Ch-related physiological molecules in the absence and presence of Ca⁺⁺. CRP1-7 models, Ch-related physiological molecules and ΔG predictions were obtained as described in the legend of Fig 2. **Numbers before the names**, PubMed ID numbers. HO, hydroxy. Ch, cholesterol. (XLSX)

S3 Table. Docking predictions of binding of Ch-related nonphysiological compounds to CRP1-7. Ch-related nonphysiological compound structures were retrieved from several libraries obtained from PubChem in a *.sdf format. To construct the library, 550 Chs, 314 colestens, 73 corticosterones, 41 dehydroepiandrosterones (DHEAs), 107 estriols, 99 pregnenolones, 196 progesterones and 107 HOChs were retrieved. Duplicated and extremely long molecules were eliminated from a total of 1487 *.sdf, resulting in a downsized library of 1093 *.pdbqt archives. The docking were performed to CRP1-7 modelled in the absence or in the presence of Ca⁺⁺ (crp ±Ca⁺⁺). **A**) Table of Ch-related compounds ordered from the lowest to the highest ΔG (free-binding energies) in Kcal/mol after docking to CRP1-7. **Yellow background**, data used to derive Table 1. **B**) Distribution of ΔG in relative frequencies. **Black arrow**, cut-off ΔG value chosen to derive Table 1. **C**) Correlation between the ΔGs from the dockings using CRP +Ca⁺⁺ and CRP-Ca⁺⁺. (XLSX)

S4 Table. ssCRP1-7 binding to solid-phase 25HOCh. The binding of ssCRP1-7 to 25HOCh was assayed using plates of 96-wells coated to dryness with 0.15 to 500 µM 25HOCh dissolved in ethanol. The 25HOCh-coated plates were washed with borate buffer and incubated with ssCRP1-7 in borate buffer for 1 h in a 50 µl volume. Bound ssCRP1-7 were detected using rabbit anti-CRP p3 peptide, peroxidase labeled goat anti-rabbit IgG and OPD. Raw absorbances were measured at 492–620 nm. Absorbance obtained with empty wells were subtracted to all data. **Yellow background**, data used to derive Fig 3B. (XLSX)

S5 Table. Solid-phase binding and docking prediction raw data with their calculations of 25HOCh and the CRP5 pepscan interactions. For the 25HOCh-binding, a series of 15-mer peptides overlapping 5 amino acids from the CRP5 sequence were chemically synthesized adding an amino-terminal biotin molecule. Solid-phases were coated with 2 µg per well of 25HOCh into polystyrene 96-well plates. Binding of 0.05 µg biotinylated pepscan peptides, detection with peroxidase-labelled streptavidin and staining with OPD were then performed. For the *in silico* docking predictions, the modeled pepscan peptides with the lowest ΔG energies in solution were docked to all possible conformations of 25HOCh. **n° peptide**, position of the middle amino acid of each 15-mer peptide of the pepscan. **1,2,3,4...**, number of replicas of 25HOCh-binding or predicted 25HOCh-CRP5 conformations of 25HOCh in the 25HOCh-CRP5 complexes. **±sd**, standard deviations. **Poses**, list of ΔG of the predicted complexes for the different conformations of 25HOCh when docked to the CRP5 peptides. **docking best pose**, the pose which resulted in the best fitting to the 25HOCh-binding data. **Bold gray background**, 25HOCh-binding data which was represented in Fig 4A which was represented in Fig 4A. **Bold yellow background**, predicted Kcal/mol ΔG of peptide docking to 25HOCh which best fitted the binding data. *, non-significant highest ΔG energies > -1.1 were adjusted to -2.5 Kcal/mol for best fitting the binding data. (XLSX)

S6 Table. Number of amino acids per position after alignment among EST-derived amino acid sequences of CRP5 and CRP5 transcript variants. Transcript variants corresponding to the zebrafish *crp5* gene were retrieved from UniGene Dr.124528-Dr.162306. ORFs > 100 amino acids were translated by the Virtual Ribosome software (<http://www.cbs.dtu.dk/services/VirtualRibosome/>), numbered without their signal peptides (¹FKNL... in CRP5) and aligned to the sequence of CRP5 (BC121777). **Amino acid**, amino acids written in the three or single letter code. **Number**, different amino acids per position in CRP5 and CRP5 EST-derived variants. (XLSX)

Acknowledgments

We are grateful to Paula Perez Gonzalez who helped with the experimentation. Dr.Jose Antonio Encinar and Dra. Marcela Giudici from the IBMC-UMH, revised the docking prediction data and helped to perform gel electrophoresis experiments under native conditions, respectively. Melissa Bello-Perez was supported by the Generalidad Valenciana, fellowship ACIF/2016.

Author Contributions

Conceptualization: Luis Perez, Julio Coll.

Formal analysis: Julio Coll.

Funding acquisition: Beatriz Novoa, Luis Perez.

Investigation: Melissa Bello-Perez, Alberto Falco, Julio Coll.

Methodology: Melissa Bello-Perez, Alberto Falco.

Resources: Beatriz Novoa, Luis Perez.

Supervision: Beatriz Novoa, Luis Perez, Julio Coll.

Writing – original draft: Luis Perez, Julio Coll.

Writing – review & editing: Luis Perez, Julio Coll.

References

1. Bottazzi B, Inforzato A, Messa M, Barbagallo M, Magrini E, et al. (2016) The pentraxins PTX3 and SAP in innate immunity, regulation of inflammation and tissue remodelling. *J Hepatol* 64: 1416–1427. <https://doi.org/10.1016/j.jhep.2016.02.029> PMID: 26921689
2. Falco A, Cartwright JR, Wiegertjes GF, Hoole D (2012) Molecular characterization and expression analysis of two new C-reactive protein genes from common carp (*Cyprinus carpio*). *Dev Comp Immunol* 37: 127–138. <https://doi.org/10.1016/j.dci.2011.10.005> PMID: 22079493
3. Wang J, Tang B, Liu X, Wu X, Wang H, et al. (2015) Increased monomeric CRP levels in acute myocardial infarction: a possible new and specific biomarker for diagnosis and severity assessment of disease. *Atherosclerosis* 239: 343–349. <https://doi.org/10.1016/j.atherosclerosis.2015.01.024> PMID: 25682033
4. Braig D, Nero TL, Koch HG, Kaiser B, Wang X, et al. (2017) Transitional changes in the CRP structure lead to the exposure of proinflammatory binding sites. *Nat Commun* 8: 14188. <https://doi.org/10.1038/ncomms14188> PMID: 28112148
5. McFadyen JD, Kiefer J, Braig D, Loseff-Silver J, Potempa LA, et al. (2018) Dissociation of C-Reactive Protein Localizes and Amplifies Inflammation: Evidence for a Direct Biological Role of C-Reactive Protein and Its Conformational Changes. *Front Immunol* 9: 1351. <https://doi.org/10.3389/fimmu.2018.01351> PMID: 29946323
6. Chen R, Qi J, Yuan H, Wu Y, Hu W, et al. (2015) Crystal structures for short-chain pentraxin from zebrafish demonstrate a cyclic trimer with new recognition and effector faces. *J Struct Biol* 189: 259–268. <https://doi.org/10.1016/j.jsb.2015.01.001> PMID: 25592778
7. Bello-Perez M, Falco A, Medina-Gali R, Pereiro P, Encinar JA, et al. (2017) Neutralization of viral infectivity by zebrafish c-reactive protein isoforms. *Mol Immunol* 91: 145–155. <https://doi.org/10.1016/j.molimm.2017.09.005> PMID: 28915434
8. Inforzato A, Doni A, Barajon I, Leone R, Garlanda C, et al. (2013) PTX3 as a paradigm for the interaction of pentraxins with the complement system. *Semin Immunol* 25: 79–85. <https://doi.org/10.1016/j.smim.2013.05.002> PMID: 23747040
9. Vilahur G, Badimon L (2015) Biological actions of pentraxins. *Vascul Pharmacol* 73: 38–44. <https://doi.org/10.1016/j.vph.2015.05.001> PMID: 25962566
10. Caprio V, Badimon L, Di Napoli M, Fang WH, Ferris GR, et al. (2018) pCRP-mCRP Dissociation Mechanisms as Potential Targets for the Development of Small-Molecule Anti-Inflammatory Chemotherapeutics. *Front Immunol* 9: 1089. <https://doi.org/10.3389/fimmu.2018.01089> PMID: 29892284
11. Bang R, Marnell L, Mold C, Stein MP, Clos KT, et al. (2005) Analysis of binding sites in human C-reactive protein for Fc $\{\gamma\}$ R II , Fc $\{\gamma\}$ R IIA , and C1q by site-directed mutagenesis. *J Biol Chem* 280: 25095–25102. <https://doi.org/10.1074/jbc.M504782200> PMID: 15878871
12. Lu J, Marjon KD, Mold C, Du Clos TW, Sun PD (2012) Pentraxins and Fc receptors. *Immunol Rev* 250: 230–238. <https://doi.org/10.1111/j.1600-065X.2012.01162.x> PMID: 23046133
13. Wu Y, Potempa LA, El Kebir D, Filep JG (2015) C-reactive protein and inflammation: conformational changes affect function. *Biol Chem* 396: 1181–1197. <https://doi.org/10.1515/hsz-2015-0149> PMID: 26040008
14. Eisenhardt SU, Habersberger J, Peter K (2009) Monomeric C-reactive protein generation on activated platelets: the missing link between inflammation and atherothrombotic risk. *Trends Cardiovasc Med* 19: 232–237. <https://doi.org/10.1016/j.tcm.2010.02.002> PMID: 20382347
15. Eisenhardt SU, Thiele JR, Bannasch H, Stark GB, Peter K (2009) C-reactive protein: how conformational changes influence inflammatory properties. *Cell Cycle* 8: 3885–3892. <https://doi.org/10.4161/cc.8.23.10068> PMID: 19887916

16. Li HY, Wang J, Meng F, Jia ZK, Su Y, et al. (2016) An Intrinsically Disordered Motif Mediates Diverse Actions of Monomeric C-reactive Protein. *J Biol Chem* 291: 8795–8804. <https://doi.org/10.1074/jbc.M115.695023> PMID: 26907682
17. Wang MY, Ji SR, Bai CJ, El Kebir D, Li HY, et al. (2011) A redox switch in C-reactive protein modulates activation of endothelial cells. *FASEB J* 25: 3186–3196. <https://doi.org/10.1096/fj.11-182741> PMID: 21670067
18. Lv JM, Lu SQ, Liu ZP, Zhang J, Gao BX, et al. (2018) Conformational folding and disulfide bonding drive distinct stages of protein structure formation. *Sci Rep* 8: 1494. <https://doi.org/10.1038/s41598-018-20014-y> PMID: 29367639
19. Bello M, Falco A, Medina R, Encinar JA, Novoa B, et al. (2017) Structure and functionalities of the human c-reactive protein compared to the zebrafish multigene family of c-reactive-like proteins. *Developmental & Comparative Immunology* 69: 33–40.
20. Estepa A, Coll JM (2015) Innate multigene family memories are implicated in the viral-survivor zebrafish phenotype. *Plos One* 10: e0135483. <https://doi.org/10.1371/journal.pone.0135483> PMID: 26270536
21. Garcia-Valtanen P, Martinez-Lopez A, Lopez-Munoz A, Bello-Perez M, Medina-Gali RM, et al. (2017) Zebra Fish Lacking Adaptive Immunity Acquire an Antiviral Alert State Characterized by Upregulated Gene Expression of Apoptosis, Multigene Families, and Interferon-Related Genes. *Front Immunol* 8: 121. <https://doi.org/10.3389/fimmu.2017.00121> PMID: 28243233
22. Shrivastava AK, Singh HV, Raizada A, Singh SK (2015) C-reactive protein, inflammation and coronary heart disease. *The Egyptian Heart Journal* 67: 89–97.
23. Wu YP, Sun DD, Wang Y, Liu W, Yang J (2016) Herpes Simplex Virus Type 1 and Type 2 Infection Increases Atherosclerosis Risk: Evidence Based on a Meta-Analysis. *Biomed Res Int* 2016: 2630865. <https://doi.org/10.1155/2016/2630865> PMID: 27195284
24. Voulgaris T, Sevestianos VA (2016) Atherosclerosis as Extrahepatic Manifestation of Chronic Infection with Hepatitis C Virus. *Hepat Res Treat* 2016: 7629318. <https://doi.org/10.1155/2016/7629318> PMID: 26885388
25. Adinolfi LE, Zampino R, Restivo L, Lonardo A, Guerrera B, et al. (2014) Chronic hepatitis C virus infection and atherosclerosis: clinical impact and mechanisms. *World J Gastroenterol* 20: 3410–3417. <https://doi.org/10.3748/wjg.v20.i13.3410> PMID: 24707124
26. McKibben RA, Haberlen SA, Post WS, Brown TT, Budoff M, et al. (2016) A Cross-sectional Study of the Association Between Chronic Hepatitis C Virus Infection and Subclinical Coronary Atherosclerosis Among Participants in the Multicenter AIDS Cohort Study. *J Infect Dis* 213: 257–265. <https://doi.org/10.1093/infdis/jiv396> PMID: 26216904
27. Shah S, Ma Y, Scherzer R, Huhn G, French AL, et al. (2015) Association of HIV, hepatitis C virus and liver fibrosis severity with interleukin-6 and C-reactive protein levels. *AIDS* 29: 1325–1333. <https://doi.org/10.1097/QAD.0000000000000654> PMID: 25870985
28. Yang J, Gustavsson AL, Haraldsson M, Karlsson G, Norberg T, et al. (2017) High-affinity recognition of the human C-reactive protein independent of phosphocholine. *Org Biomol Chem* 15: 4644–4654. <https://doi.org/10.1039/c7ob00684e> PMID: 28513744
29. Trott O, Olson AJ (2010) AutoDock Vina: improving the speed and accuracy of docking with a new scoring function, efficient optimization, and multithreading. *J Comput Chem* 31: 455–461. <https://doi.org/10.1002/jcc.21334> PMID: 19499576
30. Dallakyan S, Olson AJ (2015) Small-molecule library screening by docking with PyRx. *Methods Mol Biol* 1263: 243–250. https://doi.org/10.1007/978-1-4939-2269-7_19 PMID: 25618350
31. Shityakov S, Forster C (2014) In silico predictive model to determine vector-mediated transport properties for the blood-brain barrier choline transporter. *Adv Appl Bioinform Chem* 7: 23–36. <https://doi.org/10.2147/AABC.S63749> PMID: 25214795
32. Fijan N, Petrinec Z, Sulimanovic D, Zwillichberg LO (1971) Isolation of the viral causative agent from the acute form of infectious dropsy of carp. *Veterinary Archives* 41: 125–138.
33. ICTV (2015) Implementation of taxon-wide non-Latinized binomial species names in the family *Rhabdoviridae*. *Rhabdoviridae Study Group*: 9.
34. Perez-Filgueira DM, Resino-Talavan P, Cubillos C, Angulo I, Barderas MG, et al. (2007) Development of a low-cost, insect larvae-derived recombinant subunit vaccine against RHDV. *Virology* 364: 422–430. <https://doi.org/10.1016/j.virol.2007.03.016> PMID: 17434554
35. Smith PK, Krohn RI, Hermanson GT, Mallia AK, Gartner FH, et al. (1985) Measurement of protein using bicinchoninic acid. *Anal Biochem* 150: 76–85. PMID: 3843705
36. Biro A, Cervenak L, Balogh A, Lorincz A, Uray K, et al. (2007) Novel anti-cholesterol monoclonal immunoglobulin G antibodies as probes and potential modulators of membrane raft-dependent immune functions. *J Lipid Res* 48: 19–29. <https://doi.org/10.1194/jlr.M600158-JLR200> PMID: 17023738

37. Torrent F, Villena A, Lee PA, Fuchs W, Bergmann SM, et al. (2016) The amino-terminal domain of ORF149 of koi herpesvirus is preferentially targeted by IgM from carp populations surviving infection. *Arch Virol* 161: 2653–2665. <https://doi.org/10.1007/s00705-016-2934-4> PMID: 27383208
38. Coll JM (2018) Herpesvirus infection induces both specific and heterologous anti-viral antibodies in carp. *Frontiers in Immunology* 9.
39. Neron B, Menager H, Maufrais C, Joly N, Maupetit J, et al. (2009) Mobyle: a new full web bioinformatics framework. *Bioinformatics* 25: 3005–3011. <https://doi.org/10.1093/bioinformatics/btp493> PMID: 19689959
40. Estepa A, Coll JM (1996) Pepscan mapping and fusion related properties of the major phosphatidylserine-binding domain of the glycoprotein of viral hemorrhagic septicemia virus, a salmonid rhabdovirus. *Virology* 216: 60–70. <https://doi.org/10.1006/viro.1996.0034> PMID: 8615007
41. Estepa AM, Rocha AI, Mas V, Perez L, Encinar JA, et al. (2001) A protein G fragment from the Salmonid viral hemorrhagic septicemia rhabdovirus induces cell-to-cell fusion and membrane phosphatidylserine translocation at low pH. *Journal of Biological Chemistry* 276: 46268–46275. <https://doi.org/10.1074/jbc.M108682200> PMID: 11590161
42. Biasini M, Bienert S, Waterhouse A, Arnold K, Studer G, et al. (2014) SWISS-MODEL: modelling protein tertiary and quaternary structure using evolutionary information. *Nucleic Acids Res* 42: W252–258. <https://doi.org/10.1093/nar/gku340> PMID: 24782522
43. Arnold K, Bordoli L, Kopp J, Schwede T (2006) The SWISS-MODEL workspace: a web-based environment for protein structure homology modelling. *Bioinformatics* 22: 195–201. <https://doi.org/10.1093/bioinformatics/bti770> PMID: 16301204
44. Guex N, Peitsch MC (1997) SWISS-MODEL and the Swiss-PdbViewer: an environment for comparative protein modeling. *Electrophoresis* 18: 2714–2723. <https://doi.org/10.1002/elps.1150181505> PMID: 9504803
45. Mariani V, Kiefer F, Schmidt T, Haas J, Schwede T (2011) Assessment of template based protein structure predictions in CASP9. *Proteins* 79 Suppl 10: 37–58.
46. Tanaka T, Robey FA (1983) A new sensitive assay for the calcium-dependent binding of C-reactive protein to phosphorylcholine. *J Immunol Methods* 65: 333–341. PMID: 6361145
47. Pepys MB (1981) C-reactive protein fifty years on. *Lancet* 1: 653–657. PMID: 6110874
48. Agrawal A, Xu Y, Ansardi D, Macon KJ, Volanakis JE (1992) Probing the phosphocholine-binding site of human C-reactive protein by site-directed mutagenesis. *J Biol Chem* 267: 25353–25358. PMID: 14600031
49. Volanakis JE (2001) Human C-reactive protein: expression, structure, and function. *Mol Immunol* 38: 189–197. PMID: 11532280
50. Zhu X, Xiao S, Zhou D, Sollogoub M, Zhang Y (2018) Design, synthesis and biological evaluation of water-soluble per-O-methylated cyclodextrin-C60 conjugates as anti-influenza virus agents. *Eur J Med Chem* 146: 194–205. <https://doi.org/10.1016/j.ejmech.2018.01.040> PMID: 29407950
51. Danthi P, Chow M (2004) Cholesterol removal by methyl-beta-cyclodextrin inhibits poliovirus entry. *J Virol* 78: 33–41. <https://doi.org/10.1128/JVI.78.1.33-41.2004> PMID: 14671085
52. Desplanques AS, Nauwynck HJ, Vercauteren D, Geens T, Favoreel HW (2008) Plasma membrane cholesterol is required for efficient pseudorabies virus entry. *Virology* 376: 339–345. <https://doi.org/10.1016/j.virol.2008.03.039> PMID: 18471850
53. Glisoni RJ, Castra EF, Cavallaro LV, Moglioni AG, Sosnik A (2015) Complexation of a 1-Indanone Thiosemicarbazone with Hydroxypropyl-beta-Cyclodextrin Enhances Its Activity Against a Hepatitis C Virus Surrogate Model. *J Nanosci Nanotechnol* 15: 4224–4228. PMID: 26369033
54. Fujita H, Tamai K, Kawachi M, Saga K, Shimbo T, et al. (2011) Methyl-beta cyclodextrin alters the production and infectivity of Sendai virus. *Arch Virol* 156: 995–1005. <https://doi.org/10.1007/s00705-011-0938-7> PMID: 21311919
55. Tian Z, Si L, Meng K, Zhou X, Zhang Y, et al. (2017) Inhibition of influenza virus infection by multivalent pentacyclic triterpene-functionalized per-O-methylated cyclodextrin conjugates. *Eur J Med Chem* 134: 133–139. <https://doi.org/10.1016/j.ejmech.2017.03.087> PMID: 28411453
56. Yang Q, Zhang Q, Tang J, Feng WH (2015) Lipid rafts both in cellular membrane and viral envelope are critical for PRRSV efficient infection. *Virology* 484: 170–180. <https://doi.org/10.1016/j.virol.2015.06.005> PMID: 26115164
57. Pereiro P, Forn-Cuni G, Dios S, Coll J, Figueras A, et al. (2017) Interferon-independent antiviral activity of 25-hydroxycholesterol in a teleost fish. *Antiviral Res* 145: 146–159. <https://doi.org/10.1016/j.antiviral.2017.08.003> PMID: 28789986
58. Dong H, Zhou L, Ge X, Guo X, Han J, et al. (2018) Antiviral effect of 25-hydroxycholesterol against porcine reproductive and respiratory syndrome virus in vitro. *Antivir Ther*.

59. Ji SR, Wu Y, Zhu L, Potempa LA, Sheng FL, et al. (2007) Cell membranes and liposomes dissociate C-reactive protein (CRP) to form a new, biologically active structural intermediate: mCRP(m). *FASEB J* 21: 284–294. <https://doi.org/10.1096/fj.06-6722com> PMID: 17116742
60. Gold ES, Diercks AH, Podolsky I, Podyminogin RL, Askovich PS, et al. (2014) 25-Hydroxycholesterol acts as an amplifier of inflammatory signaling. *Proc Natl Acad Sci U S A* 111: 10666–10671. <https://doi.org/10.1073/pnas.1404271111> PMID: 24994901
61. Civra A, Cagno V, Donalisio M, Biasi F, Leonardiuzzi G, et al. (2014) Inhibition of pathogenic non-enveloped viruses by 25-hydroxycholesterol and 27-hydroxycholesterol. *Sci Rep* 4: 7487. <https://doi.org/10.1038/srep07487> PMID: 25501851
62. Shrivastava-Ranjan P, Bergeron E, Chakrabarti AK, Albarino CG, Flint M, et al. (2016) 25-Hydroxycholesterol Inhibition of Lassa Virus Infection through Aberrant GP1 Glycosylation. *MBio* 7.
63. Potempa LA, Yao ZY, Ji SR, Filep JG, Wu Y (2015) Solubilization and purification of recombinant modified C-reactive protein from inclusion bodies using reversible anhydride modification. *Biophys Rep* 1: 18–33. <https://doi.org/10.1007/s41048-015-0003-2> PMID: 26942216
64. Magnadottir B, Hayes P, Gisladottir B, Bragason B, Hristova M, et al. (2018) Pentraxins CRP-I and CRP-II are post-translationally demarcated and differ in tissue specificity in cod (*Gadus morhua* L.) ontogeny. *Dev Comp Immunol* 87: 1–11. <https://doi.org/10.1016/j.dci.2018.05.014> PMID: 2977771
65. Taylor KE, van den Berg CW (2007) Structural and functional comparison of native pentameric, denatured monomeric and biotinylated C-reactive protein. *Immunology* 120: 404–411. <https://doi.org/10.1111/j.1365-2567.2006.02516.x> PMID: 17163961
66. Potempa LA, Maldonado BA, Laurent P, Zemel ES, Gewurz H (1983) Antigenic, electrophoretic and binding alterations of human C-reactive protein modified selectively in the absence of calcium. *Mol Immunol* 20: 1165–1175. PMID: 6656768
67. Falco A, Cartwright JR, Wiegertjes GF, Hoole D (2012) Molecular characterization and expression analysis of two new C-reactive protein genes from common carp (*Cyprinus carpio*). *Developmental and Comparative Immunology* 37: 127–138. <https://doi.org/10.1016/j.dci.2011.10.005> PMID: 22079493
68. Widziolek M, Prajsnar TK, Tazzymann S, Stafford GP, Potempa J, et al. (2016) Zebrafish as a new model to study effects of periodontal pathogens on cardiovascular diseases. *Sci Rep* 6: 36023. <https://doi.org/10.1038/srep36023> PMID: 27777406
69. Zieden B, Kaminskas A, Kristenson M, Kucinskiene Z, Vessby B, et al. (1999) Increased plasma 7 beta-hydroxycholesterol concentrations in a population with a high risk for cardiovascular disease. *Arterioscler Thromb Vasc Biol* 19: 967–971. PMID: 10195924

PUBLICACIÓN 4

TÍTULO: Zebrafish C-reactive protein isoforms inhibit SVCV replication by blocking autophagy through the interaction with cell membrane cholesterol

COAUTORES: Melissa Belló Pérez, Patricia Pereiro González, Julio Coll Morales, Beatriz Novoa García, Luis Perez García-Estañ, Alberto Falcó Graciá.

REVISTA: Autophagy (enviada a fecha 15/05/19)

**Zebrafish C-reactive protein isoforms inhibit SVCV replication by blocking
autophagy through the interaction with cell membrane cholesterol**

Melissa Bello-Perez¹, Patricia Pereiro², Julio Coll³, Beatriz Novoa², Luis Perez^{1,*}and Alberto Falco^{1,*}

¹Instituto de Investigación, Desarrollo e Innovación en Biotecnología Sanitaria de Elche (IDiBE) and Instituto de Biología Molecular y Celular (IBMC), Miguel Hernández University (UMH), 03202 Elche, Spain.

²Instituto de Investigaciones Marinas (IIM), Consejo Superior de Investigaciones Científicas (CSIC), 36208 Vigo, Spain.

³Instituto Nacional de Investigaciones y Tecnologías Agrarias y Alimentarias (INIA), Dpto. Biotecnología, 28040 Madrid, Spain.

To whom correspondence should be addressed:

* Dr. Alberto Falco, Institute of Research, Development and Innovation in Biotechnology of Elche (IDiBE) and Molecular and Cellular Biology Institute (IBMC), Miguel Hernández University (UMH), Edificio Torregaitán. Avenida de la Universidad. 03202 Elche (Alicante, Spain). Tel.: +34-96 65 89 53; Fax +34- 96 665 87 58; E-mail: alber.falco@umh.es

* Dr. Luis Perez, Institute of Research, Development and Innovation in Biotechnology of Elche (IDiBE) and Molecular and Cellular Biology Institute (IBMC), Miguel Hernández University (UMH), EdificioTorregaitán. Avenida de la Universidad. 03202 Elche (Alicante, Spain). Tel.: +34-96 65 84 35; Fax +34-96 665 87 58; E-mail: luis.perez@umh.es

E-mail addresses:

M.B.-P., melissa.bello@goumh.es

P.P., patriciapereiro@iim.csic.es

J.C., juliocoll@inia.es

B.N., beatriznovoa@iim.csic.es

L.P., luis.perez@umh.es

A.F., alber.falco@umh.es

Abstract

In the present work, the mechanisms involved in the recently reported antiviral activity against fish spring viremia of carp rhabdovirus (SVCV) are explored for the isoforms of zebrafish C-reactive like-protein (CRP1-7), confirming them to induce an antiviral state in the host. Experimental evidence ruled out the blocking of the attachment/binding step of the viral replication cycle as well as the direct inhibition of the G protein fusion activity or the stimulation of the host's interferon system. Further results showed that the antiviral protection conferred by CRP1-7 was mainly due to the inhibition of autophagic processes, and then adding extra and unexpected properties to the extensive list of activities reported for CRPs. In this sense, given the high affinity of CRPs for cholesterol and the described influence of the cholesterol balance in lipid rafts on autophagy, both methyl- β -cyclodextrin (a cholesterol-complexing agent) and 25-hydroxycholesterol (with reported antiviral properties) were used to further explore such activity from CRPs. In this way, all these compounds revealed to exert antiviral activity by affecting autophagy in a similar manner. Thus, in this work we propose that CRP reduces autophagy activity by initially disturbing cholesterol ratios in the host cellular membranes, what in turn affects the intracellular regulation of reactive oxygen species, as suggested from the abrogation of the anti-SVCV activity from these cholesterol-mediated modulators with antioxidant N-acetyl cysteine treatments. Altogether, this knowledge on the autophagy reducing activity of primitive vertebrate CRPs sheds light on their antiviral mechanisms, opening a new research field with potential medical implications.

Keywords

CRP, zebrafish, rhabdovirus, SVCV, antiviral, autophagy, 25-HOC, MBCD, cholesterol, endocytosis

Introduction

The fine-tuned response of the human plasma C-reactive protein (CRP) levels to infection, inflammation or trauma, makes this predominant acute phase protein (APP) one of the most studied health biomarkers, which has been associated with predictive significance to cardiovascular risks and diseases.¹⁻³ In humans, CRP is the prototypic APP². Thus, in response to an acute phase response (APR) inducing stimulus, the pro-inflammatory mediator interleukin 6 (IL6) mediates the production and release into the blood of CRP from primarily the liver⁴. As a consequence, circulating CRP levels may increase by as much as 10³-fold from barely detectable basal concentrations².

Human CRP is the canonical member of the pentraxin protein family^{3,5}. Pentraxins have an annular pentameric structural symmetry of its circulating form, as described for human ones,⁶ and their monomers are characterized by the presence of a C-terminal domain of about 200 amino acid residues containing the so-called “pentraxin signature”, an 8 amino acid residue-long conserved sequence (HxCxS/TWxS).⁷⁻⁹ Those pentraxins consisting in just this basic domain are termed “classical” or short pentraxins and entail CRP and serum-amyloid P component (SAP),³ while the presence of an additional N-terminal unrelated region classifies them into “fusion” or long pentraxins, which prototypic representative is the pentraxin 3 (PTX3).¹⁰ Human CRP and SAP show high degree of sequence identity (51%)⁹, analogous molecular structures and functions^{6,11,12} and overlapping ligand specificities.^{8,13} Then, it is not surprising that short pentraxins show species-, as well as strain- and gender- (i.e. hormonal-), interchangeable acute phase reactivity.^{2,14-18}

The polarized planar structure of circulating CRP molecules with opposite ligand-recognition and multifunctional-effector faces defines them as soluble pattern-recognition receptors endowed with crucial innate immune activities.^{1,13} It is extensively reported the ability of human pentameric CRP to recognize and bind, in a Ca²⁺-dependent manner, surface-exposed phospholipid heads, preferentially phosphorylcholine.¹⁹ Phosphorylcholine works not only as pathogen-associated molecular pattern (PAMP) since it is present in the lipoteichoic acid and LPS of some gram-positive and -negative bacteria, respectively,^{13,20-22} but also as danger-associated molecular pattern (DAMP) due to its phospholipase A2-mediated exposition^{23,24} in altered lipid bilayers of damaged, apoptotic and necrotic cells.^{20,25,26} The Ca²⁺-dependent phosphorylcholine-binding site of soluble CRP is also involved in interactions with oxidized LDL,²³ nuclear materials such as chromatin, histones, small nuclear ribonucleoproteins,^{27,28} as

PUBLICACIÓN 4

well as with polysaccharides, galactans and other compounds, which may not contain phosphorylcholine but are abundant in bacteria,²⁹ fungi^{30,31} and parasites.^{32,33}

Due to its clinical implications, CRPs have been mostly studied in humans. Thus, it is not surprising that existing comparative studies would reasonably question not only the denomination "pentraxin" in itself to this family of molecules because of the occurrence of several different oligomerization forms between species,^{34,35} but also the current classification of short pentraxins into CRPs and SAPs, whose differential properties found in humans have been shown to overlap and even be the opposite in other species.^{13,15,36,37} However, in general terms, these studies have shown that the aforementioned fundamental activities associated with short pentraxins in humans are evolutionarily conserved, what is certainly due to the sharing of both homologous sequences that correspond to functionally important motifs and analogous molecular structures.^{12,13,37-40}

In mammals, CRPs are usually overexpressed during both viral and bacterial infections;⁴¹ however, despite high serum levels of CRP level are more characteristic of bacterial infections, going up to 3 logs, those originated by viruses induce lower but significant 10¹ levels.^{2,41,42} Furthermore, the few existing studies analyzing C-reactive-like protein (CRP) levels in fish show moderate serum levels in response to both bacterial and viral infections, suggesting an antiviral effect for CRPs.⁴³⁻⁴⁵ Thus, in common carp (*Cyprinus carpio*), serum CRP level increases up to 2-, 6-and 10-fold in response to *Aeromonas salmonicida*,⁴⁶ *Aeromonas hydrophila*⁴³ and cyprinid herpesvirus-3 (CyHV-3)⁴⁴ infections, respectively.

Further positive correlations between fish CRP levels and viral infections have been established in this context by transcriptional analysis. For instance, significant upregulations of fish *crp* gene expression in several immune- and non-immune-related tissues of diverse species have been revealed in response to viruses such as CyHV-3,⁴⁴ red seabream iridovirus (RSIV),⁴⁷⁻⁴⁹ viral hemorrhagic septicemia virus (VHSV)^{50,51} and spring viremia of carp virus (SVCV).^{51,52} Similarly, higher transcriptional expression for *crp* genes were observed in common carp treated with polyinosinic:polycytidylic acid (polyI:C, a compound mimicking viral dsRNA),⁴⁵ in orally DNA-vaccinated rainbow trout (*Oncorhynchus mykiss*)⁵³ and zebrafish (*Danio rerio*) embryos microinjected with an expression plasmid encoding the *il6* gene,⁵¹ a cytokine also shown to be upregulated in response to viral infections in human.⁵⁴

In this sense, our recent findings show that all previously-identified zebrafish CRP1-7 isoforms⁵⁵ confer *in vitro* and *in vivo* isoform-dependent anti-SVCV protection⁵⁶ and exert unexpected anti-SVCV synergistic effects⁵⁶ with 25-hydroxycholesterol (25-HOC).⁵⁷

Recombinant tongue sole (*Cynoglossus semilaevis*) CRP has been also reported to enhance host resistance to RSIV infection when intraperitoneally (i.p.) co-injected with the virus inoculum.⁴⁹ However, despite their great relevance for evolutionary immunology and therapeutic potential, the corresponding mechanisms that underlie any of these CRP anti-viral effects are not yet known. The present work has been focused on these mechanistic aspects.

Results

CRP1-7 anti-SVCV activity targets host cells rather than virus

Our previous studies had shown that pre-incubation of supernatants from *epithelioma papulosum cyprinid* (EPC) cells transfected with zebrafish CRP1-7 (CRP1-7) with EPC cells inhibited SVCV infection;^{51,56} however, whether such anti-viral activity might be due to the interaction of CRP1-7 with viral particles remains to be demonstrated. In order to determine the stage of the viral cycle at which CRP1-7 might act, CRP1-7 treatments were added at different time-points within an SVCV infection (see diagram insets in Fig. 1 for further details). Thus, when either EPC cells (Fig. 1A) or SVCV (Fig. 1B) were treated with CRP1-7 prior to the viral adsorption stage, similar inhibitory activity on SVCV replication was observed for all CRPs (CRP2-6 inhibition range of 47.1-76.2%) except for CRP1 and CRP7. In these assays, non-significant differences among different exposure times (i.e., 2h and 20 h) were obtained and 2 h pre-treatments were enough to achieve maximum inhibitions within these experimental settings (Fig. 1A, B). Also, moderate SVCV replication inhibitions were found when treatments were restricted to the adsorption stage (Fig. 1C), what it can be considered as a 0 h pre-treatment with SVCV as in Fig. 1B. Actually, significant inhibitory effects were found for CRP2, 4 and 5 ($55.6 \pm 11.8\%$, $54.2 \pm 6.2\%$ and $46.6 \pm 16.3\%$, respectively) in comparison to the control treatment (supernatants from EPC cells transfected with green fluorescent protein (GFP)) (Fig. 1C). Taken together these results suggest that CRP antiviral activity may be due to a protective effect on the EPC cells. On the contrary, the duration of the treatment when added just after the adsorption stage did significantly affect the inhibitory activity ($P<0.001$). Particularly, the inhibitory effect of CRP2-7 on SVCV replication significantly increased when these treatments lasted 20 h (52.3-84.2%) in comparison to the 2 h ones (12.1-27.7%), which were not significantly higher than their corresponding GFP controls (Fig. 1D).

It should be noted that, using this same methodology, we also proceeded to determine that the antiviral activity induced by CRP1-7 is actually due to their content on the corresponding CRPs. For this purpose, the ligand binding capacity of the CRPs for 25-HOC that

is described in our previous work⁵⁶ was used to deplete each CRP1-7. As observed in Supplementary Fig. S1, such depletion contributed significantly ($P < 0.001$) to decrease the inhibitory infection capacity of the CRP treatments. At an individual level, CRP2-6 depleted formulations significantly reduced their antiviral capacity with respect to their corresponding full supernatant. Since a direct correlation between anti-SVCV activity and CRP content could be established for CRP2-6, those were pooled to be tested in subsequent experiments (CRP-mix).

Anti-SVCV protection conferred by CRP is neither by hindering viral entry nor IFN-mediated

The time-dependent inhibitory activity observed in post-adsorption treatments with CRP (Fig. 1D) indicates that late stages of the viral replication cycle could be affected. However, this might also be a consequence of the prolonged treatment that inducing a continued protective state in the cells during viral infection and/or hindering the entry steps of the virus during several consecutive replication cycles. Since the results obtained in the pre-treatment assays (Fig. 1A-C) pointed to the latter mechanisms, subsequent efforts were focused on these possibilities.

The initial steps of the rhabdoviral replication cycle comprise the attachment of the virions to the cell surface, the binding of the rhabdoviral surface protein G to host's specific receptor/s, the endocytosis process and, finally, the fusion of viral and host endosomal membranes that allows the release of the viral genome and associated proteins into the cytosol.⁵⁸ Therefore, to study the influence of CRP1-7 on the attachment/binding of the viral particles to host cell membranes, EPC cells were inoculated with SVCV at multiplicity of infection (MOI) 1 together with CRP1-7 and incubated for 2 h at 4°C. After removing the non-attached viral particles, cell-bound SVCV were quantified by analyzing the abundance of viral n gene copies by reverse transcriptase quantitative polymerase chain reaction (RT-qPCR) (Fig. 2A). Results showed that the amount of n gene copies remained invariable regardless of the CRP1-7 treatment used. The effect of each of the CRP1-7 on the pH-dependent fusion ability of the protein G of SVCV was studied by performing a fusion assay in which, by lowering the pH of cell media to 6, the fusion conformation of the SVCV G protein located at the membrane of previously infected cells was triggered to generate cell-to-cell fusion with its surrounding cellular membranes resulting in quantifiable syncytia. Results showed that CRP1-7 did not exhibit any direct inhibitory effect on SVCV G protein-mediated membrane fusion, perhaps with the exception of CRP7 (fusion reduction of about 20% with $P < 0.05$) (Fig. 2B).

However, despite the fact that the above-mentioned assays had demonstrated that CRP1-7 did not alter the virus entry step directly (Fig. 2A, B), the analysis of viral RNA synthesis at early stages post-adsorption (Fig. 2C) by determining the levels of the viral *g* and *n* transcripts, showed that the treatment with CRP-mix decreased the expression levels of those viral genes as early as 4-5 h post-adsorption and suggests the implication of another inhibitory mechanism. For this reason, the ability of CRP1-7 to trigger the IFN system, the host's typical and evolutionary-conserved response to viral infections,⁵⁹ was examined. However, CRP1-7 did not significantly change the transcript levels of the IFN-stimulated *mx* gene (Fig. 2D). Similarly, conditioned supernatants from EPC cells treated with CRP1-7 for 2 h and collected 20 h later, potentially containing IFN if inducible by CRP1-7, did not protect EPC cells from SVCV infection (Fig. 2E).

CRP1-7 modulate the transcription of autophagy-related genes in vitro and in vivo

So far it seemed that CRP1-7 cause their anti-SVCV neutralizing activity by promoting an IFN-independent antiviral state in the treated cells. Thus we proceeded to explore such observation in an homologous experimental system constituted by the zebrafish-derived ZF4 cell line, since the EPC cell line comes from fat-head minnow (*Pimephales promelas*), another fish species within the same family (*Cyprinidae*).⁶⁰ Thus, the pre-treatment of ZF4 cells with CRP1-7 and CRP-mix for 2 h also protected from the infection with SVCV (Fig. 3A) like in EPC cells (Fig. 1A). Likewise, the analysis of the progression of the viral replication *in vitro* at early stages post-adsorption in ZF4 (Fig. 3B) exhibited also an analogous profile to that observed in EPC cells (Fig. 2C). For instance, the CRP-mix induced similar inhibition levels of SVCV replication in ZF4 and EPC cells (≥ 2 -fold at 4 h post-adsorption).

In agreement with the data obtained using EPC cells, the CRP-mix did not positively regulate the IFN-response in ZF4 (Fig. 3C). On the contrary, the analysis of the transcriptional response of both zebrafish *mxa* and *mxe* revealed to be significantly reduced over time by CRP-mix ($P < 0.001$ for both *mxa* and *mxe*). Remarkably, *mxa* lowest levels (2.5 folds at 2 h post-treatment) were already restored to basal levels at 4 h post-treatment, while *mxe* ones did not fully stabilize from their lowest levels (over 5 folds at 4 h post-treatment), at even the latest post-treatment time-point checked, which in this set of experiments with ZF4 cells extended to 20 h. Additionally, the transcript levels of the genes coding for zebrafish IFN γ 1 and 2 (*ifnphi1* and *ifnphi2*, respectively) showed similar profiles than *mxa*, reaching upregulations at 5 (*ifnphi1*, 1.7 ± 0.04 folds, $P < 0.01$) and 20 h (*ifnphi1*, 1.8 ± 0.2 , $P < 0.01$; *ifnphi2*, 2.1 ± 0.1 , $P < 0.01$) from their

corresponding lower levels at 0 h (*ifnphi1*, 0.6 ± 0.1 , $P<0.01$; *ifnphi2*, 0.4 ± 0.04 , $P<0.05$) (Supplementary Fig. S2). However, such small up-regulation of IFN-related genes could not explain observed antiviral protection rates.⁵⁹

We proceeded to investigate whether autophagy, recently associated with an evolutionarily-conserved antiviral response,⁶¹⁻⁶³ was involved in the neutralization of SVCV by CRP1-7. For this purpose, the transcript levels of some relevant genes related to the autophagic route were determined: *beclin1*, *wipi1*, *lc3a*, *atg5*, *gabarp* and *ambra1*. The results revealed that some of them were stimulated by CRP-mix in ZF4 cells (Fig. 3D). Particularly, *wipi1*, *ambra1* and *lc3a* transcript levels were moderately elevated (1.5 to 3.5 folds; $P<0.05-0.001$) during the initial stages after treatment with CRP-mix compared to control treatments (GFP). These transcriptional levels started to stabilize 5 h post-treatment and were fully restored after 20 h, except for *lc3a*, which was reduced (~2 folds, $P<0.05$). Similarly, the analysis of the transcriptional levels of the above mentioned autophagy-related genes in immune-related tissues such as spleen, liver and head kidney, after zebrafish were i.p. injected with the CRP-mix 2 days before, revealed not only that autophagy was transcriptionally modulated *in vivo* by CRPs, but also that such response was tissue-dependent. The highest levels were found in spleen for *beclin1* and *wipi1* and kidney for *wipi1* (Fig. 3E).

CRPs increase autophagosomes and modify their tissue distribution

Autophagy levels were further studied by analyzing the distribution of LC3 (a well described autophagy marker)^{64,65} in ZF4 cells treated with CRP-mix and GFP. Microscopic quantification of cytosolic LC3-positive fluorescent green-labelled puncta (a visible indicator of LC3 recruitment) showed increased autophagosome numbers after CRP-mix treatments (2.3 ± 0.6 folds, $P<0.05$) (see representative microscopic images and the resulting quantification graph in Fig. 4A).

To determine the influence of selected CRPs on the modulation of the autophagy *in vivo*, the fluorescence of GFP-LC3 was visualized at low magnification in GFP-LC3 transgenic zebrafish larvae. For this, one-cell embryo stage zebrafish were microinjected 3 days before observation with the pMCV1.4 plasmid coding for zebrafish *crp1*, 4 and 5, as well as *il6*. The recombinant overexpression of CRPs resulted in increased fluorescence specially in the yolk, indicating augmented basal autophagy levels in this organ compared to empty plasmid-injected larvae (Fig. 4B). Among the *crp* genes tested, *crp5* was the most active in inducing such effect; however, *il6* caused not only higher, but also wider-distributed fluorescence (Fig. 4B). Only LC3

fluorescence induced by *crp5* and *il6* was detected on the dorsal root ganglia. In this context, the analysis of LC3 induction of CRPs by IL6 revealed that, after i.p.injection of IL6 in EPC-transfected supernatants, the levels of transcripts of *crp3* (1.8 ± 0.1 folds, $P < 0.001$) and *crp5* (5.1 ± 0.8 folds, $P < 0.01$) significantly increased in zebrafish liver tissues, while the transcription of the other *crp* gene isoforms remained unchanged (Fig. S3).

Inhibition of autophagy with CRPs inhibits SVCV infection

The *in vitro* LC3 recruitment was also analyzed in response to SVCV in the presence/absence of CRP-mix (Fig. 5A). Thus, after infecting ZF4 cells with SVCV (MOI 1) for 4 h, no modulation of autophagosomes was apparent (0.7 ± 0.1 folds) in comparison to uninfected (GFP) control cells (1.0 ± 0.3). Further results showed that when SVCV infection was carried out in combination with the CRP-mix, autophagosomes significantly increased respect to SVCV infection alone (2.6 ± 1.1 folds) but remained similar to the CRP-mix treatment alone (2.3 ± 0.6 , Fig. 4A).

In line with these findings, the analysis of transcript expression of autophagy-related genes *in vitro* at early stages (0-5 h) after SVCV infection in the presence of the CRP-mix (Fig. 5B) revealed that the presence of SVCV caused a 2 h delay in the transcriptional modulation induced by CRP-mix treatments (Fig. 3D). In contrast, SVCV infection did not reduce the transcription levels of any of the autophagy-related genes, leading instead to increased transcription levels of *wipi1* (3.5 ± 1.1 folds at 4 h, $P < 0.01$; 4.9 ± 1.1 folds at 5 h, $P < 0.001$) and *atg5* (4.0 ± 0.6 folds at 5 h, $P < 0.001$). Regarding *lc3a*, significant increased levels were already detected at 3 h (1.9 ± 0.6 folds, $P < 0.05$) and remained high until the endpoint of the time-course (2.0 ± 0.3 folds at 4 h, $P < 0.05$; 2.4 ± 0.2 folds at 5 h, $P < 0.01$). These results also contrasted with the almost negligible transcript levels found for these genes in an identical time-course experiment but in the absence of CRPs (Supplementary Fig. S4). In this latter case, only significant reductions were observed for *wipi1* and *lc3a* at 0 h (~2 folds in both cases in comparison to non-infected cells).

Although the above commented results suggest that CRPs might be inducing autophagy, this is yet a controversial issue in rhabdovirus infections.^{63,66-69} In this context, Fig. 5C shows that the pre-treatment of ZF4 cells with 3-methyladenine (3-MA), an inhibitor of PI3K-III and therefore an autophagy inhibitor,⁷⁰ neutralizes SVCV replication in a concentration-dependent manner, reaching neutralization levels of $87.4 \pm 1.6\%$ at the maximum concentration used (1 mM for 20 h), and thus confirming the requirement of the autophagic

process for SVCV replication. In turn, this result also suggests, at least in the present case, that the true effect of CRPs on autophagy is inhibitory. To check this hypothesis, the ability to neutralize the infection of SVCV was used as a functional assay in combination with some autophagy modulators comprising the inhibitors 3-MA and chloroquine (CQ, inhibitor of lysosome/endosome fusion)⁷¹ and the enhancer rapamycin (acting on mTOR)⁶⁴. Thus, Fig. 5D shows that while the treatment with the autophagy inhibitors neutralized the infectivity of SVCV (as it had already been shown for 3-MA in Fig. 5C), their antiviral effect was higher in combination with the CRP-mix. On the other hand, the treatment with 25 µM of rapamycin during 4 h favored the replication of SVCV (neutralization levels dropped to -78.9 ± 30.9%), but this enhancing effect was reversed by adding the CRP-mix (50.8 ± 1.4%) (Fig. 5C).

25-HOC and methyl-β-cyclodextrin (MBCD) interfere with the autophagocytic process

By using the experimental approach described above to study the involvement of autophagy in the antiviral effect of CRPs, we proceeded to test whether this mechanism was also associated with the antiviral activity of 25-HOC,^{57,72} a compound previously reported to act synergistically with CRPs.⁵⁶ Additionally, since the regulation of cholesterol had been already linked to the modulation of autophagy,⁷³ the effect of MBCD, a molecule with cholesterol-binding properties,^{74,75} was also tested.

First, this methodology was validated by comparing GFP (1.0 ± 0.3 folds) to CQ treatments (11.3 ± 0.4 folds, $P < 0.001$) (Fig. 6A), an aforementioned autophagy inhibitor of the last steps of the autophagic process with an autophagosome cumulative effect⁷¹. In this regard, autophagosome levels for CQ solvent control, i.e. 2.5% ethanol, were 0.5 ± 0.1 folds (Supplementary Fig. S5A). Then, the ability to modulate the recruitment of LC3 was analyzed in ZF4 cells in response to 25-HOC and MBCD in the presence/absence of CRP-mix. As Fig. 6B shows, after treating ZF4 cells with 25-HOC (10 µg/mL) or MBCD (4 mM) for 4 h, no modulation of the autophagosome was observed in any case (0.9 ± 0.2 folds for 25-HOC and 1.2 ± 0.2 folds for MBCD); whilst in combination with the CRP-mix, upregulations were found for both compounds, 16.1 ± 2.8 folds for 25-HOC and 7.3 ± 1.4 folds for MBCD, in comparison to the corresponding treatments without the CRP-mix ($P < 0.05$).

SVCV neutralizing assays performed by combining either 25-HOC or MBCD with the autophagy modulators (Fig. 6C) showed that the combinations of any of the cholesterol-targeting compounds with the autophagy inhibitors 3-MA or CQ increased the SVCV neutralizing activity of 25-HOC and MBCD when added alone. In contrast, the autophagy

enhancer rapamycin, which increased SVCV infectivity when added alone (neutralization levels of $-78.7 \pm 30.9\%$), reverted the SVCV neutralization induced by both 25-HOC (from $48.2 \pm 10.3\%$ to $-0.3 \pm 6.9\%$, $P < 0.001$) and MBCD (from $31.7 \pm 2.0\%$ to $-24.3 \pm 3.9\%$, $P < 0.001$). Similarly, the treatment with N-acetyl cysteine (NAC) (Fig. 6D), a hijacker of reactive oxygen species (ROS) with the ability to block/inhibit autophagy,⁷⁶ did not affect the replication of SVCV when used alone, but it did revert the inhibitory effect induced by the CRP-mix, 25-HOC and/or MBCD by ~50% (Fig 6C).

Discussion

The present work provides evidence on the antiviral activity mediated by CRP1-7, which is mainly due to the induction of a protective state in the host fish cells, rather than to a hampering effect on the viral particles. Evidence showed that the pre-incubation of the host cells with CRP1-7 before the inoculation of the virus is sufficient to inhibit viral infectivity (Fig. 1A and 3A). In this line, the time-independent nature observed in the neutralization properties of most CRP1-7 when co-incubated with the virus also supports this hypothesis and suggests that such antiviral activity is mainly due to the coexistence of CRPs and cells during the adsorption step (Fig. 1B, C); however, an isoform-specific action on viral replication with milder effects cannot be excluded yet. In addition, the inability of CRP1-7 to alter virus binding (Fig. 2A) together with their inhibitory effect on viral transcription at 4 h post-adsorption (Fig. 2C and 3B) suggests an early blockade of SVCV replication. In this context, only a few cases have been reported in which pentraxins directly interact with the viral particles or viral proteins, such as human SAP⁷⁷ and PTX3⁷⁸ against influenza A virus, but there are numerous studies describing different immunomodulatory properties of pentraxins on different cell types, although never related to antiviral protection.⁷⁹⁻⁸¹

The IFN system is an immune strategy widely used by lower vertebrates that is characterized by a very rapid response to a viral threat.⁵⁹ The activation of this system confers an antiviral state to the cells⁸² through the induction of effector molecules capable of limiting viral replication.⁸³ In this work, evidence showed that CRP1-7 do not trigger the IFN response since the incubation of both EPC and ZF4 cells with CRPs not only did not induce the expression of relevant *mx* nor *ifn* isoforms, but they were even repressed in some cases (Fig. 2D and 3C), what it is in accordance with other studies in humans.⁸⁴ Those results were also consistent with the lack of activity observed for conditioned media from EPC cells treated with CRP1-7 (Fig. 2E).

On the contrary, this work demonstrated for the first time that CRPs modulate the autophagic process at several levels, i.e., transcription (Fig. 3D, E), autophagic flux (Fig. 4A) and tissue distribution (Fig. 3E and 4B). Furthermore, such effect was not affected by the presence of SVCV (Fig. 5A, B). So far, such activity of CRPs had been only tangentially addressed by associating high levels of circulating mammalian CRPs with autophagic processes in the context of different dysfunctions/diseases. In this regard, a recent study using a transgenic approach describes significantly-reduced autophagy fluxes in the kidney from autophagy reporter mouse lines over-expressing rabbit CRP, and that such effect was rescued with rapamycin, what in turn it also reduced collateral renal injury.⁸⁵

The interaction of autophagy with the immune response to infections has been known for a long time.⁶¹ In the specific case of diseases of viral origin, it has been described that many viruses, including those of fish, activate/need autophagy for their replication.^{68,69,76,86-88} In this regard, there are some previous studies that have analyzed the influence of the autophagy on SVCV infection;^{63,67,68} however, the conclusions of these studies are contradictory when interpreting the activation of autophagy, as either a negative regulatory mechanism,^{63,67} or, more recently, a mechanism required by the virus for its replication⁶⁸. In view of this controversy, before checking whether the antiviral activity of the CRP1-7 is due to their ability to modulate autophagy, we first needed to clarify their effect on SVCV replication. Thus, in this work we showed that the autophagic process is required for SVCV replication, since infectivity is neutralized by the autophagy blockers CQ (Fig. 5D) and 3-MA (Fig. 5C, D). In any case, autophagy in fish has been under study only recently and therefore there is the possibility of data misinterpretations in the pioneering studies.

Additionally, autophagy blocking assays carried out by using CQ support the results observed with 3-MA. Inhibition of SVCVreplication was potentiated when the autophagy blockers were used in combination with CRPs, MBCD or 25-HOC. Therefore, together with the decrease in the neutralization of the infection when combining each of these three compounds with the autophagy-enhancer rapamycin,⁶⁴ these results indicate that the inhibition of SVCV infection observed when cells were treated with CRPs, MBCD or 25-HOC is due tothe blockade of either autophagy or an element common to autophagy and viral endocytosis pathways, as it has been also reported previously for the rabies virus.⁶⁶ For instance, in this sense there has been already described that autophagosomes may fuse with intermediate endosomes within a viral infection to form amphisomes.⁸⁹⁻⁹¹ Since CRP treatment of the cells resulted in an accumulation of autophagosomes, we suggest that the inhibitory effect on autophagy occurs at a late stage such as the fusion of autophagosomes and lysosomes, in a similar fashion as CQ^{71,92,93}.

Considering that lysosomes are vulnerable to oxidative stress,⁹⁴ in order to understand the mechanism by which CRPs, 25-HOC and MBCD might block the fusion of the autophagosome/intermediate endosome/amphisome with the lysosome, the possible involvement of ROS in this process was analyzed. The results showed a significant reduction of the antiviral effect of the three compounds after treatment with the oxidative stress inhibitor NAC,⁷⁶ suggesting that all three may cause their blocking effect on autophagy by increasing ROS levels. Such mechanism has been described for other autophagy inhibitors.⁹² Briefly, an increase of the ROS concentration induces an increase of the lysosomal pH that inhibits both the fusion of the lysosome with the autophagosome⁹² and the fusion conformation of the SVCV G protein that allows the viral particles to enter host's cytosol.^{58,95} Furthermore, these results would also be supported by the observed downregulation of the IFN system observed in response to CRP1-7, since it has also been described that the induction of the antiviral activity of the IFN system is sensitive to changes in the pH of lysosomes/endosomes produced by the CQ treatment.⁹⁶

In this work, we propose that CRPs, MBCD and 25-HOC increase the levels of intracellular ROS because of the sequestration/imbalance of membrane cholesterol, as it has been already described to induce the formation of ROS.^{97,98} In fact, the induction of ROS generation as a consequence of the interaction of the monomeric form of human CRP with lipid rafts in human and rat peripheral blood mononuclear cells has been also observed.⁹⁹ Thus, the high affinity for cholesterol described for MBCD^{74,75} and CRPs^{56,100,101} suggests they may display a cholesterol-sequestering activity with blocking effects on ROS-dependent autophagy. In the case of 25-HOC, when added to cells, would also impair lipid rafts composition with similar inhibitory consequences for autophagy. In contrast, other oxysterols, for instance 24S-hydroxycholesterol (24S-HOC),^{102,103} 7-ketocholesterol (7KC), 7β-hydroxycholesterol (7β-HOC)¹⁰³ and 27-HOC,¹⁰⁴ have been shown to activate autophagy. In this line, the modulation of autophagy in response to an exogenous lipid load both *in vitro* and *in vivo* has been already demonstrated. For instance: the treatment of hepatocytes with some lipids reduced the co-localization of lipid droplets with lysosomal-associated membrane protein 1 and the increase of fats in the diet of mice markedly decreased the number of autophagosomes that contain lipid droplets.¹⁰⁵ In fact, the treatment of ZF4 cells with cholesterol significantly increased the amount of intracellular autophagosomes and inhibited SVCV infectivity the same way as 25-HOC (Fig. S5A, B). Moreover, such inhibition was reverted by its use in combination with the cholesterol-sequestering MBCD (Fig. S5B). Therefore, we hypothesize that any imbalance in the cholesterol content of host's cellular membrane affects the ROS generation and consequently disturbs both

PUBLICACIÓN 4

the autophagic and SVCV replication processes (Fig. 7). In line with this hypothesis, there are studies that correlate the integrity of the lipid rafts with the upregulation of autophagy, mainly from the observation of the accumulation of autophagosomes and the increase of LC3B-II levels.^{74,75} However, considering our results and some recent advances on the study of autophagy, an inhibition of a late autophagic step cannot be entirely ruled out.⁷¹

Among the multiple physiological properties of some oxysterols, the ability to inhibit viral infections of 25-HOC^{72,106-109} and 27-HOC¹¹⁰ are some of the best described. According to our results, 25-HOC, as well as CRP2-6 and MBCD, inhibits the replication of SVCV *in vitro* by a mechanism related to ROS generation and autophagy. Nevertheless, treatment of cells with 25-HOC prior to infection with enveloped viruses blocks the fusion of the viral and cell membranes.^{72,111} This fact would fit in our proposed model since the ROS generation both increases the lysosomal pH and reduces the lysosomal fusion capacity with autophagosomes and endosomes, thus limiting the pH-dependent fusogenicity of the G protein of SVCV.

To conclude, this work proposes (Fig. 7) that SVCV requires some of the autophagic machinery to complete its entry steps into the host. Additionally, the treatment with either CRP2-6, 25-HOC, MBCD or any of their combinations induces the generation of ROS via the disruption of the cholesterol-rich membrane domains in the host cell membranes, increasing lysosomal pH as a consequence. SVCV replication would be then reduced not only by altering the low pH-dependent fusogenic capacity of the SVCV G protein, but mostly because an inefficient fusion of lysosomes with autophagosomes/intermediate endosomes/amphisomes. Since, there are evidences of the conservation of these mechanisms in higher vertebrates; this study may be pioneering in redirecting a research field with potential for a wide range of therapeutic applications.

Materials and Methods

Cell lines and virus

EPC cells from fat-head minnow, the most widely used cell line for research on fish viruses and the diagnosis of fish viral diseases, were purchased from the American Type Culture Collection (ATCC, Manassas, VA, USA, Ref. No. CRL-2872).⁶⁰ EPC cell monolayers were grown in Dutch-modified Roswell Park Memorial Institute (RPMI)-1640 culture medium (Sigma, St. Louis, USA), supplemented with 10% fetal bovine serum (FBS) (Sigma), 2 mM glutamine, 1 mM sodium pyruvate, 50 µg/mL gentamicin and 2 µg/mL of fungizone (Gibco BRL-Invitrogen, Carlsbad, CA, USA). The zebrafish embryonic fibroblast ZF4 cell line was

purchased from the ATCC (Ref. No. CRL-2050). ZF4 cells were cultured in Dulbecco's modified Eagle's medium (DMEM, Gibco BRL-Invitrogen) supplemented with 10% FBS and 100 µg/mL of primocin (InvivoGen, San Diego, CA, USA). Both cell lines were maintained at 28°C in a 5% CO₂ atmosphere.

The SVCV isolate 56/70 from common carp was replicated in EPC cells at 22°C in an atmosphere without CO₂ supply and by using previously described culture media for cell growth except for 2% FBS (infection media). After 7 days post-infection, infective supernatants were harvested, clarified by centrifugation at 4,000 g and 4°C for 30 min, aliquoted and stored at -80°C until use. Virus titers were determined by the focus forming assay as it is described below.

Animals

The adult XL wild type zebrafish of 700–900 mg of body weight (3–4 cm long) and embryos from transgenic GFP-Lc3 zebrafish that were used in this study were obtained by natural spawning from mating adults at one of the host institution facilities (Instituto de Investigaciones Marinas-CSIC, Vigo, Spain). Fish were maintained at 28°C in 30 L re-circulating water tanks by following established protocols.¹¹² Prior to handling, fish were anaesthetized by immersion in 100 mg/L tricaine methanesulfonate (MS-222) (Sigma). End-point fish euthanasia was performed by overdosing at 500 mg/L.

All experimental procedures with live zebrafish were performed in accordance with the Spanish Law for Animal Experimentation (Royal Executive Order, 53/2013) and the European Union directive 2010/63/UE. Animal trials procedures were approved by the local government ethics committee on animal experimentation (Dirección General de Agricultura, Ganadería y Pesca, Generalitat Valenciana) and the Project Evaluation Board of Miguel Hernández University (permit no. UMH.IBM.JFG.01.14), as well as the CSIC National Committee on Bioethics under approval number ES360570202001/16/FUN01/PAT.05/tipoE/BNG.

Production of CRP1-7-enriched, -depleted and -conditioned supernatants

The pMCV1.4 plasmids coding for each CRP1-7 from our previous studies^{51,56} were used as described therein to obtain cell-free supernatants enriched in CRP1-7 isoforms from 4-day transfected EPC cells. Likewise, their CRP content was characterized by ELISA, western blot and cholesterol-binding affinity.^{51,56} Similarly, the pMCV1.4 constructs with the genes coding for

PUBLICACIÓN 4

either GFP or zebrafish IL6 were used to obtain control supernatants without CRPs and supernatants enriched in IL6. For some particular experiments, a CRP2-6 equally mixed solution of supernatants (CRP-mix) was employed for different experiments. All supernatants were stored at -80°C until use.

To demonstrate that the antiviral activity of the CRP1-7 supernatants were due to the CRP1-7 proteins rather than to other possible CRP-induced EPC-derived compounds, the supernatants were CRP depleted by incubating them with solid-phase immobilized 25-HOC (Sigma), a lipid for which most CRP1-7 showed the highest affinity in our previous work.⁵⁶ Briefly, wells from Maxisorb 96-well plates (Nunc, Roskilde, Denmark) were coated to dryness with 100 µM of ethanol-dissolved 25-HOC and were kept dried until use. Then, after washing them 3 times with phosphate buffered saline (PBS), 100 µL of 4-fold-diluted CRP1-7 supernatants were added per well and incubated for 2 h. Finally, depleted supernatants were collected and stored at -80°C until use.

To produce CRP-conditioned supernatants, EPC cell monolayers were incubated for 2h at 22°C with CRP1-7 and, after 3 washes with EPC growth media, replaced with fresh EPC growth media and further incubated for 24 h at 22°C. Finally, these supernatants were collected, clarified as described before, aliquoted and stored at -80°C until use.

In vitro SVCV infectivity assays

To explore the effects of the experimental treatments on the replication of SVCV, several different infection assays on EPC and ZF4 cells were performed. In general, cells grown on 96-well plates were inoculated with SVCV supernatants in infection media at a MOI of 10⁻² SVCV per cell (unless stated otherwise) and incubated together for 2 h at a temperature of 4°C (the low temperature chosen to delay viral replication during the initial adsorption/binding step and synchronize viral replication). Then, the viral inoculants were removed, and the EPC cell monolayers washed 3 times with infection media in order to eliminate unattached SVCV particles. Subsequently, fresh infection media was added, and plates further incubated for 20h at 22°C.

Variations on this common procedure were used to investigate potential interactions of CRPs with either cells or SVCV. Thus, such variations were made by incubating i) CRP1-7 with SVCV or EPC before viral adsorption (pre-adsorption treatments), ii) CRP1-7 and cells together during the SVCV adsorption step (adsorption treatment) and iii) adding CRP1-7 after the SVCV

adsorption step (post-adsorption treatment). Diagrams describing such experimental designs are shown in Fig. 1A. After every incubation step, cell monolayers were washed 3 times with infection media.

SVCV focus forming assay

To assess the effect of the treatments on viral infectivity *in vitro*, SVCV-infection foci of 5-20 cells were immune-labelled to be quantified as previously described.¹¹³ Briefly, at 20h post-adsorption, cell monolayers were fixed with 4% formalin (Sigma) in PBS for 20 min and incubated for 24 h at 4°C with a 1:300 dilution of polyclonal anti-SVCV (BioX Diagnostics SA, Jemelle, Belgium) in antibody (Ab)-dilution buffer made of PBS containing 1% bovine serum albumin (BSA), 1% goat serum and 0.5% Triton X-100 (Sigma). After 3 washes with PBS, there was another incubation period with a FITC-labeled goat anti-mouse antibody (Sigma) diluted 1:300 in Ab-dilution buffer for 45 min at room temperature and protected from light. Finally, cell monolayers were washed 3 times with PBS again and immunofluorescence-labeled foci counted or photographed by means of a fluorescence DMI 3000B inverted microscope with an EL6000 compact light source and a DFC3000G digital camera (Leica, Bensheim, Germany). Data were expressed as percentages of neutralization, calculated by the formula: 100 - (number of foci in the treatment samples / number of foci in the control samples) × 100.

G protein-mediated fusion assays in SVCV-infected EPC cell monolayers

To assess the effect of the treatments on the ability of the SVCV surface G protein to fuse membranes, the G-dependent fusion activity was induced by lowering the pH of infected EPC cell monolayers and quantified by counting syncytia as previously described.¹¹³ Briefly, at 20 h post-adsorption, cell media was removed from SVCV infected EPC cell monolayers, which were washed 3times with infection media and then treated with CRP1-7 for 2 h at 22°C. After another 3 washes, G-dependent fusion was triggered by incubating the EPC cell monolayers with infection media at pH 6 (fusion media) for 30 min, washed 3 times again and subsequently incubated with infection media at pH 7.5 for 2h at 22°C. Finally, cell monolayers were fixed with cold methanol (-20°C) for 15 min, air dried, stained with Giemsa (5 mg/mL in PBS), washed 3 times with PBS and air dried. Syncytia resulting from the fusion of adjacent cells were then counted and photographed with mentioned-above microscope. Percentage of G protein-mediated syncytia was calculated by the formula: 100 × number of syncytia in treated EPC cell

PUBLICACIÓN 4

monolayers / number of syncytia in control (GFP-treated) EPC cell monolayers. Three different assays each by triplicate were performed per experiment. Results were shown as mean and standard deviations (s.d.).

Virus-cell binding assay

To study whether CRP1-7 inhibited the binding of SVCV to EPC cells SVCV supernatants (MOI 1) in the absence (GFP) or presence of CRP1-7 were incubated with EPC cell monolayers during the adsorption step (2 h at 4°C) and then washed 3 times with infection media to remove unattached SVCV. Thereafter, cell-bound SVCV was estimated by measuring the number of viral genomes derived from the detection copies of the SVCV *n* gene (primer sequences are shown in Supplementary Table S1), by RT-qPCR as described later.

Determination of SVCV replication levels in EPC cells at early stages post-adsorption

To determine whether CRPs affect SVCV replication at early stages post-adsorption, both EPC and ZF4 cell monolayers were incubated with CRP-mix for 2 h at 22°C. Then, cells were washed 3 times with infection media and inoculated with SVCV at MOI of 10⁻² for a further 2-h incubation at 4°C. After another 3 washes, fresh infection media was added and plates further incubated at 22°C. Infected cells were collected at 0, 1, 2, 3, 4 and 5 h post-adsorption for the subsequent analysis of their viral replication levels by performing RT-qPCR on SVCV *n* and *g* gene transcripts (primer sequences are shown in Supplementary Table S1).

Analysis of the transcriptional modulation of the interferon (IFN) system and autophagy

To assess whether CRPs were affecting the IFN system and/or autophagy at a transcriptional level, EPC cells were treated with CRP1-7 for 2 h at 22°C, washed 3 times with infection media and further incubated at 22°C. Samples were collected at 20 h post-treatment for the subsequent RT-qPCR analysis of the transcripts of *mx*, an IFN-stimulated gene commonly used as one of the best reporters of the IFN system response.⁵⁹ A similar procedure was followed with ZF4 cells except by using the CRP-mix and collecting samples at 1, 2, 3, 4, 5 and 20 h post-treatment. The genes analyzed in this latter case were the *mx* paralogs *mxa* and *mxe*, the IFN ϕ coding genes *ifnphi1* and *ifnphi2*, and the autophagy-related *beclin1*, *lc3a*, *wipi1*, *atg5*, *gabarp*, *ambra1* genes (primer sequences are shown in Supplementary Table S1).

Injection of CRP-mix and IL6 into adult zebrafish

Four adult zebrafish were i.p. injected with 5 µL of GFP, CRP-mix or IL6 supernatants. Two days post-injection, spleen, liver and head kidney tissues were individually dissected, immersed in RNAlater (Ambion, Austin, TX, USA) and stored at -80°C until they were analyzed by RT-qPCR (primer sequences are shown in Supplementary Table S1) as described below.

RNA isolation, cDNA synthesis and qPCR

Total RNA was extracted from cultured cells and tissue organs using the E.Z.N.A. HP Total RNA and E.Z.N.A. HP Tissue RNA kits (Omega Bio-tek, Norcross, GA, USA), respectively. The samples were then treated with DNase (Turbo DNA-free™ Kit, Ambion Inc., Austin, TX, USA), to eliminate residual genomic DNA, by following manufacturer's instructions. Each cultured cell sample was obtained by pooling four wells from 96-well plates. RNA concentrations were estimated with a Nanodrop 1000 spectrophotometer (Thermo-fisher Scientific, Waltham, MA, USA). Isolated RNA samples were stored at -80°C until use.

For the synthesis of cDNA, 0.5µg of isolated RNA from each sample were used. The Moloney murine leukemia virus (M-MuLV) reverse transcriptase (Gibco BRL-Invitrogen) was used as previously described.⁴⁵

The qPCR was performed by using an ABI PRISM 7300 thermocycler (Applied Biosystems, NJ, USA). Reactions were conducted in 20 µL reaction volumes, including 2 µL of cDNA, 900 nM of each corresponding forward and reverse primer (Sigma) (primer sequences are shown in Supplementary Table S1) and 10 µL of with SYBR Green PCR master mix (Life Technologies, Paisley, UK). Non-template controls were added for each gene analysis. All reactions were performed using technical duplicates. Cycling conditions were an initial denaturing step (10 min at 95°C), followed by 40 cycles of 1 min at 65°C and 1 min at 95°C, and finally an extension step of 10 min at 65°C. Melting curves were checked for inconstancies in each reaction. Results were obtained by normalizing the number transcripts of each target gene respective to corresponding endogenous reference's ones (transcripts of the *ef1a* gene for EPC cells and 18S ribosomal RNA for zebrafish tissues) from the same sample. A variation of Livak and Schmittgen's method¹¹⁴ by the formula $2^{Ct\text{ ref.} - Ct\text{ target}}$ was used. Results were normalized to the expression of the corresponding housekeeping gene transcription and, when stated, also relative to control samples calculated by the formula: transcript levels in treated samples / transcript levels in control samples.

Immunofluorescence assays and confocal microscopy

For these experiments, there were selected several compounds because of their anti-SVCV activity (25-HOC ($C_{27}H_{46}O_2$)), their interaction with membrane cholesterol balance (MBCD, 25-HOC and cholesterol ($C_{27}H_{46}O$)) or their autophagy modulating properties (CQ, 3-MA, NAC and, rapamycin), all of them provided by Sigma. Stock solutions (40 mM MBCD in PBS; 0.4 mg/mL 25-HOC and cholesterol in ethanol; 0.1 M CQ in H_2O ; 0.6 M NAC in H_2O and 0.2 M 3-MA in H_2O) were stored at -20°C until use.

ZF4 monolayers grown at 80% of confluence onto 24-well plates with 12-mm glass coverslips were treated with the following compounds in 500 μL of ZF4 infection media for 4 h at 22°C: CQ(25 μM), 3-MA (10 μM), 25-HOC (10 $\mu g/mL$, including 2.5% ethanol), MBCD (4 mM), cholesterol (10 $\mu g/mL$, including 2.5% ethanol), SVCV (MOI 1), GFP and CRP-mix, and the combinations CRP-mix (or GFP) with either SVCV, 25-HOC or MBCD. Non-treated cells were also included as a control. After the treatment, cells were washed 3 times with infection media and fixed with 2% formalin for 15 min at 4°C. After 3 washes with PBS, cells were blocked with 1% BSA and 0.5% Triton X-100 (Sigma) (blocking buffer) in PBS for 1 h, washed again and then incubated overnight at 4°C with a 1:200 dilution in blocking buffer of mouse anti-LC3B monoclonal antibody (NanoToolsAntikörperteknik GmbH & Co., Teningen, Germany). After washing, cells were incubated with the secondary antibody Alexa Fluor®488 goat anti-mouse IgG (1:500 dilution in blocking buffer) for 1h at room temperature, as well as stained with a DNA-specific dye 4,6-diamido-2-phenylindole (DAPI) solution (0.1 $\mu g/mL$) (Molecular Probes-Life Technologies, Paisley, UK) for nuclear localization. Finally, cell samples were washed 3 times and mounted using ProLong Antifade Reagents (Life Technologies). Confocal images were captured by using a TSC SPE confocal microscope and LAS AF software (all Leica).

Determination of intracellular autophagosomes

The quantification of autophagosomes was carried out by means of the analysis of the immunofluorescence images with the software ImageJ v1.52a (US National Institutes of Health, Bethesda, MD, USA). For this, the FITC-derived fluorescence from each image was measured by applying a threshold of 25 brightness in the green spectra, which excluded the background and selected fluorescence-labelled puncta. DAPI-stained nuclei were counted manually. Data is represented as the normalization of the selected fluorescent area per cell for each treatment compared to control by the formula: average fluorescent area for each cell from treated

monolayers / average fluorescent area for each cell from control (GFP-treated) monolayers. For each treatment three images were analyzed from two different experiments (about 100 cells were analyzed per treatment).

Visualization of GFP-Lc3-recombinant zebrafish embryos injected with CRPs and il6 coding plasmids

To test the effects of CRPs and IL6 in the process of autophagy *in vivo*, groups of 30 one-cell stage embryos of GFP-Lc3 zebrafish¹¹⁵ were microinjected with 2nL of PBS containing 150 pg of either pMCV1.4, pMCV1.4-crp1, 4 or 5 or pMCV1.4-il6. The microinjections were performed with glass microcapillary pipettes (WPI, Sarasota, FL, USA) incorporated into a MN-151 micromanipulator and an IM-30 microinjector (Narishige, Tokyo, Japan). The resulting 3-day hatched larvae were anesthetized (by adding 200 µL of 0.05% MS-222 solution to a Petri plate with 10 mL of water), photographed using a Multi-Zoom AZ100 microscope equipped with a DS-Ri1 digital camera (Nikon, Melville, NY), and images processed with the LAS AF software (Leica).

Determination of the effect of autophagy inhibitors and cholesterol-interacting compounds on SVCV replication

The anti-SVCV activity of CRP, 25-HOC and MBCD was compared in the presence and absence of some relevant autophagy modulators (in particular, 3-MA, CQ, rapamycin and NAC). Briefly, EPC monolayers at 22°C were first incubated with either 3-MA (1 mM and a 0-1 mM gradient, 20 h), CQ (25 µM, 30 min), rapamycin (25 µM, 4 h) or NAC (1 mM, 20 h), washed 3 times with infection media and then treated for 2 h with either GFP, CRP-mix, 10 µg/mL of 25-HOC or 1 mM MBCD. Similarly, the effect of cholesterol on SVCV infectivity was assessed with and without the presence of MBCD. Thus, EPC cell monolayers were treated with MBCD (1 mM), cholesterol (0.5 and 1 mM) or MBCD (1 mM) with cholesterol (either 0.5 or 1 mM) for 2 h at 22°C. Treated EPC cell monolayers were then washed with RPMI 2% FBS medium 3 times and infected with SVCV (MOI 10⁻²) for the subsequent determination of the number of foci of infection as described above.

Statistical analysis

Data are shown as means and s.d. Resulting data sets were subjected to the most appropriate statistical analysis depending on each particular experimental design. Differences between two samples within a dataset were analyzed by Student's t-test or multiple Student's t-

PUBLICACIÓN 4

test corrected by using the Holm-Sidak method, whilst one- and two-way ANOVA and Sidak's multiple comparison tests to determine differences between groups. Prism v7 (Graphpad software, La Jolla, CA) was used for creating the graphs and statistical analysis. The $P < 0.05$, $P < 0.01$ and $P < 0.001$ statistical differences were indicated as a, b and c, respectively, when compared to the corresponding control groups.

Graphics

Image processing and diagram drawing were performed with Adobe Photoshop CC 2017 (Adobe Systems Inc, San Jose, CA, USA).

Supplementary Materials: Table S1 and Figures S1-5.

Funding: This work was supported by the Spanish Ministry of Science and Innovation under Grant AGL2014-51773-C3-1-R; Xunta de Galicia (GAIN) under Grant IN607B 2016/12; and Generalitat Valenciana and Fondo Social Europeo (FSE) 2014-2020 under Grant ACIF/2016/207.

Acknowledgments: We thank Ms. Paula Pérez and Dr. Ángeles Gómez for technical assistance, Drs Judit Castro and Lucía Sanchez for their methodological support in confocal observations, Drs. José Antonio Encinar and Victoriano Mulero for their valuable comments and Mr. Diego Sanz for graphical support. The authors gratefully acknowledge deceased Dr. Amparo Estepa for original ideas and inspiration.

Disclosure statement: The authors declare no potential conflict of interest.

References

- [1] Vilahur G, Badimon L. Biological actions of pentraxins. *Vascul Pharmacol* 2015; 73:38-44.
- [2] Pepys MB, Hirschfield GM. C-reactive protein: a critical update. *J Clin Invest* 2003; 111(12):1805-12.
- [3] Pepys MB, Baltz ML. Acute phase proteins with special reference to C-reactive protein and related proteins (pentaxins) and serum amyloid A protein. *Adv Immunol* 1983; 34:141-212.
- [4] Hurlmann J, Thorbecke GJ, Hochwald GM. The liver as the site of C-reactive protein formation. *The Journal of Experimental Medicine* 1966; 123(2):365.
- [5] Tillett WS, Francis T. Serological Reactions in Pneumonia with a Non-Protein Somatic Fraction of Pneumococcus. *J Exp Med* 1930; 52(4):561-71.
- [6] Shrive AK, Cheetham GM, Holden D, Myles DA, Turnell WG, Volanakis JE, Pepys MB, Bloomer AC, et al. Three dimensional structure of human C-reactive protein. *Nat Struct Biol* 1996; 3(4):346-54.
- [7] Nguyen NY, Suzuki A, Boykins RA, Liu TY. The amino acid sequence of Limulus C-reactive protein. Evidence of polymorphism. *J Biol Chem* 1986; 261(22):10456-65.
- [8] Garlanda C, Bottazzi B, Bastone A, Mantovani A. Pentraxins at the crossroads between innate immunity, inflammation, matrix deposition, and female fertility. *Annu Rev Immunol* 2005; 23:337-66.
- [9] Tharia HA, Shrive AK, Mills JD, Arme C, Williams GT, Greenhough TJ. Complete cDNA sequence of SAP-like pentraxin from Limulus polyphemus: implications for pentraxin evolution. *J Mol Biol* 2002; 316(3):583-97.
- [10] Introna M, Breviario F, d'Aniello EM, Golay J, Dejana E, Mantovani A. IL-1 inducible genes in human umbilical vein endothelial cells. *Eur Heart J* 1993; 14 Suppl K:78-81.
- [11] Emsley J, White HE, O'Hara BP, Oliva G, Srinivasan N, Tickle IJ, Blundell TL, Pepys MB, et al. Structure of pentameric human serum amyloid P component. *Nature* 1994; 367(6461):338-45.
- [12] Srinivasan N, White HE, Emsley J, Wood SP, Pepys MB, Blundell TL. Comparative analyses of pentraxins: implications for protomer assembly and ligand binding. *Structure* 1994; 2(11):1017-27.
- [13] Armstrong PB. Comparative biology of the pentraxin protein family: evolutionarily conserved component of innate immune system. *Int Rev Cell Mol Biol* 2015; 316:1-47.
- [14] de Beer FC, Baltz ML, Munn EA, Feinstein A, Taylor J, Bruton C, Clamp JR, Pepys MB. Isolation and characterization of C-reactive protein and serum amyloid P component in the rat. *Immunology* 1982; 45(1):55-70.
- [15] Pepys MB, Baltz M, Gomer K, Davies AJ, Doenhoff M. Serum amyloid P-component is an acute-phase reactant in the mouse. *Nature* 1979; 278(5701):259-61.
- [16] Rudnick CM, Dowton SB. Serum amyloid P (female protein) of the Syrian hamster. Gene structure and expression. *J Biol Chem* 1993; 268(29):21760-9.
- [17] Mortensen RF, Beisel K, Zeleznik NJ, Le PT. Acute-phase reactants of mice. II. Strain dependence of serum amyloid P-component (SAP) levels and response to inflammation. *J Immunol* 1983; 130(2):885-9.
- [18] Rubio N, Sharp PM, Rits M, Zahedi K, Whitehead AS. Structure, expression, and evolution of guinea pig serum amyloid P component and C-reactive protein. *J Biochem* 1993; 113(3):277-84.
- [19] Thompson D, Pepys MB, Wood SP. The physiological structure of human C-reactive protein and its complex with phosphocholine. *Structure* 1999; 7(2):169-77.
- [20] Agrawal A, Singh PP, Bottazzi B, Garlanda C, Mantovani A. Pattern recognition by pentraxins. *Adv Exp Med Biol* 2009; 653:98-116.

- [21] Serino L, Virji M. Phosphorylcholine decoration of lipopolysaccharide differentiates commensal Neisseriae from pathogenic strains: identification of licA-type genes in commensal Neisseriae. *Mol Microbiol* 2000; 35(6):1550-9.
- [22] Volanakis JE, Kaplan MH. Specificity of C-Reactive Protein for Choline Phosphate Residues of Pneumococcal C-Polysaccharide. *Proceedings of the Society for Experimental Biology and Medicine* 1971; 136(2):612-14.
- [23] Chang M-K, Binder CJ, Torzewski M, Witztum JL. C-reactive protein binds to both oxidized LDL and apoptotic cells through recognition of a common ligand: Phosphorylcholine of oxidized phospholipids. *Proceedings of the National Academy of Sciences of the United States of America* 2002; 99(20):13043-48.
- [24] Hack CE, Wolbink G-J, Schalkwijk C, Speijer H, Hermens WT, van den Bosch H. A role for secretory phospholipase A2 and C-reactive protein in the removal of injured cells. *Immunology Today* 1997; 18(3):111-15.
- [25] Ciurana CL, Hack CE. Competitive binding of pentraxins and IgM to newly exposed epitopes on late apoptotic cells. *Cell Immunol* 2006; 239(1):14-21.
- [26] Poon IK, Hulett MD, Parish CR. Molecular mechanisms of late apoptotic/necrotic cell clearance. *Cell Death Differ* 2010; 17(3):381-97.
- [27] Du Clos TW. The interaction of C-reactive protein and serum amyloid P component with nuclear antigens. *Mol Biol Rep* 1996; 23(3-4):253-60.
- [28] Robey FA, Jones KD, Tanaka T, Liu TY. Binding of C-reactive protein to chromatin and nucleosome core particles. A possible physiological role of C-reactive protein. *J Biol Chem* 1984; 259(11):7311-6.
- [29] Higginbotham JD, Heidelberger M, Gotschlich EC. Degradation of a pneumococcal type-specific polysaccharide with exposure of group-specificity. *Proc Natl Acad Sci U S A* 1970; 67(1):138-42.
- [30] Baldo BA, Fletcher TC, Pepys J. Isolation of a peptido-polysaccharide from the dermatophyte *Epidermophyton floccosum* and a study of its reaction with human C-reactive protein and a mouse anti-phosphorylcholine myeloma serum. *Immunology* 1977; 32(6):831-42.
- [31] Jensen TD, Schonheyder H, Andersen P, Stenderup A. Binding of C-reactive protein to *Aspergillus fumigatus* fractions. *J Med Microbiol* 1986; 21(2):173-7.
- [32] Pied S, Nussler A, Pontent M, Miltgen F, Matile H, Lambert PH, Mazier D. C-reactive protein protects against preerythrocytic stages of malaria. *Infect Immun* 1989; 57(1):278-82.
- [33] Culley FJ, Harris RA, Kaye PM, McAdam KP, Raynes JG. C-reactive protein binds to a novel ligand on *Leishmania donovani* and increases uptake into human macrophages. *J Immunol* 1996; 156(12):4691-6.
- [34] Shrive AK, Metcalfe AM, Cartwright JR, Greenhough TJ. C-reactive protein and SAP-like pentraxin are both present in *Limulus polyphemus* haemolymph: crystal structure of *Limulus* SAP. *J Mol Biol* 1999; 290(5):997-1008.
- [35] Chen R, Qi J, Yuan H, Wu Y, Hu W, Xia C. Crystal structures for short-chain pentraxin from zebrafish demonstrate a cyclic trimer with new recognition and effector faces. *J Struct Biol* 2015; 189(3):259-68.
- [36] Amatayakul-Chantler S, Dwek RA, Tennent GA, Pepys MB, Rademacher TW. Molecular characterization of *Limulus polyphemus* C-reactive protein. II. Asparagine-linked oligosaccharides. *Eur J Biochem* 1993; 214(1):99-110.
- [37] Schwalbe RA, Dahlback B, Coe JE, Nelsetuen GL. Pentraxin family of proteins interact specifically with phosphorylcholine and/or phosphorylethanolamine. *Biochemistry* 1992; 31(20):4907-15.
- [38] Coe JE, Ross MJ. Hamster female protein, a sex-limited pentraxin, is a constituent of Syrian hamster amyloid. *J Clin Invest* 1985; 76(1):66-74.

- [39] Bello-Perez M, Falco A, Medina R, Encinar JA, Novoa B, Perez L, Estepa A, Coll J. Structure and functionalities of the human c-reactive protein compared to the zebrafish multigene family of c-reactive-like proteins. *Dev Comp Immunol* 2017; 69:33-40.
- [40] Pathak A, Agrawal A. Evolution of C-Reactive Protein. *Frontiers in Immunology* 2019; 10(943).
- [41] Cray C. Acute phase proteins in animals. *Prog Mol Biol Transl Sci* 2012; 105:113-50.
- [42] Ansar W, Ghosh S. C-reactive protein and the biology of disease. *Immunol Res* 2013; 56(1):131-42.
- [43] MacCarthy EM, Burns I, Irnazarow I, Polwart A, Greenhough TJ, Shrive AK, Hoole D. Serum CRP-like protein profile in common carp *Cyprinus carpio* challenged with *Aeromonas hydrophila* and *Escherichia coli* lipopolysaccharide. *Dev Comp Immunol* 2008; 32(11):1281-9.
- [44] Pionnier N, Adamek M, Miest JJ, Harris SJ, Matras M, Rakus KL, Irnazarow I, Hoole D. C-reactive protein and complement as acute phase reactants in common carp *Cyprinus carpio* during CyHV-3 infection. *Dis Aquat Organ* 2014; 109(3):187-99.
- [45] Pionnier N, Falco A, Miest JJ, Shrive AK, Hoole D. Feeding common carp *Cyprinus carpio* with beta-glucan supplemented diet stimulates C-reactive protein and complement immune acute phase responses following PAMPs injection. *Fish Shellfish Immunol* 2014; 39(2):285-95.
- [46] Pionnier N, Falco A, Miest J, Frost P, Irnazarow I, Shrive A, Hoole D. Dietary beta-glucan stimulate complement and C-reactive protein acute phase responses in common carp (*Cyprinus carpio*) during an *Aeromonas salmonicida* infection. *Fish Shellfish Immunol* 2013; 34(3):819-31.
- [47] Choi KM, Shim SH, An CM, Nam BH, Jeong JM, Kim JW, Park CI. Functional characterisation and expression analysis of recombinant serum amyloid P isoform 1 (RbSAP1) from rock bream (*Oplegnathus fasciatus*). *Fish Shellfish Immunol* 2015; 45(2):277-85.
- [48] Hwang SD, Bae JS, Jo DH, Kim KI, Cho MY, Jee BY, Park MA, Park CI. Gene expression and functional characterization of serum amyloid P component 2 in rock bream, *Oplegnathus fasciatus*. *Fish Shellfish Immunol* 2015; 47(1):521-7.
- [49] Wang T, Zhang J. CsPTX1, a pentraxin of *Cynoglossus semilaevis*, is an innate immunity factor with antibacterial effects. *Fish Shellfish Immunol* 2016; 56:12-20.
- [50] Estepa A, Coll J. Innate Multigene Family Memories Are Implicated in the Viral-Survivor Zebrafish Phenotype. *PLoS One* 2015; 10(8):e0135483.
- [51] Bello-Perez M, Falco A, Medina-Gali R, Pereiro P, Encinar JA, Novoa B, Perez L, Coll J. Neutralization of viral infectivity by zebrafish c-reactive protein isoforms. *Mol Immunol* 2017; 91:145-55.
- [52] Medina-Gali R, Bello-Perez M, Martinez-Lopez A, Falco A, Ortega-Villaizan MM, Encinar JA, Novoa B, Coll J, et al. Chromatin immunoprecipitation and high throughput sequencing of SVCV-infected zebrafish reveals novel epigenetic histone methylation patterns involved in antiviral immune response. *Fish Shellfish Immunol* 2018; 82:514-21.
- [53] Ballesteros NA, Saint-Jean SS, Encinas PA, Perez-Prieto SI, Coll JM. Oral immunization of rainbow trout to infectious pancreatic necrosis virus (IPNV) induces different immune gene expression profiles in head kidney and pyloric ceca. *Fish Shellfish Immunol* 2012; 33(2):174-85.
- [54] Mogensen TH, Paludan SR. Molecular pathways in virus-induced cytokine production. *Microbiol Mol Biol Rev* 2001; 65(1):131-50.
- [55] Falco A, Cartwright JR, Wiegertjes GF, Hoole D. Molecular characterization and expression analysis of two new C-reactive protein genes from common carp (*Cyprinus carpio*). *Dev Comp Immunol* 2012; 37(1):127-38.

- [56] Bello-Perez M, Falco A, Novoa B, Perez L, Coll J. Hydroxycholesterol binds and enhances the anti-viral activities of zebrafish monomeric c-reactive protein isoforms. *PLOS ONE* 2019; 14(1):e0201509.
- [57] Pereiro P, Forn-Cuní G, Dios S, Coll J, Figueras A, Novoa B. Interferon-independent antiviral activity of 25-hydroxycholesterol in a teleost fish. *Antiviral research* 2017; 145:146-59.
- [58] Pöhlmann S, Simmons G. *Viral entry into host cells*. Springer; 2013.
- [59] Winton J, Batts W, deKinkelin P, LeBerre M, Bremont M, Fijan N. Current lineages of the epithelioma papulosum cyprini (EPC) cell line are contaminated with fathead minnow, *Pimephales promelas*, cells. *J Fish Dis* 2010; 33(8):701-4.
- [60] Langevin C, Aleksejeva E, Passoni G, Palha N, Levraud JP, Boudinot P. The antiviral innate immune response in fish: evolution and conservation of the IFN system. *J Mol Biol* 2013; 425(24):4904-20.
- [61] Kirkegaard K, Taylor MP, Jackson WT. Cellular autophagy: surrender, avoidance and subversion by microorganisms. *Nat Rev Microbiol* 2004; 2(4):301-14.
- [62] Shelly S, Lukinova N, Bambina S, Berman A, Cherry S. Autophagy is an essential component of *Drosophila* immunity against vesicular stomatitis virus. *Immunity* 2009; 30(4):588-98.
- [63] Garcia-Valtanen P, Ortega-Villaizan Mdel M, Martinez-Lopez A, Medina-Gali R, Perez L, Mackenzie S, Figueras A, Coll JM, et al. Autophagy-inducing peptides from mammalian VSV and fish VHSV rhabdoviral G glycoproteins (G) as models for the development of new therapeutic molecules. *Autophagy* 2014; 10(9):1666-80.
- [64] Klionsky DJ, Abeliovich H, Agostinis P, Agrawal DK, Aliev G, Askew DS, Baba M, Baehrecke EH, et al. Guidelines for the use and interpretation of assays for monitoring autophagy in higher eukaryotes. *Autophagy* 2008; 4(2):151-75.
- [65] Mizushima N. Methods for monitoring autophagy. *The international journal of biochemistry & cell biology* 2004; 36(12):2491-502.
- [66] Liu J, Wang H, Gu J, Deng T, Yuan Z, Hu B, Xu Y, Yan Y, et al. BECN1-dependent CASP2 incomplete autophagy induction by binding to rabies virus phosphoprotein. *Autophagy* 2017; 13(4):739-53.
- [67] Espin-Palazon R, Martinez-Lopez A, Roca FJ, Lopez-Munoz A, Tyrkalska SD, Candel S, Garcia-Moreno D, Falco A, et al. TNFalpha Impairs Rhabdoviral Clearance by Inhibiting the Host Autophagic Antiviral Response. *PLoS Pathog* 2016; 12(6):e1005699.
- [68] Liu L, Zhu B, Wu S, Lin L, Liu G, Zhou Y, Wang W, Asim M, et al. Spring viraemia of carp virus induces autophagy for necessary viral replication. *Cell Microbiol* 2015; 17(4):595-605.
- [69] Peng J, Zhu S, Hu L, Ye P, Wang Y, Tian Q, Mei M, Chen H, et al. Wild-type rabies virus induces autophagy in human and mouse neuroblastoma cell lines. *Autophagy* 2016; 12(10):1704-20.
- [70] Vinod V, Padmakrishnan CJ, Vijayan B, Gopala S. 'How can I halt thee?' The puzzles involved in autophagic inhibition. *Pharmacol Res* 2014; 82:1-8.
- [71] Mauthe M, Orhon I, Rocchi C, Zhou X, Luhr M, Hijlkema KJ, Coppes RP, Engedal N, et al. Chloroquine inhibits autophagic flux by decreasing autophagosome-lysosome fusion. *Autophagy* 2018; 14(8):1435-55.
- [72] Liu S-Y, Aliyari R, Chikere K, Li G, Marsden MD, Smith JK, Pernet O, Guo H, et al. Interferon-inducible cholesterol-25-hydroxylase broadly inhibits viral entry by production of 25-hydroxycholesterol. *Immunity* 2013; 38(1):92-105.
- [73] Piscianz E, Vecchi Brumatti L, Tommasini A, Marcuzzi A. Is autophagy an elective strategy to protect neurons from dysregulated cholesterol metabolism? *Neural Regen Res* 2019; 14(4):582-87.

- [74] Shi Y, Tan SH, Ng S, Zhou J, Yang ND, Koo GB, McMahon KA, Parton RG, *et al.* Critical role of CAV1/caveolin-1 in cell stress responses in human breast cancer cells via modulation of lysosomal function and autophagy. *Autophagy* 2015; 11(5):769-84.
- [75] Huang FC. The critical role of membrane cholesterol in salmonella-induced autophagy in intestinal epithelial cells. *Int J Mol Sci* 2014; 15(7):12558-72.
- [76] Li M, Li J, Zeng R, Yang J, Liu J, Zhang Z, Song X, Yao Z, *et al.* Respiratory syncytial virus replication is promoted by autophagy-mediated inhibition of apoptosis. *Journal of virology* 2018; 92(8):e02193-17.
- [77] Job ER, Bottazzi B, Gilbertson B, Edenborough KM, Brown LE, Mantovani A, Brooks AG, Reading PC. Serum amyloid P is a sialylated glycoprotein inhibitor of influenza A viruses. *PLoS One* 2013; 8(3):e59623.
- [78] Reading PC, Bozza S, Gilbertson B, Tate M, Moretti S, Job ER, Crouch EC, Brooks AG, *et al.* Antiviral activity of the long chain pentraxin PTX3 against influenza viruses. *The Journal of Immunology* 2008; 180(5):3391-98.
- [79] Kim Y, Ryu J, Ryu MS, Lim S, Han KO, Lim IK, Han KH. C-reactive protein induces G2/M phase cell cycle arrest and apoptosis in monocytes through the upregulation of B-cell translocation gene 2 expression. *FEBS Lett* 2014; 588(4):625-31.
- [80] Pasceri V, Willerson JT, Yeh ET. Direct proinflammatory effect of C-reactive protein on human endothelial cells. *Circulation* 2000; 102(18):2165-8.
- [81] Torzewski M, Rist C, Mortensen RF, Zwaka TP, Bienek M, Waltenberger J, Koenig W, Schmitz G, *et al.* C-reactive protein in the arterial intima: role of C-reactive protein receptor-dependent monocyte recruitment in atherosclerosis. *Arterioscler Thromb Vasc Biol* 2000; 20(9):2094-9.
- [82] Ke F, Zhang Q-Y. Aquatic animal viruses mediated immune evasion in their host. *Fish & shellfish immunology* 2018.
- [83] Poynter SJ, DeWitte-Orr SJ. Fish interferon-stimulated genes: the antiviral effectors. *Developmental & Comparative Immunology* 2016; 65:218-25.
- [84] She S, Xiang Y, Yang M, Ding X, Liu X, Ma L, Liu Q, Liu B, *et al.* C-reactive protein is a biomarker of AFP-negative HBV-related hepatocellular carcinoma. *International journal of oncology* 2015; 47(2):543-54.
- [85] Bian A, Shi M, Flores B, Gillings N, Li P, Yan SX, Levine B, Xing C, *et al.* Downregulation of autophagy is associated with severe ischemia-reperfusion-induced acute kidney injury in overexpressing C-reactive protein mice. *PloS one* 2017; 12(9):e0181848.
- [86] Kim JY, Wang L, Lee J, Ou J-hJ. Hepatitis C virus induces the localization of lipid rafts to autophagosomes for its RNA replication. *Journal of virology* 2017; 91(20):e00541-17.
- [87] Tu Z, Gong W, Zhang Y, Feng Y, Liu Y, Tu C. Inhibition of Rabies Virus by 1, 2, 3, 4, 6-Penta-O-galloyl- β -D-Glucose Involves mTOR-Dependent Autophagy. *Viruses* 2018; 10(4):201.
- [88] Li C, Liu J, Zhang X, Wei S, Huang Y, Huang X, Wei J, Qin Q. Fish autophagy protein 5 exerts negative regulation on antiviral immune response against iridovirus and nodavirus. *Frontiers in Immunology* 2019; 10:517.
- [89] Hurwitz SN, Cheerathodi MR, Nkosi D, York SB, Meckes DG. Tetraspanin CD63 bridges autophagic and endosomal processes to regulate exosomal secretion and intracellular signaling of Epstein-Barr virus LMP1. *Journal of virology* 2018; 92(5):e01969-17.
- [90] Panyasrivanit M, Khakpoor A, Wikan N, Smith DR. Co-localization of constituents of the dengue virus translation and replication machinery with amphisomes. *Journal of General Virology* 2009; 90(2):448-56.
- [91] Khakpoor A, Panyasrivanit M, Wikan N, Smith DR. A role for autophagolysosomes in dengue virus 3 production in HepG2 cells. *Journal of General Virology* 2009; 90(5):1093-103.
- [92] Zheng K, Li Y, Wang S, Wang X, Liao C, Hu X, Fan L, Kang Q, *et al.* Inhibition of autophagosome-lysosome fusion by ginsenoside Ro via the ESR2-NCF1-ROS pathway

- sensitizes esophageal cancer cells to 5-fluorouracil-induced cell death via the CHEK1-mediated DNA damage checkpoint. *Autophagy* 2016; 12(9):1593-613.
- [93] Redmann M, Benavides GA, Berryhill TF, Wani WY, Ouyang X, Johnson MS, Ravi S, Barnes S, *et al.* Inhibition of autophagy with baflomycin and chloroquine decreases mitochondrial quality and bioenergetic function in primary neurons. *Redox biology* 2017; 11:73-81.
- [94] Terman A, Kurz T, Gustafsson B, Brunk U. Lysosomal labilization. *IUBMB life* 2006; 58(9):531-39.
- [95] Le Blanc I, Luyet P-P, Pons V, Ferguson C, Emans N, Petiot A, Mayran N, Demaurex N, *et al.* Endosome-to-cytosol transport of viral nucleocapsids. *Nature cell biology* 2005; 7(7):653.
- [96] Chelbi-Alix M, Thang MN. Chloroquine impairs the interferon-induced antiviral state without affecting the 2', 5'-oligoadenylate synthetase. *Journal of Biological Chemistry* 1985; 260(13):7960-64.
- [97] Hsu SP, Kuo JS, Chiang H-C, Wang H-E, Wang Y-S, Huang C-C, Huang Y-C, Chi M-S, *et al.* Temozolomide, sirolimus and chloroquine is a new therapeutic combination that synergizes to disrupt lysosomal function and cholesterol homeostasis in GBM cells. *Oncotarget* 2018; 9(6):6883.
- [98] Lee S-J, Jung YH, Kim JS, Lee HJ, Lee SH, Lee K-H, Jang KK, Choi SH, *et al.* A *Vibrio vulnificus* VvpM induces IL-1 β production coupled with necrotic macrophage death via distinct spatial targeting by ANXA2. *Frontiers in cellular and infection microbiology* 2017; 7:352.
- [99] Thiele JR, Zeller J, Kiefer J, Braig D, Kreuzaler S, Lenz Y, Potempa LA, Grahammer F, *et al.* A conformational change in C-reactive protein enhances leukocyte recruitment and reactive oxygen species generation in ischemia/reperfusion injury. *Frontiers in immunology* 2018; 9:675.
- [100] Pilely K, Fumagalli S, Rosbjerg A, Genster N, Skjoedt M-O, Perego C, Ferrante AM, De Simoni M-G, *et al.* c-reactive Protein Binds to cholesterol crystals and co-localizes with the Terminal complement complex in human atherosclerotic Plaques. *Frontiers in immunology* 2017; 8:1040.
- [101] Taskinen S, Hyvönen M, Kovanen PT, Meri S, Pentikäinen MO. C-reactive protein binds to the 3 β -OH group of cholesterol in LDL particles. *Biochemical and biophysical research communications* 2005; 329(4):1208-16.
- [102] Noguchi N, Urano Y, Takabe W, Saito Y. New aspects of 24 (S)-hydroxycholesterol in modulating neuronal cell death. *Free Radical Biology and Medicine* 2015; 87:366-72.
- [103] Nury T, Zarrouk A, Mackrill JJ, Samadi M, Durand P, Riedinger J-M, Doria M, Vejux A, *et al.* Induction of oxiapoptophagy on 158N murine oligodendrocytes treated by 7-ketocholesterol-, 7 β -hydroxycholesterol-, or 24 (S)-hydroxycholesterol: Protective effects of α -tocopherol and docosahexaenoic acid (DHA; C22: 6 n-3). *Steroids* 2015; 99:194-203.
- [104] Vurusanker B, Gargiulo S, Testa G, Gamba P, Leonarduzzi G, Poli G, Basaga H. The role of autophagy in survival response induced by 27-hydroxycholesterol in human promonocytic cells. *Redox biology* 2018.
- [105] Singh R, Kaushik S, Wang Y, Xiang Y, Novak I, Komatsu M, Tanaka K, Cuervo AM, *et al.* Autophagy regulates lipid metabolism. *Nature* 2009; 458(7242):1131.
- [106] Li C, Deng Y-Q, Wang S, Ma F, Aliyari R, Huang X-Y, Zhang N-N, Watanabe M, *et al.* 25-Hydroxycholesterol protects host against Zika virus infection and its associated microcephaly in a mouse model. *Immunity* 2017; 46(3):446-56.
- [107] Li C, Sun L, Lin H, Qin Z, Tu J, Li J, Chen K, Lin L. Glutamine starvation inhibits snakehead vesiculovirus replication via inducing autophagy associated with the disturbance of endogenous glutathione pool. *Fish & shellfish immunology* 2019; 86:1044-52.

- [108] Shawli GT, Adeyemi OO, Stonehouse NJ, Herod MR. The Oxysterol 25-Hydroxycholesterol Inhibits Replication of Murine Norovirus. *Viruses* 2019; 11(2):97.
- [109] Shrivastava-Ranjan P, Bergeron É, Chakrabarti AK, Albariño CG, Flint M, Nichol ST, Spiropoulou CF. 25-Hydroxycholesterol inhibition of Lassa virus infection through aberrant GP1 glycosylation. *MBio* 2016; 7(6):e01808-16.
- [110] Civra A, Francese R, Gamba P, Testa G, Cagno V, Poli G, Lembo D. 25-Hydroxycholesterol and 27-hydroxycholesterol inhibit human rotavirus infection by sequestering viral particles into late endosomes. *Redox biology* 2018; 19:318-30.
- [111] Zhang Y, Wang L, Huang X, Wang S, Huang Y, Qin Q. Fish Cholesterol 25-hydroxylase inhibits virus replication via regulating interferon immune response or affecting virus entry. *Frontiers in immunology* 2019; 10.
- [112] Westerfield M. The zebrafish book: a guide for the laboratory use of zebrafish (*Brachydanio rerio*). University of Oregon press; 1995.
- [113] Falco A, Medina-Gali RM, Poveda JA, Bello-Perez M, Novoa B, Encinar JA. Antiviral Activity of a Turbot (*Scophthalmus maximus*) NK-Lysin Peptide by Inhibition of Low-pH Virus-Induced Membrane Fusion. *Mar Drugs* 2019; 17(2).
- [114] Livak KJ, Schmittgen TD. Analysis of relative gene expression data using real-time quantitative PCR and the 2(-Delta Delta C(T)) Method. *Methods* 2001; 25(4):402-8.
- [115] He C, Bartholomew CR, Zhou W, Klionsky DJ. Assaying autophagic activity in transgenic GFP-Lc3 and GFP-Gabarp zebrafish embryos. *Autophagy* 2009; 5(4):520-6.



Tables**Table S1.** Primer sequences used for qPCR.

Organism	Gene	Sequence (5' - 3')	Accession. no.
<i>P. promelas</i>	<i>ef1a</i>	Fw: CTGGAGGCCAGCTCAAACAT Rv: CATTCCCTCCTTACGCTCAAC	AY643400
	<i>mx</i>	Fw: GGAGAAGAGGTTAAATGTGGATCAG Rv: TGAAGTGCCTTTTATCTTAATCT	KM099175
	18S	Fw: ACCACCCACAGAACATCGAGAAA Rv: GCCTGCGGCTTAATTGACT	NR_145818
	<i>ef1α</i>	Fw: CCACGTCGACTCCGGAAA Rv: CGATTCCACCGCATTGTAGA	AY422992.1
<i>D. rerio</i>	<i>ambra1</i>	Fw: TCTTCGAGAAAATGGCACCT RV: CTCTCTGCGTTAGGGACAGG	XM_002667669
	<i>atg5</i>	Fw: AGAGAGGCAGAACCCCTACTATC Rv: CCTCGTGTCAAACCACATTTC	NM_205618
	<i>beclin1</i>	Fw: GATCATGCGCAATGGTGGCTTC Rv: CCTCCTGTGTCCCTCAATCTT	AB266448
	<i>gabarap</i>	Fw: GTCTGACCTCACAGTTGGC Rv: TCCTGGTAGAGCAGTCCCAT	NM_001013260
	<i>lc3a</i>	Fw: CAATCAGCACAGCATGG Rv: GTAAAGGAAGCCGTCTTC	NM_214739
	<i>wipi1</i>	Fw: GTGAGAGGGTAGAGAACAG Rv: GTAACAACGACCCAACATC	XM_005164002
	<i>mxa</i>	Fw: CACAGACAATCATGCCACCT Rv: TTTGCAGCTCAAAGCAGCT	NM_182942
	<i>mxe</i>	Fw: AGTCACCCAATGTCAGTGCA Rv: GCTGAGAGATGTACTGGTC	BC095587
	<i>ifnphi1</i>	Fw: GAGCACATGAACCTCGGTGAA Rv: TGCCTATCTGCCACACATT	BC162493.1
	<i>ifnphi2</i>	Fw: CCTCTTGCCAACGACAGTT Rv: CGGTTCTTGAGCTCTCATC	BX005440.4
SVCV	<i>n-SVCV</i>	Fw: GCATTATGCCGCTCCAAGAG Rv: AGCTTGCATTGAGATCGA	U18101
	<i>g-SVCV</i>	Fw: TACAGATTGGGGATCTG Rv: ACCAACGTTCCATCAACACA	NC_002803

Figures

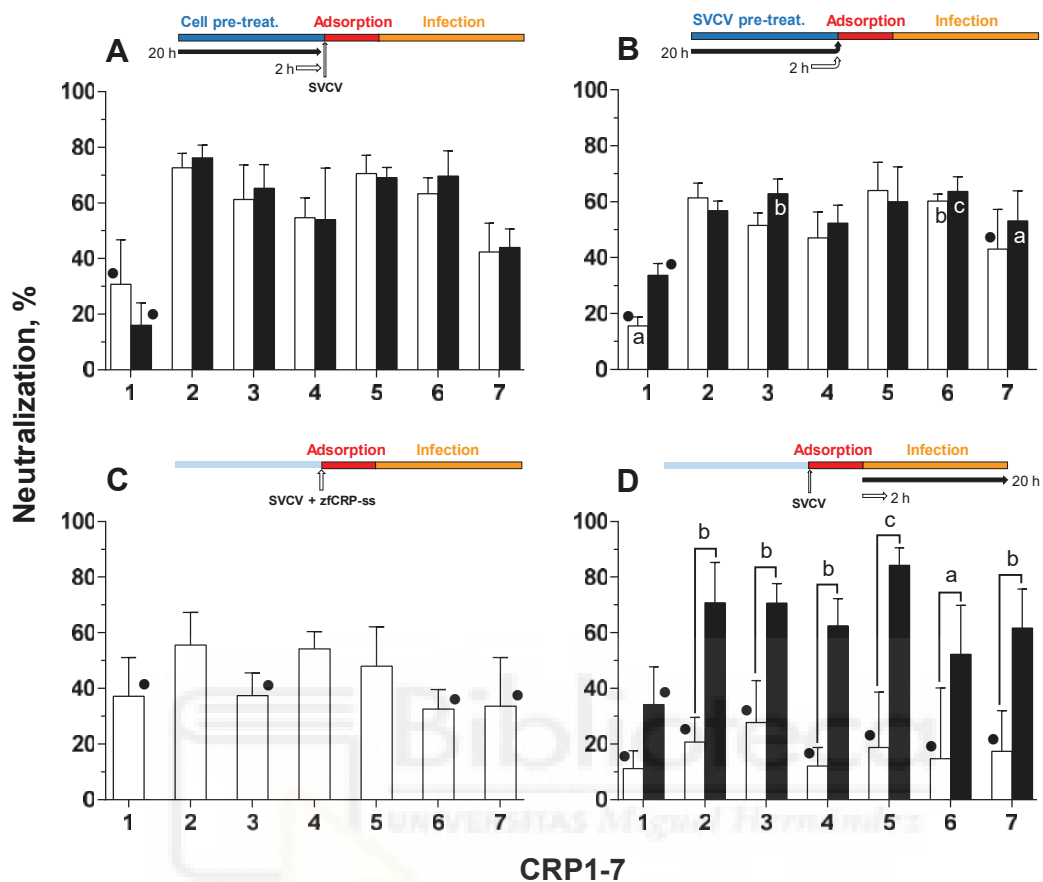


Figure 1

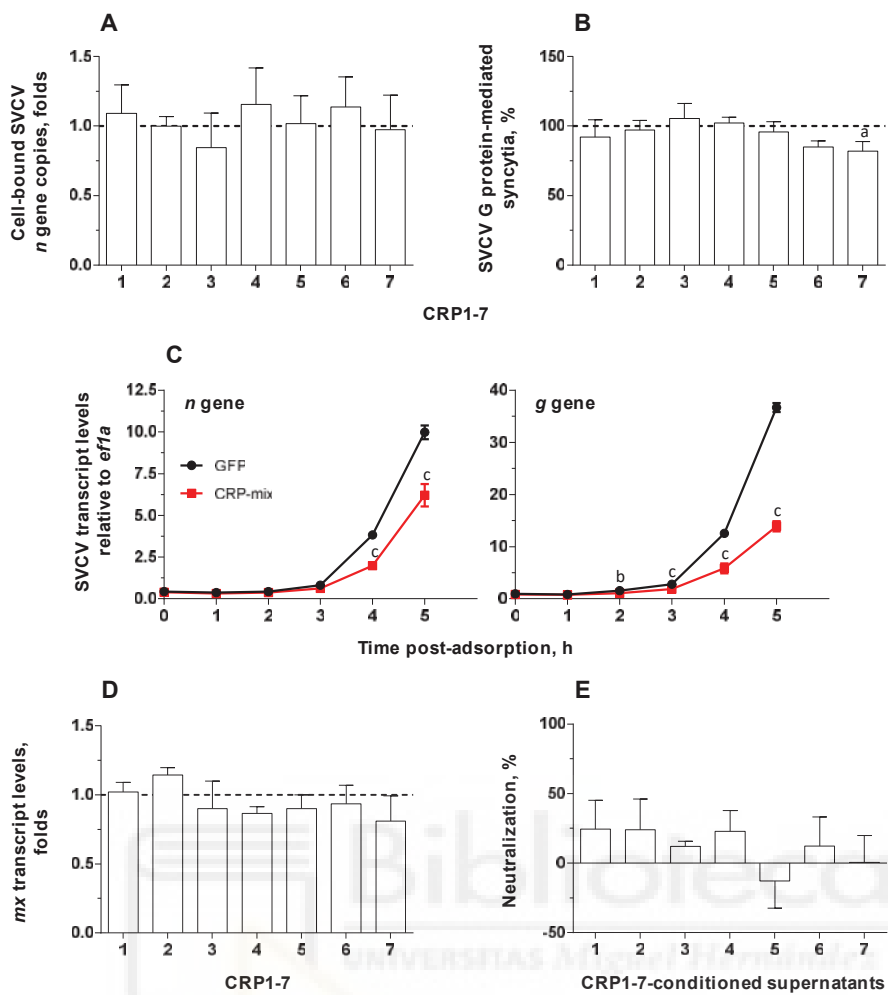


Figure 2

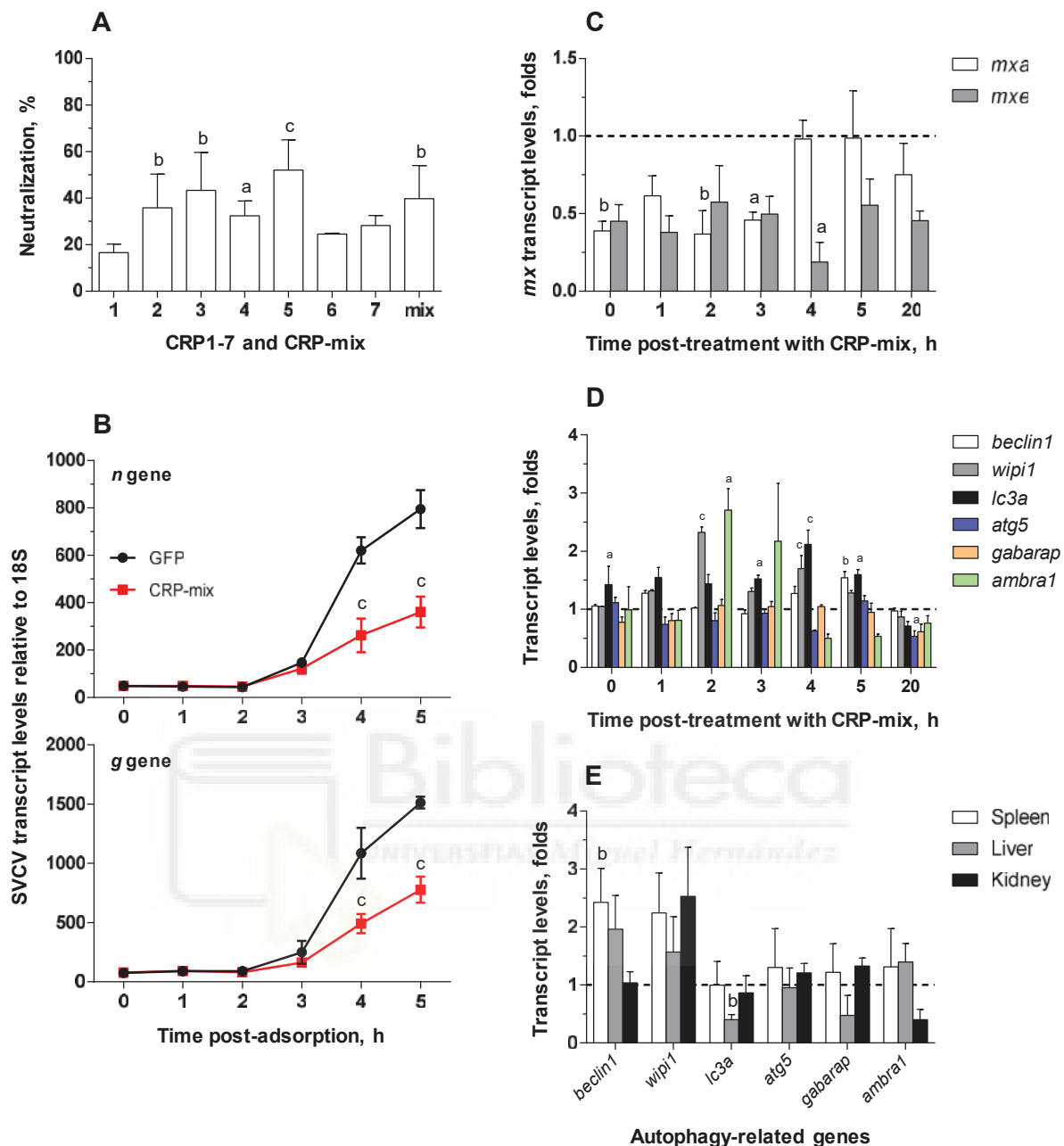


Figure 3

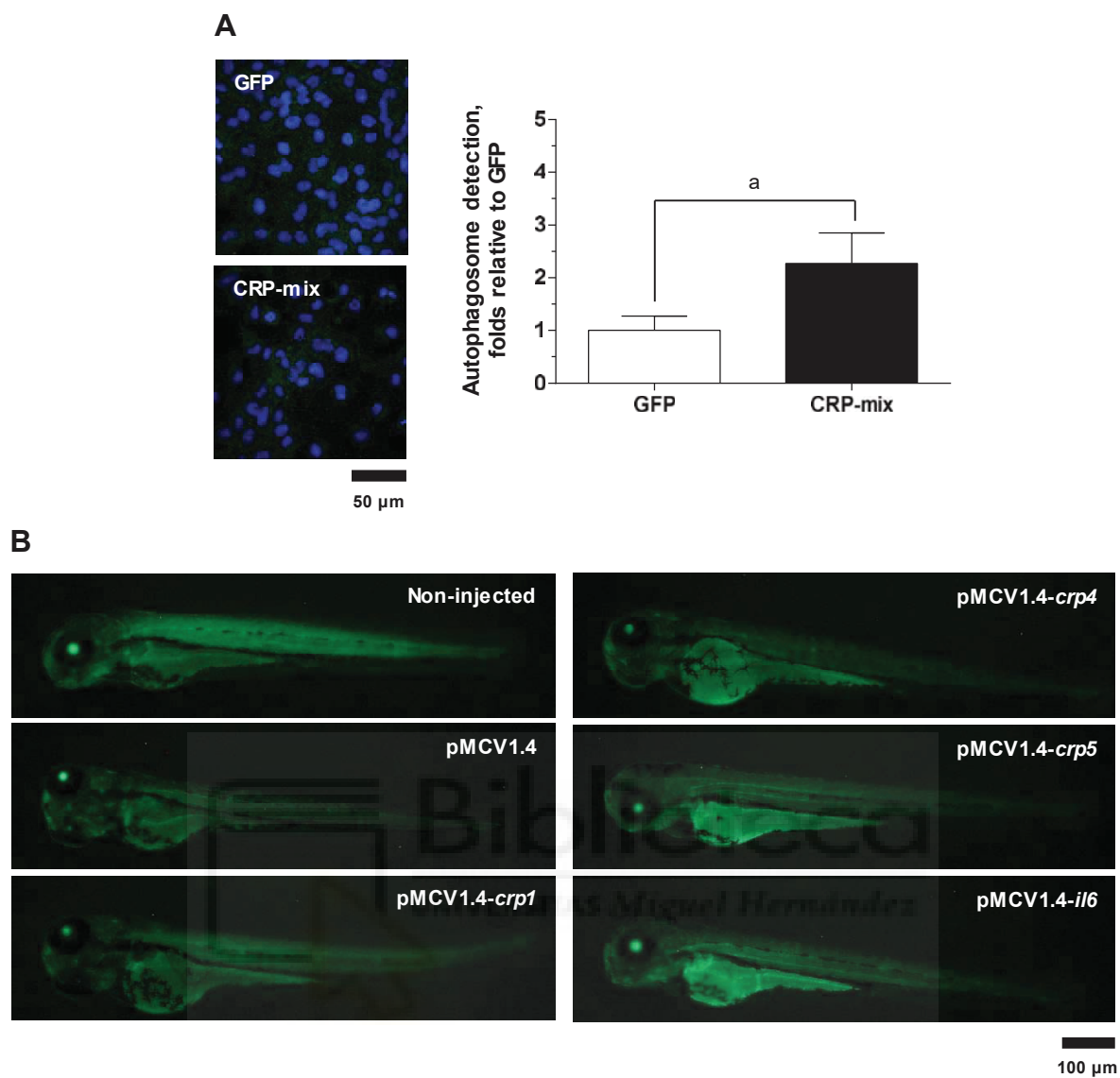


Figure 4

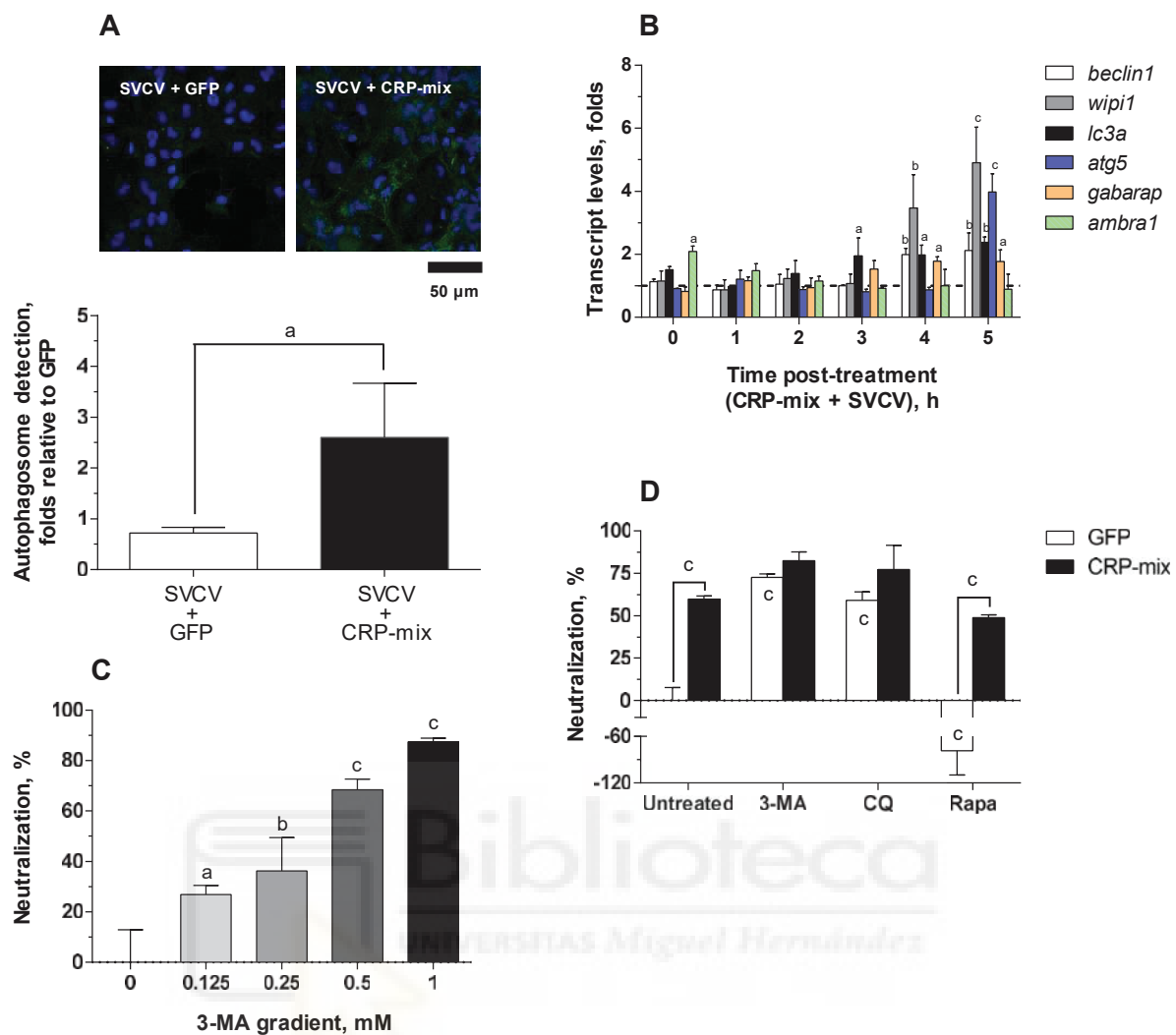


Figure 5

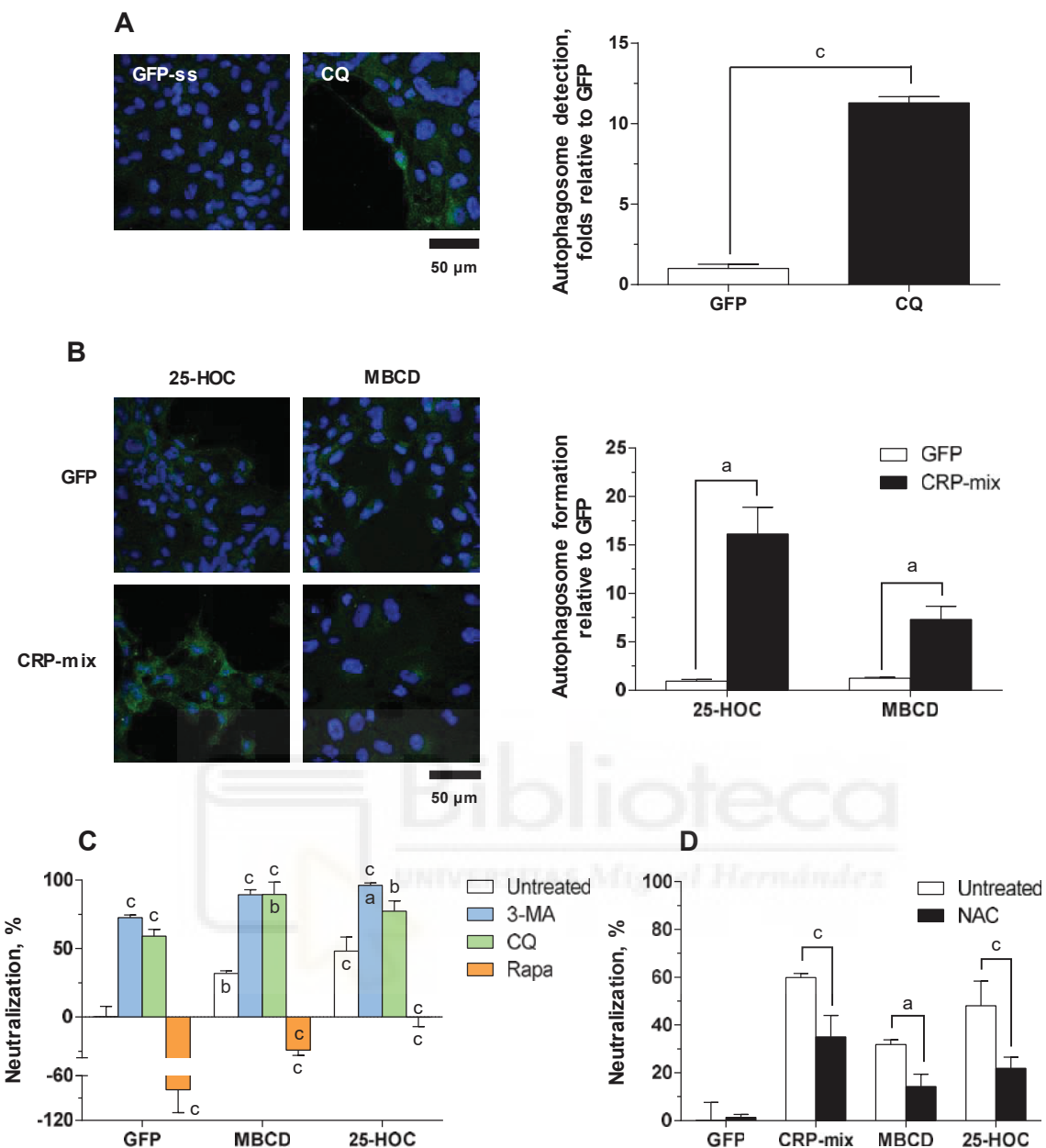


Figure 6

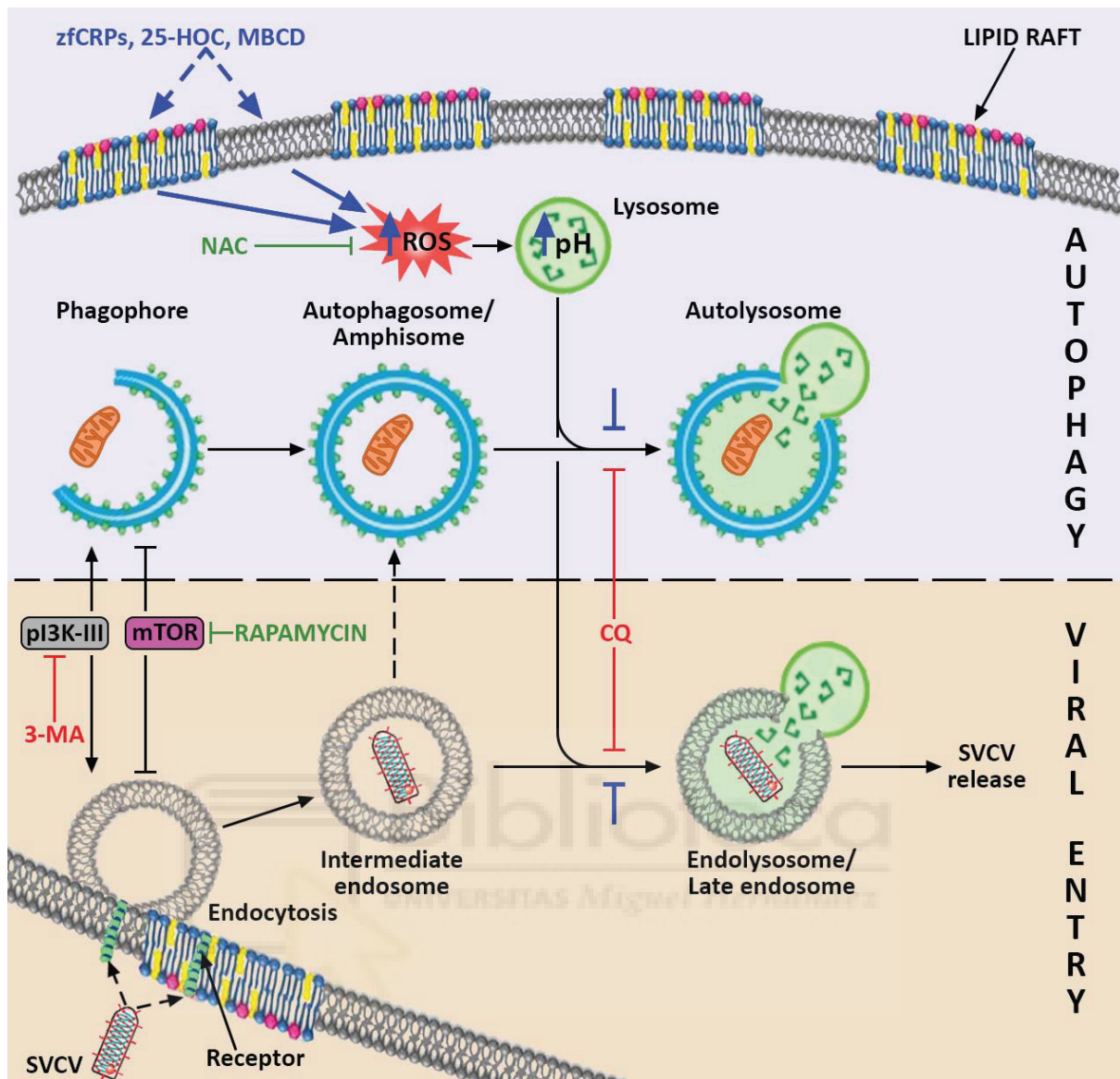


Figure 7

Supplementary figures

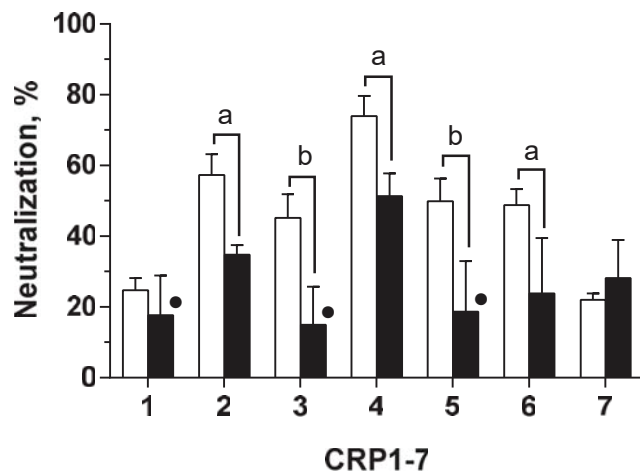


Figure S1

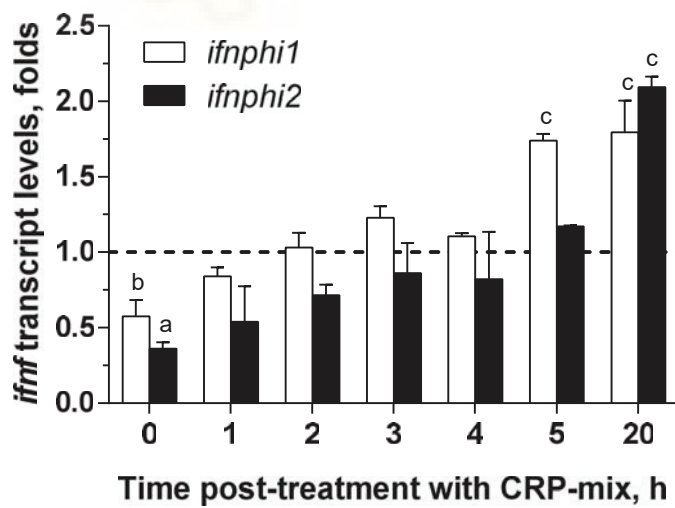


Figure S2

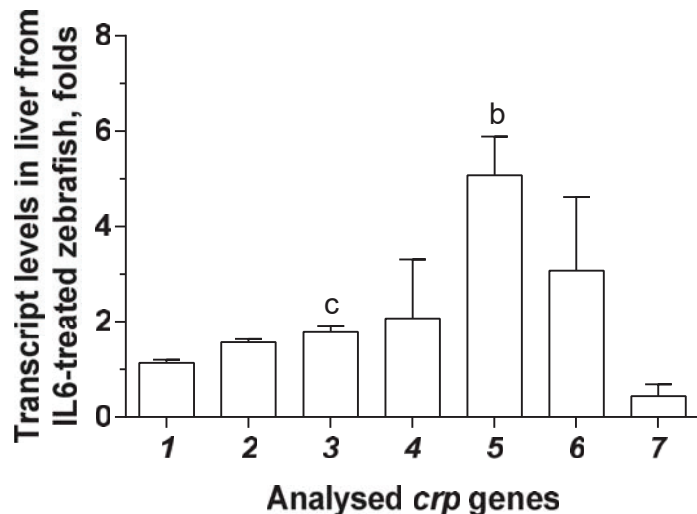


Figure S3

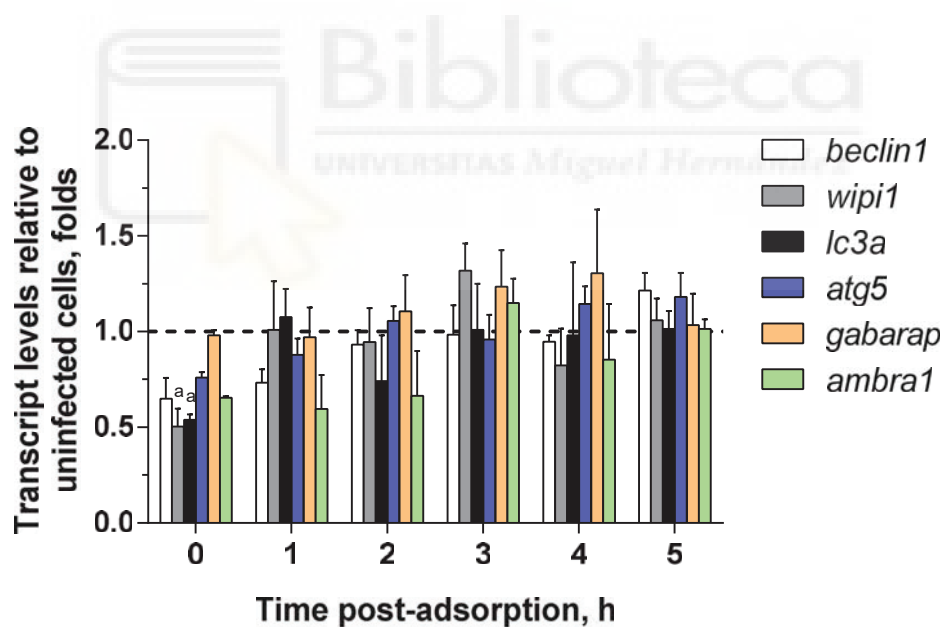


Figure S4

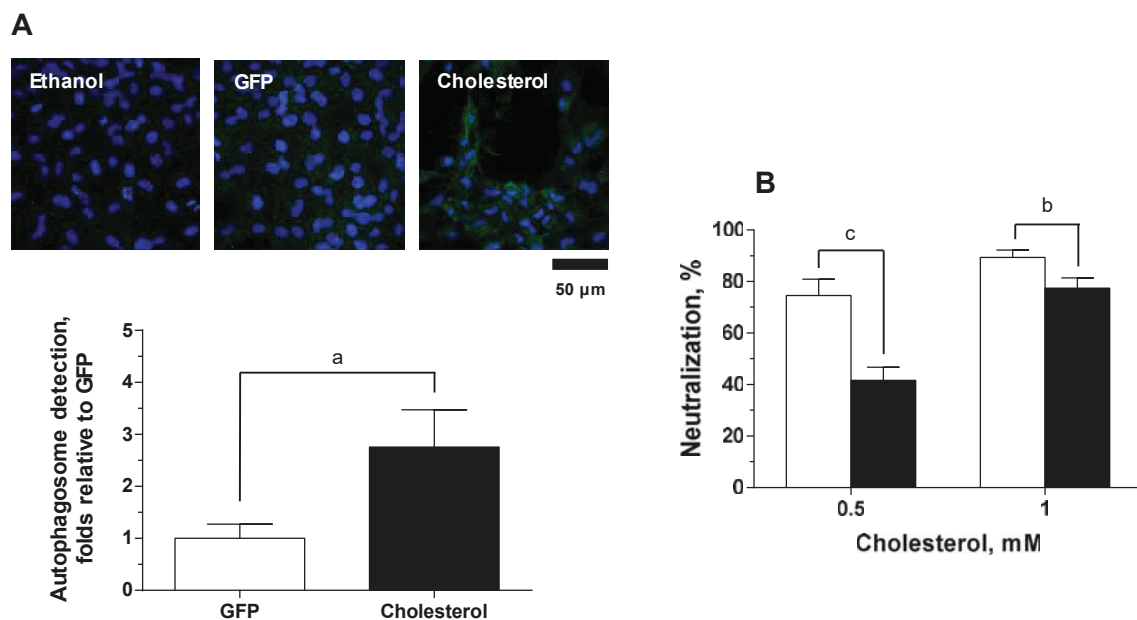


Figure S5



Figure captions

Figure 1. Effect of the treatment of CRP on the replication of SVCV in EPC cells. The neutralization activity of CRP1-7 was analyzed by adding the CRP at different points of the replication of SVCV. Each of the CRP was incubated with (A) EPC cells before virus adsorption, (B) SVCV before and during virus adsoption, (C) both EPC cells and SVCV only during virus adsoption and (D) infected EPC cells (i.e., after adsorption). The duration of co-incubations was either 2 h (white bars) or 20 h (black bars). Describing experimental timeline charts are included as insets in the top of each corresponding graph. SVCV infection was determined by the focus forming assay. Data were expressed as percentages of neutralization, which were calculated by the formula: $100 - (\text{number of fluorescent foci in the treatment group} / \text{number of fluorescent foci in the control GFP group}) \times 100$. Graphs represent the mean and s.d. of three independent experiments, each one performed in triplicate. •, indicates no significant differences between the treatment and the control (GFP treatment). The $P \leq 0.05$, $P \leq 0.01$ and $P \leq 0.001$ statistical differences were indicated as either a, b or c, respectively. Inside-bar symbols from graph (B) indicate significant differences in comparison to corresponding CRP treatments in (C). Statistically significant differences between different times within the same CRP treatment are shown with symbols over the keys connecting both groups.

Figure 2. Interaction of CRP1-7 on SVCV replication in EPC cells. (A) SVCV binding levels to EPC cell surfaces in the presence of CRP1-7. EPC cell-bound SVCV particles in the presence of CRP were quantified by the *ef1a*-relative amounts of SVCV *n* gene copies by RT-qPCR and expressed as folds of change by the formula: n gene copies in CRP1-7-treated monolayers / n gene copies in GFP-treated monolayers. (B) CRP1-7 inhibition of the fusogenic activity of SVCV G protein in the surface of SVCV-infected EPC cells. The levels of G protein-mediated syncytia of 5 or more cells in SVCV-infected EPC cell monolayers were determined by triggering cell fusion at pH 6 in the presence of CRP and expressed as percentage of counted syncytia by the formula: $100 \times (\text{number of syncytia in CRP1-7-treated monolayers} / \text{number of syncytia in GFP-treated monolayers})$. (C) Time course of SVCV replication *in vitro* at early stages post-adsorption. EPC cell monolayers were incubated for 2 h with CRP-mix before viral adsorption and SVCV replication estimated by measuring the expression of SVCV *n* and *g* gene transcripts by RT-qPCR and expressed as folds of change by the formula: $\text{SVCV } n \text{ or } g \text{ transcripts at each time point in treated or control monolayers} / \text{ef1a transcripts in corresponding monolayers}$. (D) Modulation of the IFN system by CRP1-7. The transcript levels of the IFN-response reporter *mx* gene were quantified by RT-qPCR in EPC cells 20 h after their treatment with CRP for 2 h and normalized to corresponding *ef1a* levels. Data were expressed as folds of change by the formula: $mx \text{ expression in CRP1-7-treated monolayers} / mx \text{ expression in GFP-treated monolayers}$. (E) Presence of antiviral factors in supernatants from CRP1-7-treated EPC cell monolayers. The SVCV neutralization induced by supernatants collected from EPC cells previously treated for 2 h with CRP1-7 was determined by the focus forming assay. The results are expressed relative to GFP treatments by the formula: $100 - (\text{number of fluorescent foci in the treatment group} / \text{number of fluorescent foci in the control GFP group}) \times 100$. All experiments were performed 3 times each by triplicates, except for (C) and (D) that were performed twice each by tetraplicates. Data were represented as the mean and s.d. The statistically significant different levels between them indicated with symbols as indicated in Fig. 1 and methods.

Figure 3. Effect of CRP1-7 on SVCV replication in ZF4 zebrafish cells. (A) SVCV neutralization of CRP1-7 and CRP-mix when incubated with ZF4 cells for 2 h before virus adsorption. SVCV infection was determined by the focus forming assay. The results are represented as percentages of neutralization by the formula: $100 - (\text{number of fluorescent foci in the treatment group} / \text{number of fluorescent foci in the control GFP group}) \times 100$. These experiments were performed 3 times each by triplicates. (B) Time course of SVCV replication at early stages post-adsorption. SVCV replication levels in ZF4 cells, incubated for 2 h with CRP-mix before viral

adsorption, were determined at 0-5 h by measuring the expression of SVCV *n* and *g* gene transcripts by RT-qPCR and expressed as folds of change by the formula: SVCV *n* or *g* transcripts at each time point in treated or control monolayers / 18S ribosomal transcripts in corresponding monolayers. (C) Induction of the IFN system by the CRP-mix. The transcript levels of two IFN-response reporter gene isoforms of Mx (*mxa* and *mxe*) were quantified by RT-qPCR in ZF4 cells treated with the CRP-mix for 2 h before viral infection at different times post-adsorption (0-5 and 20 h). Data were normalized to corresponding 18S ribosomal levels and expressed as in Fig. 2D. (D) Capacity of the CRP-mix to modulate autophagy-related transcripts *in vitro*. The transcript levels of relevant autophagy genes (*beclin1*, *wipi1*, *lc3a*, *atg5*, *gabarp* and *ambra1*) were quantified as described in (C). All *in vitro* gene expression studies were performed twice in triplicates. (E) Capacity of the CRP-mix to modulate autophagy-related gene transcripts *in vivo*. Four adult zebrafish were i.p. injected with CRP-mix. Two days post-injection, the transcript levels of the autophagy-related genes previously analyzed *in vitro* were quantified by RT-qPCR in spleen, liver and kidney tissues. Data are normalized to corresponding 18S ribosomal levels and expressed as folds of change by the formula: gene expression in fish injected with CRP-mix / gene expression in fish injected with GFP. All data are represented as the mean and s.d. The statistically significant level differences between them are indicated with symbols as indicated in Fig. 1 and in methods.

Figure 4. LC3 recruitment by selected CRPs *in vitro* in ZF4 cells and *in vivo* in zebrafish larvae. (A) Representative confocal images of FITC immune-labeled LC3B in ZF4 cells treated with either GFP or CRP-mix for 4 h. Nuclei were stained with DAPI. Autophagosome levels were quantified as the area (per cell) of over-threshold green fluorescence corresponding to intracellular puncta and represented as folds of change in comparison to the GFP treatment by the formula: over-threshold fluorescence per cell in CRP-mix-treated monolayers / over-threshold fluorescence per cell in GFP-treated monolayers. This experiment was performed 3 times, each of them by triplicates. Symbol “a” indicates statistically significant differences between CRP-mix and GFP treatments at the $P < 0.05$ level. (B) Representative images of GFP-LC3 transgenic zebrafish larvae at 3 days post-injection with 150 pg of pMCV1.4 or pMCV1.4-*crp1/crp4/crp5/il6* plasmid constructs. Corresponding scale bars of 50 and 100 μm are included.

Figure 5. Autophagy induced by CRP-mix on SVCV replication in ZF4 cells. (A) Representative confocal images of FITC immune-labeled LC3B in ZF4 cells treated with either GFP or CRP-mix together with SVCV for 4 h. Nuclei were stained with DAPI. Autophagosome levels were quantified as described in Fig. 4 and in methods. Scale bar of 50 μm is included. (B) Ability of the CRP-mix to modulate autophagy-related gene transcription *in vitro* during an SVCV infection. The transcript levels of the genes of relevant autophagy elements (*beclin1*, *wipi1*, *lc3a*, *atg5*, *gabarp* and *ambra1*) were quantified by RT-qPCR in ZF4 cells treated with CRP-mix for 2 h before to viral inoculum (MOI 1) at different times post-adsorption (0-5 and 20 h). This experiment was performed twice in triplicates. Data are expressed as indicated in Fig. 3. (C) Effect of the autophagy inducer 3-MA on SVCV replication. The SVCV neutralization activity of a gradient of 3-MA (0-1mM) when incubated with EPC cells for 20 h prior to virus adsorption was assessed. SVCV infection was determined by the focus forming assay. The results are represented as percentages of neutralization relative to untreated group by the formula: 100 - (number of fluorescent foci in the 3-MA-treated group / number of fluorescent foci in the non-treated group) $\times 100$. (D) Effects of the CRP-mix on the SVCV neutralizing activity of autophagy modulators *in vitro*. SVCV infectivity was assessed on EPC cells treated with 3-MA (1 mM, 20 h), CQ (25 μM , 30 min) and rapamycin (Rapa, 25 μM , 4 h), and then incubated for 2 h with the CRP-mix before infection. SVCV infection was determined by the focus forming assay and data represented as in (C) and relative to the GFP-treated group. Statistically significant differences in comparison to corresponding untreated groups and GFP are shown inside and on top of bars, respectively. Neutralization experiments were performed 3 times each by triplicates. The

statistically significant level differences are indicated with symbols as indicated in Fig. 1 and in methods.

Figure 6. Autophagy and ROS generation during the SVCV neutralizing activity induced by 25-HOC and MBCD together with CRP-mix. Representative confocal images of FITC immune-labeled LC3B in ZF4 cells treated with (A) either GFP or CQ (25 μ M) and (B) 25-HOC (10 μ g/mL) or MBCD (4 mM) alone or in combination with CRP-mix for 4 h. Nuclei were stained with DAPI. Autophagosome levels were quantified as described in Fig. 4 and in methods. Scale bar of 50 μ m is included. (C) Effect of 25-HOC and MBCD on the SVCV neutralizing activity of autophagy modulators *in vitro*. SVCV infectivity was assessed on EPC cells treated with 3-MA (1 mM, 20 h), CQ (25 μ M, 30 min) and rapamycin (Rapa, 25 μ M, 4 h), and then incubated for 2 h with 10 μ g/mL of 25-HOC or 1 mM MBCD before infection. SVCV infection was determined by the focus forming assay. Statistically significant differences in comparison to corresponding GFP and untreated groups are shown inside and on top of bars, respectively. (D) Effect of NAC on the SVCV neutralizing activity of CRP-mix, 25-HOC and MBCD *in vitro*. SVCV infectivity was assessed on EPC cells treated with NAC (1 mM, 20 h) and then incubated for 2 h with either GFP, CRP-mix, 10 μ g/mL 25-HOC or 1 mM MBCD before infection. SVCV infection was determined by the focus forming assay. The results from neutralization assays are represented as in Fig. 5. These experiments were performed 3 times by triplicates. All statistically significant level differences between treatment and corresponding control groups are indicated with symbols as in Fig 1 and in methods.

Figure 7. Proposed model for the mechanism by which CRPs, 25-HOC and MBCD interact with autophagy and SVCV entry. It is suggested that these three compounds (their proposed effects are indicated in blue) produce an imbalance in membrane cholesterol in the lipid rafts, what induces the increase of intracellular ROS. In turn, ROS stimulates the increment of lysosomal pH that reduces the fusion of lysosomes and intermediate endosomes (indicated with blue stoppers) and thus the formation of late endosomes/endolysosomes. Since SVCV requires the formation of endolysosomes because of their low pH to trigger the fusion conformation of the SVCV G protein for viral entry, this blockade impairs SVCV release into host's cytosol. The scheme shows that SVCV endocytic and autophagy pathways share common elements allowing the action of particular autophagy modulators on both of them. The potential convergence of pathways resulting in the formation of the amphisome, described for other viruses, is also indicated. The positive regulators of both routes are drawn in green and the negative ones in red.

Supplementary figure captions

Figure S1. Antiviral activity of CRP1-7-depleted supernatants. Each CRP1-7-containing supernatant was CRP depleted by incubation with immobilized 25-HOC in ELISA plates for 2 h. Whole CRP1-7 (white bars) and depleted CRP1-7 (black bars) were incubated with EPC cells for 2 h prior to SVCV adsorption (MOI 10⁻²). SVCV infection was determined by the focus forming assay. Data are expressed as percentages of neutralization by the formula: 100 - (number of fluorescent foci in the treatment group / number of fluorescent foci in the control GFP group) × 100. Data represent the mean and s.d. of two independent experiments, each performed in triplicate. •, indicates no significant differences between the treatment and the GFP control. Statistically significant differences are indicated as in Fig. 1 and in methods.

Figure S2. Assessment of the ability of CRP-mix to induce the transcription of *ifnphi1* and *2* *in vitro*. The transcript levels of *ifnphi1* and *ifnphi2* were quantified by RT-qPCR in ZF4 cells treated with CRP-mix for 2 h prior to SVCV inoculum at different times post-adsorption. Data are expressed as folds of change relative to GFP treatments by the formula: *ifn* expression in CRP-mix-treated monolayers / *ifn* expression in GFP-treated monolayers. This experiment was performed twice in tetraplicate, the results were represented as the mean and s.d. and the statistically significant differences in comparison to GFP-treatment group were indicated as in Fig. 1 and methods.

Figure S3. Assessment of the ability of IL6 to induce the expression of *crp1-7* transcripts *in vivo*. Four adult zebrafish were i.p. injected with supernatants enriched in IL6. Two days post-injection, the transcript levels of each *crp1-7* isoform from liver were quantified by RT-qPCR and normalized to 18S ribosomal levels in corresponding samples. Data were expressed as folds of change relative to GFP treatments by the formula: *crp1-7* expression in liver of zebrafish injected with IL6 / *crp1-7* expression in liver of zebrafish injected with GFP. The results are represented as the mean and s.d. and the statistically significant differences in comparison to the GFP-treated group were indicated as in Fig. 1 and methods.

Figure S4. Transcriptional modulation of autophagy by SVCV in ZF4 cells. The transcript levels of the genes of relevant autophagy elements (*beclin1*, *wipi1*, *lc3a*, *atg5*, *gabarp* and *ambra1*) were quantified at different times post-adsorption (0-5 h) by RT-qPCR in ZF4 cells treated with GFP for 2 h prior to viral inoculum (MOI 1). This experiment was performed twice in tetraplicates. Data are expressed as indicated in Fig. 3 (relative to the uninfected group). The statistically significant differences in comparison to the control group were indicated as in Fig. 1 and methods.

Figure S5. Effect of the addition of exogenous cholesterol on intracellular autophagosome levels and SVCV infection *in vitro*. (A) Representative confocal images of FITC immune-labeled LC3B in ZF4 cells treated with GFP, cholesterol, as well as ethanol (solvent control of both 25-HOC and cholesterol), for 4 h. Nuclei were stained with DAPI. Autophagosome levels were quantified as described in Fig. 4 and in methods. Scale bar of 50 µm is included. (B) Effect of cholesterol in the absence and presence of MBCD on SVCV replication *in vitro*. SVCV infectivity was assessed on EPC cells treated with cholesterol (0.5 and 1 mM) together with MBCD at either 0.5 mM (white bars) or 1 mM (black bars) for 2 h before infection. SVCV infection was determined by the focus forming assay. The results are represented as percentages of neutralization relative to the untreated group. This experiment was performed 3 times by triplicate. Statistically significant differences between cholesterol treatments with and without MBCD are indicated as in Fig. 1 and methods.

ANEXO 1

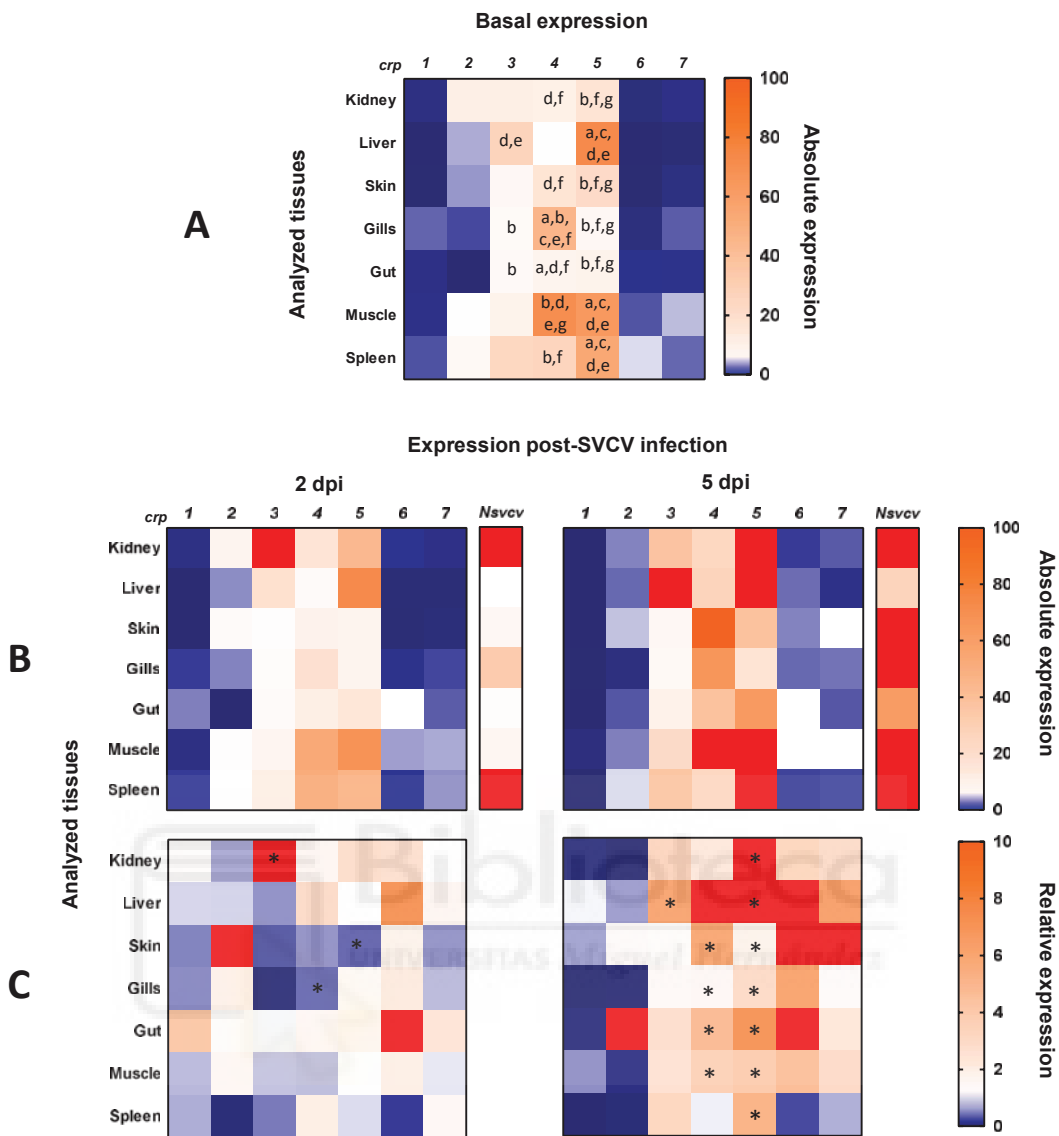
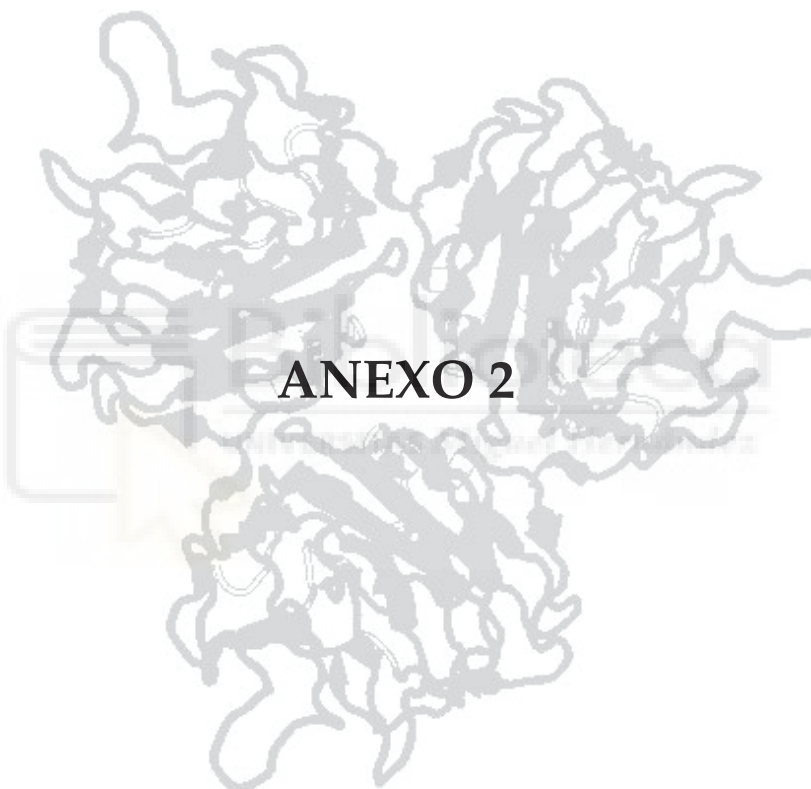


Figura 1. Matriz de expresión génica de *zfcrp1-7* y *n-SVCV* en tejidos de pez cebra adultos. A) Niveles transcripcionales de *zfcrp1-7* constitutivos. B) Niveles de transcripción de *zfcrp1-7* a 2 y 5 dpi de SVCV. C) Veces de incremento/diminución de los niveles de tránscritos de *zfcrp1-7* a 2 y 5 dpi con respecto a la expresión constitutiva. La expresión de los genes fue evaluada por RT-qPCR. Cada valor de expresión de *zfcrp* se normalizó por el valor de *ef1a* (expresión de cada gen / expresión de *ef1a*). Cada nivel de expresión se representa como un cuadrado de color en la posición correspondiente a su gen y tejido. El color depende del nivel de expresión según una escala de tres colores (azul: expresión baja, blanco: expresión media, rojo: expresión alta). Las diferencias de expresión constitutiva de una *zfcrp* entre diferentes tejidos se indican con letras. Cada letra representa un tejido: a, riñón; b, hígado; c, piel; d, branquias; e, intestino; f, músculo y g, bazo. Cuando la expresión de una *zfcrp* en un tejido es significativamente diferente a la expresión en otro ($p \leq 0,05$), en el cuadrado aparece la letra del tejido con el que presenta diferencias significativas. * indica diferencias significativas entre expresión constitutiva y expresión después de la infección.



PUBLICACIÓN 5

TÍTULO: Discovery of nonnucleoside inhibitors of polymerase from infectious pancreatic necrosis virus (IPNV)

COAUTORES: Melissa Belló Pérez, Alberto Falcó Graciá, Vicente Galiano Ibarra, Julio Coll Morales, Luis Perez García-Estañ, Jose Antonio Encinar Hidalgo

REVISTA: Drug Design, Development and Therapy

doi: 10.2147/DDDT.S171087

Discovery of nonnucleoside inhibitors of polymerase from infectious pancreatic necrosis virus (IPNV)

Melissa Bello-Pérez¹

Alberto Falcó¹

Vicente Galiano²

Julio Coll³

Luis Pérez¹

José Antonio Encinar¹

¹Molecular and Cell Biology Institute (IBMC), Miguel Hernández University (UMH), Elche, Spain; ²Department of Physics and Computer Architecture, Miguel Hernández University (UMH), Elche, Spain; ³Department of Biotechnology, Instituto Nacional de Investigación y Tecnología Agraria y Alimentaria (INIA), Madrid, Spain

Introduction: Infectious pancreatic necrosis virus (IPNV) causes serious losses in several fish species of commercial interest. IPNV is a non-enveloped double-stranded RNA virus with a genome consisting of two segments A and B. Segment B codes for the VP1 protein, a non-canonical RNA-dependent RNA polymerase that can be found both in its free form and linked to the end of genomic RNA, an essential enzyme for IPNV replication.

Materials and methods: We take advantage of the knowledge over the allosteric binding site described on the surface of the thumb domain of Hepatitis C virus (HCV) polymerase to design new non-nucleoside inhibitors against the IPNV VP1 polymerase.

Results: Molecular docking techniques have been used to screen a chemical library of 23,760 compounds over a defined cavity in the surface of the thumb domain. Additional ADMET (absorption, distribution, metabolism, excretion, and toxicity) filter criteria has been applied.

Conclusion: We select two sets of 9 and 50 inhibitor candidates against the polymerases of HCV and IPNV, respectively. Two non-toxic compounds have been tested in vitro with antiviral capacity against IPNV Sp and LWVRT60 strains in the low μM range with different activity depending on the IPNV strain used.

Keywords: IPNV, HCV, antiviral drugs, non-nucleoside inhibitors, RdRp, molecular docking

Introduction

Since the discovery of the first vaccine against smallpox in 1796 by Edward Jenner, society has relied almost entirely on the development of new vaccines to battle viral diseases. However, the world's capacity for vaccine development is currently already falling behind the rate of emergence and reemergence of dangerous viral diseases. Indeed, viral diseases are particularly troublesome, because effective treatments against most of them are lacking. For instance, approximately half the short list of US Food and Drug Administration-approved antiviral drugs are aimed at HIV1 and those remaining target only six more viruses.¹ Furthermore, resistance to existing antimicrobials is emerging, along with new viral pathogens.² Consequently, urgent efforts are necessary to accelerate novel antiviral drug discovery. One such technology that has allowed for the *in silico* screening of large amounts of compounds for targeting specific sites within functionally significant proteins is the use of bioinformatic tools. Through the use of increasingly potent computational hardware systems combined with the ever-increasing availability of detailed information on the molecular structure of relevant proteins and extensive chemical libraries, significant advances have been made in both clinical and veterinary fields.^{3,4}

Correspondence: José Antonio Encinar;
Alberto Falcó
Molecular and Cell Biology Institute,
Edificio Torregaitán, Miguel Hernández
University, Avenida de la Universidad,
Elx 03202, Alicante, Spain
Tel +34 9 665 8453
Fax +34 96 665 8758
Email jant.encinar@umh.es;
alber.falco@umh.es

Infectious pancreatic necrosis virus (IPNV) was the first virus to be isolated from fish, and is now recognized as the known causative agent of IPN disease, which mainly affects cultured salmonids.⁵ IPNV belongs to the family Birnaviridae and is a member of the genus *Aquabirnavirus*. IPNV is the prototype member of the genus *Aquabirnavirus* of the family Birnaviridae. The most characteristic macro- and histopathological symptoms of this disease are exophthalmia, skin hyperpigmentation, abdominal and pyloric petechial hemorrhages, erratic swimming, and necrosis of both the kidney and pancreas.^{5,6}

Infection outbreaks by IPNV can cause high mortality in first-feeding fry and postsmolts,^{7,8} consequently incurring high economic losses to the aquaculture industry.^{6,9,10} The mortality rate is very variable (10%–90%) and affects youngest fish to a greater extent, reaching 45%, 35%, and 7% in 1-, 2-, and 4-month-old fish, respectively.¹¹ Interestingly, while currently unlisted in the Model Aquatic Health Code of the World Organization for Animal Health, the presence of IPNV is continuously being detected worldwide in both aquacultured^{12–17} and wild fish, including several nonsalmonid species.^{15,17–19} Apart from the fact that this virus is transmitted both vertically and horizontally,^{20,21} fish that recover or are asymptotically infected often become carriers of the virus throughout their lives,^{11,22} contributing to its broad spread. Unfortunately, there is no therapy for this disease, so current protective measures are aimed at avoiding and alleviating its incidence. Such approaches have included less stressful handling of animals, use of IPN-resistant fish lines, improved management procedures, and the use of vaccination programs. In any case, the spread of the virus has been shown to be unpredictable, and there is still room to improve the protection conferred by existing vaccines, such as reducing their cost and making them more suitable to all life stages.⁹

IPNV is an enveloped virus with an icosahedral and single-shelled capsid ($T=13$ symmetry) of about 60 nm in diameter, which consists of two proteins (VP2 and VP3). Its linear dsRNA genome is bisegmented (segment A 3,097 nucleotide [nt], segment B, 2,784 nt), uncapped, and unpolyadenylated.¹⁰ Segment A is bicistronic. Among its two open reading frames (ORFs), the largest one, ORF L, codes for the proteins VP2-4 as a 106-kDa polyprotein (NH₂-pVP2-VP4-VP3-COOH) which is co-translationally cleaved by the viral protease VP4. The precursor pVP2 belongs to the major capsid protein VP2 (being most abundant overall),²³ of which VP3 is a minor capsid protein that complexes with the dsRNA genome.¹⁰ In turn, the other segment-A ORF (ORF S) is not present in all isolates. ORF S overlaps the amino-terminal end of ORF L

and encodes VP5. VP5 is variable in size (3.3–17 kDa) and a nonstructural protein that is not essential for viral infectivity, but may contribute to the virulence of the strain by presumably triggering an antiapoptotic mechanism.²⁴ Segment B contains a single ORF that encodes the VP1 protein, which is a noncanonical RNA-dependent RNA polymerase (RdRp; 94 kDa). This protein, which can be found in its free form or indistinctively linked to the end of the genomic RNA (VPg),²⁵ lacks the hallmark catalytic GDD signature in the region corresponding to the presumptive motif VI of infectious bursal disease virus.²⁶ However, it presents a spatially rearranged LDD motif (residues 653–655 from Protein Data Bank [PDB] 2YI8).²⁷ VP1 also has enzymatic activity, such as that possessed by guanylyl and methyl transferase.²⁸

Taking advantage of the knowledge obtained from previous studies on the allosteric binding site described on the surface of the thumb domain of hepatitis C virus (HCV) polymerase,²⁹ we herein explored a similar site in IPNV VP1 polymerase, allowing for the discovery of new antiviral drugs. This work describes the molecular docking results for a chemical library selected against a cavity site in the thumb domain of the RdRp of different IPNV strains, the successive filters applied for candidate compounds, and preliminary biological assays aimed at assessing antiviral capacity and specificity against two different IPNV strains for two of the selected candidates.

Materials and methods

Chemical compounds for antiviral assays

The compounds with the PubChem IDs 3274414 and 39834288 were purchased from the chemical supplier Ambinter (supplier references Amb10836885 and Amb674545, respectively) (Ambinter c/o Greenpharma Orléans, France).

Protein structure for IPNV RNA-dependent RNA-polymerase VP1 and chemical libraries

To date, five resolved structures have been deposited in the PDB for the VP1 protein of the Jasper strain of IPNV (UniProt code P22173): 2YI8, 2YI9, 2YIA, 2YIB, and 3ZED.^{30,31} However, no structures of this protein are yet deposited for the Sp (UniProt code P22174) or LWVRT60 (UniProt code A0A1B2AQF1) strains. Therefore, three-dimensional (3-D) structural models of the VP1 protein from both strains were generated by homology modeling in automated mode, using the 2YIB structure as a template.³² Briefly, a template search with BLAST and HHblits was performed against the Swiss-Model Template Library (SMTL; last update

December 6, 2017, last included PDB release December 1, 2017). The target sequence was searched with BLAST³³ against the primary amino-acid sequence contained in the SMTL. A total of 28–30 templates were found in each case. An initial HHblits profile was built using the procedure outlined in Remmert et al,³⁴ followed by one iteration of HHblits against NR20. The profile obtained was then searched against all profiles of the SMTL. A total of 140–163 templates were found in each case. For each template identified, its quality was predicted from features of the target-template alignment. Templates of the highest quality were then selected for model building. Models were built based on the target-template alignment using ProMod II. Coordinates conserved between the target and the template were copied from the template to the model. Insertions and deletions were remodeled using a fragment library. Side chains were then rebuilt. Finally, the geometry of the resulting model was regularized using a force field. In cases where loop modeling with ProMod II³⁵ did not yield satisfactory results, an alternative model was built with Modeller.³⁶ For these molecular docking studies, amino-acid sequences 31–36 and 122–157 were electronically removed in both models and template. Structures 2BRK and 2BRL of HCV NS5 RdRp from Di Marco et al²⁹ were used additionally, thereby employing nine structures for overall structural refinement. Visualization of the structures and preparation of the figures were carried out with PyMol 2.0 software.

For these experiments, a chemical library of 23,764 compounds was built using the option available at the PubChem site (<https://pubchem.ncbi.nlm.nih.gov/search/search.cgi>; in the “Identity/similarity” section) for searching structurally similar compounds to a given template. In our case, the structures of compounds 1 (PubChem ID 4369534) and 2 (PubChem ID 4369535), which were described to interact with the polymerase of HCV and to inhibit its activity,²⁹ were used as query templates. Compounds were subsequently searched with at least 70% structural identity, thus generating a chemical library to be tested in molecular docking experiments. The PubChem web application used herein to allowed for the 3-D chemical structure of all compounds retrieved to be downloaded as spatial data files.

Molecular docking procedures

Before carrying out molecular docking experiments, PDBQT files of both the protein (receptor) and the ligands of our chemical library were calculated.^{37,38} Next, the five structures and two models of VP1 proteins were subjected to a geometric optimization process using the repair function of the FoldX algorithm.³⁹ Molecular docking experiments were

performed using AutoDock Vina software version 1.1.2⁴⁰ and targeted to a grid with dimensions of 24×24×24 points centered around the cavity generated by the amino acids Glu557, Asn580, Ans624, Pro625, and Pro550 of HCV NS5 RdRp and likewise around the amino acids Trp500, Arg503, Pro495, Val494, Leu492, Leu392, Ala396, and His428 of the VP1 protein of IPNV. AutoDock Vina was set up on a lusitania2.cenits.es Linux cluster (Research, Technological Innovation, and Supercomputing Center of Extremadura, Cáceres, Spain). AutoDock Vina generates for each tested ligand a conformer docked to the binding site in the protein and calculates the Gibbs free-energy variation of the binding process. Compounds with lower ΔG (kcal/mol) outperform a first-screening filter as potential candidates for inhibitors.

Calculation of pharmacokinetic parameters and potential toxicity of inhibitor candidates

Physicochemical parameters for the best-docked compounds were calculated as described previously^{37,38} using DataWarrior version 4.7.2.⁴¹ ADMET (absorption, distribution, metabolism, excretion, and toxicity) properties were calculated with the AdmetSAR web application⁴² and DataWarrior.⁴¹ The same applications were used to calculate these parameters for the drugs included in the DrugBank database,⁴³ and they are available at the website <http://dockingfiles.umh.es/drugbank/DrugBanklist.asp>.

Cell culture and viral strains

The Chinook salmon-embryo cell line CHSE214 was purchased from the (European Collection of Authenticated Cell Cultures, Public Health England, Salisbury, UK) (91041114). It was maintained at 20°C in a 5% CO₂ atmosphere in Roswell Park Memorial Institute (RPMI) 1640 (Dutch modification) medium containing 10% FBS (Sigma-Aldrich, St Louis, MO, USA), 2 mM glutamine (Thermo Fisher Scientific, Waltham, MA, USA) and 50 µg/mL gentamicin (Thermo Fisher Scientific). Both Sp and LWVRT60 strains of IPNV were grown in CHSE214 cells at 14°C. When cytopathic effects were widespread, supernatants from infected cell cultures were clarified by centrifugation, filtered (0.22 µm), and stored in aliquots at -80°C. Virus titers were determined by end-point dilution in confluent CHSE214-cell monolayers grown in 96-well plates at 14°C in infection medium (ie, growth medium supplemented with 2% instead of 10% FBS). The Reed-Muench method⁴⁴ was used to calculate 50% tissue-culture infective dose (TCID₅₀)/mL. Average TCID₅₀/mL (and SD) for each batch was obtained from three different titrations.

Cytotoxicity assays

The potential toxicity of selected compounds on CHSE cells was analyzed by measuring changes in cell viability with MTT (Sigma-Aldrich) assays. Briefly, confluent cell monolayers in 96-well plates were treated with different concentrations of each type of compound in infection media for 24 hours (100 µL/well). Then, 0.5 mg/mL MTT from tenfold-concentrated stocks in PBS (stored at -20°C) in fresh media (100 µL/well) was used to replace treatments. MTT solutions were incubated with cells under the same conditions for an additional 4 hours. Finally, media were carefully removed and the colored formazan product dissolved in 100 µL dimethyl sulfoxide (DMSO; Merck, Kenilworth, NJ, USA) and measured at 570 nm vs reference absorbance at 620 nm with a SpectroStar Omega absorbance microplate reader (BMG LabTech, Ortenberg, Germany). OD is expressed in percentages relative to the control group consisting of untreated cells. Additional controls included corresponding compounds and solvents (DMSO for the PubChem 3274414 compound and DMSO:acetone 1:1 for the PubChem 39834288 compound up to a maximum final concentration of 0.5% v:v) at an equivalent concentration to that used at each compound concentration tested at 1, 5, 10, 20, and 50 µM. Cell viability was calculated by the formula: 100×(treated-cell absorbance/control-cell absorbance). All experiments were performed in triplicate, and results are shown as mean with SD calculated from three different experiments.

Antiviral assays

To test the influence of the selected compounds on IPNV infectivity, IPNV was added at a 0.01 multiplicity of infection in 100 µL RPMI 1640 (Dutch modification) medium supplemented with 2% FBS (infection medium) to confluent CHSE-cell monolayers grown in 96-well plates and incubated for 2 hours at 4°C (adsorption period). Then, infected cell monolayers were washed twice with PBS and compounds (PubChem ID 3274414 was dissolved in DMSO and PubChem ID 39834288 in DMSO: acetone 1:1) were added to corresponding wells in 100 µL infection medium at different concentrations of 1, 5, 10, 20, and 50 µM. The final concentration of organic solvent never exceeded 0.5% (v:v). Infected cells were further incubated with the treatments for 24 hours at 14°C. After incubation, cells were collected for quantification of the virus by reverse-transcription quantitative polymerase chain reaction (RT-qPCR). In parallel and as a control for each concentration of compound used, infected cells were also treated with the corresponding solvents at a concentration equivalent to each concentration of compound used. Positive and negative infection controls were also included.

All conditions were performed in triplicate (RT-qPCR was performed by pooling the cells of all replicates).

RNA isolation, cDNA synthesis, and RT-qPCR assays

Levels of each IPNV strain replicating in infected CHSE cells were evaluated by determining their content in viral transcripts. Therefore, RT-qPCR was performed on cDNA from CHSE-cell RNA previously used in the antiviral assays. Therein, RNA from the aforementioned collected cells was isolated using an E.Z.N.A.® Total RNA kit (Omega Bioteck, Norcross, GA, USA) following the manufacturer's guidelines. RNA concentration was assessed using a Nano-Drop 1,000 spectrophotometer (Thermo Fisher Scientific) by measuring absorbance at 260 nm. Samples were stored at -80°C until use.

In order to obtain cDNA reverse transcriptase (Moloney murine leukemia virus; Thermo Fisher Scientific), 1 µg RNA from each sample was used, as previously described.⁴⁵ RT-qPCR reactions were carried out using the ABI 7300 Real-Time PCR System (Thermo Fisher Scientific) with SYBR® Green Master Mix PowerUp SYBR Green Master Mix (Thermo Fisher Scientific). The total volume of each reaction was 20 µL and included 2 µL cDNA, 900 nM each primer, and 10 µL SYBR green PCR master mix. Nontemplate controls were performed for each gene analysis. Cycling conditions were 95°C for 10 minutes, followed by 40 cycles of 1 minute at 65°C, 15 seconds at 95°C, and finally an extension of 1 minute at 60°C and 15 seconds at 95°C. Results were obtained by normalizing the expression of the target gene respective to that of the endogenous reference using a variation of Livak and Schmittgen's method⁴⁶ by the formula $2^{C_{\text{ref}} - C_{\text{target}}}$. The endogenous gene used in this study was elongation *eif4a*. Primers used are shown in Table 1. All reactions were performed in duplicate. Results are presented as percentages of inhibition of IPNV infectivity relative to values obtained by an equivalent amount of corresponding solvent, and correspond to means with SD calculated from four different experiments.

Results and discussion

Exploring allosteric binding-site cavity from IPNVVP1 protein

Di Marco et al²⁹ reported the crystal structure of HCV RdRp (genotype 1b, strain BK) in a complex with two nonnucleoside inhibitors occupying a cavity (Figure 1A) that appeared in the thumb domain for deletion mutants lacking the 55 amino acids at the C-terminus ($\Delta C55$). Both compounds inhibited not only the purified full-length and truncated C-terminal $\Delta C55$ enzyme in a low-nanomolar range but also the replicon

Table I Primers used in this study

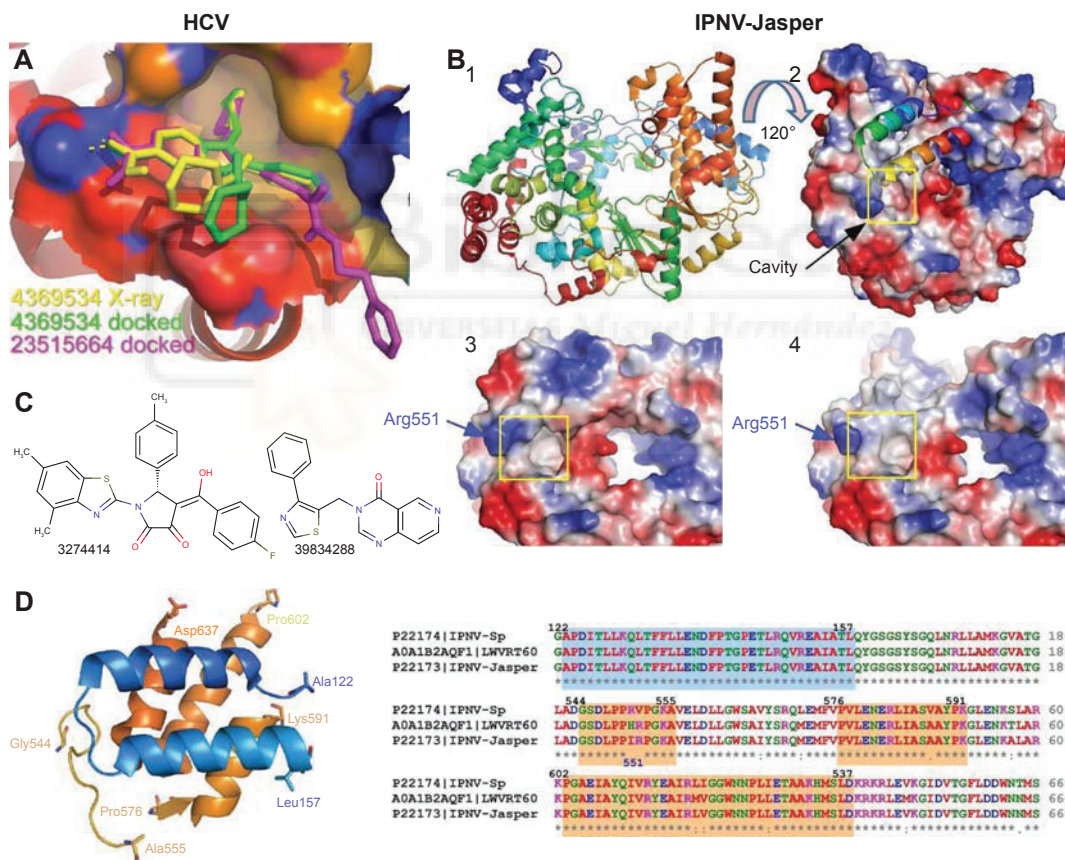
Organism ^a	Gene/segment ^b	Sequence (5'-3')	Accession ^c	Reference(s) ^d
<i>Salmo salar</i>	<i>eif1a</i>	Fw: GCCCCCTCAGGATGTCTAC Rv: CACGGCCCACAGGTACTG	BG933897	47
IPNV Sp	segA	Fw: TCTCCCGGGCAGTTCAAGT Rv: CGGTTTCACGATGGTTGTT	AJ622822	48, 49
IPNV LWVRT60	segB	Fw: TCGAGAACAAAGACCCCTGCC Rv: GACATGTGTTTGCTGCGGT	KU609619	This study

Notes: ^aOrganism (scientific name) or IPNV strain; ^btarget-organism gene or IPNV-strain genome segment; ^cGenBank accession number of target sequences; ^dstudies in which these primers have been used previously.

Abbreviations: IPNV, infectious pancreatic necrosis virus; Fw, forward; Rv, reverse.

system, although with minor affinity (15–30 times lower). This cavity is not accessible in the crystal structure of the full-length protein, and arises after displacement of the α -helix, which implies that the interaction between thumb and fingers

is weak enough to allow for a slightly open structure of the polymerase.²⁹ This observation suggests that *a priori* this domain in IPNV VP1 polymerase might also be displaced similarly by the interaction of molecules with its corresponding

**Figure 1** Cavity for the allosteric binding site in the thumb domain of viral RdRp.

Notes: (A) Allosteric binding site around the amino-acid side chains of Leu392, Ala395, Thr399, Ile424, Leu425, His428, and Phe429 of crystal structure with the PDB number 2BRK, also including the cocrystallized PubChem ID inhibitor 4369534²⁹ in yellow, the same compound docked in light green, and the best-docked PubChem ID 23515664 compound in pink. (B) Structural features of IPNV VP1 RdRp (2Y18) as ribbon representation (1), as electrostatic surface potential with the amino acid sequence 122–157 and 31–36 as ribbon (2), detail of the cavity near the Arg551 (3), and electrostatic surface potential of the deletion mutant Δ122–157 and A31–36 used for molecular docking purposes (4). (C) Chemical structure of compounds experimentally tested in this work. PubChem ID numbers included. (D) Secondary structure of the protein region that forms the cavity explored in molecular docking experiments. The right side shows the sequence alignment for this region of the protein in IPNV Jasper, Sp, and LWVRT60 strains. Blue and orange boxes indicate the amino-acid sequences for the left side.

Abbreviations: RdRp, RNA-dependent RNA polymerase; PDB, Protein Data Bank; HCV, hepatitis C virus; IPNV, infectious pancreatic necrosis virus.

homologous cavity. Therefore, potential antiviral drugs against IPNV could be designed against that cavity without generating deletion mutants.

Five high-resolution structures are known for the VP1 polymerase of the Jasper strain of IPNV. It can be observed that unlike HCV polymerase, there is a partially accessible cavity even if residues 122–157 of the thumb domain in HCV polymerase are present (Figure 1B). This cavity becomes more evident for the same structure when amino acids 122–157 are electronically removed (Figure 1B). Although no high-resolution structures of the VP1 protein are available for the Sp and LWVRT60 IPNV strains, those available in our laboratory show high sequence identity (88.7%–99.5%) with Jasper VP1. This is especially true for the three domains involved in the definition of the cavity (Figure 1D). For this reason, homology modeling of the VP1 protein using the structures of the Jasper strain as a template was carried out.³⁸ In both the available structures and resulting models, the amino-acid sequences 122–157 and 31–36 were electronically deleted and molecular docking experiments carried out on the resulting structures.

Analysis of compounds docked to cavity on surface of thumb domain

Initially, an in silico screening of our chemical library was carried out on HCV polymerase, in order to check the predictive capacity of AutoDock Vina with the compound

cocrystallized by Di Marco et al, define thresholds for the variation of Gibbs free energy (ΔG , kcal/mol) in the screening process, and find compounds with smaller ΔG values, and then potentially higher affinity, than those tested by Di Marco et al.²⁹ Collectively, such data would allow for a targeted approach in the design of potential inhibitors of the IPNV VP1 protein, as was the main objective of this study.

Figure 1A depicts compound one in yellow (PubChem 4369534), present in the crystal structure with the PDB number 2BRK.²⁹ The same compound highlighted in light green is shown superimposed after molecular docking calculations ($\Delta G = -8.75$ kcal/mol). Docked and experimental conformation of 4369534 compound had an root-mean-square deviation of 5.141 Å. Finally, one of the optimal compounds with respect to binding was calculated from our chemical library (PubChem 23515664), and is depicted in pink. Docking calculations for compound 2 (PubChem 4369535) also predicted a conformer interacting in such a cavity, in agreement with that obtained through cocrystallization-derived structures²⁹ (not shown) and with a similar ΔG value (-8.60 kcal/mol). After analysis of the docking data for our chemical library against HCV structures (2BRKA31–36, $\Delta 122$ –157 and 2BRLA31–36, $\Delta 122$ –157) we found 200 compounds (not shown) with ΔG values ≤ -9.0 kcal/mol (the ΔG value chosen as threshold based on previous calculated results for Di Marco et al's active compounds; Figure 2), and among

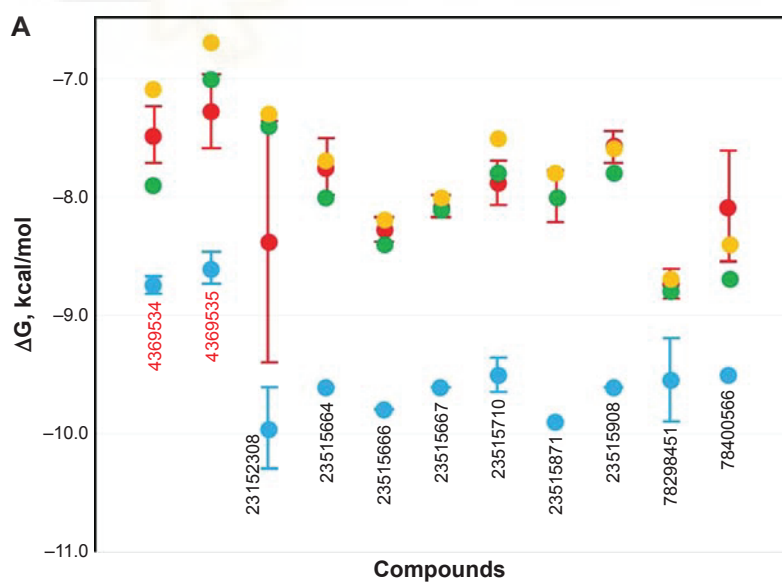


Figure 2 (Continued)

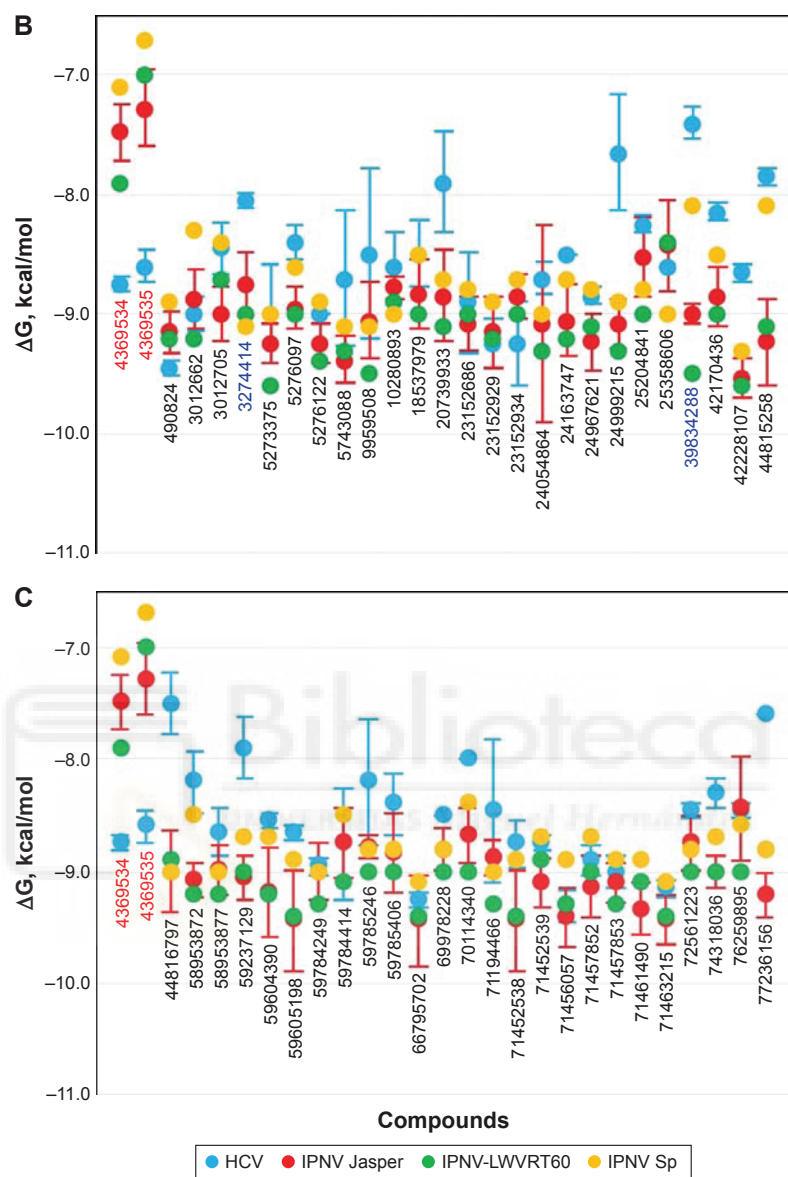


Figure 2 Comparison of Gibbs free energy (ΔG) variation for selected compounds based on molecular docking.
Notes: (A) Optimal compounds selected (minor ΔG) against HCV NS5B RdRp and their ΔG against IPNV VPI polymerase of Sp, Jasper, and LWVRT60 strains. (B, C) Optimal compounds selected against each of the three strains of IPNV and their ΔG values with respect to the remaining strains and HCV. PubChem ID number is indicated in black below each value, except for the inhibitors described by Di Marco et al³⁹ (red) and the two compounds experimentally tested in this study (blue).

Abbreviations: HCV, hepatitis C virus; RdRp, RNA-dependent RNA polymerase; IPNV, infectious pancreatic necrosis virus.

these 26 compounds with ΔG values ≤ -9.5 kcal/mol. Calculated ΔG values for compounds that primarily bind to hydrophobic sites are greater than expected when the binding site is more hydrophilic. As a consequence, in these cases the K' calculated from the value of ΔG ($K' = \exp^{\Delta G/RT}$)³⁸ did not

correspond to the experimental values in the subnanomolar range for compounds 1 and 2.

Of those 26 compounds with the lowest ΔG values, 17 were discarded, as their ADMET profiles were not optimal. In this sense, the range of optimal values was slightly

varied for different parameters with respect to other research by our group.^{37,38} Briefly, different parameters of the ADMET profile were analyzed (Figure 3) for both approved and experimental drugs included in the DrugBank

database⁴³ (these data are available at the website <http://dockingfiles.umh.es/drugbank/DrugBanklist.asp>). Eight of the nine parameters analyzed in Figure 3 show a Gaussian distribution in a frequency where 80%–90% of the

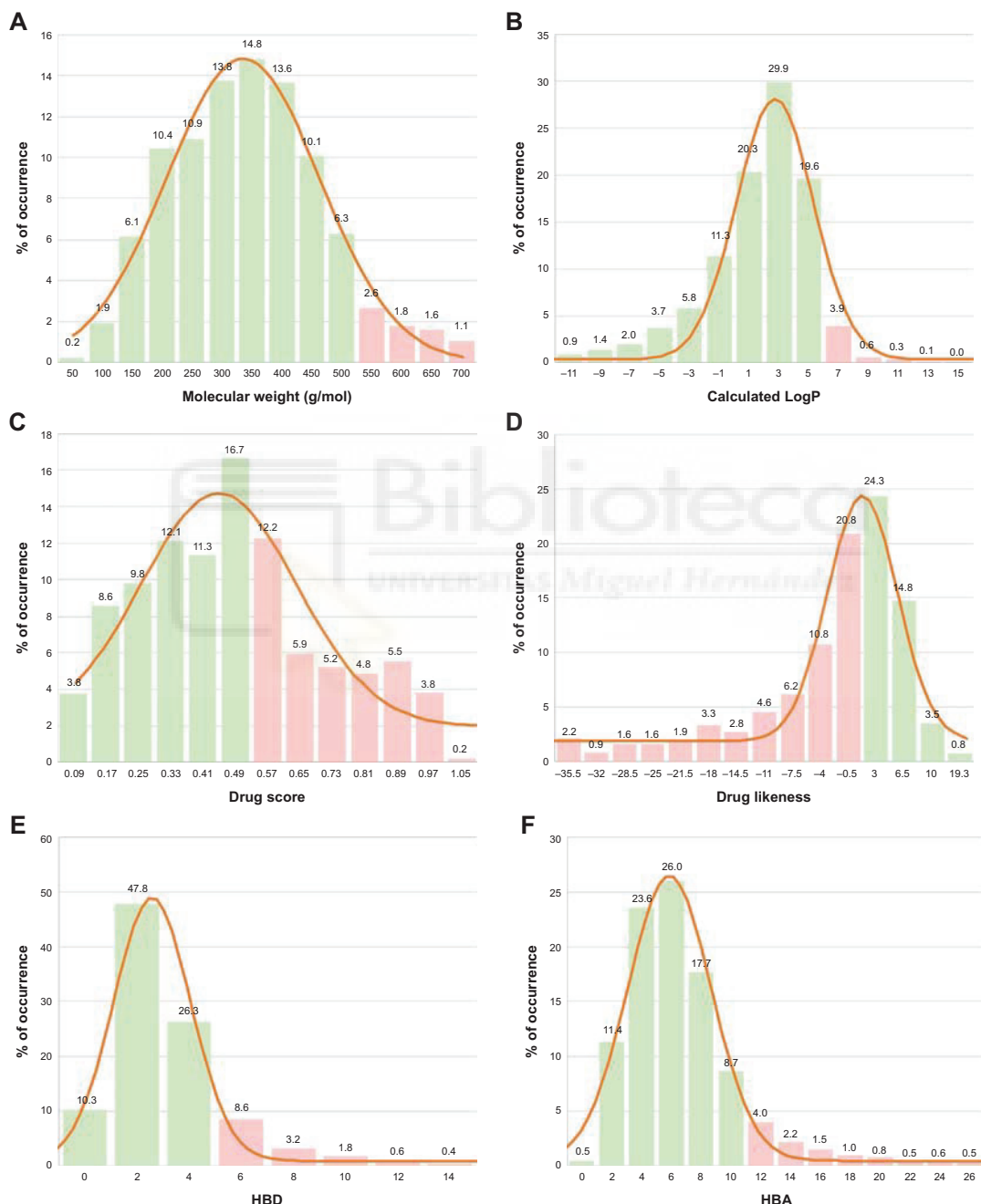


Figure 3 (Continued)

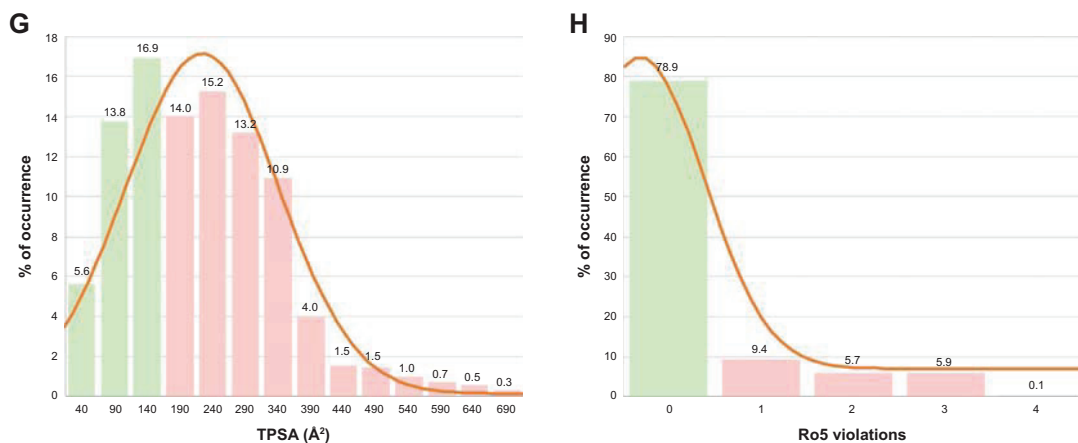


Figure 3 Analysis of physicochemical parameters of drugs included in the DrugBank database.

Notes: Distribution of molecular weight (**A**), calculated LogP (**B**), drug score (**C**), drug likeness (**D**), HBD (**E**), HBA (**F**), topological polar surface area (**G**), and violations of Lipinski et al's⁵⁰ rule of five (**H**) drugs included in the DrugBank database.⁴³ Each panel includes a curve indicating Gaussian distribution of frequency of parameter analyzed.

Abbreviations: LogP, logarithm of partition coefficient; HBD, hydrogen-bond donor; HBA, hydrogen-bond acceptor; TPSA, topological polar surface area; Ro5, rule of five.

values of these parameters varied by molecular weight, calculated logarithm of partition coefficient, drug score, drug likeness, H-bond acceptor, hydrogen (H)-bond donor, and topological polar surface area. In this manner, it can be observed that a high percentage of these drugs showed values in several parameters that are far from standard as was especially evident for drug score, drug likeness, and topological polar surface area. Moreover, up to 21% of these drugs present more than one violation of Lipinski's rules.⁵⁰ According to these data, the extreme values of these Gaussian distributions will be taken into account to be used as a screening filter for potential antiviral drugs

against IPNV. Even up to 3 violations of Lipinski's rules were admitted (See Tables 2, 4 and 6).

In Figure 2A, calculated ΔG values for selected compounds are compared to compounds 1 (4369534) and 2 (4369535)²⁹ for not only HCV but also all three IPNV strains. As expected, both compounds showed an ΔG value of almost 2 kcal/mol higher for all the IPNV strains, as they were not designed for targeting their polymerases. This occurred similarly with the nine compounds selected against HCV (Figure 2A). These data reflect the differences in the volume of the cavity and in the sequence of amino acids that define it between HCV and IPNV.

Table 2 Calculated physicochemical parameters for selected compounds against HCV NS5B RdRp based on molecular docking analysis

Compounds	Clusters	TPSA (Å²)	cLogS	MW	cLogP	HBA	HBD	Ro5 violations	Drug likeness	Drug score
4369534	1	71.77	-4.539	446.545	4.3728	6	1	0	-0.91217	0.212791182
4369535	1	65.78	-4.711	501.669	4.1731	6	1	1	2.8068	0.290325582
23152308	2	61.08	-6.189	532.686	7.695	6	1	2	1.9041	0.129071139
23515664	3	84.22	-5.904	467.567	5.5929	6	2	1	-1.0435	0.219641626
23515666	3	70.14	-7.345	465.474	5.868	5	1	1	-8.1071	0.141128842
23515667	3	64.35	-7.269	466.458	6.0954	5	1	1	-8.6848	0.136743667
23515710	3	84.22	-5.634	453.54	5.1385	6	2	1	0.17978	0.311684528
23515871	3	127.31	-5.795	468.512	4.0863	8	3	0	-0.002769	0.335480502
23515908	3	84.22	-5.522	439.514	4.7084	6	2	0	-0.0094093	0.338105422
78298451	4	156.22	-6.052	605.649	2.8246	11	2	2	1.045	0.316872425
78400566	5	115.46	-6.249	538.602	4.52	9	2	1	-8.1363	0.102868689

Notes: Compounds in bold are inhibitors of the HCV polymerase experimentally tested.²⁹ Compound names obtained from PubChem. Each cluster groups compounds with structures with up to 80% structural similarity.⁵⁰

Abbreviations: HCV, hepatitis C virus; RdRp, RNA-dependent RNA polymerase; TPSA, topological polar surface area; cLogS, calculated logarithm of solubility; MW, molecular weight; cLogP, calculated logarithm of partition coefficient; HBA, hydrogen-bond acceptor; HBD, hydrogen-bond donor; Ro5, rule of five.

Table 3 Predicted molecular pharmacokinetic properties of selected compounds against HCV NSSB RdRp

Compounds ADME	BBB	HIA	Caco2	Caco2 permeability (LogP _{app} , cm/s)	Pgp substrate inhibitor I	Pgp substrate inhibitor II	CYP450 2c9	CYP450 2d6	CYP450 3a4	CYP450 2c9	CYP450 2d6	CYP450 3a4	CYP450 2c19	CYP450 3a4	CYP450 2c19	CYP450 3a4	ROCT inhibitor
4369534	+	-	-	0.5784	+	+	-	-	-	-	-	-	-	-	-	-	Low
4369535	+	+	-	0.8928	+	+	-	-	-	-	-	-	-	-	-	-	Low
23152308	+	+	+	1.4709	+	-	+	-	-	+	-	-	-	-	-	-	High
23515664	+	+	-	0.468	+	-	+	-	-	-	-	-	-	-	-	-	High
23515666	+	+	-	0.9467	-	-	+	-	-	+	-	-	-	-	-	-	High
23515667	+	+	-	0.9213	-	-	+	-	-	+	-	-	-	-	-	-	High
23515710	+	+	-	0.4514	+	-	+	-	-	-	-	-	-	-	-	-	High
23515871	+	+	-	0.3009	-	-	-	-	-	-	-	-	-	-	-	-	Low
23515908	+	+	-	0.4909	+	-	+	-	-	-	-	-	-	-	-	-	High
78298451	-	+	-	0.0684	+	-	+	-	-	-	-	-	-	-	-	-	Low
78400566	+	-	-	0.2807	+	-	-	-	-	-	-	-	-	-	-	-	Low

Notes: Compounds in bold are inhibitors of the HCV polymerase experimentally tested.²⁹ All parameters calculated using <http://lmmnd.ecust.edu.cn:8000/predict/site>.⁴²

Abbreviations: HCV, hepatitis C virus; RdRp, RNA-dependent RNA polymerase; ADME, absorption, distribution, metabolism, elimination; BBB, blood-brain barrier; HIA, human intestinal absorption; P_{app}, apparent permeability coefficient; IP, inhibitory promiscuity; ROCT, renal organic cation transporter.

Table 4 Predicted toxicity assessment of selected compounds against HCV NSSB RdRp

Toxicity profile	4369534	4369535	23152308	23515664	23515666	23515667	23515710	23515871	23515908	78298451	78400566
Mutagenic ^a	None										
Tumorigenic ^a	None										
RE ^a	High										
Irritant ^c	None										
HERG inhibition I ^b	Weak										
HERG inhibition II ^b	-	-	+	+	+	+	+	+	+	+	+
Ames toxicity ^b	-	-	-	-	-	-	-	-	-	-	-
Carcinogens ^b	-	-	-	-	-	-	-	-	-	-	-
FT (pLC ₅₀ , mg/L) ^b	High, 1.3334	High, 1.2745	High, 1.0762	High, 1.5414	High, 1.037	High, 0.6405	High, 1.4738	High, 1.3289	High, 1.4462	High, 1.1014	High, 1.174
TPT (pIC ₅₀ , mg/L) ^b	High, 0.388	High, 0.5375	High, 0.4226	High, 0.3794	High, 0.6917	High, 0.9935	High, 0.3714	High, 0.3363	High, 0.3439	High, 0.4889	High, 0.4499
Honeybee toxicity ^b	Low										
Biodegradation ^b	-	-	III								
Acute oral toxicity ^b	III	III	Not required								
Carcinogenicity (three-class) ^b	Not required										
RAT (LD ₅₀ , mol/kg) ^b	2.2189	2.696	2.701	2.2834	2.8229	2.6911	2.3196	2.5033	2.3824	2.7072	2.4479

Notes: Toxicity data was expressed as the negative logarithm of 50% growth inhibitory concentration (pIC50). The value of LD50 for a substance is the dose required to kill half the members of a tested population after a specified test duration. Compound names from PubChem. Calculated using DataWarrior⁴¹ version 4.7.2.^b Calculated using <http://lmmnd.ecust.edu.cn:8000/predict/site>.⁴²
Abbreviations: HCV, hepatitis C virus; RdRp, RNA-dependent RNA polymerase; RE, reproductive effectiveness; FT, fish toxicity; IC₅₀, lethal concentration at 50%; TPT, *Tetrahymena pyriformis* toxicity; RAT, rat acute toxicity.

Table 5 Calculated physicochemical parameters for selected compounds against IPNV VPI RdRp based on molecular docking analysis

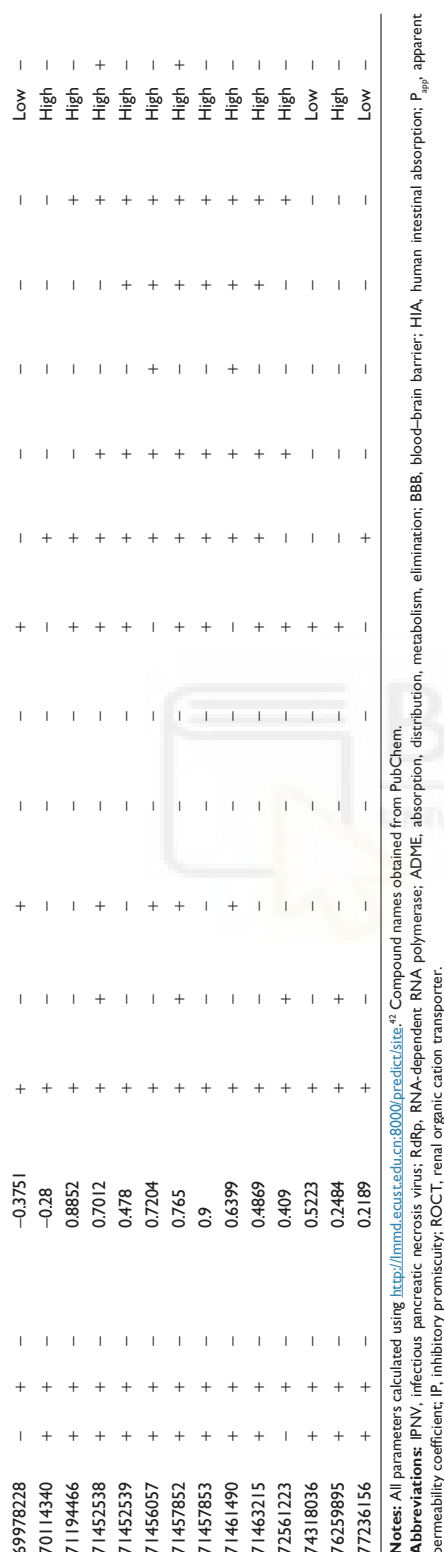
Compounds	Clusters	TPSA (Å ²)	cLogS	MW	cLogP	HBA	HBD	Ro5 violations	Drug likeness	Drug score
10280893	1	163.14	-3.464	552.641	2.285	12	4	2	-1.0971	0.371867727
18537979	1	166.38	-2.435	553.629	1.2329	13	4	2	1.4422	0.579621051
20739933	2	96.11	-7.217	480.566	4.8776	7	3	0	1.5843	0.239607744
58953872	2	96.11	-7.487	494.593	5.2196	7	3	1	1.5843	0.269858554
23152686	3	109.24	-6.054	534.614	6.0037	8	3	2	-0.32674	0.118698802
23152929	3	71.94	-6.041	490.605	6.689	6	2	1	-0.27206	0.119642868
23152934	3	61.08	-5.704	504.632	6.8218	6	1	2	0.72092	0.141347709
66795702	3	71.94	-6.112	504.632	6.9757	6	2	2	0.98293	0.134739208
24054864	4	86.21	-7.442	489.53	5.8066	7	1	1	1.7705	0.120414447
24163747	5	86.21	-6.787	479.535	5.2461	7	1	1	-1.2712	0.117405963
24967621	6	80.15	-6.17	481.594	4.6727	6	2	0	2.0585	0.358603377
71452538	6	58.22	-5.759	469.627	5.4654	5	1	1	1.9467	0.340567283
71456057	6	67.01	-6.488	491.633	5.484	5	2	1	1.6836	0.287416263
71457852	6	58.22	-5.489	455.6	5.1234	5	1	1	3.955	0.40928884
71457853	6	80.15	-6.514	495.621	5.0166	6	2	1	2.1942	0.317209639
71461490	6	79.9	-5.717	492.621	4.5371	6	2	0	1.6836	0.375823294
71463215	6	80.15	-6.538	495.621	5.0706	6	2	1	1.1437	0.290088161
24999215	7	93.45	-4.726	495.577	4.3431	7	2	0	3.6601	0.485783392
25204841	8	47.09	-6.513	448.568	5.4178	5	0	1	1.453	0.307833286
25358606	9	76.9	-5.43	482.538	3.7813	8	0	0	7.4652	0.479134432
3012662	10	131.39	-7.516	669.78	6.2485	10	3	2	1.3775	0.164791551
3012705	10	131.39	-7.055	617.704	4.7679	10	3	1	1.4271	0.2342033
5743088	10	115.46	-6.249	538.602	4.52	9	2	1	-8.1363	0.102868689
3274414	11	98.74	-6.306	472.539	5.3692	5	1	1	-1.5436	0.158941452
39834288	12	86.69	-3.251	320.375	1.8408	5	0	0	4.6379	0.855850841
42170436	13	126.05	-6.307	469.5	3.6969	9	3	0	0.35709	0.273696271
42228107	14	119.34	-5.288	477.483	3.0042	10	2	0	4.5258	0.523365319
44815258	15	120.35	-3.385	588.666	4.4852	10	2	1	0.49074	0.379468126
44816797	15	124.26	-3.804	584.634	5.1162	10	2	2	0.94695	0.353975046
490824	16	109.47	-7.253	551.645	5.2766	9	2	2	-1.7804	0.151308017
5273375	17	143	-5.987	605.697	4.7129	11	4	2	-0.3175	0.216436088
5276097	18	77.24	-7.315	489.573	6.4855	6	1	1	-4.5325	0.124874159
5276122	19	97.55	-7.057	574.679	6.3309	8	1	2	-0.29605	0.123835809
59237129	20	94.56	-4.486	438.533	3.7911	7	4	0	-0.55945	0.411185665
59604390	21	63.15	-5.468	462.551	4.6925	6	1	0	6.4596	0.15810365
59605198	21	63.15	-5.782	480.542	4.7933	6	1	0	5.1196	0.142503799
59784249	22	121.03	-6.033	518.575	3.0633	9	4	1	4.9822	0.425742108
59785406	22	121.03	-5.618	490.522	2.4327	9	4	0	3.8764	0.492489568
59784414	23	110.17	-7.855	530.586	2.7996	9	3	1	4.7368	0.351433623
59785246	24	110.17	-5.611	504.549	2.6026	9	3	1	6.019	0.480801976
9959508	25	139.29	-5.4	561.527	3.4903	11	3	2	-2.4649	0.227350159
69978228	25	189.61	-4.132	582.619	2.1062	13	5	2	3.1151	0.515992208
70114340	26	162.36	-2.901	504.553	2.1538	10	5	1	3.9231	0.676691765
71194466	27	109	-7.502	489.534	4.1577	8	3	0	3.3098	0.343673151
71452539	28	76.24	-5.85	485.626	4.3657	6	2	0	0.56667	0.339399549
72561223	29	110.17	-4.503	510.596	2.0128	9	3	1	5.1802	0.579372462
74318036	30	112.47	-6.421	572.751	4.478	9	5	1	2.2466	0.14379847
76259895	31	96.76	-6.713	483.57	3.1192	8	3	0	4.4867	0.414597223
77236156	32	141.84	-4.624	584.634	3.3632	10	4	1	-0.75495	0.305553124

Notes: Compound names obtained from PubChem. Each cluster groups compounds with structures with up to 80% structural similarity.⁵⁰

Abbreviations: IPNV, infectious pancreatic necrosis virus; RdRp, RNA-dependent RNA polymerase; TPSA, topological polar surface area; cLogS, calculated logarithm of solubility; MW, molecular weight; cLogP, calculated logarithm of partition coefficient; HBA, hydrogen-bond acceptor; HBD, hydrogen-bond donor; Ro5, rule of five.

Table 6 Predicted molecular pharmacokinetic properties of selected compounds against IPNV VP1 RdRp

Compounds	ADME	BBB	HIA	Caco2	Caco2 permeability (LogP _{app} , cm/s)	Pgp substrate inhibitor I	Pgp substrate inhibitor II	CYP450 2c9	CYP450 2d6	CYP450 3a4	CYP450 2c19	CYP450 3a4	CYP450 2d6	CYP450 2c9	CYP450 3a4	IP	ROCT inhibitor
490824	-	-	-	-	0.5656	+	-	-	-	-	-	-	-	-	-	-	Low
3012662	-	-	-	-	0.0447	+	-	-	-	-	-	-	-	-	-	-	Low
3012705	-	-	-	-	0.0648	+	-	-	-	-	-	-	-	-	-	-	Low
3274414	-	-	-	-	1.5102	-	-	-	-	-	-	-	-	-	-	-	High
5273375	-	-	-	-	0.2038	-	-	-	-	-	-	-	-	-	-	-	Low
5276097	-	-	-	-	1.0397	-	-	-	-	-	-	-	-	-	-	-	High
5276122	-	-	-	-	0.2336	-	-	-	-	-	-	-	-	-	-	-	High
5743088	-	-	-	-	0.2807	-	-	-	-	-	-	-	-	-	-	-	Low
9959508	-	-	-	-	0.619	-	-	-	-	-	-	-	-	-	-	-	High
10280893	-	-	-	-	0.3982	-	-	-	-	-	-	-	-	-	-	-	High
185337979	-	-	-	-	0.427	-	-	-	-	-	-	-	-	-	-	-	High
20739933	-	-	-	-	0.8745	-	-	-	-	-	-	-	-	-	-	-	High
23152686	-	-	-	-	-0.0731	-	-	-	-	-	-	-	-	-	-	-	Low
23152929	-	-	-	-	0.7433	-	-	-	-	-	-	-	-	-	-	-	High
23152934	-	-	-	-	1.2391	-	-	-	-	-	-	-	-	-	-	-	High
24054864	-	-	-	-	0.6356	-	-	-	-	-	-	-	-	-	-	-	High
24163747	-	-	-	-	0.4231	-	-	-	-	-	-	-	-	-	-	-	High
24967621	-	-	-	-	0.4959	-	-	-	-	-	-	-	-	-	-	-	High
24999215	-	-	-	-	-0.0142	-	-	-	-	-	-	-	-	-	-	-	High
25204841	-	-	-	-	0.7521	-	-	-	-	-	-	-	-	-	-	-	High
25358606	-	-	-	-	1.2873	-	-	-	-	-	-	-	-	-	-	-	Low
39834288	-	-	-	-	1.4452	-	-	-	-	-	-	-	-	-	-	-	High
42170436	-	-	-	-	0.9813	-	-	-	-	-	-	-	-	-	-	-	High
42228107	-	-	-	-	0.851	-	-	-	-	-	-	-	-	-	-	-	Low
44815258	-	-	-	-	0.4878	-	-	-	-	-	-	-	-	-	-	-	High
44816797	-	-	-	-	0.5363	-	-	-	-	-	-	-	-	-	-	-	High
58953872	-	-	-	-	0.8745	-	-	-	-	-	-	-	-	-	-	-	High
58953877	-	-	-	-	0.8745	-	-	-	-	-	-	-	-	-	-	-	High
59237129	-	-	-	-	0.5357	-	-	-	-	-	-	-	-	-	-	-	High
59604390	-	-	-	-	1.4041	-	-	-	-	-	-	-	-	-	-	-	High
59605198	-	-	-	-	1.2794	-	-	-	-	-	-	-	-	-	-	-	High
59784249	-	-	-	-	1.2234	-	-	-	-	-	-	-	-	-	-	-	High
59784414	-	-	-	-	0.7756	-	-	-	-	-	-	-	-	-	-	-	High
59785246	-	-	-	-	0.4222	-	-	-	-	-	-	-	-	-	-	-	High
59785406	-	-	-	-	0.6464	-	-	-	-	-	-	-	-	-	-	-	High
66795702	-	-	-	-	1.0637	-	-	-	-	-	-	-	-	-	-	-	High



In Figure 2B and C, the ΔG values of the selected compounds docked against the IPNV VP1 of all three strains are compared. For each strain, compounds with ΔG values ≤ -9 kcal/mol were selected. The ΔG values of these compounds are also shown against HCV. All these compounds were also within the range of values of the ADMET profile (see Tables 3, physicochemical parameters; 5 ADME; 7 toxicity). Although the chemical library used in molecular docking experiments was obtained from the PubChem database, not all deposited compounds are commercially available, and thus only some can be tested experimentally. In fact, this is the third (and very relevant) filter that joins the two previous filters for a final proposal of candidates for antiviral compounds. A total of 50 compounds were proposed as potential antiviral compounds (Figure S1) for the three strains of IPNV. Careful observation of the ΔG values of these 50 compounds for all IPNV strains (Figure 2B and C) reveals that for some the ΔG values can vary up to more than 1 kcal/mol between the Sp and LWVRT60 strains. This was especially true for compounds 3012662, 39834288, 44815258, and 58953872. However, for many others, the differences were negligible. Taking this observation into consideration, in order to assess if different ΔG values between the IPNV strains reflected different rates of inhibition of compounds against the Sp and LWVRT60 strains, two compounds with two different ΔG patterns were selected for testing in vitro. The compounds selected for further in vitro assays were 3274414 and 39834288 (Figure 1C).

Determination of cell viability of CHSE cells after treatment with compounds 3274414 and 39834288

Cellular cytotoxicity induced by the selected experimental compounds was evaluated by an MTT cell-viability assay (Figure 4). For these assays, CHSE cells were treated with a range of concentrations of each compound (0–50 μ M). In parallel, treatments with equivalent amounts of the corresponding compound solvents were performed. After 24 hours, cell viability was determined by MTT as described in the “Materials and methods” section. As shown in Figure 5, CHSE cells were more sensitive to 3274414 than 39834288. For treatments with 3274414, no significant toxic effect was observed in the concentration range tested of 0–20 μ M ($95.4\% \pm 4.6\%$ at 20 μ M). Cell viability slightly decreased to $74.9\% \pm 2.9\%$ for 3274414 at 50 μ M. In contrast, at this concentration (the highest tested), cell viability was $88.3\% \pm 3.9\%$ for 39834288. In turn, both solvents at any concentration showed cell-viability percentages close to 100%.

Table 7 Predicted toxicity assessment of selected compounds against IUPAC VPI RDRP

Toxicity profile	490824	3012662	3012705	3274414	5273375	5276097	5276122	5743088	9959508	10280893
Mutagenic ^a	None									
Tumorigenic ^a	None	None	None	None	None	None	High	None	None	None
RE ^a	None	None	None	Low	None	None	None	None	None	None
Irritant ^a	None									
HERG inhibition I ^b	Weak									
HERG inhibition II ^b	–	+	–	–	+	–	+	+	+	+
Ames toxicity ^b	–	–	–	–	–	–	–	–	–	+
Carcinogens ^b	–	–	–	–	–	–	–	–	–	+
FT (pLC ₅₀ mg/L) ^b	High, 1.4493	High, 1.3364	High, 1.289	High, 0.9135	High, 1.2677	High, 1.1508	High, 1.2322	High, 1.174	High, 1.2936	High, 1.3447
TPT (pGIC ₅₀ µg/L) ^b	High, 0.5062	High, 0.4142	High, 0.4114	High, 0.7454	High, 0.5388	High, 0.6038	High, 0.4499	High, 0.5237	High, 0.5237	High, 0.4871
Honeybee toxicity ^b	Low									
Biodegradation ^b	–	–	–	–	–	–	–	–	–	–
Acute oral toxicity ^b	III									
Carcinogenicity (three-class) ^b	Not required									
RAT (LD ₅₀ mg/kg) ^b	1.8935	2.3915	2.4206	2.4636	2.4041	2.4488	2.2312	2.4479	2.5923	2.7713
Toxicity profile	18537979	20739933	23152686	23152929	23152934	24054864	24163747	24961721	24999215	25204841
Mutagenic ^a	None	Low	None	None	None	High	High	High	None	None
Tumorigenic ^a	None									
RE ^a	None	None	None	High	None	None	None	None	None	None
Irritant ^a	None									
HERG inhibition I ^b	Weak									
HERG inhibition II ^b	+	–	+	+	+	–	–	–	–	+
Ames toxicity ^b	–	–	–	–	–	–	–	–	–	–
Carcinogens ^b	–	–	–	–	–	–	–	–	–	–
FT (pLC ₅₀ mg/L) ^b	High, 1.3752	High, 1.4731	High, 1.4335	High, 1.4518	High, 1.2124	High, 0.8885	High, 1.0083	Low, 1.4958	Low, 1.3529	Low, 1.4985
TPT (pGIC ₅₀ µg/L) ^b	High, 0.4549	High, 0.4749	High, 0.3475	High, 0.3764	High, 0.3721	High, 0.5479	High, 0.4754	High, 0.2529	High, 0.4765	High, 0.5004
Honeybee toxicity ^b	Low									
Biodegradation ^b	–	–	–	–	–	–	–	–	–	–
Acute oral toxicity ^b	III									
Carcinogenicity (three-class) ^b	Not required									
RAT (LD ₅₀ mg/kg) ^b	2.8539	2.2733	2.2743	2.3865	2.4794	2.2269	2.2662	2.4844	2.6327	2.5284
Toxicity profile	25358606	39834288	42170436	42228107	44815258	44816797	58933872	58953877	59237129	59604390
Mutagenic ^a	None	Low	None	High						
Tumorigenic ^a	None	None	Low	None	None	None	None	None	None	High
RE ^a	None									
Irritant ^a	None	None	None	None	None	None	Weak	Weak	Weak	Weak
HERG inhibition I ^b	Weak	Weak	Weak	Weak	Weak	Weak	+	–	+	+
HERG inhibition II ^b	+	–	–	–	–	–	–	–	–	–
Ames toxicity ^b	–	–	–	–	–	–	–	–	–	–
Carcinogens ^b	–	–	–	–	–	–	–	–	–	–

	FT (pLC ₅₀ , mg/L) ^b	TPT (pIGC ₅₀ , µg/L) ^b	Honeybee toxicity ^b	High, 1.1439	High, 1.4429	High, 1.1606	High, 1.4331	High, 1.4499	High, 1.3925	High, 1.4731	High, 1.4749	Low, 1.9838	High, 1.2676
	Biodegradation ^b		Honeybee toxicity ^b	High, 0.4812	High, 0.5824	High, 0.6336	High, 0.4559	High, 0.5352	High, 0.532	High, 1.4749	High, 0.4749	High, 0.6335	High, 0.3329
	Acute oral toxicity ^b		Carcinogenicity (three-class) ^b	Low	Low	Low	Low						
	RAT (LD ₅₀ , mol/kg) ^b		Carcinogenicity (three-class) ^b	Not required	Not required	Not required	Not required						
Toxicity profile	59005198	59784249	59784414	59785246	59785406	66795702	69978228	70114340	71194466	71452558			
Mutagenic ^a	High	None	None	None	None	None	None	None	None	None	None	None	None
Tumorigenic ^a	High	None	None	None	None	None	None	None	None	None	None	None	None
RE ^a	None	None	None	None	None	None	None	None	None	None	None	None	None
Irritant ^c	None	None	None	None	None	None	None	None	None	None	None	None	None
HERG inhibition I ^b	Weak	+	Weak	+	+	Weak	+	Weak	+	Weak	+	Weak	Weak
HERG inhibition II ^b	+	+	+	+	+	+	+	+	+	+	+	+	+
Ames toxicity ^b	–	–	–	–	–	–	–	–	–	–	–	–	–
Carcinogens ^b	–	–	–	–	–	–	–	–	–	–	–	–	–
FT (pLC ₅₀ , mg/L) ^b	High, 1.1918	High, 0.9868	High, 0.965	High, 1.1446	High, 1.335	High, 1.4583	Low, 1.3099	Low, 2.0819	High, 1.5963	Low, 1.4317			
TPT (pIGC ₅₀ , µg/L) ^b	High, 0.5055	High, 0.622	High, 0.4835	High, 0.4416	High, 0.4223	High, 0.3263	High, 0.4834	High, 0.2969	High, 0.3216	High, 0.3877			
Honeybee toxicity ^b	Low	Low	Low	Low	Low	Low	Low	Low	Low	Low	Low	Low	Low
Biodegradation ^b	–	–	–	–	–	–	–	–	–	–	–	–	–
Acute oral toxicity ^b	–	–	–	–	–	–	–	–	–	–	–	–	–
Carcinogenicity (three-class) ^b	Not required	Not required	Not required	Not required	Not required	Not required	Not required	Not required	Not required	Not required	Not required	Not required	Not required
RAT (LD ₅₀ , mol/kg) ^b	2.6089	2.6679	2.6756	2.6682	2.6564	2.4875	2.5076	2.5428	2.3759	2.2774			
Toxicity profile	71452539	71456057	71457852	71457853	71461490	71463215	72561223	74318036	76259895	77236156			
Mutagenic ^a	None	None	None	None	None	None	None	None	None	None	None	None	None
Tumorigenic ^a	None	None	None	None	None	None	None	None	None	None	None	None	None
RE ^a	None	None	None	None	None	None	None	None	None	None	None	None	None
Irritant ^c	None	None	None	None	None	None	None	None	None	None	None	None	None
HERG inhibition I ^b	Weak	+	Weak	+	+	Weak	+	Weak	+	Weak	+	Weak	Weak
HERG inhibition II ^b	+	+	+	–	–	–	–	–	–	–	–	–	–
Ames toxicity ^b	–	–	–	–	–	–	–	–	–	–	–	–	–
Carcinogens ^b	–	–	–	–	–	–	–	–	–	–	–	–	–
FT (pLC ₅₀ , mg/L) ^b	Low, 1.6115	Low, 1.6589	High, 1.3639	High, 1.246	Low, 1.7366	Low, 1.5449	High, 1.1057	High, 1.329	High, 1.3351	High, 1.4949			
TPT (pIGC ₅₀ , µg/L) ^b	High, 0.3166	High, 0.2518	High, 0.4052	High, 0.3028	High, 0.2401	High, 0.234	High, 0.5002	High, 0.5396	High, 0.4232	High, 0.5486			
Honeybee toxicity ^b	Low	Low	Low	Low	Low	Low	Low	Low	Low	Low	Low	Low	Low
Biodegradation ^b	–	–	–	–	–	–	–	–	–	–	–	–	–
Acute oral toxicity ^b	–	–	–	–	–	–	–	–	–	–	–	–	–
Carcinogenicity (three-class) ^b	Not required	Not required	Not required	Not required	Not required	Not required	Not required	Not required	Not required	Not required	Not required	Not required	Not required
RAT (LD ₅₀ , mol/kg) ^b	2.4763	2.601	2.686	2.5399	2.6534	2.5176	2.6378	2.4561	2.4322	2.4325			

Notes: ¹Toxicity data was expressed as the negative logarithm of 50% growth inhibitory concentration (pIGC₅₀). The value of LD₅₀ for a substance is the dose required to kill half the members of a tested population after a specified test duration. Compound names from PubChem. ^aCalculated using DataWarrior[®] version 4.7.2; ^bcalculated using <http://lmmdeuse.edu.cn/8000/predictsite/>. ^cIC₅₀ calculated using IC₅₀ calculator.

Abbreviations: IPNV, infectious pancreatic necrosis virus; RdRp, RNA-dependent RNA polymerase; RE, reproductive effectiveness; FT, fish toxicity; IC₅₀, lethal concentration at 50%; TPT, *Tetrahymena pyriformis* toxicity; RAT, rat acute toxicity.

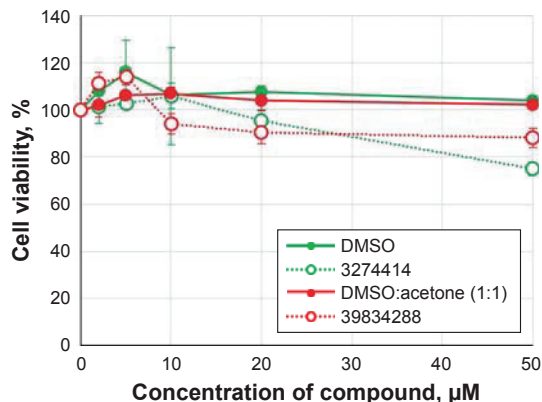


Figure 4 Viability of CHSE cells after treatment with PubChem 3274414 and 39834288 compounds.

Notes: CHSE monolayers were treated with increasing concentrations of 3274414 and 39834288 compounds dissolved in DMSO and DMSO:acetone (1:1), respectively; and equivalent amounts of the corresponding solvents (0.5 μ L/well), for 24 hours at 14°C before performing the MTT assay. Cell viability is shown as the percentage relative to non-treated cells, taken as an average (\pm SD) from three independent experiments performed in triplicate.

Abbreviation: DMSO, dimethyl sulfoxide.

Determination of anti-IPNV activity induced by selected compounds

Infected CHSE cells were further incubated with different concentrations of selected compounds (3274414 or 39834288) for 24 hours. Viral loads were subsequently measured as the total abundance of viral transcripts quantified by RT-qPCR. As shown in Figure 5, different inhibition patterns were observed dependent on the compound and IPNV strain used. When the compounds induced antiviral activity, this occurred in a dose-dependent manner.

For the 3274414 compound, both IPNV strains were inhibited following a similar pattern. At the maximum concentration tested (50 μ M), the infectivity of both viral strains was reduced by approximately 50% (Figure 5A). The potency of this compound was lower than that induced by mycophenolic acid or ribavirin,⁴⁸ which at 1 μ M both inhibited the infectivity of IPNV Sp up to 90%. Our docking data showed that 3274414–polymerase interactions were only hydrophobic and involved residues Lys554, Ala555, Glu557, and Asn580. The compound showed the same orientation in its binding to the polymerase in all three IPNV strains.

For the 39834288 compound, its antiviral capacity was markedly different (Figure 5B), exhibiting no effect upon the Sp strain. In contrast, its potency was found to be greater than that of compound 3274414 against the LWVRT60 strain, reducing its infectivity by 80% at 20 μ M. By adjusting

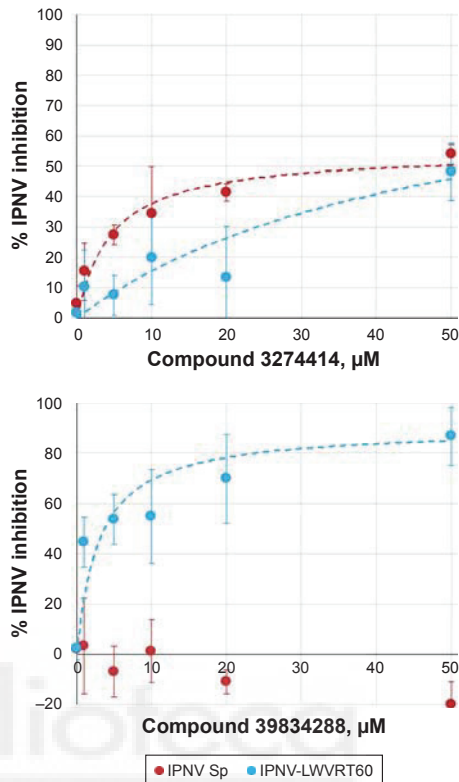


Figure 5 Percentage of inhibition of infectivity of both IPNV Sp and LWVRT60 strains after treatment with PubChem 3274414 or 39834288 compound.

Notes: CHSE monolayers infected with 0.01 TCID₅₀/mL of either IPNV Sp or IPNV LWVRT60 were treated after viral adsorption with increasing concentrations (1, 5, 10, 20, and 50 μ M) of either PubChem 3274414 or 39834288 compounds. After 24 hours, the amount of replicating virus was determined by RT-qPCR. Results are presented as percentage inhibition of infection produced by compounds (inhibitor) in comparison to corresponding organic solvent controls (vehicle), shown as the average (\pm SD) from four independent experiments. Dashed lines are the fit to a dose-response curve % IPNV inhibition = Bottom + (Top-Bottom)/(1 + (IC₅₀/[inhibitor])^{Hill_Slope}) with a Hill slope of 1.

Abbreviations: IPNV, infectious pancreatic necrosis virus; TCID₅₀, 50% tissue-culture infective dose; RT-qPCR, reverse-transcription quantitative polymerase chain reaction.

the parameters to a Hill equation, an IC₅₀ of 3.1 μ M was calculated. The estimated IC₅₀ value for compound 3274414 was about 15 μ M for both Sp and LWVRT60 strains. These IC₅₀ values are comparable with those of other nonnucleoside inhibitors designed to block the RNA-template tunnel of RdRp dengue virus 2.⁵¹ The compounds (NTD1, -2, and -29) analyzed therein showed no toxicity up to 50 μ M and presented IC₅₀ values of 7.2, 0.7, and 1.5 μ M, respectively. In spite of showing inhibitory activity against the recombinant viral polymerase, the antiviral activity of NTD1 and NTD2 compounds in cell cultures could not be

demonstrated.⁵¹ Selective inhibition of one virus subtype over other subtypes has been previously for small-molecule inhibitors of influenza A virus, although the molecular basis of such specificity remained obscure.⁵²

The interactions of 39834288–polymerase (H-bonds between the compound and the residues Pro552, Glu557, and, Asn623) predicted by molecular docking were similar for the three IPNV strains (Figure 6A). Therefore, the question remained as to how compound 39834288 showed no activity against the Sp strain. The calculation of position for the compounds docked to the cavity in the surface of the thumb was made in the absence of residues 31–36 and 122–157. Therefore, it is understandable that they did not show differences in 39834288–polymerase interactions. However, cell-culture assays for antiviral activity were carried out with the full enzyme. Binding of the inhibitor in the cavity is only possible if the loop 122–157 is displaced, especially for the compound 39834288, which would have large clashes (Figure 6B), as it is located in the full protein (2YI8). As would be expected, based upon 3274414–polymerase docking-calculated interactions, a much smaller rearrangement of loop 122–157 would be required to accommodate compound 39834288. In this sense, the binding energy of loop 122–157 to the domain that forms the cavity

(residues Asp523 to Asp691) was calculated using FoldX software.³⁹ These data showed that although there were neither differences between the three strains for the numbers of hydrogen-bonds (Asp124–Ala588, Thr146–Asn624, Tyr159–Glu594, Asp124–Arg612, Asp124–Tyr613, Thr146–Asn624, Gln149–Asn580, and Ile154–Tyr589), saline bridges (Asp124–Arg612) nor the interface area (about 1,060 Å²), there were appreciable differences in the global calculation of binding free-energy variation. The calculated ΔG for the binding of both domains was –36.9 kcal/mol for the LWRVT60 strain and –38.1 kcal/mol for the Sp strain. In other words, the rearrangement of loop 122–155 was more energy-expensive for the polymerase of the Sp strain than for LWRVT60. Such may also explain the observed inability of compound 39834288 to displace this loop in the Sp strain, resulting in negligible activity of its polymerase and in turn its infectivity.

Conclusion

The results presented herein are compatible with the existence of an allosteric regulation site in the IPNV VP1 polymerase. From a library of 23,760 compounds, nine and 50 were predicted as antiviral drug candidates against HCV and IPNV polymerases, respectively (Figure 7). Two nontoxic

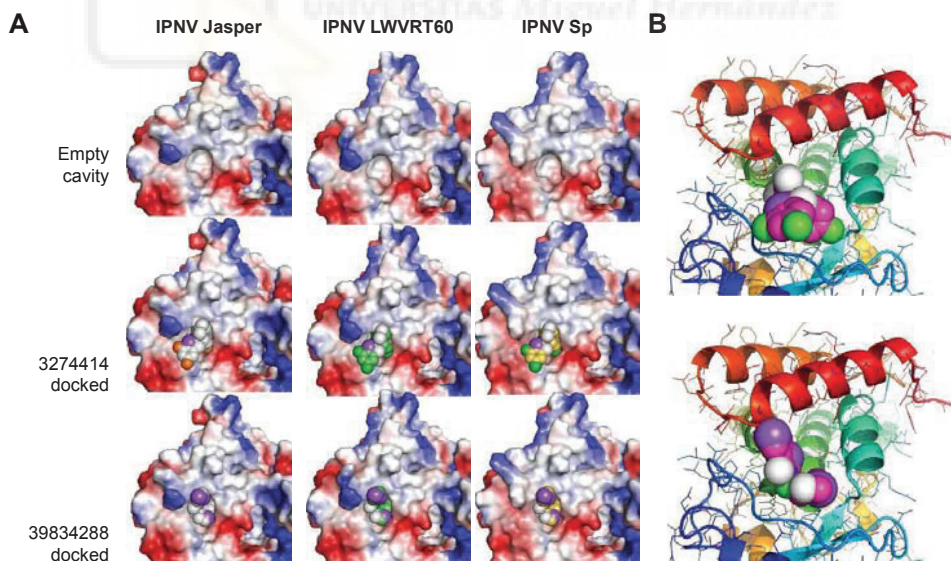


Figure 6 Structural details of docked compounds on cavity.

Notes: (A) Electrostatic surface potential without (empty cavity) and with the best-docked PubChem 3274414 and 39834288 compounds in IPNV Jasper (2YI8), Sp (homology model), and LWRVT60 (homology model) strains. (B) Clashes of docked 3274414 (upper) and 39834288 (lower) compounds with the IPNV VP1 Sp strain with the amino-acid sequence 122–157 depicted in red.

Abbreviation: IPNV, infectious pancreatic necrosis virus.

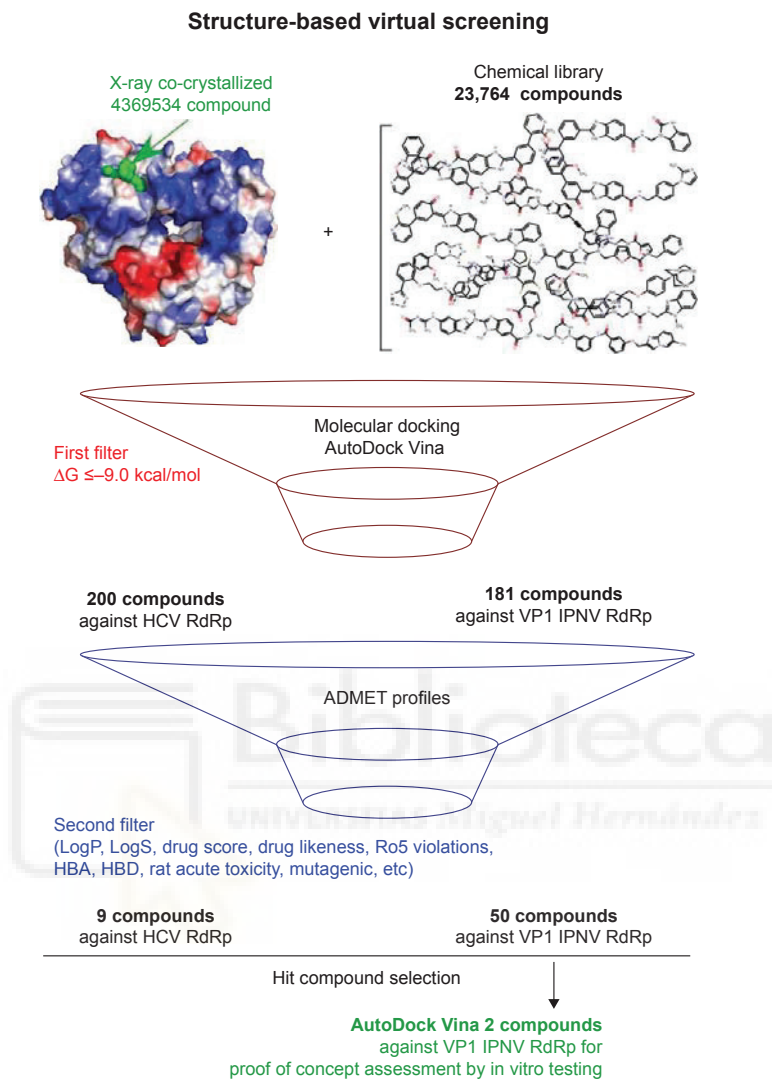


Figure 7 Schematic workflow for the hit-compound selection.

Notes: Virtual screening workflow and procedure used for selecting hits whose bioactivity was experimentally tested. The number of compounds that passed each step are shown. From an initial set of 23,764 compounds, 50 compounds were identified as putative VP1 IPNV RdRp inhibitors (first and second filters). Two of the 50 compounds were selected for proof-of-concept assessment by in vitro testing.

Abbreviations: IPNV, infectious pancreatic necrosis virus; RdRp, RNA-dependent RNA polymerase; HCV, hepatitis C virus; ADMET, absorption, distribution, metabolism, excretion, and toxicity; LogP, logarithm of partition coefficient; LogS, logarithm of solubility; Ro5, rule of five; HBA, hydrogen-bond acceptor; HBD, hydrogen-bond donor.

compounds were tested in vitro, and showed antiviral activity against IPNV in the low-micromolar range.

Acknowledgments

Special thanks are due to Dr Amparo Estepa Pérez, who has passed away, but contributed to financing this work. MBP is financed by the Generalidad Valenciana, fellowship ACIF/2016. We are grateful to Research, Technological Innovation, and the Supercomputing Center of Extremadura

(CénitS) for allowing us to use their supercomputing facilities (Lusitania II). This work was supported by the Programa Estatal de Investigación, Desarrollo e Innovación Orientada a los Retos de la Sociedad project AGL2014-51773-C3-1-R of the Ministerio de Economía y Competitividad of Spain. We thank Dr Beatriz Novoa (Instituto de Investigaciones Marinas, Consejo Superior de Investigaciones Científicas, Vigo, Spain) for providing the IPNV LWVRT60 strain. Technical support from Angeles Gómez is also acknowledged.

Dr Matthew Mold (Keele University, Newcastle, UK) provided some assistance with the English. We thank the anonymous reviewers for their constructive comments, which helped us to improve the manuscript.

Author contributions

JAE, LP, and AF conceived and designed the experiments and wrote the paper, MBP, JC, and AF conducted the in vitro experiments, JAE and VG conducted the in silico molecular docking experiments and the DrugBank analysis, and LP and JAE were responsible for funding acquisition. All authors contributed to the general discussion of the manuscript. All authors contributed toward data analysis, drafting and revising the paper and agree to be accountable for all aspects of the work.

Disclosure

The authors report no conflicts of interest in this work.

References

1. de Clercq E. Antivirals: current state of the art. *Future Virol.* 2008;3(4):393–405.
2. Griffiths PD. A perspective on antiviral resistance. *J Clin Virol.* 2009;46(1):3–8.
3. Awoonor-Williams E, Walsh AG, Rowley CN. Modeling covalent-modifier drugs. *Biochim Biophys Acta.* 2017;1865(11 Pt B):1664–1675.
4. Raghavendra NM, Pingili D, Kadasi S, Mettu A, Prasad S. Dual or multi-targeting inhibitors: the next generation anticancer agents. *Eur J Med Chem.* 2018;143:1277–1300.
5. Wolf K, Snieszko SF, Dunbar CE, Pyle E. Virus nature of infectious pancreatic necrosis in trout. *Proc Soc Exp Biol Med.* 1960;104:105–108.
6. Munro ES, Midtlyng PJ. Infectious pancreatic necrosis and associated aquatic birnaviruses. In: Woo P, Bruno D, editors. *Fish Diseases and Disorders.* 2nd ed. Wallingford, UK: CABI; 2011:1–65.
7. Guy DR, Bishop SC, Brotherstone S, et al. Analysis of the incidence of infectious pancreatic necrosis mortality in pedigree Atlantic salmon, *Salmo salar* L., populations. *J Fish Dis.* 2006;29(11):637–647.
8. Rønneseth A, Wergeland HI, Devik M, Evensen O, Pettersen EF. Mortality after IPNV challenge of Atlantic salmon (*Salmo salar* L.) differs based on developmental stage of fish or challenge route. *Aquaculture.* 2007;271(1–4):100–111.
9. Dhar A, LaPatra S, Orry A, Allnutt F. Infectious pancreatic necrosis virus. In: Woo P, Cipriano R, editors. *Fish Viruses and Bacteria: Pathobiology and Protection.* Wallingford, UK: CABI; 2017:1–12.
10. Delmas B, Mundt E, Vakharia VN, Wu JL. Family – Birnaviridae. In: King AM, Carstens EB, editors. *Virus Taxonomy: Ninth Report of the International Committee on Taxonomy of Viruses.* London: Academic Press; 2012:499–507.
11. Lvov DK, Shchelkanov MY, Alkhovsky SV, Deryabin PG. Double-stranded RNA viruses. In: Lvov DK, Shchelkanov MY, Vladimirovich S, Alkhovsky SV, Deryabin PG, editors. *Zoonotic Viruses in Northern Eurasia: Taxonomy and Ecology.* Boston: Academic Press; 2015: 113–133.
12. Büyükekiz AG, Altun S, Hansen EF, et al. Infectious pancreatic necrosis virus (IPNV) serotype Sp is prevalent in Turkish rainbow trout farms. *J Fish Dis.* 2018;41(1):95–104.
13. Holopainen R, Eriksson-Kallio AM, Gadd T. Molecular characterisation of infectious pancreatic necrosis viruses isolated from farmed fish in Finland. *Arch Virol.* 2017;162(11):3459–3471.
14. Mamrinez RA, Vera T, Villalba MV, et al. Molecular characterization of infectious pancreatic necrosis virus strains isolated from the three types of salmonids farmed in Chile. *Virol J.* 2017;14(1):17.
15. Ogut H, Altuntas C, Parlak R. Viral surveillance of cultured rainbow trout in the eastern Black Sea, Turkey. *J Aquat Anim Health.* 2013;25(1):27–35.
16. Ruane NM, McCarthy LJ, Swords D, Henshilwood K. Molecular differentiation of infectious pancreatic necrosis virus isolates from farmed and wild salmonids in Ireland. *J Fish Dis.* 2009;32(12):979–987.
17. Wallace IS, McKay P, Murray AG. A historical review of the key bacterial and viral pathogens of Scottish wild fish. *J Fish Dis.* 2017;40(12):1741–1756.
18. Crane MS, Hardy-Smith P, Williams LM, et al. First isolation of an aquatic birnavirus from farmed and wild fish species in Australia. *Dis Aquat Organ.* 2000;43(1):1–14.
19. Moreno P, Oliveira JG, Labella A, et al. Surveillance of viruses in wild fish populations in areas around the Gulf of Cadiz (South Atlantic Iberian Peninsula). *Appl Environ Microbiol.* 2014;80(20):6560–6571.
20. Delmas B, Mundt E, Vakharia V, Wu J. Family Birnaviridae. In: King AM, Carstens EB, editors. *Virus Taxonomy: Ninth Report of the International Committee on Taxonomy of Viruses.* London: Academic Press; 2012:499–507.
21. Molloy SD, Pietrak MR, Bricknell I, Bouchard DA. Experimental transmission of infectious pancreatic necrosis virus from the blue mussel, *Mytilus edulis*, to cohabitating Atlantic salmon (*Salmo salar*) smolts. *Appl Environ Microbiol.* 2013;79(19):5882–5890.
22. Munro ES, Gahlawat SK, Acosta F, Ellis AE. In infectious pancreatic necrosis virus carrier Atlantic salmon, *Salmo salar* L., post-smolts, almost all kidney macrophages ex vivo contain a low level of non-replicating virus. *J Fish Dis.* 2006;29(1):43–48.
23. Chevalier C, Lepault J, Erk I, da Costa B, Delmas B. The maturation process of pVP2 requires assembly of infectious bursal disease virus capsids. *J Virol.* 2002;76(5):2384–2392.
24. Santi N, Song H, Vakharia VN, Evensen O. Infectious pancreatic necrosis virus VP5 is dispensable for virulence and persistence. *J Virol.* 2005;79(14):9206–9216.
25. Magyar G, Chung HK, Dobos P. Conversion of VP1 to VPg in cells infected by infectious pancreatic necrosis virus. *Virology.* 1998;245(1):142–150.
26. Duncan R, Mason CL, Nagy E, Leong JA, Dobos P. Sequence analysis of infectious pancreatic necrosis virus genome segment B and its encoded VP1 protein: a putative RNA-dependent RNA polymerase lacking the Gly-Asp-Asp motif. *Virology.* 1991;181(2):541–552.
27. Koonin EV, Wolf YI, Nagasaki K, Dolja VV. The Big Bang of picorna-like virus evolution antedates the radiation of eukaryotic supergroups. *Nat Rev Microbiol.* 2008;6(12):925–939.
28. Dobos P. In vitro glycanylation of infectious pancreatic necrosis virus polypeptide VP1. *Virology.* 1993;193(1):403–413.
29. Di Marco S, Volpari C, Tomei L, et al. Interdomain communication in hepatitis C virus polymerase abolished by small molecule inhibitors bound to a novel allosteric site. *J Biol Chem.* 2005;280(33):29765–29770.
30. Graham SC, Sarin LP, Bahar MW, et al. The N-terminus of the RNA polymerase from infectious pancreatic necrosis virus is the determinant of genome attachment. *PLoS Pathog.* 2011;7(6):e1002085.
31. Bahar MW, Sarin LP, Graham SC, et al. Structure of a VP1-VP3 complex suggests how birnaviruses package the VP1 polymerase. *J Virol.* 2013;87(6):3229–3236.
32. Biasini M, Bienert S, Waterhouse A, et al. SWISS-MODEL: modelling protein tertiary and quaternary structure using evolutionary information. *Nucleic Acids Res.* 2014;42:W252–W258.
33. Altschul SF, Madden TL, Schäffer AA, et al. Gapped BLAST and PSI-BLAST: a new generation of protein database search programs. *Nucleic Acids Res.* 1997;25(17):3389–3402.
34. Remmert M, Biegert A, Hauser A, Söding J. HHblits: lightning-fast iterative protein sequence searching by HMM-HMM alignment. *Nat Methods.* 2011;9(2):173–175.

35. Guex N, Peitsch MC. SWISS-MODEL and the Swiss-PdbViewer: an environment for comparative protein modeling. *Electrophoresis*. 1997; 18(15):2714–2723.
36. Sali A, Blundell TL. Comparative protein modelling by satisfaction of spatial restraints. *J Mol Biol*. 1993;234(3):779–815.
37. Encinar JA, Fernández-Ballester G, Galiano-Ibarra V, Micol V. In silico approach for the discovery of new PPAR γ modulators among plant-derived polyphenols. *Drug Des Devel Ther*. 2015;9:5877–5895.
38. Galiano V, García-Valtanen P, Micol V, Encinar JA. Looking for inhibitors of the dengue virus NS5 RNA-dependent RNA-polymerase using a molecular docking approach. *Drug Des Devel Ther*. 2016;10: 3163–3181.
39. Schymkowitz J, Borg J, Stricher F, Nys R, Rousseau F, Serrano L. The FoldX web server: an online force field. *Nucleic Acids Res*. 2005;33: W382–W388.
40. Trott O, Olson AJ. AutoDock Vina: improving the speed and accuracy of docking with a new scoring function, efficient optimization, and multithreading. *J Comput Chem*. 2010;31(2):455–461.
41. Sander T, Freyss J, von Korff M, Rufener C. DataWarrior: an open-source program for chemistry aware data visualization and analysis. *J Chem Inf Model*. 2015;55(2):460–473.
42. Cheng F, Li W, Zhou Y, et al. AdmetSAR: a comprehensive source and free tool for assessment of chemical ADMET properties. *J Chem Inf Model*. 2012;52(11):3099–3105.
43. Law V, Knox C, Djoumbou Y, et al. DrugBank 4.0: shedding new light on drug metabolism. *Nucleic Acids Res*. 2014;42:D1091–D1097.
44. Reed LJ, Muench H. A Simple method of estimating fifty per cent endpoints. *Am J Epidemiol*. 1938;27(3):493–497.
45. Falco A, Chico V, Marroquín L, Perez L, Coll JM, Estepa A. Expression and antiviral activity of a beta-defensin-like peptide identified in the rainbow trout (*Oncorhynchus mykiss*) EST sequences. *Mol Immunol*. 2008;45(3): 757–765.
46. Livak KJ, Schmittgen TD. Analysis of relative gene expression data using real-time quantitative PCR and the $2^{-\Delta\Delta C_t}$ method. *Methods*. 2001; 25(4):402–408.
47. Sobhkhz M, Joensen LL, Tollersrud LG, Strandsgaard G, Thim HL, Jørgensen JB. A conserved inhibitory role of suppressor of cytokine signaling 1 (SOCS1) in salmon antiviral immunity. *Dev Comp Immunol*. 2017;67:66–76.
48. Marroquín L, Estepa A, Perez L. Inhibitory effect of mycophenolic acid on the replication of infectious pancreatic necrosis virus and viral hemorrhagic septicemia virus. *Antiviral Res*. 2008;80(3):332–338.
49. García I, Galiana A, Falco A, Estepa A, Perez L. Characterization of an infectious pancreatic necrosis (IPN) virus carrier cell culture with resistance to superinfection with heterologous viruses. *Vet Microbiol*. 2011; 149(1–2):48–55.
50. Lipinski CA, Lombardo F, Dominy BW, Feeney PJ. Experimental and computational approaches to estimate solubility and permeability in drug discovery and development settings. *Adv Drug Deliv Rev*. 2001;46(1–3):3–26.
51. Niyomrattanakit P, Chen YL, Dong H, et al. Inhibition of dengue virus polymerase by blocking of the RNA tunnel. *J Virol*. 2010;84(11): 5678–5686.
52. Yuan S, Chu H, Ye J, et al. Identification of a novel small-molecule compound targeting the influenza A virus polymerase PB1-PB2 interface. *Antiviral Res*. 2017;137:58–66.

PUBLICACIÓN 6

TÍTULO: Viral interference between infectious pancreatic necrosis virus and spring viremia of carp virus in zebrafish

COAUTORES: Melissa Belló Pérez, Regla María Medina Gali, Julio Coll Morales, Luis Perez García-Estañ.

REVISTA: Aquaculture

doi: <https://doi.org/10.1016/j.aquaculture.2018.10.039>

Volumen 500, Febrero 2019, Páginas 370-377.

1 **Title: Viral interference between infectious pancreatic necrosis virus and spring viremia of
2 carp virus in zebrafish**

3

4 Authors: Melissa Bello-Perez^{a(1)}, Regla Medina-Gali^{a(1)}, Julio Coll^b, Luis Perez^{*a}

5

6

7 ^a Instituto de Biología Molecular y Celular, Universidad Miguel Hernández de Elche, 03202
8 Elche, Spain

9 ^b Instituto Nacional de Investigaciones Agrarias, 28040 Madrid, Spain

10

11

12 (1) Both authors contributed equally to this work.

13 (*) Corresponding author

14

15

16 E-mail addresses

17 reglita2000@yahoo.com

18 melissa.bello@goumh.umh.es

19 juliocollm@gmail.com

20 luis.perez@umh.es

21 **Abstract**

22 Fish birnaviruses and rhabdoviruses are major causes of diseases that pose a threat to
23 the fish farming industry. In this work we investigated the interaction between IPNV
24 (birnavirus) and SVCV (rhabdovirus) in a zebrafish model where SVCV is lethal while IPNV
25 causes asymptomatic infection. Two situations were analyzed: 1) A primary IPNV infection
26 followed by a second challenge with SVCV; 2) SVCV as the first infection and a second
27 challenge with IPNV. Irrespective of the order of infections, IPNV increased survival of SVCV-
28 infected fish, reflecting viral interference that correlated with the inhibition of SVCV RNA
29 synthesis. In contrast, in some instances a synergistic effect occurred between SVCV and IPNV:
30 IPNV replication was enhanced in mixed infections with SVCV compared to the single IPNV
31 infection. Expression of host immune response genes *illb*, *mx* and *gig2* was modulated
32 differently depending on the order of virus infections: while higher levels of expression of *illb*,
33 *mx* and *gig2* were found in fish infected first with IPNV, those three genes were down-regulated
34 in fish infected with SVCV and then challenged with IPNV.

35 This first report of mixed birnavirus/rhabdovirus infections in zebrafish may help to
36 identify those factors associated to disease resistance and cross-protection in fish, with practical
37 implications for the development of new strategies for virus control in aquaculture.

38

39

40

41 *Keywords:* zebrafish; IPNV; SVCV; zebrafish; viral interference

48 **1. Introduction**

49 Double or even multiple viral infections have been reported in several species of fish
50 (Alonso, 2003; Kotob, 2016; Lin, 2017; Tafalla, 2006; Wiik-Nielsen, 2016). The study of the
51 interplay between two viruses and its impact on the severity of disease and development of
52 mortality in fish has shed some practical information on the host responses to viral challenge
53 that correlate to disease resistance and vaccine efficacy (Emmenegger, 2017).

54 Spring viremia of carp virus (SVCV) is the causative agent of spring viremia of carp
55 disease. It belongs to the Rhabdoviridae family of viruses with negative sense single stranded
56 RNA genome (Ashraf, 2016). Natural outbreaks of spring viremia of carp have been recorded in
57 common carp and other cyprinid species (OIE, 2017). Infectious pancreatic necrosis virus
58 (IPNV) causes disease in salmon and rainbow trout and has the ability to establish persistent
59 infections in a number of fish species (Julin, 2014). IPNV is a member of the family
60 Birnaviridae, viruses with double-stranded RNA genome. Both IPNV and SVCV are present
61 endemic in continental Europe (OIE, 2017). Thus, there is a possibility of IPNV and SVCV
62 coexistence in fish, although dual IPNV/SVCV infections have not been encountered so far, it is
63 perfectly possible due to the overlapping temperature range of both viruses and the ability of
64 IPNV to infect a wide range of species. SVCV infection of zebrafish by bath immersion has
65 been extensively studied before (Encinas, 2013; Medina-Gali, 2018b; Sanders, 2003).
66 Experimental infection of IPNV on zebrafish has also been reported (LaPatra, 2000). Thus, from
67 a practical point of view double IPNV/SVCV challenge of zebrafish can be a suitable
68 experimental model to study potential viral interference and host immune response in fish.

69 When two viruses coincide in a host they often compete for the cellular machinery
70 resulting in what is called viral interference. In fish, there is a body of evidence on IPNV-
71 induced interference over other viruses both *in vitro* and *in vivo*. In cell culture, primary IPNV
72 persistent infection blocks the replication of VHSV rhabdovirus in a subsequent infection
73 (García, 2011; Parreño, 2017). In vivo, IPNV infection often leads to the suppression of the
74 secondary virus challenge (Byrne, 2008; Johansen and Sommer, 2001; Lopez-Vazquez, 2017).
75 In mixed infections the final outcome depends on the interaction of the two pathogens, their

76 relative optimal temperatures and how they alter the host immune response. Heterologous
77 interference is often associated to the activation of the non-specific protection exerted by the
78 innate immune system (Lopez-Vazquez, 2017; Pakingking, 2004; Rosaeg, 2017; Vendramin,
79 2018). While it is widely accepted that SVCV is an inducer of the interferon pathway and other
80 cytokines (Aggad, 2009; Encinas, 2013; Feng, 2016; Medina-Gali, 2018b), contradictory results
81 have shown both stimulation as well as down-regulation of innate immune response key genes
82 (i.e. *ifn*, *mx*) by IPNV infection (Collet, 2007; Ingerslev, 2009; Lockhart, 2007; Lopez-Vazquez,
83 2017; Nombela, 2017; Skjesol, 2009).

84 Therefore, it would be interesting to assess the potential for viral interference between
85 two unrelated viruses (IPNV and SVCV) within the host. In this study we show that a first
86 IPNV infection of zebrafish induces a blockade over a subsequent SVCV infection.
87 Furthermore, it is also described for the first time the IPNV infection at an early time after
88 SVCV infection stops SVCV-induced disease and mortality in zebrafish.

89

90 **2. Materials and methods**

91 2.1. Cell and virus culture.

92 EPC cells were purchased from the American Type Culture Collection (ATCC number
93 CRL-2872). The cell line was maintained at 28 °C in a 5% CO₂ atmosphere in RPMI Dutch
94 modified (Gibco, Invitrogen corporation, UK) cell culture medium buffered with 20 mM
95 HEPES and supplemented with 10% fetal calf serum (FCS, Sigma, St. Louis, USA), 1 mM
96 piruvate, 2 mM glutamine (Sigma), 50 µg/ml gentamicin (Sigma) and 2.5 µg/ml fungizone
97 (Gibco).

98 Rainbow trout gonad cells (RTG-2) were purchased from SIGMA Aldrich (Sigma). The
99 cell line was maintained at 28 °C in a 5% CO₂ atmosphere in minimum essential medium
100 (MEM) supplemented with 10% FCS (Sigma), 1 mM piruvate, 2 mM glutamine (Sigma), 50
101 µg/ml gentamicin (Sigma) and 2.5 µg/ml fungizone (Gibco) .

102 The spring viremia of carp virus SVCV isolate 56/70 was grown in the EPC cell line at
103 22 °C by using RPMI medium supplemented with 2% FCS. Supernatants from SVCV infected

104 EPC cell monolayers were harvested at 7 days p.i. and clarified by centrifugation at 4000 r.p.m.
105 for 30 min and kept in aliquots at -70 °C. SVCV titers were measured by a methylcellulose
106 plaque assay (Encinas, 2013, García-Valtanen, 2017).

107 The infectious pancreatic necrosis virus (IPNV Sp strain) was grown in the RTG-2 cell
108 line at 14 °C in MEM + 2% FCS. Supernatants from IPNV infected RTG-2 cell monolayers
109 were harvested at 7 days p.i. and clarified by centrifugation at 4000 r.p.m. for 30 min and kept
110 in aliquots at -70 °C. Virus titration (TCID50/ml) was performed by the end-point dilution.

111

112 2.2. Virus infection and sampling.

113 Zebrafish (with average body weight 0.35-0.4 g) was used in two consecutive infection
114 trials IPNV + SVCV and SVCV + IPNV, in order to evaluate the effect of the viral interference.
115 The experiments were conducted following the established procedures approved by the ethics
116 committee on animal experimentation of the local government (Dirección General de
117 Agricultura, Ganadería y Pesca, Generalitat Valenciana) and registered under permit number
118 2016 / VSC / PEA / 00182. Fish were acclimatized for two weeks at 21°C prior to virus
119 challenge.

120 **IPNV + SVCV.** Zebrafish (80 fish) were intraperitoneally (i.p.) injected with 2×10^6 TCID50
121 of IPNV per fish, and after 2 or 30 days infected by bath immersion in 2×10^4 pfu/ml of SVCV
122 (Fig.1, IPNV + SVCV). A single SVCV-infected and a non-infected control group were treated
123 in parallel. Five days post SVCV infection head kidney, liver and spleen of 5 fish/treatment
124 were collected and pooled. Mortality was monitored for 19 days. Fish were kept at 21°C along
125 the challenge period.

126 **SVCV + IPNV.** Zebrafish (80 fish) were infected by bath immersion in 2×10^4 pfu/ml of
127 SVCV for 90 minutes. After 2 or 30 days fish were intraperitoneally injected with 2×10^6
128 TCID50 of IPNV per fish (Fig.1, SVCV + IPNV). Head kidney, liver and spleen were collected
129 and pooled at 3 days post-infection (dpi) for analysis. Mortality was monitored for 15 days. Fish
130 were kept at 21°C along the challenge period.

131

132 2.3. RNA extraction, cDNA synthesis and qPCR assays.

133 To evaluate transcript expression in adult zebrafish by reverse transcriptase and
134 quantitative polymerase chain reaction (RT-qPCR), the internal organs from 5 fish per group
135 were excised and pooled. RNA extraction was performed using the E.Z.N.A HP Tissue RNA kit
136 (Omega Bio-tek, Norcross, GA, USA) according to the manufacturer's instructions and stored at
137 -80 °C until use. Then, the cDNA was obtained using the reverse transcriptase (Moloney murine
138 leukemia virus, Invitrogen) as previously described (Chico, 2006).

139 Quantitative PCR was carried out in real time using the ABI PRISM 7300 system
140 (Applied Biosystems, NJ, USA) and SYBR Green PCR master mix (Life Technologies, United
141 Kingdom). Reactions were performed in a final volume of 20 µL containing 2 µL of cDNA, 900
142 nM of each primer and 10 µL of SYBR Green PCR master mix. The conditions of the
143 polymerase chain reaction were: 95°C for 10 min, 40 cycles at 65°C 1 min, 95°C for 1 min, and
144 extension for 10 min. The analysis of gene expression was performed by the $2^{-\Delta Ct}$ method (Livak
145 and Schmittgen, 2001), where ΔCt is determined by the formula target gene Ct value - efla gene
146 Ct value from the target Ct value. The sequences of the primers used in the assays are shown in
147 Table S1. Differential folds were calculated by the formula, normalized mean expression of
148 infected fish/normalized mean expression of control fish.

149

150 2.4. Data analysis and statistics

151 Statistical analysis was performed using the Graph Pad Prism v5.0 software. Survival
152 plots were generated using the Kaplan-Meier method. To compare the datasets of the different
153 treatments with their respective untreated controls, Tukey tests were performed. When
154 applicable, significant differences were represented as asterisks (*, **, ***) indicating p <0.05,
155 p<0.01 and p<0.001 values, respectively.

156

157 3. Results

158 3.1. IPNV and SVCV single infections.

159 Adult zebrafish infected with IPNV by intraperitoneal injection (2×10^6 TCID50 per
160 fish) did not show any clinical signs. The small percent of mortality (5%) that was observed
161 could be attributed to stress and handling of fish (Fig.2A). After 30 days of IPNV infection,
162 when the apparently healthy fish were tested for IPNV RNA they yielded positive results,
163 indicating that they had become IPNV carriers (not shown). In contrast, fish infected with
164 SVCV by bath immersion (2×10^4 pfu/ml) experienced great mortality rates (Fig.2B).

165

166 3.2. IPNV infection protects against subsequent SVCV infection (IPNV+SVCV).

167 The first experimental trial consisted of infection of zebrafish with IPNV by i.p.
168 injection (2×10^6 TCID50 per fish) followed by bath immersion in 2×10^4 pfu/ml SVCV 2 or
169 30 days later (Fig.1, IPNV + SVCV). Our results show that the survival rates in the
170 IPNV+SVCV groups was higher (73% survival in the IPNV2d+SVCV group and 56% survival
171 in the IPNV30d+SVCV group) than those infected with SVCV only (20% survival, Fig.2B).
172 Thus, the results in the IPNV2d+SVCV and IPNV30d+IPNV conditions suggest that IPNV
173 protects zebrafish from SVCV lethal effects, delaying mortality and increasing survival.

174

175 3.3. IPNV and SVCV replication in IPNV+SVCV infections.

176 To further analyze the interference phenomenon the replication of IPNV and SVCV was
177 examined by measuring IPNV A segment and SVCV N gene levels in samples from a pool of
178 internal organs by RT-qPCR. SVCV RNA in fish previously infected with IPNV either 2 days
179 or 30 days earlier showed significantly lower levels at 5 days post SVCV infection compared to
180 fish infected only with SVCV (Fig.3B), suggesting that the presence of IPNV inhibited
181 subsequent SVCV replication. Unexpectedly, IPNV replication increased after SVCV
182 superinfection (Fig.3A), although great variability in IPNV RNA levels among individuals was
183 observed in the IPNV+SVCV groups.

184

185 3.4. Transcription of interleukin 1 β (*illb*), *mx* and *gig2* genes in IPNV + SVCV infections.

186 To evaluate if the innate immune response could be involved in the observed cross-
187 protection of IPNV against SVCV three genes characteristically associated to fish response to
188 virus infection were analyzed: *illb*, *mx* and *gig2* (Fig.4). SVCV infection of zebrafish led to
189 enhanced expression of the three genes. In the IPNV+SVCV groups, modulation of *illb*, *mx* and
190 *gig2* transcription by the first virus (IPNV) was observed, with all three genes showing higher
191 expression levels compared to single SVCV infection. However, none of the selected genes
192 were overexpressed in response to IPNV alone.

193

194 3.5. IPNV infection protects against previous SVCV infection (SVCV+IPNV).

195 We set a new trial intended to check if the viral interference phenomenon would still
196 occur if the order on viral infections was reversed. Thus, one SVCV bath infection was followed
197 by i.p. injection of IPNV 2 days or 30 days later (Fig.1, SVCV + IPNV). Fish challenged with
198 SVCV had a ≈33% survival, while the SVCV+IPNV2d group had a greater survival rate (≈78%,
199 Fig.5). This result suggests that IPNV injection at an early time (2dpi SVCV) prevented SVCV
200 disease progression. At later times (30 dpi SVCV) fish were not experienced SVCV disease or
201 mortality any longer and therefore survival was not affected by IPNV.

202

203 3.6. Viral replication in SVCV + IPNV-infected fish.

204 Replication of SVCV and IPNV was measured in the experimental groups by RT-
205 qPCR. Samples were harvested at 3 dpi with IPNV. SVCV transcript expression was
206 significantly lower in fish that were superinfected with IPNV 30 days after SVCV infection
207 compared to the SVCV infected group (Fig.6A). In fish superinfected with IPNV 2 days after
208 SVCV, SVCV RNA levels were also lower but not statistically significant.

209 IPNV replication was significantly enhanced in survivors of SVCV challenge
210 (SVCV30d + IPNV) but not in fish infected with SVCV for only 2 days (SVCV2d + IPNV,
211 Fig.6B).

212

213 3.7. Changes in selected genes transcription in SVCV + IPNV infected fish.

214 To investigate the impact of the second IPNV infection on host innate response, samples
215 from internal organs of zebrafish were collected to measure expression levels of *illb*, *mx* and
216 *gig2* genes. Transcription of all three genes was maximal in the SVCV30d group (Fig.7). When
217 IPNV was administered to the SVCV-infected fish at 30 days post SVCV infection a
218 significantly lower expression of the antiviral transcripts was observed. Again, IPNV failed to
219 stimulate the expression of any of the three selected genes.

220

221 **4. Discussion**

222 Viral interference is defined as the suppression of one virus replication by a subsequent
223 infection with the same (homologous) or different (heterologous) virus. In this study we have
224 demonstrated in vivo interference between IPNV and SVCV when IPNV was administered
225 either before or after SVCV. We had observed previously a characteristic interference of IPNV
226 over heterologous viruses in IPNV-carrier cell cultures (García, 2011; Parreño, 2017). Since that
227 interference phenomenon was observed on a cyprinid cell line (EPC), we aimed to replicate this
228 situation in vivo on a cyprinid fish species. Zebrafish is susceptible to SVCV infection
229 displaying clinical signs and experiencing high mortalities (Encinas, 2013; García-Valtanen,
230 2017). In contrast, IPNV was capable of replicating in zebrafish but without clinical signs and
231 no mortality (LaPatra, 2000). To the best of our knowledge IPNV + SVCV coinfections of fish
232 under natural conditions have not been found so far. There are however a number of reports that
233 examined experimental IPNV coinfections with other rhabdoviruses (Alonso, 1999; Byrne,
234 2008; Rodriguez, 2005).

235 Protection against a second viral infection has been observed in survivors of dsRNA
236 virus infections which usually had turned into asymptomatic carriers (Kotob, 2016; LaPatra,
237 1995). This protective effect seems to last as long as the fish carries the virus from the first
238 infection (Lund, 2016). However, that is not always the case since in some instances cross-
239 protection declines over time (Pakingking, 2004). Therefore, we decided to perform a second
240 infection at 2 (early) and 30 (late) days after the first virus infection. Our results indicate that
241 infection of zebrafish with IPNV suppresses the replication of SVCV irrespective of the order

242 and time of viral infection. Our findings are in agreement with previous reports showing the
243 protective effect of a first IPNV infection of trout against the IHNV rhabdovirus (Alonso, 2003;
244 Byrne, 2008; López-Vazquez, 2017) or the ISAV orthomyxovirus (Johansen and Sommer,
245 2001). Although salmonid fish are the primary targets of IPNV, birnavirus infection protected
246 against subsequent VHSV infection in flounder (Pakingking, 2004), suggesting that the IPNV-
247 mediated viral interference is not restricted to salmonids.

248 Although viral interference is characteristic of dsRNA viruses such as birnaviruses and
249 reoviruses (Vendramin, 2018) is also possible to find interference phenomena between ssRNA
250 and dsRNA viruses in fish (Wiik-Nielsen, 2016). Herein, interference of SVCV over IPNV was
251 not observed. On the contrary, our results suggest a synergistic effect of SVCV over IPNV
252 replication. Although this was not expected, we were not the first to find stimulation of one
253 virus by co-infection with another virus (Lin, 2017). The synergistic effect may be attributed to
254 immunosuppression of the host by one of the pathogens, facilitating the replication of the
255 second virus. Such situation does not appear to be the case here since SVCV did activate *mx* and
256 *gig2* gene expression. The synergistic effect may also be related to a negative effect of the
257 primary SVCV infection on the host ability to produce neutralizing antibodies. This would be
258 consistent with the stimulation of IPNV replication found in the fish infected with IPNV 30
259 days after SVCV, but not in fish infected with IPNV only 2 days after SVCV (too early for the
260 antibody response to play any part). Finally, one likely explanation for the interference
261 phenomenon is the induction of antiviral genes of the innate immune response by the first virus
262 that inhibits the replication of the second invading virus. We selected *mx* and *gig2* genes for
263 further analysis since they are amongst the most important antiviral genes induced by dsRNA
264 viruses in fish (He, 2017; López-Vázquez, 2016; Nombela, 2017; Vendramin, 2018; Xiao,
265 2016). Furthermore, recent findings highlighted the role of *gig2* gene in zebrafish upon SVCV
266 infection (Medina-Gali, 2018a). We also tested interleukin 1 β (*il1b*) as it is a widely accepted
267 marker of stimulation by pathogen associated molecular patterns or PAMPs (Carballo, 2017;
268 Tafalla, 2006; Varela, 2017; Zou, 2016). In some cases up-regulation of interferon and *mx* genes
269 by the first infection has been linked to the antiviral effect on the second pathogen (Rosaeg,

270 2017). In our hands, infection of zebrafish with IPNV before SVCV resulted in enhanced *illb*,
271 *mx* and *gig2* transcription levels. In contrast, in zebrafish infected with IPNV 30 days after
272 SVCV *illb*, *mx* and *gig2* transcription was reduced compared to the single SVCV in correlation
273 to a diminished SVCV replication. Thus, we may conclude that by interfering with SVCV
274 replication, IPNV would prevent the upregulation of host response genes. Nevertheless, an
275 explanation for the heterologous viral interference may not be always straightforward. For
276 instance, the piscine reovirus (PRV) protection against salmonid alphavirus (SAV) infection in
277 Atlantic salmon did not seem to be related to activation of typical antiviral genes (Lund, 2016).
278 On this regard, we have found a lack of correlation between in vitro and in vivo results. IPNV
279 activates *mx* expression in EPC cells (García, 2011; Jurado, 2013) but down-regulates *mx*
280 expression in vivo zebrafish. This discrepancy may be due to the fact that the EPC cell line is
281 not derived from *Danio rerio* (zebrafish) but instead is originated from *Pimephales promelas*
282 (fathead minnow). Moreover, a second IPNV infection is not capable of blocking SVCV
283 replication in EPC cells (unpublished results). Thus, the EPC cell line may not be a perfect
284 model for the in vivo zebrafish situation.

285

286 **5. Conclusions**

287 Altogether, the results presented here show the protective effect of both a preceding and
288 a subsequent infection with the birnavirus IPNV against the rhabdovirus SVCV. We present
289 evidence that the host immune response depended on the order of viral infections. In zebrafish
290 infected with IPNV a second infection with SVCV enhanced some host innate responses,
291 whereas in zebrafish infected with SVCV, a second infection with IPNV inhibited those
292 responses. The cause of such inhibition is not clear but our data point to the conclusion that
293 IPNV interference over a primary SVCV infection is a consequence of the suppression of
294 SVCV replication, while the interference of IPNV over a subsequent SVCV infection is likely
295 related to the establishment of an antiviral state by IPNV that make the fish better responders to
296 the second infection.

297 The study of the causes of the induction of an antiviral state after the first virus opens
298 new avenues of research in fish immunology that may ultimately lead to the identification of the
299 key factors underlying disease resistance in fish.

300

301 **Acknowledgements**

302 Technical assistance from Angeles Gómez (IBMC) is acknowledged. We would like to
303 thank José Antonio Perez de Gracia, Yolanda Miralles and all the personnel in the Animal
304 Research Facility at UMH for their work and dedication.

305

306 **Authors' contribution**

307 M. Bello-Perez and R. Medina-Gali contributed equally to this work.

308

309 **Funding**

310 This research was supported by Program “*I+D+I Orientada a los Retos de la Sociedad*”
311 funded by Ministerio de Economía y Competitividad of Spain (Grant AGL2014-51773-C3) and
312 Grant BIO2017-82851. Melissa Bello's contract is funded by Generalitat Valenciana fellowship
313 ACIF/2016/207.

314

315 **References**

316 Aggad, D., M. Mazel, P. Boudinot, K. E. Mogensen, O. J. Hamming, R. Hartmann, S. Kotenko,
317 P. Herbomel, G. Luftfalla, and JP. Levraud. 2009. The two groups of zebrafish virus-induced
318 interferons signal via distinct receptors with specific and shared chains. *J. Immunol.* 183:3924-
319 3931.

320 Alonso, M., I. Rodríguez, and S. S. Perez-Prieto. 1999. Viral coinfection in salmonids:
321 infectious pancreatic necrosis virus interferes with infectious hematopoietic necrosis virus.
322 Arch. Virol. 144:657-673.

323 Alonso, M., S. Rodriguez, and S. I. Perez-Prieto. 2003. Virulence of infectious hematopoietic
324 necrosis virus and infectious pancreatic necrosis virus coinfection in rainbow trout
325 (*Oncorhynchus mykiss*) and nucleotide sequence analysis of the IHNV glycoprotein gene. Arch.
326 Virol. 148:1507-1521.

327 Ashraf, U., Y. Lu, L. Lin, J. Yuan, M. Wang, and X. Liu. 2016. Spring viremia of carp virus:
328 recent advances. *J. Gen. Virol.* 97:1037-1051.

- 329 Byrne, N., J. Castric, J. Cabon, and C. Quentel. 2008. Study of the viral interference between
330 infectious pancreatic necrosis virus (IPNV) and infectious haematopoietic necrosis virus
331 (IHNV) in rainbow trout (*Oncorhynchus mykiss*). Fish Shellfish Immunol. 24:489-497.
- 332 Carballo, C., E. Garcia-Rosado, J. J. Borrego, and C. Alonso. 2016. SJNNV down-regulates
333 RGNNV replication in European sea bass by the induction of the type I interferon system. Vet.
334 Res. 47:6-16.
- 335 Chico, V., N. Gomez, A. Estepa, and L. Perez. 2006. Rapid detection and quantitation of viral
336 hemorrhagic septicemia virus in experimentally challenged rainbow trout by real-time RT-PCR.
337 J. Virol. Methods 132:154-159.
- 338 Collet, B., E. S. Munro, S. Gahlawat, F. Acosta, J. Garcia, C. Roemelt, J. Zou, C. J. Secombes,
339 and A. E. Ellis. 2007. Infectious pancreatic necrosis virus suppresses type I interferon signalling
340 in rainbow trout gonad cell line but not in Atlantic salmon macrophages. Fish Shellfish
341 Immunol. 22:44-56.
- 342 Emmenegger, E., S. Biacchesi, E. Mérour, J. Glenn, A. D. Palmer, M. Bremont, and G. Kurath.
343 2017. Virulence of a chimeric recombinant infectious haematopoietic necrosis virus expressing
344 the spring viraemia of carp virus glycoprotein in salmonid and cyprinid fish. J. Fish Diseases
345 doi.org/10.1111/jfd.12678.
- 346 Encinas, P., P. Garcia-Valtanen, B. Chinchilla, E. Gomez-Casado, A. Estepa, and J. Coll. 2013.
347 Identification of multipath genes differentially expressed in pathway-targeted microarrays in
348 zebrafish infected and surviving spring viremia carp virus (SVCV) suggest preventive drug
349 candidates. PLoS ONE 8:e73553.
- 350 Feng, H., Q.-M. Zhang, Y. Zhang, Z. Li, J. Zhang, Y.-W. Xiong, M. Wu, and J.-F. Gui. 2016.
351 Zebrafish IRF1, IRF3 and IRF7 differentially regulate IFNΦ1 and IFNΦ3 expression through
352 assembly of homo- or heteroprotein complexes. J. Immunol. 197:1893-1904.
- 353 Garcia, I., A. Galiana, A. Falco, A. Estepa, and L. Perez. 2011. Characterization of an infectious
354 pancreatic necrosis (IPN) virus carrier cell culture with resistance to superinfection with
355 heterologous viruses. Vet. Microbiol. 149:48-55.
- 356 Garcia-Valtanen, P., A. Martinez-Lopez, A. Lopez-Muñoz, M. Bello-Perez, R. M. Medina-Gali,
357 M. Ortega-Villaizan, M. Varela, A. Figueras, V. Mulero, B. Novoa, A. Estepa, and J. Coll.
358 2017. Zebra fish lacking adaptive immunity acquire an antiviral alert state characterized by
359 upregulated gene expression of apoptosis, multigene families, and interferon-related genes.
360 Front. Immunol. 8:121-doi:10.3389/fimmu.2017.00121.
- 361 He, L., A. Zhang, Y. Pei, P. Chu, Y. Li, R. Huang, L. Liao, Z. Zhu, and Y. Wang. 2017.
362 Differences in responses of grass carp to different types of grass carp reovirus (GCRV) and the
363 mechanism of hemorrhage revealed by transcriptome sequencing. BMC Genomics 18:452.
- 364 Ingerslev, H. C., A. Ronneseth, E. F. Pettersen, and H. I. Wergeland. 2009. Differential
365 expression of immune genes in Atlantic salmon (*Salmo salar* L.) challenged intraperitoneally or
366 by cohabitation with IPNV. Basic Immunol. 69:90-98.

- 367 Johansen, L. H. and A.-I. Sommer. 2001. Infectious pancreatic necrosis virus infection in
368 Atlantic salmon *Salmo salar* post-smolts affects the outcome of secondary infections with
369 infectious salmon anaemia virus or *Vibrio salmonicida*. Dis. Aquat. Org. 47:109-117.
- 370 Julin, K., L. H. Johansen, A.-I. Sommer, and J. B. Jorgensen. 2014. Persistent infections with
371 infectious pancreatic necrosis virus (IPNV) of different virulence in Atlantic salmon, *Salmo*
372 *salar* L. J. Fish Diseases 38:1005-1019.
- 373 Jurado, M. T., P. Garcia-Valtanen, A. Estepa, and L. Perez. 2013. Antiviral activity produced by
374 an IPNV-carrier EPC cell culture confers resistance to VHSV infection. Vet. Microbiol.
375 166:412-418.
- 376 Kotob, M. H., S. Menanteau-Ledouble, G. Kumar, M. Abdelzaher, and M. El-Matbouli. 2016.
377 The impact of co-infections on fish: a review. Vet. Res. 47:98.
- 378 LaPatra, S. E., L. Barone, G. R. Jones, and L. I. Zon. 2000. Effects of infectious hematopoietic
379 necrosis virus and infectious pancreatic necrosis virus infection on hematopoietic precursors of
380 the zebrafish. Blood Cells Mol. Dis. 26:445-452.
- 381 LaPatra, S. E., K. A. Lauda, and G. R. Jones. 1995. Aquareovirus interference mediated
382 resistance to infectious hematopoietic necrosis virus. Vet. Res. 26:455-459.
- 383 Lin, Q., X. Fu, N. Li, Q. Wan, W. Chen, Y. Huang, Z. Huang, J. Li, L. Zhao, and L. Lin. 2017.
384 Co-infections of infectious spleen and kidney necrosis virus and Siniperca chuatsi rhabdovirus
385 in Chinese perch (*Siniperca chuatsi*). Microb. Pathog. 11:422-430.
- 386 Livak, K. L. and T. D. Schmittgen . 2001. Analysis of relative gene expression data using real-
387 time quantitative PCR and the 2-DDT method. Methods 25:402-408.
- 388 Lockhart, K., A. J. A. McBeath, B. Collet, M. Snow, and A. E. Ellis. 2007. Expression of Mx
389 mRNA following infection with IPNV is greater in IPN-susceptible Atlantic salmon post-smolts
390 than in IPN-resistant Atlantic salmon parr. Fish Shellfish Immunol. 22:151-156.
- 391 Lopez-Vazquez, C., M. C. Alonso, C. P. Dopazo, and I. Bandín. 2017. In vivo study of viral
392 haemorrhagic septicaemia virus and infectious pancreatic necrosis virus coexistence in
393 Senegalese sole (*Solea senegalensis*). J. Fish Diseases 40:1129-1139.
- 394 Lund, M., M. V. Rosaeg, A. Krasnov, G. Timmerhaus, I. B. Nyman, V. Asperhaug, E. Rimstad,
395 and M. K. Dahle. 2016. Experimental Piscine orthoreovirus infection mediates protection
396 against pancreas disease in Atlantic salmon (*Salmo salar*). Vet. Res. 47:107.
- 397 Medina-Gali, R., M. Bello-Perez, A. Martinez-Lopez, A. Falco, M. Ortega-Villaizan, J. A.
398 Encinar, B. Novoa, J. Coll, and L. Perez. 2018a. Chromatin immunoprecipitation and high
399 throughput sequencing of SVCV-infected zebrafish reveals novel epigenetic histone
400 methylation patterns involved in antiviral immune response. Fish Shellfish Immunol. 82:514-
401 521.
- 402 Medina-Gali, R., M. Ortega-Villaizan, L. Mercado, B. Novoa, J. Coll, and L. Perez. 2018b.
403 Beta-glucan enhances the response to SVCV infection in zebrafish. Dev. Comp. Immunol.
404 84:307-314.

- 405 Nombela, I., A. Carrion, S. Puente-Marin, V. Chico, L. Mercado, L. Perez, J. Coll, and M.
406 Ortega-Villaizan. 2017. Infectious pancreatic necrosis virus triggers antiviral immune response
407 in rainbow trout red blood cells, despite not being infective. F1000 Res. 6:1968.
- 408 OIE. 2017. Manual of Diagnostic Test for Aquatic Animals. http://www.oie.int/fileadmin/Home/eng/Health_standards/aahm/current/chapitre_svc.pdf.
- 410 Pakkingking, R., Y. Okinaka, K. Mori, M. Arimoto, K. Muroga, and T. Nakai. 2004. In vivo and
411 in vitro analysis of the resistance against viral haemorrhagic septicaemia virus in Japanese
412 flounder (*Paralichthys olivaceus*) preceedingly infected with aquabirnavirus. Fish Shellfish
413 Immunol. 17:1-11.
- 414 Parreño, R., L. Almagro, M. Bello-Perez, R. Medina-Gali, A. Estepa, and L. Perez. 2017.
415 Restricted replication of viral hemorrhagic septicemia virus (VHSV) in a birnavirus-carrier cell
416 culture. Arch. Virol. 162:1037-1041.
- 417 Rodriguez, S., M. Alonso, and S. S. Perez-Prieto. 2005. Comparison of two birnavirus-
418 rhabdovirus coinfections in cell lines. Dis. Aquat. Org. 67:183-190.
- 419 Rosaeg, M. V., M. Lund, I. B. Nyman, T. Markussen, V. Asperhaug, H. Sindre, M. K. Dahle,
420 and E. Rimstad. 2017. Immunological interactions between Piscine orthoreovirus and Salmonid
421 alphavirus infections in Atlantic salmon. Fish Shellfish Immunol. 64:308-319.
- 422 Sanders, G. E., W. N. Batts, and J. R. Winton. 2003. Susceptibility of zebrafish (*Danio rerio*) to
423 a model pathogen, spring viremia of carp virus. Comp. Med. 53:514-521.
- 424 Skjesol, A., T. Aamo, M. N. Hegseth, B. Robertsen, and J. B. Jorgensen. 2009. The interplay
425 between infectious pancreatic necrosis virus (IPNV) and the IFN system: IFN signaling is
426 inhibited by IPNV infection. Virus Res. 143:53-60.
- 427 Tafalla, C., S. Rodriguez, and S. I. Perez-Prieto. 2006. Immunological consequences of the
428 coinfection of brown trout (*Salmo trutta*) with infectious hematopoietic necrosis virus (IHNV)
429 and infectious pancreatic necrosis virus (IPNV). Aquaculture 256:15-22.
- 430 Varela, M., A. Figueras, and B. Novoa. 2017. Modelling viral infections using zebrafish: innate
431 immune response and antiviral research. Antiviral Res. 139:59-68.
- 432 Vendramin, N., A. L. Farias Alencar, T. M. Ibburg, M. K. Dahle, O. Wessel, A. B. Olsen, and N.
433 J. Olesen. 2018. Piscine orthoreovirus infection in Atlantic salmon (*Salmo salar*) protects
434 against subsequent challenge with infectious hematopoietic necrosis virus (IHNV). Vet. Res.
435 49:30-doi: 10.1186/s13567-018-0524-z.
- 436 Wiik-Nielsen, J., M. Alarcón, B. B. Jensen, O. Haugland, and A. B. Mikalsen. 2016. Viral co-
437 infections in farmed Atlantic salmon, *Salmo salar* L., displaying myocarditis. J. Fish Diseases
438 39:1495-1507.
- 439 Xiao, J., J. Yan, H. Chen, J. Li, Y. Tian, L. Tang, and H. Feng. 2016. Mx1 of black carp
440 functions importantly in the antiviral innate immune response. Fish Shellfish Immunol. 58:584-
441 592.
- 442 Zou, J. and C. J. Secombes. 2016. The function of fish cytokines. Biology 5:doi:
443 10.3390/biology5020023.

444 **Figure captions**

445 Fig.1. Experimental design of zebrafish infections and sample collection timelines.

446

447 Fig.2. IPNV + SVCV infections of zebrafish. Kaplan-Meier survival plots of zebrafish infected
448 first with IPNV and secondly with SVCV. (A) Zebrafish (25 fish/group) were intraperitoneally
449 injected with IPNV (2×10^6 TCID50/fish). (B) At 2 days or 30 days after IPNV infection fish
450 were infected with SVCV by bath immersion (2×10^4 pfu /ml) and mortality was recorded for
451 19 days.

452

453 Fig.3. Viral loads of IPNV and SVCV based on RT-qPCR evaluation. Data represent relative
454 values respect to *eflα* expression. Five individuals were sampled for each group. (*) Asterisks
455 indicate ($p < 0.05$) differences in IPNV-A segment (A) or SVCV N gene RNA levels (B).
456 Internal organs from SVCV-infected fish were harvested at 5 days post infection.

457

458 Fig.4. Relative expression of *mxab*, *gig2l* and *illb* gene transcripts in internal organs of fish (n =
459 5) infected with IPNV and SVCV as indicated. Data are referred to uninfected controls (value =
460 1, dotted line). Time of sampling for SVCV-infected fish was 5 dpi. Results are expressed as the
461 mean±SD. Statistical significance in immune gene expression between two groups is indicated
462 (*, $p < 0.05$; ** $p < 0.01$; ***, $p < 0.001$).

463

464 Fig.5. SVCV + IPNV infections of zebrafish. Kaplan-Meier survival plots of zebrafish infected
465 first with IPNV and secondly with SVCV. (A) Zebrafish (25 fish/group) were infected with
466 SVCV by bath immersion (2×10^4 pfu/ml). (B) Fish were intraperitoneally injected with IPNV
467 2×10^6 TCID50/fish at 2 or 30 days after SVCV infection. Mortalities were recorded for 15
468 days.

469

470 Fig.6. Viral loads of SVCV and IPNV based on RT-qPCR evaluation. Five individuals were
471 sampled for each experimental group. *, ** indicate significant ($p < 0.05$, $p < 0.01$) differences in

472 SVCV N gene (A) or IPNV-A segment RNA levels (B). Fish infected with IPNV were
473 harvested at 3 dpi.

474

475 Fig.7. Relative expression of *mxab*, *gig2l* and *il1b* gene transcripts in internal organs of fish (n =
476 5) infected with SVCV and IPNV as indicated. Data are referred to uninfected controls (value =
477 1, dotted line). Time of sampling for IPNV-infected fish was 3 dpi. Results are expressed as the
478 mean±SD. Statistical significance in immune gene expression between two groups is indicated
479 (**, p<0.01; ***, p< 0.001).



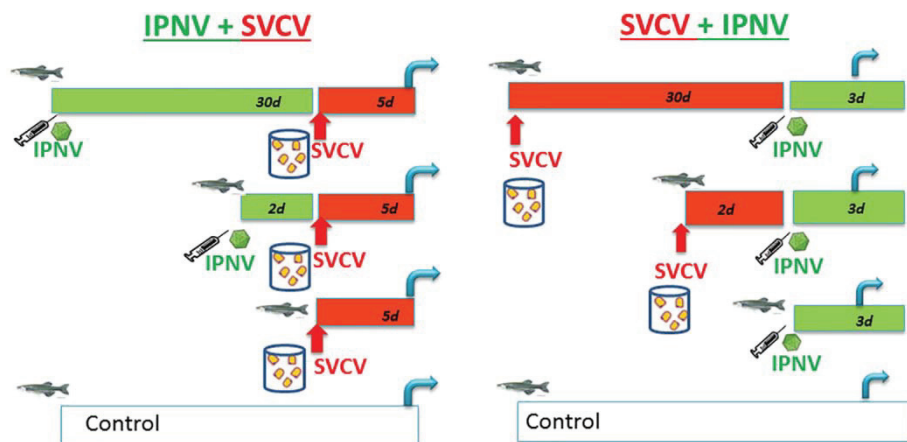


Figure 1.

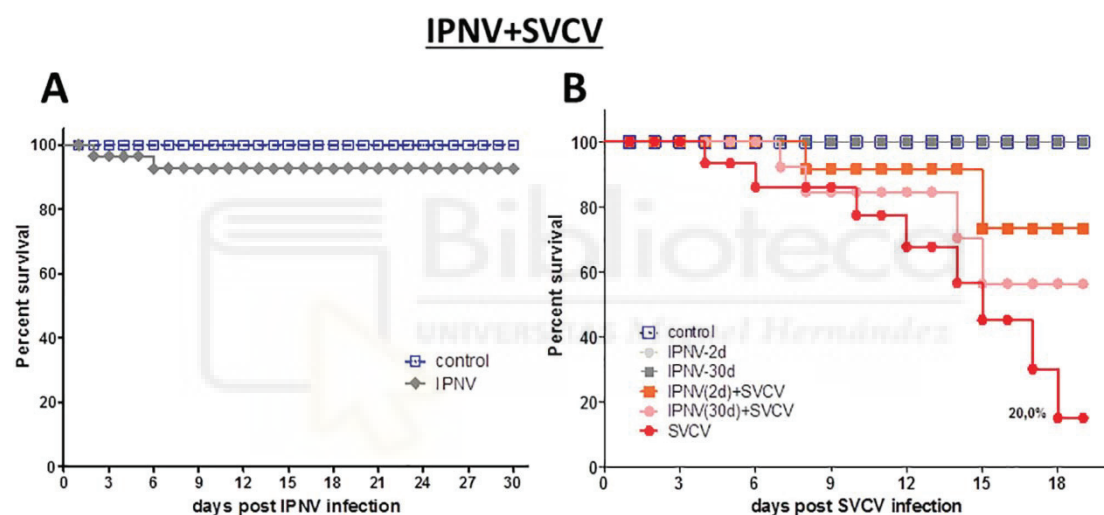


Figure 2.

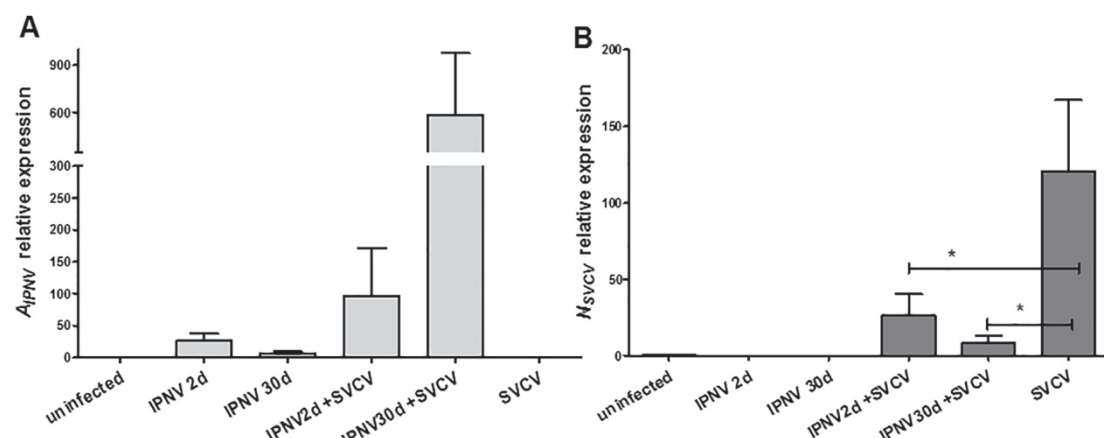


Figure 3.

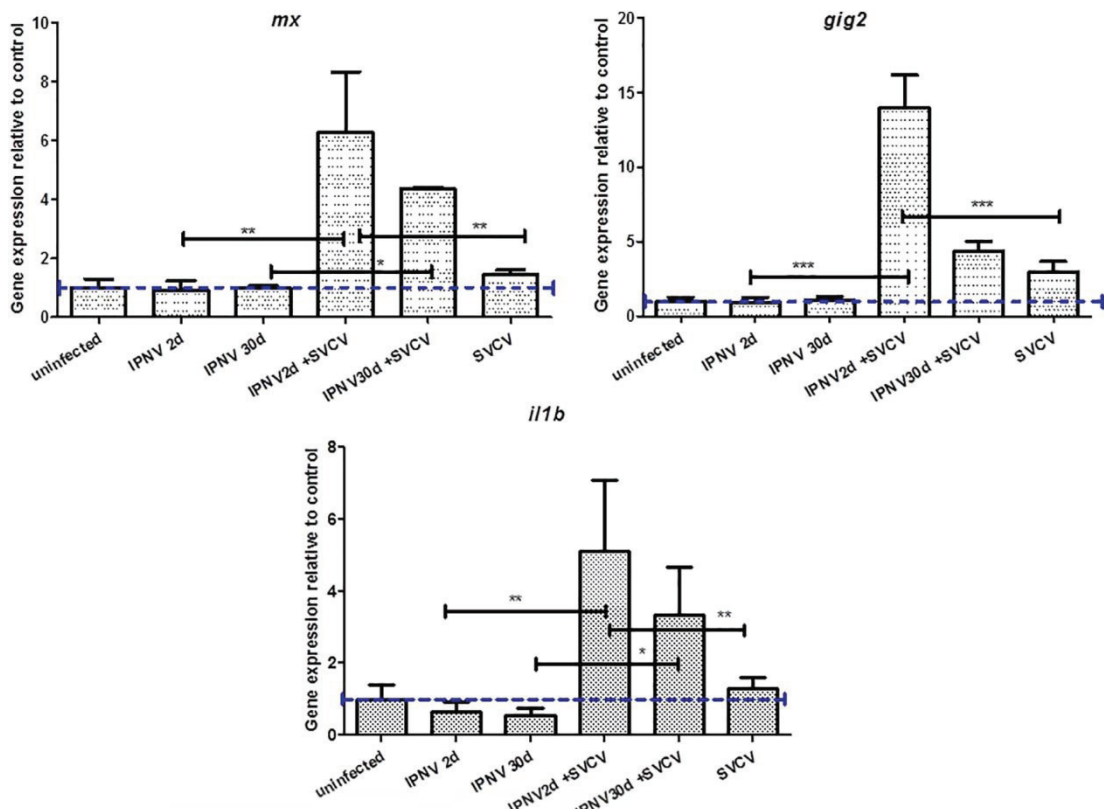


Figure 4.

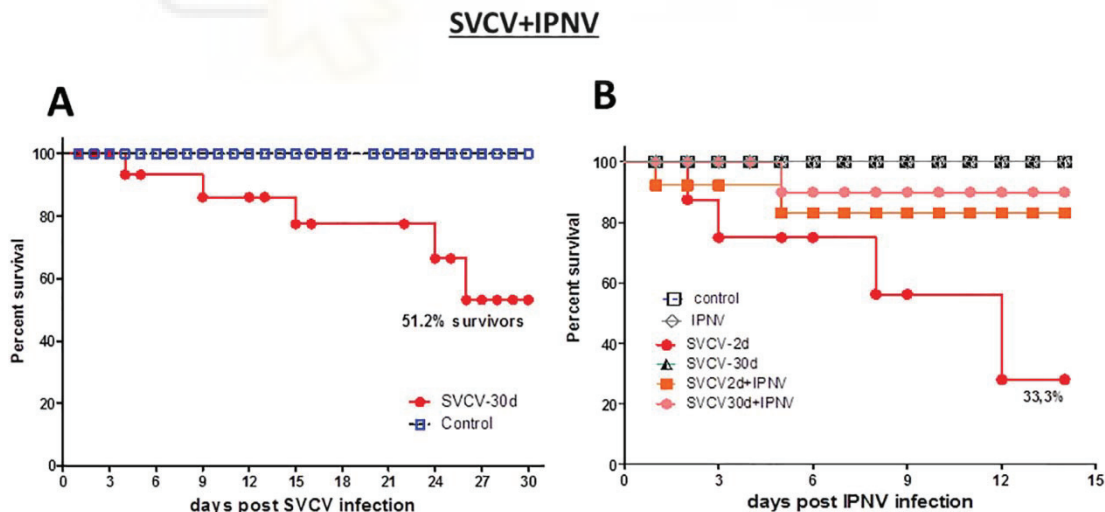


Figure 5.

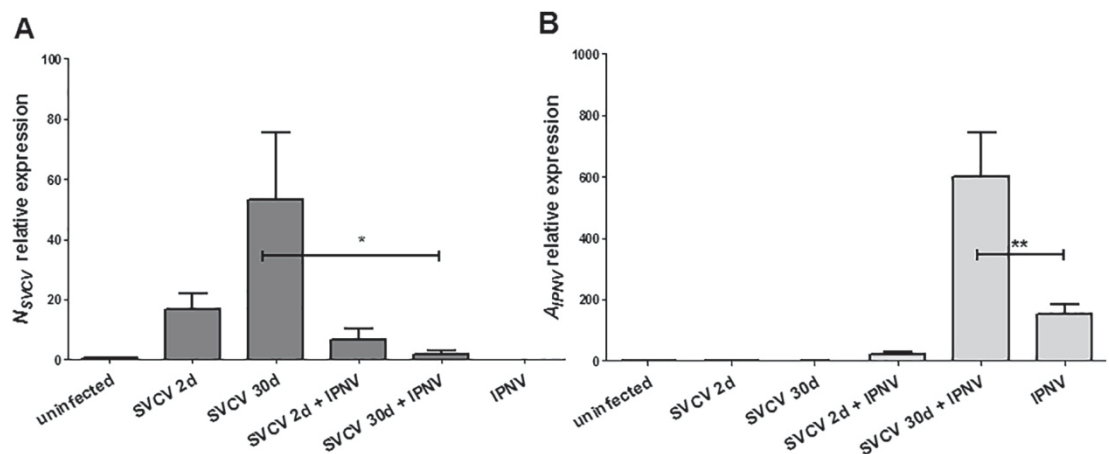


Figure 6.

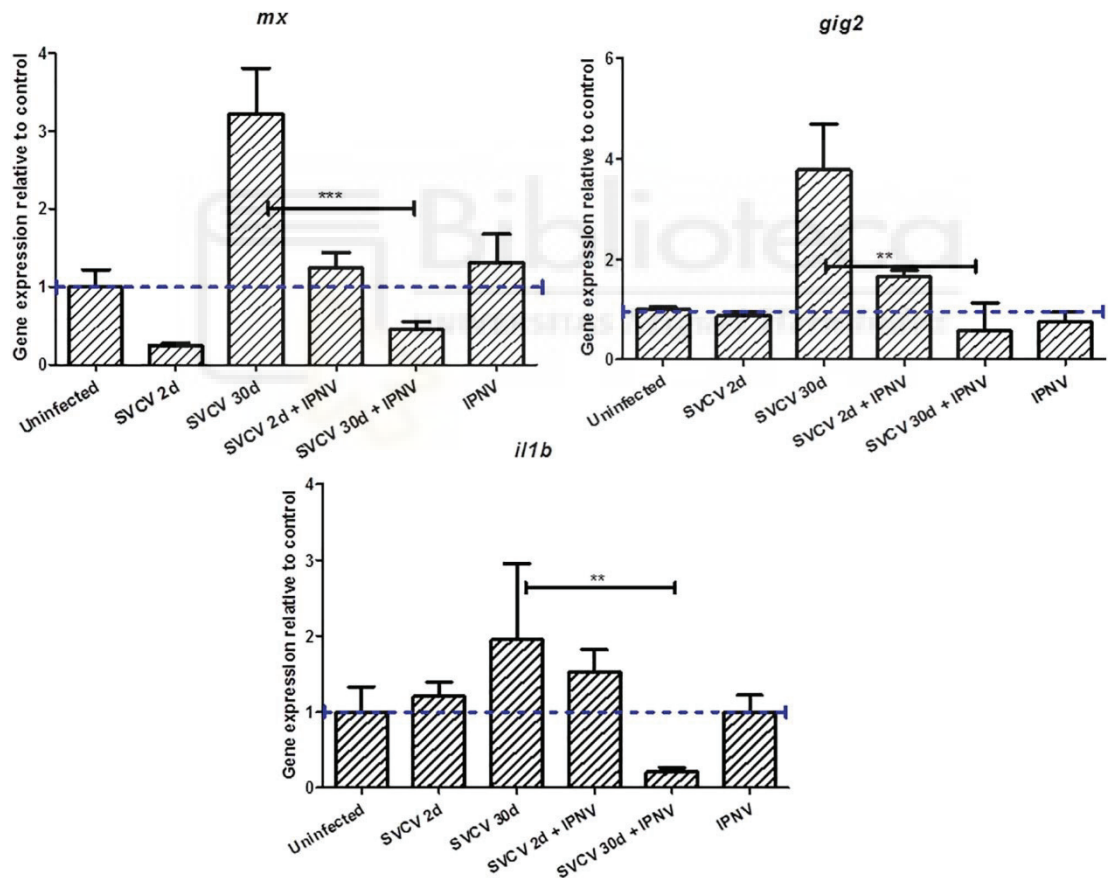


Figure 7.